

THÈSE / UNIVERSITÉ DE RENNES 1

sous le sceau de l'Université Bretagne Loire

pour le grade de

DOCTEUR DE L'UNIVERSITÉ DE RENNES 1

Mention : Électronique

Ecole doctorale MATISSE

présentée par

Seljan Josip

Préparée à l'unité de recherche (UMR CNRS 6164, IETR)
Institute d'Électronique et de Télécommunications de Rennes
Université de Rennes 1

**Modélisation
électromagnétique
rapide de structures
SIW par équations
intégrales**

**Thèse soutenue à l'Université de
Rennes 1
le 24/10/2016**

devant le jury composé de :

Hélène ROUSSEL

Professeur, UPMC Paris / *rapporteur*

Francesco ANDRIULLI

Professeur, Télécom Bretagne / *rapporteur*

Matteo ALBANI

Professeur, Université de Siena / *examineur*

Massimiliano CASALETTI

Maitre de Conférences, UPMC Paris / *examineur*

Ronan SAULEAU

Professeur, IETR Rennes / *directeur de thèse*

« To all the ladies and gentlemen, who made this all so probable...»

Alex Chilton

ACKNOWLEDGEMENTS

To almost no exception, a Ph.D. programme, as well as the acknowledgements section of a thesis, cannot be brought to an end without a significant amount of poor attempts at humour, pretension, false self-importance, misplaced quotes and overall cheesiness, in no particular order. In fact, gradually these become indispensable tools one uses again and again during her/his career.

However, rarely can one acquire proficiency in the aforementioned areas without serious help from those he holds dear, whether professionally or personally. Well, to be fair, even the ones he would hold down to a railroad track. This section is dedicated to those without whom I wouldn't have made it this far.

A great "Hvala!" to prof. Zvonimir Sipus for getting me into this mess in the first place, and for fooling me into thinking that I'm capable of more than simple subtraction and addition. The joke's on you, Zvonimir!

A huge "Merci beacoup!" to prof. Ronan Sauleau and a just as big "Grazie mille!" to dr. Mauro Ettorre for this wonderful opportunity, continuing support and a no small number of kicks in the hind when I needed them. Without your drive, enthusiasm and honesty, the closest I would've gotten to doing science would have been the time I successfully mixed toothpaste, bleach and laundry detergent into an effective ant repellent when I was 7. (At this point, a sincere apology is due to the ant community of Karlovac, Croatia.). Unfortunately, I still consider it my greatest scientific achievement to this day.

To professors Guido Valerio and Massimiliano Casaletti, I cannot even begin to express the gratitude for the kindness, acceptance, guidance and genuine care for this poor schmuck. I am now aware that I will never fully master even a passage of Felsen's, but you've shown me that it is, at least, possible in theory. For a handful of people. If that metaphorical hand has been involved in some kind of a freakish buzz saw accident.

Now, as anyone who has taken a psychology class in high school knows, according to Maslow, one cannot do well in sitting behind a monitor for long hours crunching lines of dubious code, if one hasn't had a proper hangover, seen a good movie at the cinema (bad ones serve their purpose as well), or had a good laugh the weekend before. And for that, friends, you need good company. A disgustingly humungous "Thaaank you!" goes to Adrien, Mario, Erio, Anda, Francesco the First of Rome, Francesco the Second of His Name, Danny Boy, Johnny Boy, Shoaib, Bassam, David, Marco, Giorgio, Valentina, and all the ones that will be seriously offended when they don't find their name on this list. Without you, my sanity would only be something discussed once a year by my parole committee. And, without some of you I would've never gotten close to almost making the night bus sing "Bohemian Rhapsody" in unison.

A big shout out goes to Artem, Benjamin, Sami, Laurent & Laurent, Maxim, Tao and the rest of the IETR inmates for making my stay and cigarette breaks there fun and stimulating.

To Dunja, Amael, Stelios, Antoine, Anastasia, Nikki, Colette and the rest of the wonderful gallery of wanderers, I wish to express my deepest thanks for taking me in and showing me that there is life in Rennes beyond the Rue de la Soif. Moreover, thank you for all the unsuccessful attempts at trying to get me to dance or speak whole sentences in French. I know for sure that the latter was especially excruciating for you.

Next, a thanks or two to the two people bearing a great deal responsibility for the mess to follow after this section - I would like to thank and, hopefully, someday repay at least in part for all the support, kindness and encouragement my wonderful parents Berica and Nenad have given me during these long, long four-plus years.

Modelisation rapid des structures SIW par equations integrals – Josip Seljan – April, 2015

At the very end, I would like to thank the one person who has never given up on me, helped me push through the bad days, been there to make my good days even better, and whose unfaltering love, understanding and kindness have made my life complete. This thesis is dedicated to you, Tamara.

ABSTRACT

With constant demand for larger band and more compact RF devices, the rapid shift to higher frequency regions, as high as the W-band (75 to 110 GHz), forces microwave designers to both transfer existing technologies to and invent new ones for these bands. The major obstacles encountered in this endeavour are the problem of efficient field confinement, problematic electrical contacts, high dielectric losses, and difficult integration between devices realized with different technologies, to name a few. To overcome these issues, several competing technologies emerged in the past two decades. One of the most promising is the *substrate-integrated waveguide (SIW) paradigm*. Its key concept is, as its name clearly indicates, the possibility of integrating waveguides into substrates, most often done by embedding densely-packed metal and dielectric cylinders into substrates bounded by highly-conductive layers, e.g. PCB-type ones. Doing so mitigates most of the aforementioned issues since. In addition, it provides unprecedented freedom in the range of devices that can be realized. Though commonly planar, these devices may have guide narrow walls of almost arbitrary shape and can be easily integrated with ones realized in alternative technologies, such as the coplanar-waveguide or microstrip technology. The richness in design possibilities, robustness and solid performance has led to a very large number of SIW devices, some of them finding place in commercial applications. However, aside from the simplest ones, they comprise a large number of elements and often have complex layouts. Hence, they present a challenge from a designer's perspective, necessitating numerical analysis and optimization. The most common solvers used for that purpose are based on FEM, FDTD/FDFD, and MoM, or merge several methods. Though they are up to the task for a vast range of structures, faster and more accurate ones are highly sought for.

This thesis is concerned with a hybrid mode-matching/MoM method suited to the analysis of a vast range of planar SIW structures. It relies on an efficient modal representation of fields in parallel-plate waveguides, loaded with either *single or multi-layer* planar dielectrics, containing circular-cylindrical posts; it enables the construction of linear systems whose solutions yield post-scattered field amplitudes. This problem is what we refer to as *mode-matching*, and provides means of fast computation of field in presence of metal and dielectric posts, as they are the most common elements in an SIW device. Now, since a significant share of such devices use narrow rectangular slots as coupling and radiating elements, we propose an MoM-based approach to their analysis. Through the application of the equivalence principle, each slot is short-circuited and replaced by equivalent magnetic currents; the procedure effectively partitions the larger problem into several smaller ones, each pertaining to a single region bounded by parallel PEC plates (a single parallel-plate waveguide). Enforcing the boundary conditions at surfaces of slots and performing Petrov-Galerkin weighting, we obtain a linear system whose solutions are the amplitudes of magnetic currents. From there we proceed to the computation of relevant quantities such as S, Y and Z parameters. We provide empirical criteria for choosing the number of modes/basis functions sufficient for high accuracy. Moreover, we present approximation techniques and show how to exploit symmetries inherent in SIW devices to speed up the method even further.

To stress the features rendering our approach advantageous over the alternatives, we compare it to ones found in literature representing what we believe to be the most successful attempts. We present the results of analysis of several SIW structures of varying complexity, obtained by our in-house code based on the method exposed here, and compare them against the ones obtained with a standard commercial solver. The obtained results show excellent accuracy and efficiency of the proposed method, confirming its advantage over commercial software. The speed-up factor, the robustness and generality make it an attractive tool to be used in design and optimization of SIW devices.

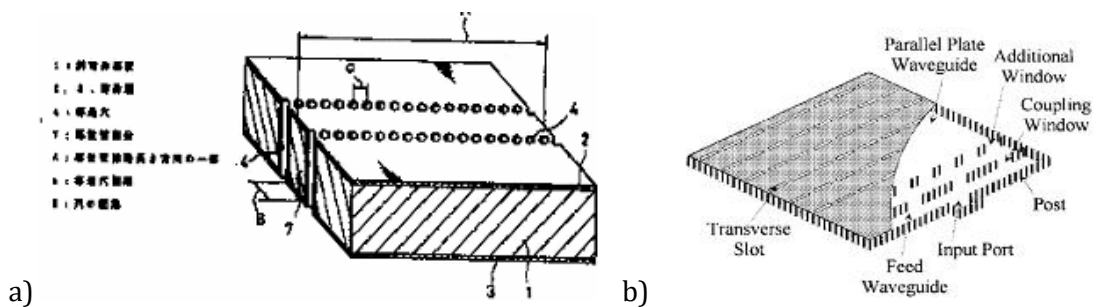
RESUMÉ DE THÈSE

Introduction et objectifs

Des défis majeurs se posent aujourd'hui à toute tentative de conception des dispositifs électroniques aux hyper-fréquences au-delà d'environ 20 GHz. Notamment : a) confinement difficile des champs électromagnétiques, b) pertes diélectriques et métalliques importantes, c) intégration entre technologies différentes, et d) difficulté de fabrication des dispositifs en système monolithique. La technologie en substrat intégré offre des nombreux avantages pour le développement de dispositifs guidant (*substrate-integrated waveguide, SIW*) aux hyper-fréquences [1]. Cette technologie combine simplicité et flexibilité pour surmonter les limites des technologies plus consolidées, telles que le microruban, ainsi que les nouvelles et moins conventionnelles, telles que le « bed of nails ».

La prémisse à la base de cette technologie est à la fois simple et puissante. Les conducteurs métalliques verticaux qui confinent les champs dans un guide d'onde sont remplacés par une série de trous verticaux métallisés faits dans le substrat. Ces trous, très proches entre eux, forment une barrière qui empêche la fuite de l'énergie dans l'espace autour (figure R.1).

Figure R.1 a) Guide d'onde brevetée par Shigeki (prise de [2]), b) Première antenne mis en œuvre dans la technologie SIW par Hirokawa et Ando (1998) (prise de [3])



Cette stratégie permet de réaliser des structures plus complexes, en raison de la flexibilité dans le placement des trous et à la facilité de fabrication. En effet, un grand nombre de dispositifs micro-ondes a été réalisé dans la technologie SIW dans les 20 dernières années, allant des filtres [4], coupleurs directionnels [5], circulateurs [6], jonctions T-magiques, plans diplexeurs, etc. . De surcroît, un certain nombre de dispositifs actifs ont été également mis en œuvre, comme des oscillateurs à rétroaction [7], diode Gunn, amplificateurs et mixeurs électriques mono-transistor. Par conséquent, tous les ingrédients nécessaires pour réaliser des dispositifs en SIW sont disponibles. En fait, l'une des tendances de la recherche actuelle dans ce domaine est orientée vers la réalisation de systèmes autonomes sur un seul substrat [8], car les structures SIW peuvent avoir des pertes et un couplage inter-circuit beaucoup plus faibles que les technologies alternatives.

En dépit de tous leurs avantages, les appareils SIW sont composés d'un très grand nombre d'éléments, ce qui complique, par conséquent, leur conception. Ceci est principalement dû aux interactions, souvent difficiles à prédire, en particulier dans des structures électriquement grandes. Bien qu'un certain nombre de règles de conception, rapides et approchées, aient été inventées (voir par exemple [9]), elles peuvent servir uniquement dans la première étape de conception. Malheureusement, la complexité et la généralité des structures à analyser empêchent la dérivation des formules analytiques suffisamment précises. Ce problème a poussé des efforts importants dans le développement d'un grand

nombre de méthodes d'analyse rapide. Ces méthodes peuvent être grossièrement divisées en deux typologies. Les méthodes analytiques approchées-, reposant sur des approximations à partir de formulations intégrales ou différentielles ([10], [11], [12]) et les méthodes rigoureuses (full wave). Les approximations sont souvent faite grâce à quelques symétries spécifiques (telles que périodicité ou symétrie miroir) ou en négligeant des effets d'ordre supérieur, ou avec sur des paramètres obtenus empiriquement à travers une procédure d'interpolation.

Les méthodes full wave, d'autre part, représentent les effets complexes de la diffusion sans approximations, sur la base soit des différences finies / éléments finis ou de la méthode des moments (MoM, [13], [14], [15]). Des méthodes hybrides peuvent aussi fusionner plusieurs approches décrites dessus. [16]. Bien que certains des ouvrages cités représentent des méthodes puissantes et flexibles, leur dénominateur commun est le manque général de généralité et d'efficacité. Ils reposent sur des scénarios trop spécifiques et donc restrictifs, et les résultats ne peuvent pas toujours être satisfaits dans un dispositif pratique.

En manque de méthodes full wave rapides et précises adaptées à l'analyse d'une vaste classe de dispositifs SIW, les objectifs du travail développé dans le cadre de cette thèse sont formulés ci-dessous:

- concevoir et mettre en œuvre une méthode numérique d'analyse pour modéliser une grande variété de dispositifs SIW avec une grande précision et de relativement faibles ressources de calcul (par rapport aux solveurs commerciaux standard), y compris des scénarios impliquant des milieux diélectriques planaire en couches dans PPWs.
- explorer les caractéristiques générales des dispositifs SIW utilisant l'analyse mis au point en fonction des propriétés modales des champs.

Le premier objectif est motivé par l'absence d'outils fiables au moment de la conception de cette thèse. Bien que certaines méthodes aient été mises au point, ils ne pouvaient pas gérer une grande variété de géométries. Cette limitation est due soit au caractère approché de la méthode d'analyse, ou à l'inefficacité de calcul liée au nombre très large des inconnues à déterminer.

Le deuxième objectif est mûri pendant le travail de thèse en raison du cadre mathématique adopté pour la formulation du problème. Notamment, une méthode particulière de synthèse de champ modal, décrite dans les prochaines sections, s'est avérée la meilleures pour obtenir une plus rapide convergence des algorithmes utilisés. Cette décomposition modale permet l'expression du champ total en plusieurs ondes de nature différente : ondes rayonnantes, ondes guidées par la PPW, ondes diffractées par les trous etc. Ce résultat permet d'identifier les processus physiques qui contribuent le plus au champ total et, par conséquent, élaborer des lignes directrices sur des règles simplifiées pour la conception des dispositifs. En outre, elle a conduit à l'amélioration de l'efficacité de l'algorithme sur la base d'approximations qui évitent le calcul de certaines interactions entre composants.

Analyse des dispositifs SIW

Un certain nombre de méthodes pour l'analyse efficace des structures de SIW planaires ont été conçues et appliquées au fil des ans. Dans cette thèse, une méthode hybride est présentée, fusionnant la méthode des moments et la méthode de raccordement modal, capable de gérer la résolution de SIW planaires assez généraux. Ceux-ci incluent la présence de plusieurs guides d'ondes SIW planaires empilés et couplés par des fentes, de guides composés d'un nombre arbitraire de couches diélectriques planes, de structures fermées ainsi que des dispositifs rayonnants.

En comparaison à d'autres méthodes similaires, notre méthode porte l'avantage clé de formuler un problème scalaire au lieu d'un problème vectoriel. Afin de trouver la fonction de Green dyadique de la SIW, les méthodes mentionnées reposent sur ce qu'on appelle la procédure Ohm-Rayleigh. Essentiellement, on trouve d'abord des ensembles complets de fonctions *vectorielles* satisfaisant les équations de Maxwell-Heaviside (vecteurs propres de la structure analysée). Ceux-ci sont obtenus par la différenciation des fonctions scalaires (correspondant à des modes caractéristiques du problème de la valeur limite en question). Ensuite, on procède à l'expansion de la fonction de Green dyadique en termes des vecteurs propres, obtenant une représentation spectrale complète; une transformée de Fourier inverse est enfin effectuée, ce qui donne la représentation spatiale souhaitée. Cependant, il faut être extrêmement prudent dans l'exercice de la transformée inverse, car des singularités spectrales doivent être prises en compte dans l'évaluation de la self-admittance (ou self-impédance) du dispositif. En outre, la procédure est assez fastidieuse en raison de plusieurs développements en séries de fonctions et intégrations spectrales, en liaison avec des régularisations pas très intuitives qui doivent être appliquées pour rendre les intégrales convergentes. Une autre difficulté, plus conceptuelle que technique, est un certain manque d'intuitivité (cette méthode ne se prête pas une interprétation physique simple) par rapport à la méthode de Schwinger-Marcuvitz-Felsen que nous avons appliquée.

D'autre part, nous démontrons comment construire la fonction de Green dyadique nécessaire à partir de potentiels scalaires, que nous dérivons avec ce que nous croyons être une manière élégante - conceptuellement claire, physiquement interprétable et mathématiquement cohérente. Nous montrons comment le dyadique de Green pour PPWs avec milieux diélectriques homogènes par morceaux est construit et régularisé, la régularisation étant d'une importance capitale dans l'application ultérieure de la méthode Petrov-Galerkin.

Une méthode numérique est finalement jugée par son efficacité - sa capacité d'obtenir des résultats suffisamment précis dans un temps de calcul acceptable. Dans notre cas, le concept clé permettant la formulation d'une méthode efficace est l'utilisation d'une représentation du champ à l'aide de lignes de transmission radiales : les fonctions représentant le champ sont exprimées comme produits de fonctions radiales de Bessel ou Hankel et d'harmoniques azimutaux (exponentielles imaginaires). Comme la plupart des structures laissent propager un seul mode guidé (habituellement celui d'ordre inférieur, le mode fondamental), les modes d'ordre supérieur seront atténués. Par conséquent, leur fonctions de Hankel, qui décrivent la dépendance radiale des champs, seront exponentiellement amorties. Il en résulte que seul un nombre réduit de modes sera nécessaire pour représenter avec précision le champ total. Des arguments similaires sont applicables aux modes azimutaux décrivant la variation angulaire des courants et des champs. S'il est bien conçu, un dispositif SIW contiendra des trous dont la circonférence sera faible par rapport à la longueur d'onde des champs se propageant dans le guide. Par conséquent, un petit nombre de fonctions azimutales sera en mesure de reconstituer la variation angulaire de champs et de courants autour de chaque trou.

En conclusion, cette représentation nous permet de représenter efficacement les champs électromagnétiques incidents (en fonction de sources), et les champs diffractés par trous et fentes. Les systèmes linéaires liés à cette représentation, dont les solutions donnent les amplitudes des champs diffractés par des trous métallisés ou diélectriques, résultent donc de taille réduite, et seront également considérés dans les travaux.

De plus, nous montrons comment évaluer numériquement les champs à l'intérieur de dispositifs empilés constitués par un certain nombre de guides SIW reliés entre eux par des fentes rectangulaires. Le couplage des fentes est étudié avec une méthode des moments, formulée pour des structures fermées et ouvertes. Nous montrons comment construire des systèmes linéaires à l'aide d'une méthode de moments en réutilisant des quantités déjà calculées pendant l'analyse du raccordement modale, et, par conséquent, réduisant le temps

d'exécution. Plusieurs méthodes ad-hoc sont présentées pour réduire le nombre d'inconnues et des calculs, qui aboutissent à une accélération significative des temps de calcul de l'ordre de N , où N est le nombre de cellules élémentaires d'un dispositif modulaire (par exemple, constitué d'un certain nombre de guides identiques). Une procédure automatisée qui pourrait être capable de reconnaître de manière autonome les motifs de répétition et les symétries d'un dispositif général sera un prochain développement des futures recherches dans ce sujet.

Les résultats des simulations numériques qui illustrent l'efficacité de la méthode seront présentés dans le chapitre 3 de cette thèse. En synthétisant, de nombreux calculs menés en comparaison avec un logiciel commercial électromagnétique (Ansys HFSS) montrent l'avantage significatif de notre méthode sur le logiciel commercial. La précision, ci-définie comme l'accord entre les quantités calculées à la fois avec le solveur commercial et le code MATLAB basé sur notre méthode, est excellente dans toutes les structures considérées. Des différences mineures existent, visibles dans les diagrammes de rayonnement au-dessous d'un niveau de -20 dB, et peuvent être considérées comme négligeables. En ce qui concerne les paramètres S , l'accord est également excellent, même pour les dispositifs SIW multicouches. Bien que les « waveguide ports » en régime monomodal soient utilisés dans la présente analyse, une extension de la méthode, couvrant le cas de plusieurs modes qui se propagent dans chaque porte est déjà en cours de validation. En ce qui concerne le temps de calcul, notre méthode est nettement plus rapide que le solveur commercial, étant de 4 à environ 20 fois plus rapide (selon la structure considérée). En outre, l'utilisation de la mémoire de notre code est très inférieure en raison d'un nombre d'inconnues significativement plus faible et des méthodes d'accélération appliquées. Le grand nombre d'inconnues est, de fait, ce qui limite l'applicabilité du logiciel commercial à l'analyse des grandes structures : à un certain point, le nombre d'inconnues devient tellement large que même les ordinateurs haut de gamme ne sont plus en mesure de stocker toutes les données nécessaires pour la solution du problème. Dans tous ces cas, notre approche peut être appliquée de manière fiable.

Un résumé des résultats les plus importants de la thèse est donné ci-dessous:

- I. L'extension du formalisme Schwinger-Marcuvitz-Felsen à PPWs remplies avec des milieux diélectriques multicouche.
- II. Extraction cohérente des singularités de la fonction dyadique de Green.
- III. L'application du formalisme ci-décrit pour étudier SIW planaires empilées et couplées à travers des fentes rectangulaires.
- IV. Expressions généralisées pour l'admittance des fentes dans les dispositifs de SIW remplies avec des milieux diélectriques multicouche.
- V. Réduction significative du temps de calcul et de la mémoire nécessaire par rapport aux logiciels commerciaux, à parité de précision.

Bien que la méthode présentée dans cette thèse puisse être appliquée à une grande variété de dispositifs SIW, certaines caractéristiques pourraient ajouter un ajustement complet de l'outil d'analyse pour gérer des scénarios pratiques. La première de ces caractéristiques est le traitement des pertes métalliques et diélectriques. En effet, la plupart des structures sont conçues pour minimiser lesdites pertes, qui dans certains cas peuvent être négligées ; il est pourtant souvent important de pouvoir évaluer les pertes, surtout si les fréquences opérationnelles tombent dans les domaines des ondes millimétriques ou des TeraHertz. L'évaluation des pertes nécessiterait une représentation de champ différent, en fonction de la conductivité des surfaces métalliques. Notamment, la présence de surfaces métalliques avec pertes, à condition que la conductivité soit suffisamment élevée, peut être prise en compte par les conditions aux limites de Leontovich [17], et ainsi représentées comme des surfaces d'impédances. En général, cela conduira à des ensembles de modes TM et TE mutuellement non orthogonaux, c'est-à-dire, les surfaces à pertes provoquent un couplage entre les modes de la structure. Cette approche a été appliquée, par exemple, dans

[18], [19] et [20], mais aucune tentative de généraliser le cas d'un PPW multicouche n'a été fait. Si, d'autre part, la conductivité considérée est faible, les objets métalliques deviennent pénétrables et peuvent être modélisés, par exemple, comme diélectriques avec pertes. Cela conduit alors à un problème plus difficile, étant donné que le spectre de l'opérateur vertical devient continu (bien que le spectre discret sera présents également).

Comme décrit dans la section 2.2.1, la méthode ci-présentée suppose des plaques métalliques de largeur infinie. Dans les cas les plus pratiques, même pour des réseaux de fentes, la troncature ne produit pas d'effets de bord significatifs comme du rayonnement dans des directions non désirées. Néanmoins, il pourrait être utile d'inclure des corrections dues à la diffraction aux bords des structures dans les prochains développements. Cela pourra être fait en utilisant une formulation appropriée de la théorie de la diffraction (voir par exemple [21]).

Conclusion et perspectives

Une méthode numérique doit être jugée par la précision de ses prédictions. Bien qu'elle puisse être simple ou élégante, elle peut aussi échouer à fournir des résultats qui correspondent à la réalité. À partir de séries de tests, nous avons rassemblé les caractéristiques principales de la performance de la méthode, et en avons déduits les points forts et les faiblesses de celle-ci.

Les discussions précédentes peuvent être résumées à l'ensemble des déclarations suivantes :

- I. La méthode présentée dans ce travail constitue un cadre conceptuel simple pour résoudre les problèmes de diffusion dans des systèmes SIW pouvant contenir :
 - a. Panneau diélectrique simple ou multi-couches,
 - b. Cylindres métallique et diélectriques de rayon arbitraire,
 - c. Fentes de couplage et fentes rayonnantes

En tant que telle, elle permet de traiter une grande variété de problèmes rencontrés dans la conception des dispositifs SIW. La simplicité conceptuelle et la cohérence mathématique, ainsi que son champ de représentation avantageux permettent de développer rapidement des routines numériques applicables à la fois à la conception et à l'analyse. En outre, cette même représentation sur le terrain se prête à l'application des techniques d'approximation asymptotique, ce qui pourrait accélérer l'analyse par un ordre de grandeur (voir par exemple [22]).

- II. A en juger par les tests numériques effectués, la méthode est applicable à la fois
 - a. dispositifs fermés (résonance) de forme arbitraire (bien sûr, à condition que le guide d'ondes en question est plan), et
 - b. dispositifs rayonnants dont les éléments rayonnants sont des fentes rectangulaires (bien que la méthode puisse être généralisée à des éléments de forme arbitraire).
- III. Du point de vue de l'utilisation des ressources de calcul HFSS, notre code surpasse le solveur FEM d'HFSS dans tous les scénarios simulés, avec un facteur de réduction du temps de calcul allant de 3 à 24, et un facteur de réduction de la mémoire vive utilisée allant de 1.1 jusqu'à 29, en fonction du nombre d'éléments de DUT (dispositifs en cours de test) et des fonctions de base utilisées. Les chiffres les plus bas apparaissent lorsque le nombre d'éléments et le nombre de fonctions de base sont élevés, ce qui donne lieu à de grands systèmes linéaires qui doivent être

résolus de manière itérative. Cependant, dans la plupart des cas, il est suffisant de considérer pas plus de deux modes longitudinaux, sept modes azimutaux (i.e. les modes avec le nombre d'onde azimutal dans l'intervalle $[-3, 3]$) et cinq fonctions de base de la fente; de nombreux problèmes en requièrent même moins pour une précision excellente.

- IV. En raison de sa généralité, l'approche proposée est applicable à un large éventail de profils diélectriques (i.e. configurations d'épaisseurs de couche et permittivités); la seule stipulation étant que le cadre multi-couches ne peut être utilisé pour les appareils rayonnants chargés de plaques diélectriques dont les couches respectives ont des valeurs de permittivité similaires («similaire» signifiant $|\varepsilon_i - \varepsilon_j| / \varepsilon_{i,j} < 5\%$ pour toutes couches i, j). En outre, le nombre d'inconnues augmente significativement moins avec l'augmentation de la permittivité et/ou de l'épaisseur d'une couche diélectrique par rapport à HFSS. Ceci est dû à l'utilisation de forme fermée des fonctions propres à la stratification de coordonnées, par opposition aux maillages tétraédriques à base HFSS.

D'autre part, la méthode possède quelques limitations qui pourraient faire l'objet de travaux futurs:

- I. Pour l'instant, l'analyse de systèmes diélectriques ou de composants métalliques à pertes n'est pas pris en charge. L'inclusion de ces pertes serait une caractéristique importante, en particulier à des fréquences supérieures à 20 GHz.
- II. L'applicabilité de la méthode pour de très grands/complexes dispositifs nécessite une analyse plus approfondie. Bien qu'il ait été démontré qu'elle fonctionne bien pour les appareils comportant plusieurs centaines d'éléments (jusqu'à environ 700), il est nécessaire d'étudier la stabilité et la convergence lorsque le nombre d'éléments est de l'ordre de plusieurs milliers. Il est tout à fait possible que les routines de résolution alternatives pour les systèmes linéaires pertinents devront être adoptées.
- III. Les fentes de forme arbitraire doivent être prises en charge, comme une partie importante des dispositifs pratiques reposent des formes non-canoniques, comme des os de chien et des fentes croisées. A cet effet, on pourrait utiliser une base générale telles que les fonctions de Rao-Wilton-Glisson. L'inconvénient dans ce cas, bien sûr, serait l'augmentation du temps de calcul due à la fois à la triangulation et le calcul d'un plus grand nombre de termes d'admittance par rapport à l'approche de base.
- IV. Le code MATLAB développé, basé sur la méthode proposée, doit être optimisé pour une exécution plus rapide et une plus petite empreinte mémoire, pour permettre la manipulation de structures plus grandes sur une gamme moyenne de configurations. À l'heure actuelle, le code est une implémentation simple de l'algorithme proposé, sans techniques de gestion de la mémoire ou d'optimisation de code. Par conséquent, il doit être réécrit dans un langage plus rapide, de préférence compilé, tel que le C ++ ou le FORTRAN. Une accélération possible pourrait être réalisée par déroulage de boucles [23] en raison de la présence d'un grand nombre de boucles *for* et *while*. Une accélération significative peut être réalisée par une parallélisation en utilisant un GPU (par exemple par le portage du code CUDA C ++), une technique prenant de l'ampleur dans la communauté de l'électromagnétisme numérique en raison de la large disponibilité de processeurs graphiques puissants. Quant à la question de l'empreinte mémoire, principalement due au stockage de grandes matrices générées par les sous-routines mode-matching/MoM, on pourrait simplement stocker lesdites matrices à sur fichiers formatés, les effacer de la mémoire vive (RAM) et les charger de nouveau si nécessaire. Bien sûr, la lecture du disque dur est beaucoup plus lente que la RAM, mais l'avantage potentiel est la possibilité d'analyser des structures plus grandes

sur les postes avec une RAM limitée. En outre, en raison de la présence de matrices creuses, le format de stockage standard des matrices creuses peut être utilisé.

TABLE OF CONTENTS

1 INTRODUCTION.....	1
1.1 PLANAR MICROWAVE SYSTEMS - BASICS.....	2
1.2 WHY SIW?.....	4
1.3 TOO MANY POSTS IN THE WAVEGUIDE – THE ANALYSIS OF SIW-TYPE DEVICES	13
1.4 AIMS OF THE THESIS.....	15
1.5 WHAT LIES AHEAD - THESIS OUTLINE.....	16
1.6 A NOTE ON NOTATION, UNITS AND ALL THAT	17
2 HYBRID MODE-MATCHING/ MOM FOR SIW DEVICES.....	18
2.1 MODELING A GENERIC SIW DEVICE – GENERAL CONSIDERATIONS	19
2.1.1 <i>Initial Assumptions and Simplifications</i>	19
2.1.2 <i>Splitting the Problem Domain</i>	21
2.2 THE INTERIOR AND EXTERIOR PROBLEMS	23
2.2.1 <i>The Interior Problem</i>	24
2.2.2 <i>Let There Be Light – Exciting the SIW</i>	74
2.2.3 <i>The Exterior Problem</i>	78
2.3 THE SLOT THICKENS – MIXING MODE MATCHING AND THE METHOD OF MOMENTS	79
2.3.1 <i>From Slots to Equivalent Currents</i>	79
2.3.2 <i>Admittance Calculation</i>	84
2.3.3 <i>The Excitation Vector of the MoM System</i>	89
2.3.4 <i>Calculating the Input/Output Parameters</i>	90
2.4 FAST IS NOT FAST ENOUGH – SPEEDING UP THE METHOD EVEN FURTHER.....	92
2.5 CONCLUSION AND FUTURE DEVELOPMENT	95
3 RESULTS.....	98
3.1 POST-SCATTERING IN CLOSED SIW STRUCTURES.....	98
3.1.1 <i>Waveguide resonator</i>	98
3.1.2 <i>SIW Waveguide Filter</i>	103
3.2 RADIATING STRUCTURES.....	107
3.2.1 <i>Waveguide slot array</i>	108
3.2.2 <i>Two-layer dielectric loaded slot array</i>	110
3.2.3 <i>Five-waveguide slot array</i>	118
3.2.4 <i>Corporate-fed stacked waveguide slot array</i>	125
3.3 CONCLUSION AND FUTURE WORK.....	129
4 REFERENCES.....	132
5 APPENDICES	140

LIST OF TABLES

TABLE 3.1 GEOMETRICAL PARAMETERS OF THE CLOSED RESONATOR SIW STRUCTURE	99
TABLE 3.2 MESH PROPERTIES AND RUNTIMES FOR THE SIW CLOSED RESONATOR.....	100
TABLE 3.3 MESH PROPERTIES AND RUNTIMES FOR THE SIW CLOSED RESONATOR LOADED WITH A LAYERED DIELECTRIC.....	101
TABLE 3.4 GEOMETRICAL PARAMETERS OF THE MULTILAYERED SIW FILTER	103
TABLE 3.5 GEOMETRICAL PARAMETERS OF THE SIW 8-SLOT ARRAY	108
TABLE 3.6 MESH PROPERTIES AND RUNTIMES FOR THE SIW 8-SLOT ARRAY	110
TABLE 3.7 MESH PROPERTIES AND RUNTIMES FOR THE SIW TWO-LAYER SLOT ARRAY.....	112
TABLE 3.8 GEOMETRICAL PARAMETERS OF THE FIVE-WAVEGUIDE SIW SLOT ARRAY	118
TABLE 3.9 SOLUTION DATA FOR THE FIVE-WAVEGUIDE, TWO-LAYER SLOT ARRAY WITH $t = (0.9, 0.1)h$, $\epsilon_r = (2.2, 1)$	120
TABLE 3.10 SOLUTION DATA FOR THE FIVE-WAVEGUIDE, TWO-LAYER SLOT ARRAY WITH $t = (0.5, 0.5)h$, $\epsilon_r = (2.2, 5.5)$	122
TABLE 3.11 UNIT-CELL GEOMETRICAL PARAMETERS OF THE CORPORATE-FED, STACKED WAVEGUIDE ARRAY	126
TABLE 3.12 SOLUTION DATA FOR THE FIVE-WAVEGUIDE, TWO-LAYER CORPORATE-FED SLOT ARRAY	128

LIST OF FIGURES

FIGURE 1.1 MICROSTRIP LINE CROSS-SECTIONAL VIEW, TAKEN FROM [25]	2
FIGURE 1.2 COMMERCIAL W-BAND MIXER (TAKEN FROM MICROWAVES101.COM)	3
FIGURE 1.3 A) WAVEGUIDE LINE PATENTED BY SHIGEKI (TAKEN FROM [2]), B) FIRST ANTENNA IMPLEMENTED IN SIW TECHNOLOGY BY HIROKAWA AND ANDO (1998) (TAKEN FROM [3]).....	4
FIGURE 1.4 A) TE_{01} FIELD DISTRIBUTION OF A RECTANGULAR WAVEGUIDE OVER THE CROSS-SECTION (THE ELECTRIC FIELD IS DEPICTED BY SOLID LINES, THE MAGNETIC FIELD BY DASHED ONES) B) SURFACE CURRENT DISTRIBUTION ON THE NARROW WALL	5
FIGURE 1.5 CIRCULAR-CAVITY SIW FILTER AT 14.6 GHz (TAKEN FROM [27])	6
FIGURE 1.6 TOP VIEW OF A SHORT SECTION OF AN SIW GUIDE	6
FIGURE 1.7 COMPARISON OF THE FREQUENCY DEPENDENCE OF LOSSES BETWEEN SIW AND RWG STRUCTURES (TAKEN FROM [29])	8
FIGURE 1.8 : SIW SLOT ARRAYS; A) PILLBOX SLOT ARRAY AT 77 GHz (TAKEN FROM [32]), B) KA-BAND SIW ROTMAN LENS (TAKEN FROM [33]).....	8
FIGURE 1.9 SIW 16 32 SLOT ARRAY (TAKEN FROM [14]); A) TOP VIEW (SLOT ARRAY), B) BOTTOM VIEW (FEEDING NETWORK)	9
FIGURE 1.10 3-WAVEGUIDE SIW ROTMAN LENS (TAKEN FROM [34]: A) TOP VIEW (ARRAY), B) FEED LAYOUT, C) MOUNTING PLATE AND CONNECTOR LAYOUT	10
FIGURE 1.11 3-D 128-ELEMENT SIW ARRAY (TAKEN FROM [39])	11
FIGURE 1.12 LTCC OVERSIZED RECTANGULAR SLOT ARRAY (TAKEN FROM [30])	12
FIGURE 1.13 THE EFFECT OF AIR-GAP THICKNESS ON THE DIELECTRIC/OVERALL LOSSES IN THE OVERSIZED LTCC GUIDE (TAKEN FROM [30]).....	12
FIGURE 2.1 SCHEMATIC OF A GENERIC SIW DEVICE	19
FIGURE 2.2 APPLICATION OF THE EQUIVALENCE PRINCIPLE	22
FIGURE 2.3 SECTION OF AN INTERIOR SIW REGION.....	24
FIGURE 2.4 THE PRINCIPAL VOLUME GEOMETRY.....	34
FIGURE 2.5 TRANSVERSELY UNBOUNDED, VERTICALLY PARALLEL-PLATE BOUNDED REGION	39
FIGURE 2.6 NETWORK SCHEME FOR THE TM ADMITTANCE GREEN'S FUNCTION CALCULATION	47
FIGURE 2.7 TOPOLOGY OF THE GREEN'S FUNCTION SINGULARITIES IN THE PLANE	48
FIGURE 2.8 NETWORK SCHEME FOR THE TE IMPEDANCE GREEN'S FUNCTION CALCULATION	51
FIGURE 2.9 A PPW FILLED WITH A LONGITUDINALLY STRATIFIED DIELECTRIC	53
FIGURE 2.10 NETWORK SCHEME OF A TM PROBLEM IN A LONGITUDINALLY STRATIFIED, PIECEWISE- CONTINUOUS MEDIUM.....	56
FIGURE 2.11 NETWORK SCHEME OF A TE PROBLEM IN A LONGITUDINALLY STRATIFIED, PIECEWISE- CONTINUOUS MEDIUM.....	58
FIGURE 2.12 A) GEOMETRY OF A TYPICAL SIW POST ; B) TYPICAL POST-SCATTERING PROBLEM	61
FIGURE 2.13 GEOMETRICAL PARAMETERS RELATED TO THE GEGENBAUER ADDITION THEOREM.....	63
FIGURE 2.14 COAXIAL PORT MODEL USED IN THE ANALYSIS	75
FIGURE 2.15 JUNCTION BETWEEN A RECTANGULAR AND AN SIW GUIDE	77
FIGURE 2.16 SLOT COORDINATES AND CHARACTERISTIC LENGTHS; A COLOUR PLOT OF THE FIRST-ORDER BASIS FUNCTION CURRENT DISTRIBUTION..	80

FIGURE 2.17 WAVE INTERACTION IN A MULTI-WAVEGUIDE SIW DEVICE	94
FIGURE 3.1 CLOSED RESONATOR SIW STRUCTURE FED BY COAXIAL PORTS.....	99
FIGURE 3.2 S-PARAMETERS OF THE CLOSED SIW RESONATOR; A) S_{11} , B) S_{21}	99
FIGURE 3.3 S-PARAMETERS OF THE TWO-LAYER DIELECTRIC LOADED SLOT ARRAY: A) MAGNITUDE, B) S_{11} , C) S_{21} PHASE	101
FIGURE 3.4 S-PARAMETERS OF THE SINGLE-LAYER DIELECTRIC LOADED RESONATOR VERSUS THE "ALMOST" SINGLE-LAYER RESONATOR: A) MAGNITUDE; B) PHASE	102
FIGURE 3.5 LAYOUT OF THE SIW MULTILAYERED, THREE-POLE CHEBYSHEV FILTER.....	103
FIGURE 3.6 S-PARAMETERS OF THE MULTILAYERED SIW FILTER WITH $\epsilon_r = (2.2, 3.3)$, $t = (0.5, 0.5) \times h$	104
FIGURE 3.7 S-PARAMETERS OF THE MULTILAYERED SIW FILTER WITH $\epsilon_r = (2.2, 3.3)$, $t = (0.9, 0.1) \times h$	104
FIGURE 3.8 S-PARAMETERS OF THE MULTILAYERED SIW FILTER WITH $\epsilon_r = (2.2, 6.15)$, $t = (0.5, 0.5) \times h$	105
FIGURE 3.9 S-PARAMETERS OF THE MULTILAYERED SIW FILTER WITH $\epsilon_r = (2.2, 6.15)$, $t = (0.8, 0.2) \times h$	106
FIGURE 3.10 S-PARAMETERS OF THE ORIGINAL SIW THREE-POLE CHEBYSHEV FILTER [109]	107
FIGURE 3.11 LAYERED-DIELECTRIC LOADED WAVEGUIDE CROSS-SECTION (NO POSTS SHOWN FOR CLARITY)	108
FIGURE 3.12 SIW 8-SLOT ARRAY; A COAXIAL PORT FEED IS USED	108
FIGURE 3.13 SIW 8-SLOT ARRAY RADIATION PATTERN AT 23.15 GHz; A) $\phi = 0^\circ$ PLANE, B) $\phi = 90^\circ$ PLANE	109
FIGURE 3.14 SIW 8-SLOT ARRAY RADIATION PATTERN AT 25.15 GHz; A) $\phi = 0^\circ$ PLANE, A) $\phi = 90^\circ$ PLANE	109
FIGURE 3.15 S_{11} MAGNITUDE AND PHASE OF THE SINGLE-LAYER DIELECTRIC-LOADED SLOT ARRAY	110
FIGURE 3.16 TWO-LAYER SLOT ARRAY NORMALIZED DIRECTIVITY AT: A) $\phi = [0, 90]^\circ$ PLANES, 21.6 GHz; B) $\phi = [0, 90]^\circ$ PLANES, 22.6 GHz.....	111
FIGURE 3.17 TWO-LAYER SLOT ARRAY WITH $\epsilon_r = (2.2, 1.1)$: A) NORMALIZED DIRECTIVITY IN THE $\phi = 0^\circ$ PLANE, B) NORMALIZED DIRECTIVITY IN THE $\phi = 90^\circ$ PLANE, C) S_{11}	113
FIGURE 3.18 TWO-LAYER SLOT ARRAY WITH $\epsilon_r = (2.2, 5.5)$: A) NORMALIZED DIRECTIVITY IN THE $\phi = 0^\circ$ PLANE, B) NORMALIZED DIRECTIVITY IN THE $\phi = 90^\circ$ PLANE, C) S_{11}	115
FIGURE 3.19 TWO-LAYER SLOT ARRAY WITH $\epsilon_r = (2.2, 8.8)$: A) NORMALIZED RADIATION PATTERN IN THE $\phi = 0^\circ$ PLANE, B) NORMALIZED RADIATION PATTERN IN THE $\phi = 90^\circ$ PLANE, C) S_{11}	116
FIGURE 3.20 FIVE-WAVEGUIDE SIW SLOT ARRAY.....	118

FIGURE 3.21 TWO-LAYER DIELECTRIC, FIVE WAVEGUIDE SLOT ARRAY RADIATION PATTERN AT - A) 24.1 GHz, $\phi = 0^\circ$ PLANE, B) 24.1 GHz, $\phi = 90^\circ$ PLANE, C) 25.1 GHz, $\phi = 0^\circ$ PLANE, D) 25.1 GHz, $\phi = 90^\circ$ PLANE, E) 26.1 GHz, $\phi = 0^\circ$ PLANE, F) 26.1 GHz, $\phi = 90^\circ$ PLANE	119
FIGURE 3.22 RADIATION PATTERNS OF THE FIVE-WAVEGUIDE SLOT ARRAY WITH $t = (0.5, 0.5)h$, $\epsilon_r = (2.2, 5.5)$: A) 25 GHz, B) 26 GHz, C) 27 GHz.....	121
FIGURE 3.23 $\phi = 0^\circ$ PLANE RADIATION PATTERNS OF THE FIVE-WAVEGUIDE SLOT ARRAY IN THE WITH $t = (0.1, 0.9)h$, $\epsilon_r = (2.2, 6.15)$ AT (26, 27) GHz.....	123
FIGURE 3.24 $\phi = 0^\circ$ PLANE RADIATION PATTERNS OF THE FIVE-WAVEGUIDE SLOT ARRAY IN THE WITH $t = (0.9, 0.1)h$, $\epsilon_r = (2.2, 6.15)$ AT (26, 27) GHz.....	123
FIGURE 3.25 REALIZED GAIN CONVERGENCE WITH RESPECT TO THE RADIATION BOX HEIGHT (FOR THE TWO-LAYER, FIVE WAVEGUIDE SLOT ARRAY); A) $\phi = 0^\circ$ PLANE, B) $\phi = 90^\circ$ PLANE.....	124
FIGURE 3.26 CORPORATE-FED SLOT ARRAY LAYOUT: A) EXPLODED VIEW, B) SIDEVIEW SCHEMATIC (TAKEN FROM TEKKOUK ET AL. [34]).....	126
FIGURE 3.27 NORMALIZED DIRECTIVITY OF THE CORPORATE-FED SLOT ARRAY IN THE $\phi = 0^\circ$ PLANE AT A) 14.1 GHz AND B) 15.1 GHz.....	127
FIGURE 3.28 THE NORMALIZED RADIATION PATTERN OF A 5-CELL CORPORATE-FED SLOT ARRAY AT 15.1 GHz, $\phi = 0^\circ$ PLANE.....	129

LIST OF ABBREVIATIONS AND ACRONYMS

SIW – Substrate Integrated Waveguide

PPW – Parallel-Plate Waveguide

MoM – Method of Moments

FEM – Finite Element Method

FDTD – Finite Difference Method

GF – Green’s Function

DGF – Dyadic Green’s Function

SDP – Steepest Descent Path

SIP – Sommerfeld Integration Path

LIST OF APPENDICES

APPENDIX A – DERIVATION OF DUAL TE S-POTENTIALS AND THE REGULARIZATION OF THE GREEN’S DYADIC	141
APPENDIX B – DIELECTRIC-POST SCATTERING IN AN SIW DEVICE	151
APPENDIX C – BIBLIOGRAPHY RELATED TO THE THESIS	160
BIOGRAPHY	162

1 INTRODUCTION

Time and time again, over a wide range of disciplines, it has been proven that ingenuity has its roots in simplicity. Microwave engineering holds no exemption to this fact. The constant demand for higher performance in terms of efficiency, bandwidth and mechanical resilience dictates the use of ever-increasingly complex designs. On the other hand, ease of fabrication with its implicit benefit of low-cost mass production place significant constraints on the overall complexity. However, as it has been demonstrated over and over, if one is in possession of simple enough *building blocks* of a system, both the complexity and ease of fabrication issues can be mitigated at once. A direct example of this is the microstrip technology [24]. By using thin strips of conducting material placed on a conductor backed dielectric slab, one can realize transmission lines, intermediate elements such as phase shifters, cross-overs etc., as well as radiating elements based on radiating patches, enabling one to realize complete transceiver systems in a single technology. Moreover, such systems can be fabricated by conventional means such as the printed-circuit-board technique (PCB), allowing high-precision mass production.

With the shift of microwave technology application to higher frequencies, even as high as the D-band, there is need of a simple, flexible and reliable framework for realizing efficient devices fulfilling diverse tasks. Unfortunately, in this region, conventional technologies suffer from debilitating drawbacks, such as high dielectric losses and difficult fabrication, rendering them inefficient and/or costly. The *substrate integrated waveguide* (SIW) paradigm is a promising candidate capable of overcoming the aforementioned difficulties, which has been gaining momentum over the past two decades, primarily due to its simplicity and flexibility. In this chapter, we discuss its foundations, merits and potential, as well as review the common design and analysis methods applied to it. In Section 1.1 we present a brief overview of the existing planar microwave technologies and basic system requirements encountered in practice nowadays. In Section 1.2 we discuss and review the SIW technology in relation to the aforementioned requirements, comparing it to conventional technologies. Section 1.3 deals with the most common methods of analysis applied to SIW devices, and serves as both a state-of-the-art and motivation for the work exposed in this thesis. Section 1.4 is concerned with the aims of this thesis relating to the analysis and design of novel SIW devices. We conclude this chapter with Section 1.5, in which we outline the structure of this thesis.

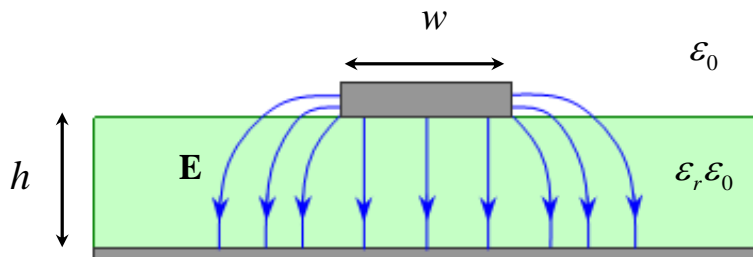
1.1 Planar microwave systems - basics

An overwhelming majority of all microwave systems used today belong to the class of planar systems. This comes as no surprise as they are simpler to implement and fabricate, owing to their relatively simpler geometry. Moreover, common planar fabrication processes such as the printed circuit board (PCB) or low-temperature co-fired ceramics (LTCC) technique allow precise and quick fabrication, making planar microwave systems even more attractive.

A typical microwave system is composed of a number of modules, depending on the purpose, but can generally be divided into a transmitting and a receiving network, though in practice they often overlap. The transmitting part consists of integrated circuits and devices which generate, process and amplify signals to be transmitted, which are then passed to the antenna feeding network. The feeding network consists of a number of passive and active devices, such as filters, amplifiers, cross-overs etc., whose purpose is to further process the signal and distribute it properly to the end module – the antenna system. The antenna system consists of a single antenna or, more commonly, of an array of radiating elements, serving to transmit the signal to a receiver. One notes that it is advantageous to have the ability to implement all the necessary parts using the same or similar technologies and, in the end, to integrate them easily on a single housing. This, indeed, is the most common case in practice, where all the modules are mounted and interconnected on a common wafer/substrate.

The most common microwave technologies are the stripline/microstrip and planar waveguide technology. Microstrip technology relies on the use of planar strips printed on dielectric substrates backed by conducting sheets, which serve as quasi-TEM transmission lines. In Figure 1.1, a schematic of a general microstrip transmission line is shown, along with the electric field lines of the dominant propagating mode.

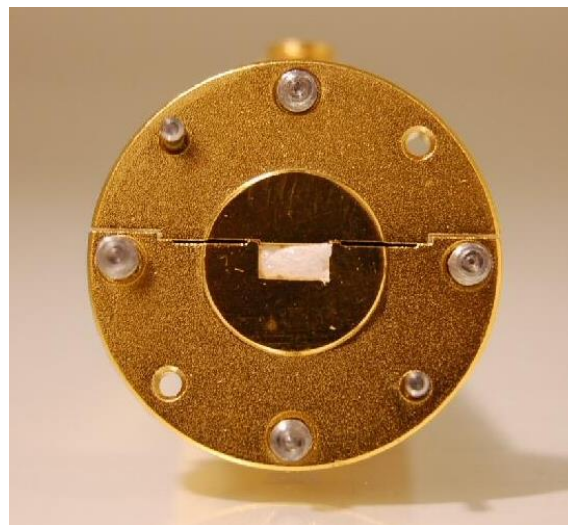
Figure 1.1 Microstrip line cross-sectional view, taken from [25]



The idea is the following – an exciting electromagnetic wave can couple to the structure by inducing oppositely flowing currents on the strip and the backing conductor, respectively. The propagating wave will be present both in the dielectric and air, as can be seen from the field lines, which implies that no TEM mode can exist. Thus, the energy is carried by hybrid waves. However, in practice, the strip is made narrow (smaller than the guiding wavelength), and the substrate thickness and permittivity are chosen so as to a) allow propagation of a single mode, and b) make the wave number transverse to the propagation direction as small as possible (at least an order of magnitude less than in the propagation direction). Thereby, a dominant quasi-TEM mode usually carries the major portion of the energy. However, if the substrate thickness becomes large enough, or a high permittivity substrate is used, surface waves can be induced which may be detrimental to the functioning of the device, e.g. cause cross-talk between lines or increase the sidelobe level of patch arrays. Because of its low profile and diversity in terms of the number of elements that can be realized in it, as well as the possibility of integration with other planar technologies such as planar waveguides, microstrip technology has become commonplace,

whole transceiver systems being realized solely in it. However, at higher frequencies its inadequacies become apparent. Since a low-thickness substrate has to be used, dielectric and conductor losses can be high due to current hotspots. To overcome these drawbacks, one possibility is to use either a parallel-plate or a rectangular waveguide (PPW and RWG from here on, respectively) as the basic building block. The electromagnetic field, now confined by metal plates, will be transferred more efficiently since the geometrical spreading is diminished by the presence of additional/larger scattering boundaries. The trade-off is the relatively more complicated design of common devices such as phase-shifters, matching elements, filters etc. The losses in metal are decreased as well, since the currents now flow on wide plates instead of thin strips. However, rectangular waveguides (RWG) are more common in practice due to superior field confinement. At moderate frequencies, up to approximately 50 GHz, it is relatively simple to fabricate a rectangular waveguide. At higher frequencies, starting from the V-band (50-75 GHz), this poses a challenge since the losses will increase dramatically with any imperfection introduced. For example, as shown in Figure 1.2, junctions of individual parts of the guide have to be carefully designed and leak-proofed so as to assure low losses due to leakage. This particular device, a W-band mixer, is made of two conjoined parts. The junction is right where the dominant TE_{01} mode has a current maximum (see [26] Ch. 8 for mode definition). This is unwise since small contact imperfections may lead to large drops in the power transmitted due to strong current leakage there.

Figure 1.2 Commercial W-band mixer (taken from Microwaves101.com)



Another great problem is how to realize the narrow walls of an RWG if the size is less than a few millimeters. Either the broadwall is bent at the edge or the narrow wall is cut from a sheet of metal and soldered or welded to the broadwall. The first option may require a large compressing force if the sheet being bent is thick and sturdy. Moreover, bending may result in a narrow wall with a curved corner, potentially adversely affecting the propagation inside the waveguide, since the corners may have a radius of curvature comparable to the wavelength. Welding and soldering also become challenging at higher frequencies due to thin layers of metal used and structural irregularities in the form of bumps which are introduced by high-temperature welding probes. In addition, the welding/soldering may change the integrity of the metal at the junction, lowering its conductivity and consequently increasing propagation losses. Hence, high-quality rectangular waveguides are generally difficult and expensive to manufacture. Another drawback of a full-plate narrow wall is that it is difficult to realize walls of general shape, e.g. circular, elliptic etc.

In addition, from the production point of view, microwave devices should be easily integrated into full, self-contained front-end systems. Therefore, modularity and ease of integration are highly prized features. Unfortunately, technologies such as the microstrip paradigm or the coplanar waveguide technology suffer from inherent inter-circuit coupling at higher frequencies, requiring complicated and costly solutions to overcome this drawback.

To summarize, paramount problems of planar device design encountered at higher frequencies are the following:

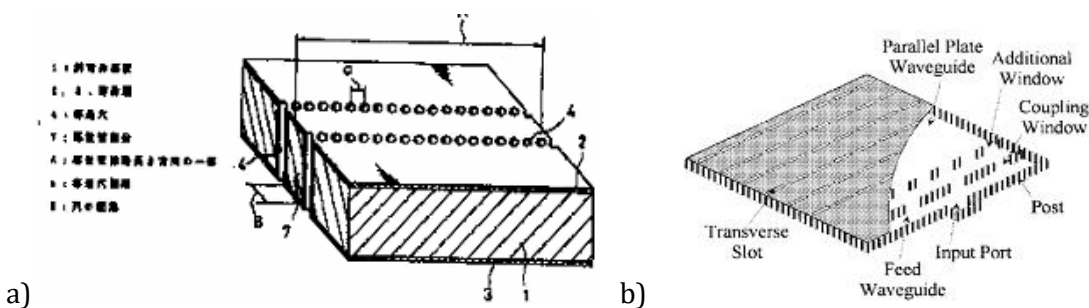
- difficult waveguide construction by conventional fabrication techniques
- conductor and dielectric losses
- sound electrical contacts
- translation of lower-frequency designs and concepts
- integration of different technologies
- complete system-on-substrate design

In the next section we shall review a technology which successfully overcomes these drawbacks.

1.2 Why SIW?

With all the aforementioned issues in mind, a new technology began to take shape over the past two decades, based on a simple realization – since most RWG-based devices operate in the dominant-mode regime which has electric field lines orthogonal to the guiding axis, it is not necessary to use a full-plated narrow wall, but merely one that confines fields of such polarization well; any higher-order mode will leak quickly out of the guide. A narrow wall composed of an array of vertical metal strips or cylinders is the simplest such structure. The earliest use of this concept can be traced back to a patent by Shigeki [2], shown in the following figure, whereas the first antenna fabricated in SIW technology, also shown here, followed in 1998 [3].

Figure 1.3 a) Waveguide line patented by Shigeki (taken from [2]), b) First antenna implemented in SIW technology by Hirokawa and Ando (1998) (taken from [3])

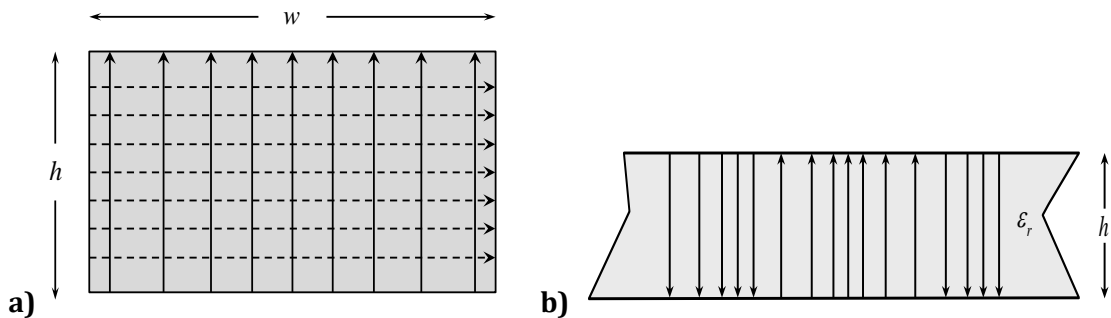


To better illustrate the concept, consider first a conventional rectangular waveguide of width larger than its height and its dominant mode TE_{01} field distribution (Figure 1.4). The electric field of that mode is transverse to the propagation direction, and hence the surface currents supported by the narrow wall are as well, as shown in the same figure. Now, one way to arrive at the concept of substrate integrated waveguide is to ask the question – how much of the narrow wall can one remove and in which manner so that the field inside the

waveguide is the least perturbed (“perturbed” meaning differing from the original field), while still allowing efficient propagation?

First, let us, for example, excise thin rectangular strips along the propagation direction from the narrow wall. This solution leads to a violent interruption of the current flow (see Figure 1.4 below), leading to significant charge accumulation on the slots left after the excision and, consequently, strong radiation. Such an arrangement leads to dramatic leakage, and may be used to create leaky wave antennas, making it a poor guide.

Figure 1.4 a) TE_{01} field distribution of a rectangular waveguide over the cross-section (the electric field is depicted by solid lines, the magnetic field by dashed ones) b) Surface current distribution on the narrow wall



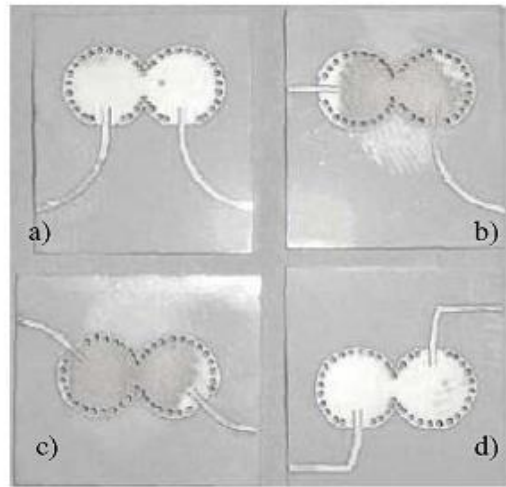
On the other hand, if we were to excise strips in the direction of the current flow, and if the slots are not too wide (i.e. on the order of 0.1λ and less), the dominant mode surface current will not be perturbed dramatically because the currents will meander slightly around each slot, leading to similar propagation characteristics as in the original waveguide, and strong field confinement. The slots may extend from the bottom to the top since the currents are not further disturbed.

However, strips, if too thin, may not be able to support the weight of the upper plate, thus requiring a dielectric slab to do so. It is for this reason metal cylinder arrays have claimed precedence over alternative elements. Namely, if tightly-spaced metal posts of small circumference with respect to the wavelength are placed instead of strip, the field will be strongly confined to the guide, and the size of the posts will not perturb it significantly.

The additional advantage of metal cylinders is the relatively easy fabrication and simple embedding into the guide - vertical holes are drilled in the guide and cylinders are plugged in and soldered to both the bottom and top plate, or electroplated. This technique allows one to integrate the waveguide directly into a substrate; hence the name - *substrate integrated waveguides*. One can easily note that such a procedure grants unprecedented freedom in the construction of sidewalls of arbitrary shape. Devices taking advantage of this newfound freedom are numerous (see e.g. Potelon *et al.* [27], [28]), a fine example of which is shown in the following figure.

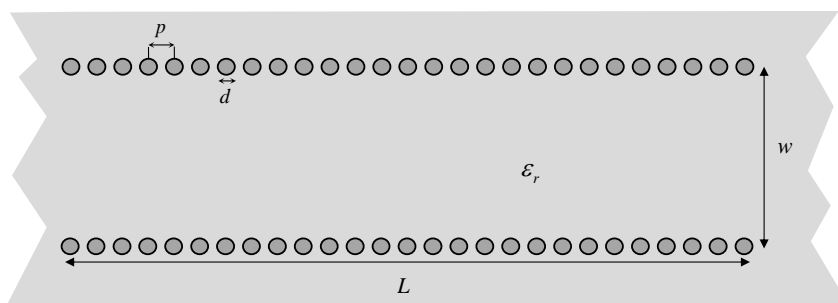
It shows four 14.6 GHz second-order bandpass filters realized by two circular cavities formed by circular fences composed of metal posts and closed from below and above by metal caps, integrated into a planar substrate. They are coupled by capacitive irises and fed by microstrip lines. Such a design would be challenging to realize using other techniques due to problematic integration of a circular wall into the substrate.

Figure 1.5 Circular-cavity SIW filter at 14.6 GHz (taken from [27])



It is obvious that with this flexibility, it is possible to easily merge different geometries, and create devices harvesting their best features. As can be noted, the diversity of SIW-type devices is grand, a generic such device being quite complex from the analysis point of view. Therefore, some simple empiric formulas for leakage loss and the equivalent width of post-based SIW guides, along with simple design guidelines have been found by a number of authors to aid the design. Here we mention the most commonly used ones. An SIW guide, shown in Figure 1.6, will behave as a conventional RWG if the ratio of the distance between two consecutive posts (period) is in the range $0.22\lambda_g < p < 0.29\lambda_g$, λ_g being the wavelength in the dielectric slab the guide is loaded with. Otherwise, a bandgap in the operating frequency range may occur, since an SIW linear guide is a quasi-periodic structure. In addition, the post diameter should be chosen as $0.11\lambda_g < d < 0.14\lambda_g$. The reason for these peculiar numbers is the following – if a post is too thin, the structure becomes mechanically fragile. On the other hand, having posts too thick leads to a dispersion characteristic which might possess a bandgap, and the fields may be appreciably distorted near the posts. Therefore, there inherently exists a trade-off between structural integrity and dispersion characteristics. The last criterion an SIW should satisfy concerns the height of the waveguide – namely, it should be kept between $0.3\lambda_g < h < 0.5\lambda_g$. If it is too large, higher-order modes readily propagate, and if the height is too small, the current density on bounding plates becomes high enough to cause severe conductor losses.

Figure 1.6 Top view of a short section of an SIW guide



If these design rules are adhered to, the equivalent guide width, representing the width of a rectangular guide having equivalent dispersion characteristics, can be well-approximated by [9]

$$w_{eq} = w - 1.08 \frac{d^2}{p} + 0.1 \frac{d^2}{w} , \quad (1.1)$$

where w denotes the distance between post fences, measured between the lines connecting centres of respective posts in each fence, and d being the diameter of a post. The above approximation holds well if $p/d < 3$ and $d/w < 0.2$. It should be stressed these approximations hold for SIW guides mimicking conventional rectangular guides. If the geometry is more complex, more refined numerical methods are necessary to characterise the propagation. These will be discussed in the following section.

The leakage is another crucial issue of an SIW device. Since the post-fence effectively behaves like a thin-wire polarizer, it is intuitively clear that the field becomes less confined with increasing inter-post distances. Different authors use different conventions, but the inter-post distance is typically kept below $0.1\lambda_g$ in most practical designs, guaranteeing leakage losses lower than 10^{-3} Np/rad .

The frequency and geometry dependence of dielectric and conductor losses, on the other hand, are inherited from the rectangular guide ([29], Figure 1.7). As concerns the dielectric losses, they can be mitigated exclusively by a judicious choice of substrate, which can be either monolithic, or tailored (see e.g. [30]). The reason is that dielectric losses are related to the electric field spatial power density $|\mathbf{E}|^2$, the volume of the dielectric in question, and its material loss tangent. In more detail, the dielectric losses, for most materials used in microwave devices, can be attributed to the dipole relaxation mechanism, which can be phenomenologically incorporated as the imaginary part of the dielectric constant. Then it can be shown (see e.g. [31, p. 267]) that the time-averaged heating rate of a material sample of volume V due to the monochromatic field \mathbf{E} of frequency ω can be expressed as

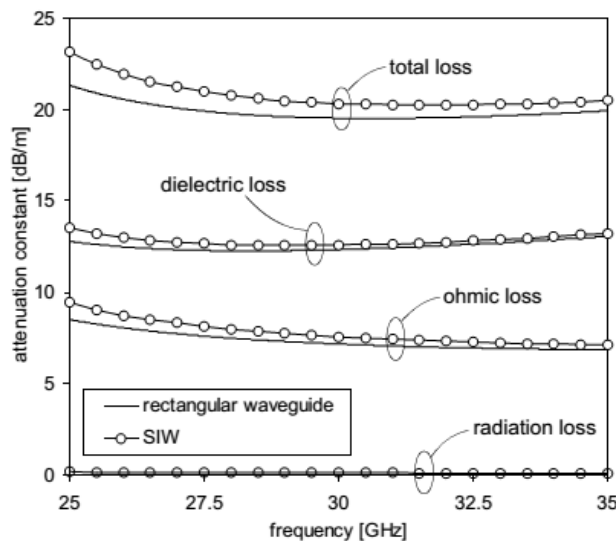
$$Q = \frac{1}{2} \int_V \omega \varepsilon'' |\mathbf{E}(\mathbf{r})|^2 d\mathbf{r} , \quad (1.2)$$

from which it is evident that, given a material with losses described by ε'' , the only way to decrease losses is to either decrease the average power density of the electric field, or to reduce the volume of the sample. Now, in order to lower the average power density of the electric field, one can try, for example, to increase the height of the waveguide (we denote the height increment by Δh) along with the height of the dielectric, resulting in a larger geometrical spreading of the field, lowering the power density by a factor of $1/\Delta h$. On the other hand, the volume of the substrate increases linearly with Δh , provided the remaining dimensions are kept the same. This results in exactly the same losses as before the height increase due to mutual compensation of said effects. Therefore, only the reduction in the loss tangent will reduce the losses. This is accomplished by either choosing a monolithic material slab of lower loss tangent, or tailoring the dielectric in such a way as to decrease the field density in the overall dielectric volume.

Similar arguments show that conductor losses remain the same upon increasing the height – current density is lowered by the same factor the conducting material necessary to increase the height is increased. Hence, lowering the conductor losses can be accomplished by using a high-conductivity metal such as gold, copper or aluminium, or by “steering” the field away from metal boundaries by confining it more to a dielectric medium, though one

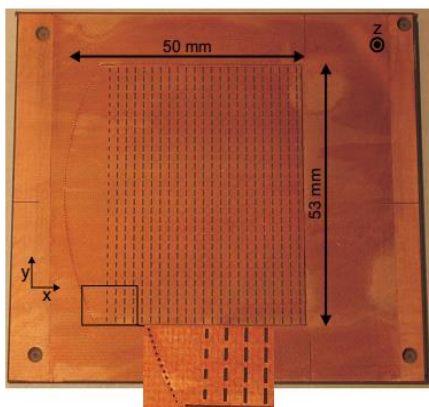
must be careful if a lossy dielectric is used. A graph is shown in the following figure, depicting the comparison of frequency dependences of losses between an SIW guide and an equivalent rectangular waveguide over the [25, 35] GHz range; it can be readily observed that the dielectric losses dominate over the conductor and radiation leakage losses, and the losses are comparable between the guides, following similar trends. Now, if one is inclined to design a radiating device using the SIW paradigm, virtually all the standard methods pertaining to RWG- and PPW-based antennas are available. However, slot arrays (see Figure 1.8) are the most common among the many radiating devices due to the ease of fabrication by etching slots on metal planes, simple control of the radiation pattern and good matching capabilities of slots. In addition, such arrays can be implemented at high frequencies in free bands, such as the Ka-band, finding application in sensing and detection (e.g. in automotive radar systems).

Figure 1.7 Comparison of the frequency dependence of losses between SIW and RWG structures (taken from [29])

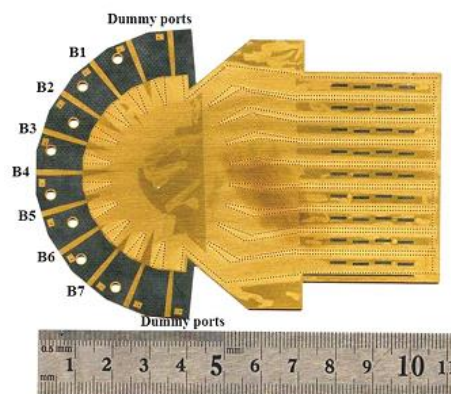


With the migration of mobile communication to higher frequencies, as is envisioned e.g. in the 5G standard, SIW technology may become commonplace as highly-directive arrays with good scanning capabilities can be easily realized in it, at a relatively low cost. As an example of an SIW array, Figure 1.8 a) shows a prototype pillbox slot array at 77 GHz, intended for use as part of an automobile radar system.

Figure 1.8 : SIW slot arrays; a) pillbox slot array at 77 GHz (taken from [32]), b) Ka-band SIW Rotman Lens (taken from [33])



a)

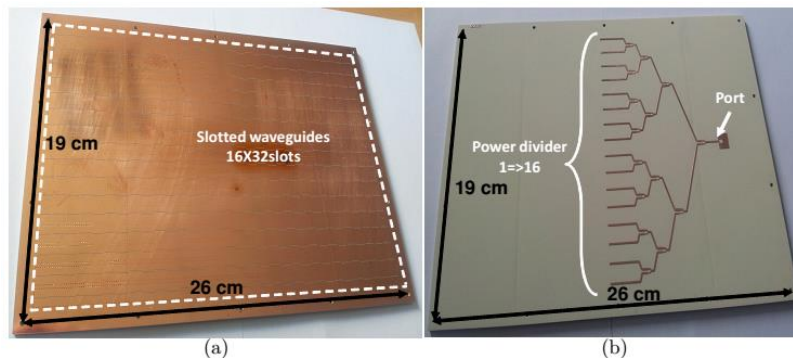


b)

It consists of two PPW guides connected by coupling slots etched in the intermediate plate. A parabolic post-fence at the far end of the feeding PPW guide, running from the lowermost to the uppermost plate reflects the spill-over power back to coupling slots and tailors the wavefront of the wave illuminating the slot array at the uppermost plate. The whole system has a surface of 50 mm × 53 mm and is only 1 mm thick. The half-power beamwidths in the E- and H-plane are 11.5 and 5.5 degrees, respectively, while the overall efficiency is larger than 50%. The set-up was fabricated in PCB technology at a smaller cost than would be if alternative technologies were employed. From this example, it is clear that the SIW paradigm allows straightforward scaling of well-known concepts to higher frequencies, while maintaining simplicity of fabrication and decent efficiency. Figure 1.8 b) [33] shows another fine example of the vast possibilities in design inherent to SIW technology. It is a Rotman lens, operating at 28.5 GHz consisting of 9 stripline-to-SIW-guide transitions, launching a field tailored by both exciting different combinations of ports as well as tuning the SIW-guide widths. This field then feeds a 9-waveguide slot array which, in turn, radiates into free-space. The authors have shown that firing different port combinations at a time allows relatively simple beam-steering with the additional bonus of narrow beams (≤ 22 degrees of -3 dB beam-width) and good matching (-15 dB at the operating frequency).

A more recent example, shown in the following figure, is a variant of the slot array designed for 14.25 GHz [34].

Figure 1.9 SIW 16 32 slot array (taken from [14]); a) top view (slot array), b) bottom view (feeding network)

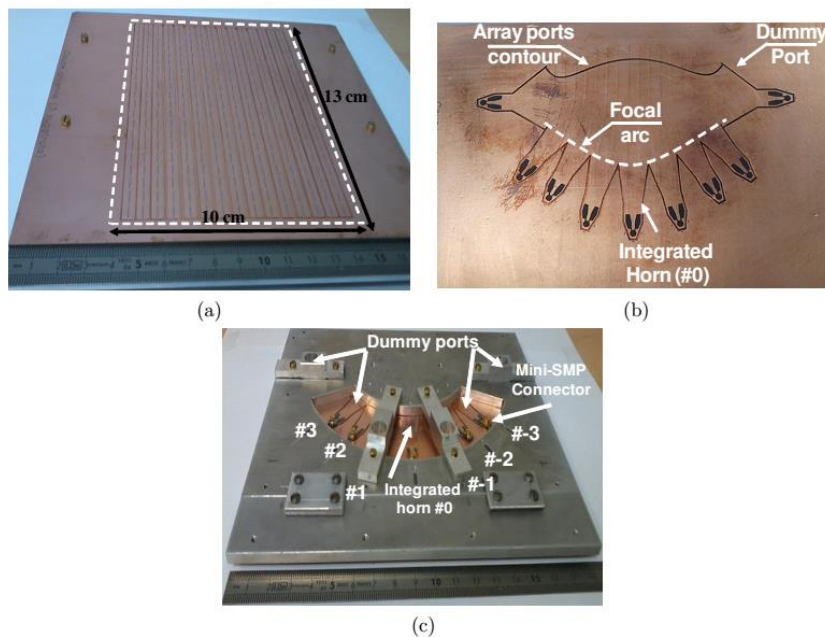


It consists of two stacked larger 26 cm × 19 cm ($12.35\lambda_0 \times 9.03\lambda_0$ at the operating frequency) waveguides. The bottom guide is partitioned into 16 smaller waveguides by metal post fences. It is fed by a 1/16 stripline-type power divider, delivering power to each subguide, exactly at the centre where a coupling slot is located. Each subguide has two coupling slots located at its top plate (the lower plate of the upper subguide) at approximately $0.25L_{subguide}$ and $0.75L_{subguide}$. The power is then transferred to each upper subguide which are, in turn, split further into two smaller subguides by a transverse post fence located in the middle of the larger subguide; each has 16 radiating slots etched in its top plate. Hence, the power delivered from the lower subguide is passed on at the centre of each of these smaller subguides in order to reduce the long-line effect, i.e. to create a corporate-fed array. This greatly enhances the operating band, since the phase error is reduced roughly fourfold, thus stabilizing the radiation pattern – the pointing angle is almost fixed at 0.5 degrees in the E-plane, whereas it is 0.25 in the H-plane over the [14, 14.5] GHz band. In addition, the gain is 24.11 dB at the central frequency. It should be noted that the device is efficiently fed by a stripline, owing up to relatively good matching of the

stripline-to-guide transition. This demonstrates the simple merging of disparate technologies, allowing the design of interesting hybrid devices.

Yet another example of the complexity achievable with SIW techniques, is the 3-waveguide SIW Rotman lens at 24.15 GHz [34], shown in Figure 1.10. It consists of three stacked guides of identical dimensions. The bottom one contains a lens-type feed akin to the one in [33] – seven SIW horns are each excited by an SMP connectors, while two dummy ports serve to absorb the backscattered energy. Each horn can be fired separately, allowing one to tailor the feeding field, which is coupled to a set of 15 separate phase shifters in the intermediate guide by novel star-shaped slots. This transition has a larger-than 70 % efficiency for all horn excitations aside from the extremal one (#3 in Figure 1.10 b)). The coupled field is then passed through phase shifters further tailoring the feeding field. The energy is then forwarded to the upper waveguide, comprised of 15 SIW waveguides, each harbouring 20 radiating slots in its upper plate. This transfer occurs at the middle of the radiating guide in order to reduce the phase error and, consequently, broaden the operating band. This particular design is endowed with excellent steering capabilities, good matching and low side-lobe levels, thus showing the power lying in design flexibility of SIW devices.

Figure 1.10 3-waveguide SIW Rotman lens (taken from [34]: a) top view (array), b) feed layout, c) mounting plate and connector layout



The greatest feature of SIW technology is the possibility of realizing complete systems on a single substrate. Since its advent, a plethora of devices have been realized in it, ranging from filters (see e.g. [4]), directional couplers [5], circulators [6], magic T-junctions, planar diplexers etc. In addition, a number of active devices have been implemented as well, such as feedback oscillators [7], Gunn diode oscillators, single-transistor power amplifiers and mixers. Hence, all the ingredients necessary to realize system-on-substrate devices are available. In fact, one of the current research trends in the field is geared towards the realization of self-contained systems on a single substrate [8], since SIW structures can be made to have considerably lower losses and inter-circuit coupling than the alternative technologies such as the coplanar and microstrip waveguides.

In addition, as already mentioned, novel concepts and merging different planar technologies become readily available when using the SIW paradigm. For example, a compact half-SIW half-shielded stripline structure for measuring permittivity in the 0.5 to 20 GHz range was

designed by Bang *et al.* [35]. In 2014, a bandpass SIW filter at 140 GHz with decent insertion loss of 1.9 dB was realized in LTCC technology by Wong *et al.* [36] as well. A very interesting concept was proposed by Bozzi *et al.* [37] which revolves around ink-jet printing SIW structures onto a paper substrate, paving the way to a more eco-friendly microwave component production.

Fine examples of devices integrating most of the aforementioned qualities can be found in [38], where several novel concepts are summarized, such as the so-called “LEGO” approach to building devices, exemplified by the 3-D 128 element SIW array (shown in the following figure).

Figure 1.11 3-D 128-element SIW array (taken from [39])

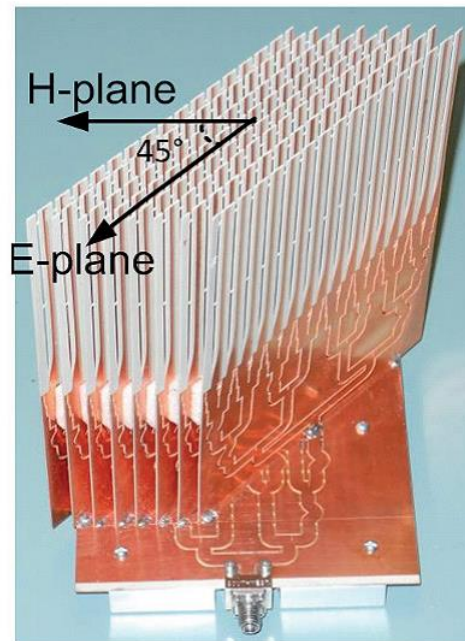


Figure 1.11 shows an 8x16 slot array, composed of a horizontal feeder in the form of an SIW guide with a 1:8 power divider, each branch delivering power to its respective SIW array placed vertically onto the feeding guide, but rotated at 45 degrees with respect to its longitudinal direction. This is done since this geometrical arrangement makes it possible to reduce the phase difference between feeding branches. Now, each radiating guide has an in-built 1:16 power divider, providing excitation to each of the 16 tapered-slot arrays; these comprise two longer longitudinal slots tailored to radiate end-fire. The LEGO approach is apparent in the assembly of the whole array – the modules used (the feeding guide and radiating ones) are fabricated independently and connected in a simple fashion, by fixing the radiating modules vertically to and soldering them onto the feeding guide directly. This provides a powerful framework due to its flexibility and the simplicity of both conception and fabrication.

An interesting concept is the introduction of tailored dielectrics into rectangular/SIW high-frequency guides to reduce the losses, an example of which is shown in the following figure. In this case, an air gap was introduced into an LTCC substrate integrated waveguide, feeding a slot array, to reduce the dielectric losses crippling the efficiency of a device at the frequency of operation (60 GHz). In essence, the presence of an air gap has the effect of redistributing the field in such a way as to lower its intensity in the volume occupied by the pertinent dielectric.

Since dielectric losses are related to the electric field density in the dielectric volume as (1.2), within the operating frequency band, it follows that the losses will be lowered; the effect of the air-gap thickness on the overall losses is shown in the following figure.

Figure 1.12 LTCC oversized rectangular slot array (taken from [30])

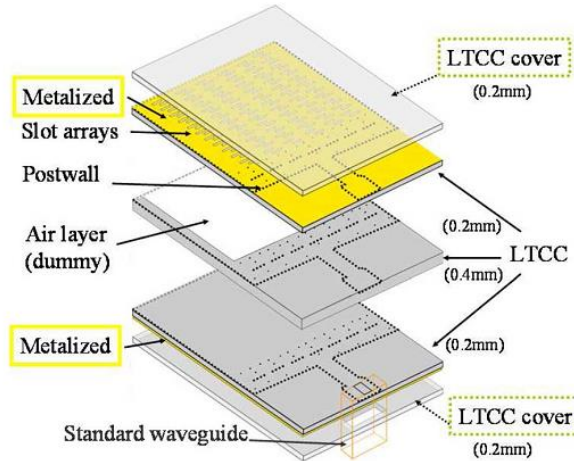
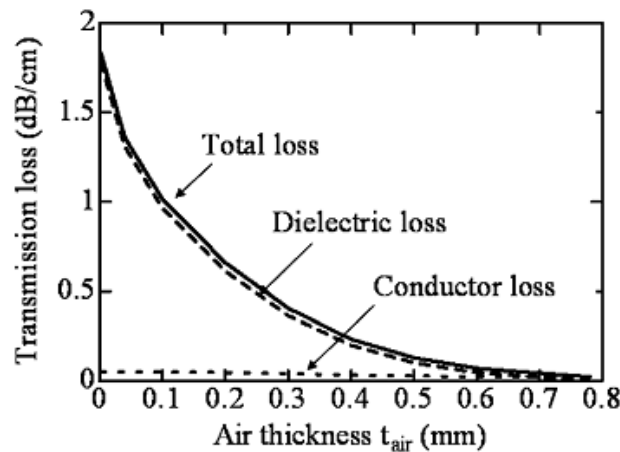


Figure 1.13 The effect of air-gap thickness on the dielectric/overall losses in the oversized LTCC guide (taken from [30])



Though the methodology of lowering the losses in this particular example can be equally applied to both rectangular and SIW guides, since it is much easier to fabricate SIW guides at higher frequencies it presents a potentially widespread framework for designing low-loss devices.

In sum, the SIW paradigm provides a simple and flexible framework for designing microwave/mm-wave devices, relying on embedding posts into suitable planar substrates to create waveguides. Since the posts can be arbitrarily arranged, devices having exotic shapes, previously infeasible to realize, can be fabricated, while maintaining the high-Q factor and losses akin to conventional rectangular waveguides. Hence, it overcomes the limitations of standard waveguides in terms of scalability to higher frequencies, and lends itself to low-cost mass production. Moreover, this technology is easily integrated with existing planar technologies such as the coplanar or microstrip guides. In addition, a large number of active and passive devices have already been designed and experimentally verified over the years, allowing one to create entire systems on a single substrate. As the transition to ever higher bands due to clutter becomes increasingly necessary, technologies

enabling simple transfer of well-established concepts from the microwave range will become dominant. A very likely candidate for the throne is the SIW technology.

1.3 Too many posts in the waveguide – the analysis of SIW-type devices

If one considers a typical SIW device for a moment, be it a simple waveguide section or a front-end system, it can be readily observed that it can be quite complex, comprising a large number of posts, slots, active devices and circuits, arranged in a complicated fashion. Hence, even a simple structure such as a rectilinear SIW-type waveguide presents a challenge in terms of detailed analysis. As mentioned in the previous subsection, a number of simple design rules and constraints have been devised over the years, extracted from experimental data and numerical data obtained from commercial electromagnetic solvers. As useful as they are in the first design, they fall short of taking into account all the complicated effects of interaction in such a device. Hence, at best these “rules” and simple formulas work in a narrow frequency and geometry-parameter range. It is then necessary to introduce more refined analysis tools to characterize the behaviour of SIW-type devices more completely. Indeed, quite a number of diverse methods have been devised to analyze SIW-type geometries. These fall into roughly two categories: approximate-analytic methods, relying on rough approximations of general integral or differential problems, often simplified by some special symmetries (such as periodicity or mirror symmetry) or neglect of higher-order effects, or based on parameters obtained empirically and usually fitted according to some interpolation scheme; the full-wave methods, on the other hand, accounting fully for complicated effects of scattering, based on either finite-difference/finite-element methods or the method of moments. Of course, hybrid methods merging several approaches are common as well. Here we briefly review several methods successfully employed to analyze SIW guides. This is by no means an exhaustive overview, but rather a bird’s-eye one with emphasis on methods either relating to the method presented in this thesis, or most commonly applied.

- Xu *et al.* [10] use a finite-difference frequency-domain (FDFD) algorithm to analyze rectilinear SIW sections, based on the imposition of periodicity in the z direction. In the x and y direction, perfectly-matching layers are set to truncate the problem domain laterally. Then the finite-difference scheme is rephrased as an eigenvalue problem from which the complex propagation constants are finally extracted, which are found to be in good agreement with the ones calculated with HFSS. The authors claim the method is applicable to arbitrary open periodic guiding sections, though the exemplary devices are exclusively rectilinear SIW sections.
- Hirokawa and Ando [12] represent metal posts by a small number of axially directed, uniform electric currents flowing on post surfaces. The authors formulate a method of moments problem with the aid of an accelerated Green’s function, the solution of which gives the propagation constant of the SIW. The method is inherently restricted to devices comprising metal posts of diameter sufficiently smaller than the dominant wavelength, for only uniform currents, having negligible variation around the diameter, to exist. This excludes, for example, 90-degree bends based on electrically larger metal posts. In addition, no device containing dielectric posts of any kind can be analyzed.
- Cassivi *et al.* [11] apply the Floquet theorem in conjunction with the boundary-integral resonant-mode expansion to calculate the generalized admittance matrix of an infinite array of SIW guide sections. The propagation constants are then extracted as the eigenvalues of the system matrix. Then the guide equivalent width

formula is fitted by a least square method. The guide sections analyzed should confine the field strongly, since the method relies on enclosure of the structure by metal walls. A major drawback of this method is its inability to analyze radiating structures and ones containing dielectric posts.

- Deslandes and Wu [9] calculate the propagation constant of an SIW guide from the reflection coefficient of a plane wave scattering off a side-wall. It is obtained by the transverse resonance technique, which relies on the knowledge of the side-wall surface impedance, obtained by the authors from an MoM procedure.
- Though not strictly related to SIW modeling, Elsherbeni and Kishk [40] formulate a multiple-scattering method for the analysis of plane-wave scattering off of axial-translation invariant dielectric and/or metal cylinders. By expanding the fields as sums of cylindrical-azimuthal modes, and applying the Gegenbauer addition theorem, through which they are able to express the total field centered in the coordinate system of a particular cylinder, the authors write down a system of coupled boundary conditions. These lead to infinite linear systems, which are truncated and solved for scattering coefficients. The method of SIW analysis presented in this thesis partially relates to this one.
- Tsang *et al.* [41] consider the problem of scattering off of metal posts in parallel-plate waveguides, specifically applied to the signal integrity analysis in high-speed electronic circuits. Firstly, the dyadic Green's function is derived in terms of the cylindrical-azimuthal vector eigenfunction expansion. The fields scattered off the posts are modeled using the same vector eigenfunctions the Green's function is expanded in, allowing simple application of boundary conditions on posts using the Gegenbauer addition theorem for cylindrical harmonics. The enforcement of boundary conditions leads to infinite linear systems which are truncated and solved, giving the scattering amplitudes of posts. The excitations considered are restricted to magnetic currents modeling the through-hole signals, and the analysis is restricted to shielded guides in dominant-mode operation, but was extended to the case of stacked-guide configurations by Chen *et al.* [42]. This particular method is used as a starting point of the method presented in this thesis.
- Wu and Kishk [13] extend the method of Elsherbeni and Kishk (1992) to scattering off of cylinders embedded in parallel-plate waveguides. By using the cylindrical eigenfunction expansion, they formulate an infinite linear system relating the incident and the scattered field amplitudes, which they truncate and solve. The problems considered do not have any variation normal to the metal plates and the method applies to closed structures. Waveguide ports are used as excitations and modeled through discretization by small sections over which the current is assumed to be uniform. An especially appealing feature of the approach is its applicability to sufficiently laterally closed structures harboring PEC, finite-conductivity or dielectric posts, in almost arbitrary arrangements. The drawback is the inability to include the effect of higher-order modes having variation in the axial direction (of cylinders); fortunately, one can turn a blind eye to this feature since in practice one almost exclusively encounters devices which support the propagation of only the lowest-order modes.
- Wu and Tsang [43] extend the analysis of Tsang *et al.* (2001) to the case of PPWs loaded with two-layer planar dielectrics. The authors approximate the effect of higher-order modes, and do not consider the presence of a general multilayered dielectric.
- Coenen [14] uses an approach based on integral equations similar to the one of Tsang. By expanding the field in terms of a radial transmission line representation, and considering solely modes having no variation across the height of the SIW guide, he is able to formulate linear systems in scattering amplitudes. Though efficient and

conceptually simple and familiar, no higher order modes are considered, as well as the radiation from apertures in metal plates. The method is successfully applied to characterization of propagation in SIW guides and to design of several waveguide components.

- Arnieri and Amendola [15], [16] use an approach similar to Tsang *et al.* to analyze post-scattering in general single-waveguide SIW devices, coupling it to an MoM procedure which takes into account the possible presence of rectangular slots. Coaxial and waveguide ports are used as excitations. The method presented in this thesis is conceptually similar to this approach.
- Diaz Caballero *et al.* [44] use an approach in the vein of Coenen and Tsang, again using the radial line representation to describe the field in an SIW guide. As Coenen, the problems the authors consider are 2D and closed. The only excitation modeled is the waveguide port. The method is formulated in such a fashion that projection integrals, which need to be performed to obtain post-scattering amplitudes, can be obtained either in an approximate analytic way or upon application of the fast Fourier transform. This renders the approach extremely efficient, even more than competing fast methods of SIW analysis, such as the one presented in [13]. As already stated, the analysis is restricted to closed structures, both laterally (by means of tight post fences) and longitudinally (by enclosing metal plates).

1.4 Aims of the thesis

With the increasing use of SIW technology, and a general lack of fast and accurate full-wave solvers suited to the analysis of a wide span of SIW devices in mind, the following objectives were formulated:

- to devise and implement a numerical method of analysis which could handle a large variety of SIW devices with high accuracy and relatively low computational resources (compared to standard commercial solvers), including scenarios involving planarly layered dielectric media in PPWs. The latter, as elaborated later in the text, should be included in order to assess the leakage loss, especially at higher frequencies, of burgeoning SIW devices loaded with layered dielectrics.
- to explore general characteristics of SIW devices using the devised analysis based on modal properties of fields.

The first objective emerged out of the unavailability of reliable software tools at the time of the conception of this thesis. Though some methods had been devised, they were not complete in the sense that they could not be applied to a wide variety of geometries, either due to restrictions coming from the approximate character of the analysis method, or computational inefficiency due to too large a number of unknowns to be solved for.

The second objective crystallized during the actual work on the thesis as a byproduct of the particular mathematical framework adopted. Namely, it was concluded that a particular modal field synthesis, described later on, would give the fastest-converging algorithm. This modal decomposition allows the resolution of the total field into several wave-species, such as the free-space waves, PPW waves, post-scattered waves etc. This allows one to identify which scattering processes contribute most significantly to the overall field and, consequently, devise rule-of-thumb guidelines for the design of devices. Additionally, it led to the improvement of the algorithm efficiency through approximations based on disregarding negligible wave interactions.

1.5 What lies ahead - thesis outline

To facilitate navigation through this work, and make its structure more transparent, here we expose its skeleton. We start the following chapter with section 2.1, containing the discussion on the types of structures we intend to analyze, along with some simplifying assumptions and restrictions. Then we venture into the analysis, considering the most general problem – a series of stacked SIW guides coupled by rectangular slots. We show how the equivalence principle enables one to simplify the problem by partitioning it into sub-problems. Section 2.2 then delves into the specifics of modeling what we refer to as the *interior* and the *exterior* problem – scattering inside an SIW guide, and radiation into a half-space, respectively. The interior problem relies on an efficient mathematical representation of fields, both the incident due to impressed sources and the post-scattered ones. We define the problem, and discuss the possible attacks on it in the form of various electromagnetic potential formulations. Then we proceed to the formulation used, deriving the necessary Green’s functions, both for single and multi-layer dielectric loaded PPWs. Here the central results of the thesis concerning the analytical part are presented, and are a) the derivation of the general-form dyadic Green’s functions in stratified-media loaded PPWs, b) the derivation of scalar potential functions involved in a) for a PPW with an arbitrary number of layers, c) the clarification of mathematical and numerical issues related to b), previously uncovered or wrongly circumvented in the existing literature, and d) the demonstration of superiority over commonly used approaches to a). Then the following subsection deals with scattering off of metal and dielectric posts in PPWs. It is shown how one can arrive to the scattered field representation from the dyadic Green’s function by way of the Gegenbauer addition theorem. The formulation of linear systems in scattering amplitudes through application of boundary conditions is demonstrated. The approximations involved, and empirical criteria for choosing the “optimal” number of electromagnetic modes are presented. The subsection after is concerned with the modeling of standard excitations in SIW devices. Namely, it is shown how the coaxial and waveguide port can be modeled and how their S and Y parameters can be computed using already calculated quantities. After that, a short subsection is devoted to the exterior problem, pertaining to half-space radiation.

With all the ingredients necessary to analyze closed SIW structures, in section 2.3 we tackle the problem of SIW devices containing narrow rectangular slots. We build upon the premise laid out in section 2.1, demonstrating how one can reconcile the presence of both circular-cylindrical posts and slots to formulate the generalized electromagnetic problem, and solve in the most straight-forward and convenient way. The latter, of course, is intimately tied to the efficiency of the method, and is especially emphasized. We show generalized expressions for *direct* slot admittances in arbitrarily stratified dielectric-loaded PPWs (“direct” meaning “without the presence of other scatterers”), encountered in the MoM problem, and suggest strategies for the computation thereof. In addition, we show how to compute *total* slot admittances using quantities already computed in the mode-matching analysis. Then, in section 2.4, we show how to improve the efficiency of the method by various techniques aiming to either a) reduce the number of modes used for the description of the electromagnetic field, thus reducing the size of linear systems arising from boundary conditions, b) to reduce the number of computations involved in evaluation of integrals occurring in the mode-matching or MoM analysis. It is demonstrated that such strategies may be easily applied, leading to significant reduction in computation time and CPU/RAM load. To conclude chapter 2, we reiterate the key concepts of our method and emphasize its advantages over the alternative approaches proposed in the literature. In addition, we

suggest further extensions and improvements of the method, some of which have already been completed during the writing of this thesis.

Chapter 3 serves to demonstrate the performance and limitations of our method through a series of numerical tests of varying complexity. Several SIW devices are simulated using an in-house MATLAB code based on the method, and the standard industry “weapon of choice” FEM solver HFSS by Ansoft. The results are compared in terms computation time and CPU/RAM load.

1.6 A note on notation, units and all that

Dear reader, I wish to impose on you the fact that though I have decided to make my life miserable by choosing this rather mathematical topic, I still have not arrived at the point where I would deliberately try to drag you down with me to the pits of notational hell, decorated with a schizophrenic unit system changing convention page to page. To prevent (or at the very least, combat) such sadism, this section sets and clarifies the choices made pertaining the common notation and units.

First of all, as is common in modern literature concerning applied electromagnetics, the unit system used throughout is, without exception, the SI system. As for the notation, we more or less follow the standard mathematical notation used in the majority of relevant literature. Scalar quantities are denoted by standard letters, whereas vectors are denoted by bold-type letters (e.g. the electric field is denoted by \mathbf{E}). On the other hand, dyadics (i.e. matrices or tensors of arbitrary rank) are denoted by underscored capital bold-type letters, e.g. the Green’s dyadic is denoted as $\underline{\mathbf{G}}$. The explicit components of a dyadic, however, are denoted in a different manner with respect to the standard electromagnetic convention. For example, the element G_{33} of the Green’s dyad is denoted as $\hat{\mathbf{z}} \otimes \hat{\mathbf{z}}$, where \otimes is the symbol of the *outer product*, instead of $\hat{\mathbf{z}}\hat{\mathbf{z}}$ as would be the case in standard literature. We opted for the former since it explicitly distinguishes between matrix elements and scalar products, thereby avoiding potential confusion.

2 HYBRID MODE-MATCHING/ MOM FOR SIW DEVICES

As demands on the performance of SIW devices increase, so does their electrical size and complexity. Unfortunately, as is always the case, their analysis and design complicate concurrently and considerably. Although one may still be able to use commercial tools for these purposes, their inherent approach to problem domain discretization may render them useless even on high-end configurations if the electrical size or the number of elements is large enough. Therefore, in the past decade, large effort has been put in devising methods of analysis and design, which would alleviate the aforementioned issues, partly at the very least. In this chapter, we describe one such method, capable of analyzing large and complex SIW geometries with great accuracy and significant time saving anywhere from one to two orders of magnitude, compared to standard EM CAD tools. Moreover, it even renders possible the analysis of devices too complex to be handled by commercial solvers. Its efficiency stems from merging the mode-matching technique, suitable to the analysis of scattering off cylindrical posts ever present in SIW devices, with the method of moments, suited to the task of accurately analyzing the effects of slot presence.

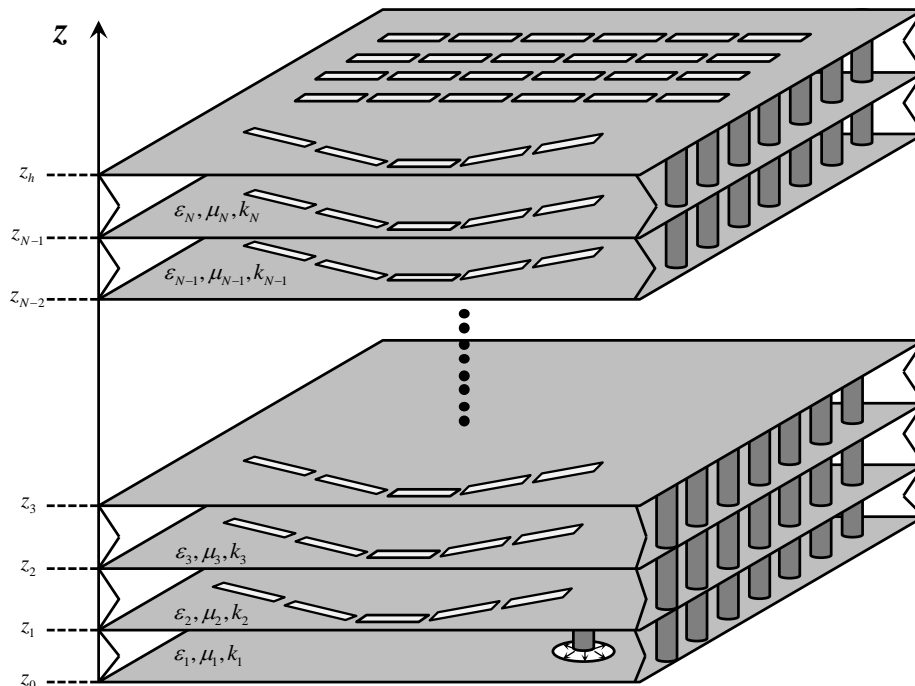
We describe the intricacies behind it in detail, following the approach presented in Casaletti *et al.* [45], [46], the exposition being as follows: in Section 2.1 we describe the general problem setup and its idiosyncrasies, which we exploit to construct an efficient mathematical model. In addition, we discuss how the problem of calculating the EM field in planar SIW devices can be simplified through the application of the equivalence principle in conjunction with the scattering superposition principle. In Section 2.2 we focus on the mathematical representation of fields radiated by sources, relying on the derivation of the PPW Green's function, both for PPWs loaded with a single dielectric and for the more general case of longitudinally stratified media. Moreover, the modelling of typical sources (coaxial cables, waveguide ports and slots) and fields scattered by posts, both PEC and dielectric, will be discussed in detail. Having collected all the necessary ingredients of the analysis, we delve into the application of derived principles to generic SIW devices in Section 2.3., which will touch upon the subject of modelling narrow slots etched in conducting plates of an SIW, with emphasis on the formulation of a method of moments problem, along with a discussion of approximate methods used for fast calculation of admittance matrix elements. Our focus is on the derivation of linear systems of scattering coefficients and the approximate methods of solution, both from a mathematical and computational perspective. In addition, we discuss the criteria according to which we choose the sufficient number of basis functions guaranteeing desired accuracy. Moreover, we show how to extend the analysis to the case of an arbitrary number of waveguides stacked on top of each other, coupled by slots in common metal plates. To conclude this chapter, we show results obtained by this method and compare it against the results obtained by commercial EM solvers, in Section 2.4.

2.1 Modeling a generic siw device – general considerations

As shown in Figure 2.1, a typical SIW device consists of

- A single or a number of parallel plate waveguides,
- Metal and/or dielectric cylindrical posts,
- Slots etched in metal plates,
- Sources (coaxial probes, waveguide ports, slot transitions etc.).
-

Figure 2.1 Schematic of a generic SIW device



Our aim is then to model this very general geometry in the most convenient way possible which will lend us use of analytical tools, while preserving accuracy and simplicity. Therefore, we have to introduce some simplifying assumptions and establish the region of their validity.

2.1.1 Initial assumptions and simplifications

Firstly, parallel plates which make up a PPW, typically made of copper, aluminium or other good conductors, restrict the propagation of the electromagnetic field in the longitudinal direction, denoted z here, whereas the field can freely propagate in transverse directions. However, a common characteristic shared by the majority of SIW devices is the enclosure of parallel plate waveguides by sidewalls, constituted by fences of tightly spaced vertical cylindrical posts of small diameter (compared to the operating wavelength). As such, these devices suffer negligible leakage in the transverse direction. Therefore, one may disregard any phenomena occurring outside of the region enclosed by post walls. Now, if one wishes to couple a device to other waveguides or the surrounding medium, slots may be etched in the metal plates which propagate the field further by virtue of displacement

currents induced on them. A good example of these traits is the pillbox-type SIW antenna, e.g. [47], [48] which actually closely resembles the device shown in the previous figure. It is typically composed of two waveguides stacked on top of each other, coupled by slots etched in the common metal plate. The bottom waveguide has a feeder embedded in it which drives the antenna. The sidewalls confine the field and guide it towards a set of coupling slots, which transfer the energy into the upper waveguide. The field then reaches the slot array in the uppermost plate, tailored to radiate a specific pattern. It should be noted that in practice the radiating elements are placed sufficiently far away from the edge of the antenna so as to minimize grating lobes due to edge diffraction. Moreover, the elementary radiator's pattern is usually such that it radiates negligibly towards the edge. These facts, although seemingly unrelated, motivate us to introduce the first simplifying assumption – we can consider the parallel plates as being *infinite* in extent. This will save us from the trouble of accounting for diffracted or fringing fields, both the ones induced at plate edges and at ends of truncated waveguides.

The second assumption is related to the conductivity of metal the plates are made of. In practice, high conductivity metals such as copper are used to realize metal plates, usually quite thin compared to the operating wavelength (less than $\lambda / 30$). Though the EM field generally will leak through plates, its amplitude is negligibly small, as long as the plates are at least a couple of skin depths thick. This leads us to consider the plates as *perfect electric conductors*. Moreover, we will consider regions separated by metal plates as *non-interacting* (of course, unless there are apertures in plates), and will remain so even when low-conductivity metals are employed, provided the thickness is large enough to kill off the field sufficiently. This assumption will prove crucial in simplifying the SIW problem, because it enables one to split the initial problem domain into subdomains, as will be discussed shortly. In addition, we shall consider the plates to have zero-thickness, since in most practical cases the thickness is small and it does not influence the field transmission through apertures. It should be stressed here, however, that plate thickness, even a relatively small one, can play a great role if a large number of slots is etched in plates, as demonstrated by Mazzinghi, Freni and Albani in [49]. The cumulative effect of individual slot phase modulation on the feeding wave may result in lower gain of slot antennas due to unwanted progressive phasing. However, in most cases of interest, this does not happen as the number of slots is usually moderate and we shall not consider it henceforth.

The next assumption concerns the metal and dielectric posts. In SIW devices, posts are typically used to realize fences, as well as lumped-like inductive elements to realize microwave filters and phase shifters. They are commonly circular-cylindrical- shaped since it is the simplest shape to realize in practice. Therefore, we will consider all posts as being of circular-cylindrical shape, although one can, in principle, model even elliptically-shaped posts using slightly more complicated special functions to describe fields scattered off of them. We stress here that all the posts considered run from the bottom to the top of a PPW they are embedded in. Posts which do not, of the kind that can be found in, e.g. , gap waveguides, cannot be taken into account by the present method.

The last assumption on geometry we will make is on the type of slots modelled by this method. In practice, the most common type of slot used is the narrow, rectangular-shaped one, having one dimension comparable to the operating wavelength (usually close to 0.5λ), the other one being an order of magnitude smaller (below $\lambda / 10$). They are easier to control than wide slots, and are commonly used as basic radiating elements in arrays, owing up to their radiation pattern which is approximately the dual of an electric dipole. Therefore, we will restrict our discussion solely to narrow slots.

Although these assumptions may seem a bit restrictive, fairly general geometries can be successfully modelled, ranging from closed resonating structures, waveguide filters, phase shifters, to complex slot arrays etc. , as will be shown in the following sections.

Finally, we should add a few remarks on the media occupying the problem domain. We will be dealing solely with non-magnetic media, although the general field formulas will have the effects of magnetization incorporated. All media are considered linear, time-invariant, piecewise-constant and lossless (although small losses may be added in proofs where convenient). The fields we will be interested in are time-harmonic, with time-dependence $e^{+j\omega t}$ suppressed.

2.1.2 Splitting the problem domain

Armed with all these starting assumptions, we can finally tackle the problem. It is obvious that a general SIW device can be quite complex, consisting of several stacked waveguides and having hundreds of posts and slots, with several feeds. Firstly, we wish to simplify the problem by splitting it into subproblems, solve them separately, and reconnect them in some fashion in order to solve the complete problem. To do this, we will employ the equivalence principle [26] as follows.

Consider a number of stacked waveguides coupled by slots and having arbitrary post configurations embedded, as shown in the previous figure (Figure 2.1). To model the effect of slots, we resort to an MoM procedure [50], i.e. we will make use of the boundary conditions on slots to reformulate the problem of field scattering off and transmission through slots into an integral equation. First, one notes that across any aperture in a metal plate, the continuity of tangential electric and magnetic fields must hold. Second, since slots are considered narrow, we can assume that only tangential electric fields induced across them will have a significant amplitude. Indeed, Stern and Elliott [51] conducted an MoM study of slot field distribution where it was established that the normal component of the electric field is roughly three orders of magnitude smaller than tangential ones, and neglecting it does not produce any noticeable changes in obtained results.

Now, according to the equivalence principle, the electromagnetic field scattered off of any body or surface can be thought of as due to equivalent currents lying on the boundary surface of the scatterer. Therefore, we enclose each slot by a box of vanishing thickness having the same dimensions as a slot, and distribute equivalent currents on its surface, as shown in Figure 2.2. (We show only two adjacent problem regions in the figure for the sake of simplicity). In applying this principle, we have several options at our disposal. We could distribute both electric and magnetic currents on the surface of the boxes, having the following form:

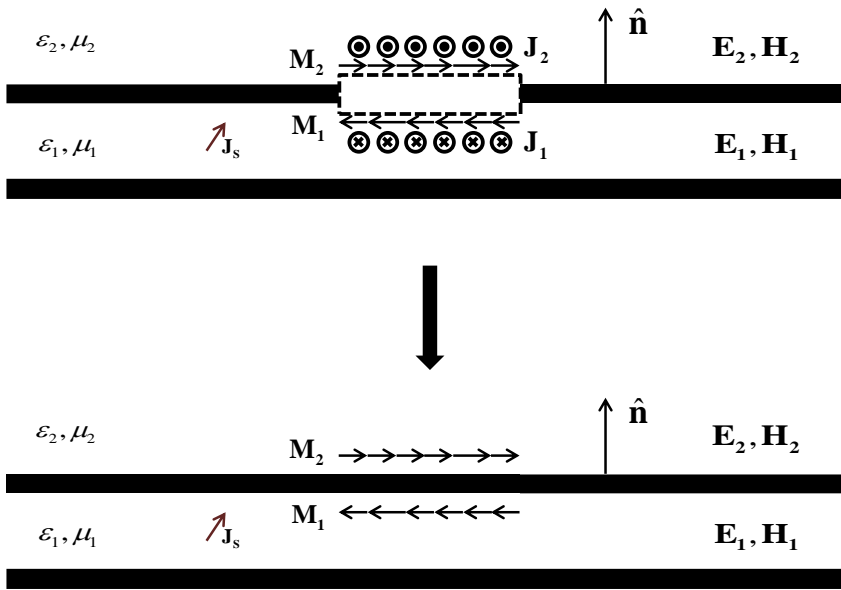
$$\begin{aligned} \mathbf{M}_i(\mathbf{r}) &= \mathbf{E}_i(\mathbf{r}) \times \hat{\mathbf{n}} \\ \mathbf{J}_i(\mathbf{r}) &= \hat{\mathbf{n}} \times \mathbf{H}_i(\mathbf{r}) \end{aligned} \quad , \mathbf{r} \in \text{slots} . \quad (2.1)$$

These currents radiate fields $\mathbf{E}_1, \mathbf{H}_1$ and $\mathbf{E}_2, \mathbf{H}_2$ into their respective regions of definition that satisfy Maxwell equations and boundary conditions, whereas we can freely choose which field they radiate into the empty volume enclosed by the box, so we will set them to zero for convenience. Unfortunately, this particular choice of equivalence leads to difficult field evaluation since, due to the presence of apertures in metal plates, no analytic Green's functions are available for such structures. However, a more convenient form of the equivalence principle is obtained upon realizing that one can fill the volume of the box with arbitrary material without altering the physics. Therefore, we fill the volumes with the same

material the plates are made of, which in our case is PEC. This has the effect of shorting out the electric currents, with only magnetic currents remaining. These currents will now be radiating above or below infinite metal plates, as shown below, and such structures possess well-known analytic Green's functions.

The currents are set to have equal magnitude but opposite direction, i.e. $\mathbf{M}_2 = -\mathbf{M}_1$, since this arrangement automatically guarantees the continuity of electric fields across slots. This is easily seen if one recalls that the radiation of magnetic dipoles is dual to electric ones. It should be noted that this holds if plates are infinitely thin. If the thickness is finite, one has to setup a waveguide problem for each slot, placing a different pair of oppositely directed currents of equal magnitude, spaced at infinitesimal distance from each other, at *each* waveguide opening.

Figure 2.2 Application of the equivalence principle



Having metallized the slots, we had “split” the problem into smaller ones, enabling us to deal with each region (PPW or half-space) separately. Placing magnetic currents, on the other hand, enables us to connect these regions upon applying boundary conditions across slots. As stated, enforcing equal magnitude and oppositely directed currents over slots is equivalent to the enforcement of the electric field continuity. However, the tangential magnetic field is continuous across slots as well, and we need to enforce this condition by stating:

$$\left[\mathbf{H}_{inc,i-1}(\mathbf{r}_q^-) + \mathbf{H}_{slots,i-1}(\mathbf{r}_q^-) \right] \times \hat{\mathbf{n}} = \left[\mathbf{H}_{inc,i+1}(\mathbf{r}_q^+) + \mathbf{H}_{slots,i+1}(\mathbf{r}_q^+) \right] \times \hat{\mathbf{n}}, \quad (2.2)$$

where the LHS is the total tangential magnetic field in waveguide $i-1$ evaluated at any point \mathbf{r}_q^- on the lower q -th slot boundary surface, i denoting the interface (plate) number, starting from the lowermost one, and the RHS is the total tangential magnetic field in waveguide $i+1$ evaluated at point \mathbf{r}_q^+ located on the upper slot boundary surface a vanishing distance δ above \mathbf{r}_q^- in the normal direction $\hat{\mathbf{n}}$. \mathbf{H}_{inc} is the field created by impressed sources, consisting of two contributions, the first being the direct source contribution:

$$\mathbf{H}_{inc,n}^{source}(\mathbf{r}) = -j\omega\epsilon_n \int_{V'} \underline{\mathbf{G}}_n(\mathbf{r}, \mathbf{r}') \cdot \mathbf{M}_S(\mathbf{r}') d\mathbf{r}', \quad (2.3)$$

accounting for the field of a source embedded in the n -th region, which is impinging directly on the slot without the presence of scatterers, and is computed by a convolution of the impressed source \mathbf{M}_S with the dyadic Green's function of the n -th region. The second contribution is the magnetic field of those same impressed sources scattered by obstacles, denoted by

$$\mathbf{H}_{scattered}^{source}(\mathbf{r}) = \sum_i \mathbf{H}_{obstacle\ i}^{source}(\mathbf{r}). \quad (2.4)$$

In our case, the only scatterers inside a PPW will be metal or dielectric posts (recall that we have replaced slots by equivalent currents), whereas no scatterers in free-space will be assumed. How to actually compute this contribution will be shown in following chapters.

Furthermore, $\mathbf{H}_{slots,n}$ is the field scattered by slots in n -th region, again consisting of a direct contribution of all the slots $\mathbf{H}_{inc,n}^{slots}$, defined as

$$\mathbf{H}_{inc,n}^{slots}(\mathbf{r}) = -j\omega\epsilon_n \sum_{slots} \int_{V'} \underline{\mathbf{G}}_n(\mathbf{r}, \mathbf{r}') \mathbf{M}_{slot}(\mathbf{r}') d\mathbf{r}', \quad (2.5)$$

\mathbf{M}_{slot} being the equivalent magnetic current of a slot in the given region, and an obstacle-scattered contribution $\mathbf{H}_{scattered}^{slots}$

$$\mathbf{H}_{scattered}^{slots}(\mathbf{r}) = \sum_i \mathbf{H}_{obstacle\ i}^{slots}(\mathbf{r}). \quad (2.6)$$

As can be seen from the discussion, we split the total field into a direct and scattered contribution, invoking the scattering superposition principle [52] which enables us to further simplify the analysis. In this way, one can make fairly general assumptions on the types of fields the scatterers create and use them to write down the total field as a sum of all the separate contributions. If one had not the ability to do so, it would hinder any attempts at analysis, since one would have to guess the proper form of the total field, which is an infeasible task.

Summa summarum, using the equivalence principle and the scattering superposition principle, we have managed to set up the problem of finding fields in an arbitrary SIW device obeying previously discussed restrictions. The problem has been divided into subproblems, one for each waveguide region, and dealing with each of them is the next topic to be discussed.

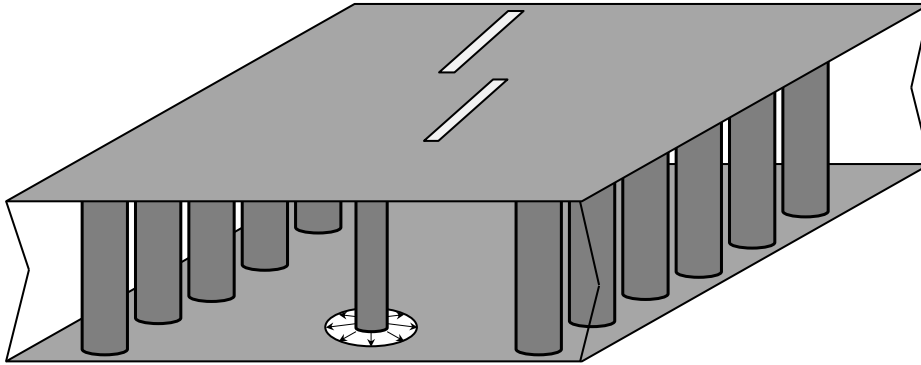
2.2 The interior and exterior problems

There are two kinds of regions in an SIW device. The first one is the waveguide region, bounded by parallel metal plates and post fences. The second one is a half-space region where, of course, free radiation occurs. In order to characterize them, one needs to be in possession of their respective field propagators, i.e. Green's functions, enabling one to calculate the fields due to arbitrary sources, impressed or induced. In this section we will deal with the specifics of the field calculation. We show how to derive the necessary Green's functions and represent post-scattered fields.

2.2.1 The interior problem

Figure 2.3 shows the general configuration of an interior region, i.e. an SIW section of an SIW device.

Figure 2.3 Section of an interior SIW region



It consists of two parallel metal plates, arbitrary sets of circular-cylindrical posts, feeds modelled as magnetic currents and possibly slots etched in either of the plates. The goal of the analysis is clear – find the total EM fields inside the region satisfying the Maxwell equations

$$\begin{aligned}
 \nabla \times \mathbf{E}(\mathbf{r}) &= -j\omega\mu\mathbf{H}(\mathbf{r}) - \mathbf{M}(\mathbf{r}) \\
 \nabla \times \mathbf{H}(\mathbf{r}) &= j\omega\varepsilon\mathbf{E}(\mathbf{r}) + \mathbf{J}(\mathbf{r}) \\
 \nabla \cdot \mathbf{E}(\mathbf{r}) &= \frac{1}{\varepsilon} \rho_e(\mathbf{r}) \\
 \nabla \cdot \mathbf{H}(\mathbf{r}) &= \frac{1}{\mu} \rho_m(\mathbf{r})
 \end{aligned} \quad , \quad (2.7)$$

subject to appropriate boundary conditions on plates, slots and posts. As discussed in the previous section, due to the linearity of Maxwell equations, we can, in principle, resolve the field into separate contributions due to sources without the presence of posts (referred to from now on as *the direct field*) and post-scattered field (*scattered field* from now on). In other words, first we remove the posts and attempt to find the field in a PPW solely due to impressed sources. Later on we will add the field scattered off of posts, whose amplitude is unknown, and enforce the boundary conditions on them to find the amplitude.

From curl equations (2.7) it follows that the vector fields satisfy the following differential equations

$$\begin{aligned}
 \nabla \times \nabla \times \mathbf{H} - k^2 \mathbf{H} &= -j\omega\varepsilon \left(\mathbf{M} - \frac{\nabla \times \mathbf{J}}{j\omega\varepsilon} \right) \\
 \nabla \times \nabla \times \mathbf{E} - k^2 \mathbf{E} &= -j\omega\mu \left(\mathbf{J} + \frac{\nabla \times \mathbf{M}}{j\omega\mu} \right)
 \end{aligned} \quad . \quad (2.8)$$

We could solve any of these two equations, and obtain the remaining field by (2.7). However, as we will transform (2.2) into an integral equation to formulate an MoM problem, we turn our attention to the H-field equation.

As one can see, we need to solve this equation for two excitations – the magnetic current \mathbf{M} and electric current \mathbf{J} . However, SIW devices are commonly fed by aperture excitations such as horns, slot-transitions and coaxial probes. It is well-known that such feeds are most conveniently modelled by equivalent magnetic currents [26]. Therefore, one rarely needs to consider the electric currents as well. Hence, we will assume that there are no impressed electric currents, i.e. $\mathbf{J} = 0$. This leaves us with the following master equation

$$\nabla \times \nabla \times \mathbf{H}(\mathbf{r}) - k^2 \mathbf{H}(\mathbf{r}) = -j\omega\epsilon \mathbf{M}(\mathbf{r}) , \quad (2.9)$$

which one has to solve for an arbitrary “acceptable” excitation \mathbf{M} . There are several ways of achieving that, such as through the use of auxiliary potentials \mathbf{A} and \mathbf{F} [53], z-directed fields [54], mixed potentials [55], Hertz potentials [56], Sommerfeld potentials [57], Debye potentials [58], and dyadic field Green’s functions [59]. All of these methods rely on the linearity of (2.9), which allows one to define a Green’s function [60] for the problem in question. These methods are well-known and a vast body of literature exists, dealing with them in detail, so a meticulous exposition might be inappropriate here. However, all of these methods are intimately related, and an understanding of one allows better understanding of the other. Therefore, we will review and compare them to each other in order to have a clearer picture of their relations, as well as respective pros and cons.

2.2.1.1 From Currents to Fields – Auxiliary Potentials

There are essentially two analytic approaches to tackling inhomogeneous Helmholtz equations – a direct path, relying on one’s ability to derive a direct vector field solution satisfying the imposed boundary conditions, either using vector modal expansions directly, or using sets of vector modes to construct the dyadic *field* Green’s function of the problem, i.e. operators connecting the sources and fields directly, and obtain the solution by convolving the driving source term with it. Then there is the indirect path, based on auxiliary vector quantities known as *auxiliary potentials* which are related to EM fields by simple differential operators. For the moment we shall focus only on the auxiliary potentials method, since it will serve as a starting point for the dyadic Green’s function method, which will be explained in much detail in the following sections. Moreover, in order to give a fair comparison of these methods, we will restrict ourselves to conditions assumed in the analysis of SIW devices – only magnetic currents serve as driving terms, and we are interested solely in the H-field. Hence, we focus primarily on solving (2.9).

We take as our first example the \mathbf{A}/\mathbf{F} potentials method. This particular method rests on two observations. The first one is that in the absence of electric charges, as is our case, the electric field is divergenceless (we prefer this term over *solenoidal*), i.e.

$$\nabla \cdot \mathbf{E}(\mathbf{r}) = 0 , \quad (2.10)$$

implying that \mathbf{E} may be constructed as a curl of some other vector function, i.e.

$$\mathbf{E}(\mathbf{r}) = \nabla \times \mathbf{F}(\mathbf{r}) . \quad (2.11)$$

Then, from the H-field curl Maxwell equation follows the result

$$\nabla \times (\mathbf{H}(\mathbf{r}) - j\omega\epsilon \mathbf{F}(\mathbf{r})) = 0 ,$$

or

$$\mathbf{H}(\mathbf{r}) = j\omega\epsilon \mathbf{F}(\mathbf{r}) - \nabla \phi_m(\mathbf{r}) , \quad (2.12)$$

where $\phi_m(\mathbf{r})$ is an arbitrary scalar function of position. (2.12) follows from the fact that any vector function obtained as the gradient of a proper scalar function is irrotational. Plugging (2.11) and (2.12) into the E-field curl Maxwell equation (2.7), one obtains the differential equation in \mathbf{F} :

$$(\nabla \times \nabla \times - k^2) \mathbf{F}(\mathbf{r}) = -\mathbf{M}(\mathbf{r}) + j\omega\mu\nabla\phi_m(\mathbf{r}) . \quad (2.13)$$

Unfortunately, this equation has an even more complicated form than (2.9) due to the presence of the gradient of the arbitrary magnetic potential. However, we will use the important concept of gauge invariance here to arrive at a simpler equation. Firstly, we note that $\nabla \times \nabla \times = \nabla(\nabla \cdot) - \nabla^2$ and replace the double curl operator in (2.13) using this identity. Secondly, the Helmholtz theorem [58] states that a properly regular vector function bounded at infinity may be written as $\mathbf{A}(\mathbf{r}) = \nabla \times \mathbf{D}(\mathbf{r}) + \nabla\varphi$. Since (2.11) holds, it follows that only the rotational part of \mathbf{F} is fixed, whereas the irrotational part can be of our choosing, since it will not contribute to the electric field. Hence, we are free to fix the divergence of \mathbf{F} any which way seems the most convenient. Upon some reflection, it turns out that we can get rid of both the *grad div*() operator on the LHS and the gradient of the potential on the RHS if we stipulate

$$\nabla \cdot \mathbf{F}(\mathbf{r}) = j\omega\mu\phi_m(\mathbf{r}) , \quad (2.14)$$

thereby simplifying (2.13) to

$$(\nabla^2 + k^2) \mathbf{F}(\mathbf{r}) = \mathbf{M}(\mathbf{r}) . \quad (2.15)$$

The solution to this equation is expressed in a simpler way than that of (2.13) and is given by

$$\mathbf{F}(\mathbf{r}) = -\int \mathbf{G}(\mathbf{r}, \mathbf{r}') \mathbf{M}(\mathbf{r}') d\mathbf{r}' , \quad (2.16)$$

$\mathbf{G}(\mathbf{r}, \mathbf{r}')$ being the scalar Green's function, which is the solution to the differential equation

$$(\nabla^2 + k^2) \mathbf{G}(\mathbf{r}, \mathbf{r}') = -\delta(\mathbf{r} - \mathbf{r}') , \quad (2.17)$$

subject to boundary conditions dictated by the E-field. Just as an illustration, the Green's function in an unbounded homogeneous and isotropic medium will take the well-known form [56]

$$\mathbf{G}(\mathbf{r}, \mathbf{r}') = \frac{e^{-jk|\mathbf{r}-\mathbf{r}'|}}{4\pi|\mathbf{r}-\mathbf{r}'|} . \quad (2.18)$$

Now one can finally obtain the full solution for the H-field in terms of the auxiliary potential \mathbf{F} as

$$\mathbf{H}(\mathbf{r}) = -j\omega\varepsilon \left\{ \int \mathbf{G}(\mathbf{r}, \mathbf{r}') \mathbf{M}(\mathbf{r}') d\mathbf{r}' + \frac{1}{k^2} \nabla \nabla \cdot \int \mathbf{G}(\mathbf{r}, \mathbf{r}') \mathbf{M}(\mathbf{r}') d\mathbf{r}' \right\} . \quad (2.19)$$

In sum, one needs to find the scalar Green's function subject to proper boundary conditions, inherited from the vector potential \mathbf{F} , which is then used as the kernel in the integral transforms above. Then, differentiation needs to be performed in order to obtain the second

term. This is performed as follows. First, we move the divergence inside the integral. Note that one should be careful at this point since a limiting procedure is necessary due to the scalar Green function's singularity at $\mathbf{r} = \mathbf{r}'$ [59]. Then, after a simple application of the chain derivative rule, along with recognizing that $\nabla = -\nabla'$ when acting on the Green's function (as it is a function of $|\mathbf{r} - \mathbf{r}'|$), and on applying Green's first identity [58] to move the divergence from the Green's function onto the current, one obtains

$$\mathbf{H}(\mathbf{r}) = -j\omega\epsilon \left\{ \int \mathbf{G}(\mathbf{r}, \mathbf{r}') \mathbf{M}(\mathbf{r}') d\mathbf{r}' - \frac{1}{k^2} \nabla \int \mathbf{G}(\mathbf{r}, \mathbf{r}') \nabla' \cdot \mathbf{M}(\mathbf{r}') d\mathbf{r}' \right\}$$

which, upon recalling that $\nabla' \cdot \mathbf{M}(\mathbf{r}') = -j\omega\rho_m(\mathbf{r}')$, finally becomes

$$\mathbf{H}(\mathbf{r}) = -j\omega\epsilon \left\{ \int \mathbf{G}(\mathbf{r}, \mathbf{r}') \mathbf{M}(\mathbf{r}') d\mathbf{r}' + \frac{1}{k^2} \nabla \int j\omega \mathbf{G}(\mathbf{r}, \mathbf{r}') \rho_m(\mathbf{r}') d\mathbf{r}' \right\}. \quad (2.20)$$

This is the standard radiation integral, its interpretation being that the total field consists of two contributions - the first due to currents, while the second one due to static charges.

The \mathbf{A} / \mathbf{F} potential method may be convenient in a multitude of problems, and it serves as the starting point of other potentials-based methods.

Hertz-Debye potentials method is one of them. It rests on the idea defining two vector potentials, pointed in a "preferred" direction, preferred usually meaning "in the stratification direction". If one defines

$$\begin{aligned} \mathbf{A}(\mathbf{r}) &= \hat{\mathbf{a}}_a A_a(\mathbf{r}) \\ \mathbf{F}(\mathbf{r}) &= \hat{\mathbf{a}}_a F_a(\mathbf{r}) \end{aligned}, \quad (2.21)$$

it is possible to decompose the fields into TM and TE components with respect to $\hat{\mathbf{a}}$ in a simple and straightforward way, if one adopts the definitions

$$\begin{aligned} \mathbf{E}_F(\mathbf{r}) &= \nabla \times \mathbf{F}(\mathbf{r}) \\ \mathbf{H}_A(\mathbf{r}) &= \nabla \times \mathbf{A}(\mathbf{r}) \end{aligned}. \quad (2.22)$$

It can be easily seen that these respective fields will be transverse to $\hat{\mathbf{a}}$, hence representing TE_a and TM_a fields (or sometimes hybrid modes), respectively. Moreover, the fields defined in this manner, being solutions to the homogeneous Helmholtz equation, may serve in the construction of dyadic Green's functions, as will be shown in the following subsection.

Depending on the problem at hand, one potential will do better than the other. The greatest power offered by the potentials approach is the degree of freedom inherent in their definition, allowing one to simplify their respective differential equations, which are, in general, easier to solve than the field vector Helmholtz equations. Moreover, they allow construction of fields in a fairly straightforward way. Coupled with the spectral domain approach [61], the potentials method becomes a powerful and versatile method capable of accounting for a plethora of problems, ranging from closed resonating devices to open, multilayered structures.

2.2.1.2 Dyadic Green's Functions

As mentioned in the previous subsection, dyadic Green's functions provide a direct way to relate currents to their fields. Though more compact in form than the auxiliary

potentials method, they accomplish the same end. Moreover, as will be shown, dyadic Green's functions are commonly derived from vector potential functions, constructible from suitable scalar potentials.

The method we adhere to is based on what we will refer to as the Schwinger-Marcuvitz-Felsen formalism (abbreviated as *SMF* from here on) [62], [63], [64], based on the use of dyadic Green's functions and will be the topic of this subsection. However, first we will focus on the general derivation and exposition of dyadic Green's functions, turning to the SMF formalism once we will have presented the alternative formalisms in sufficient detail.

We begin by noting that, since the equation (2.9) is linear, we can expect that its solution may be written as a linear superposition of some elementary contributions. What we mean by elementary is this – any source distribution may be thought of as a superposition of point sources, represented by the Dirac delta function, defined by

$$\int f(\mathbf{r}') \delta(\mathbf{r}' - \mathbf{r}) d\mathbf{r}' = f(\mathbf{r}) . \quad (2.23)$$

Generalizing this so-called sifting property of the delta function to vector functions and applying it to our case, we can write the magnetic current in (2.9) as

$$\mathbf{M}(\mathbf{r}) = \int \mathbf{M}(\mathbf{r}') \delta(\mathbf{r}' - \mathbf{r}) d\mathbf{r}' . \quad (2.24)$$

Applying a similar superposition principle, we *assume* an arbitrary H-field can be written as a linear functional, or more precisely, an integral of elementary current contributions as

$$\frac{1}{-j\omega\varepsilon} \mathbf{H}(\mathbf{r}) = \int \underline{\mathbf{G}}^{\text{HM}}(\mathbf{r}, \mathbf{r}') \cdot \mathbf{M}(\mathbf{r}') d\mathbf{r}' , \quad (2.25)$$

where we have introduced a linear operator of rank 2 (a dyad, or tensor of rank 2) $\underline{\mathbf{G}}^{\text{HM}}$, which we will refer to as the *magnetic field dyadic Green's function* [52]. In essence, we stipulated that the field \mathbf{H} is a general linear mapping of the current \mathbf{M} , the mapping being an integral transform with $\underline{\mathbf{G}}^{\text{HM}}$ as the pertinent kernel. (The existence of such a mapping is guaranteed by the Riesz representation theorem [65].) A more palpable, “physical” interpretation of $\underline{\mathbf{G}}^{\text{HM}}$ is obtained if one takes a point dipole $\mathbf{M}(\mathbf{r}') = \hat{\mathbf{a}} \delta(\mathbf{r} - \mathbf{r}')$ as the source in (2.25), $\hat{\mathbf{a}}$ being an arbitrary unit vector. Then the integration becomes a simple multiplication:

$$\mathbf{H}(\mathbf{r}) = -j\omega\varepsilon \underline{\mathbf{G}}^{\text{HM}}(\mathbf{r}, \mathbf{r}') \hat{\mathbf{a}} ,$$

and with $\underline{\mathbf{G}}^{\text{HM}}$ being defined a dyad (tensor), it represents *the magnetic field of a point dipole of moment* $-1/j\omega\varepsilon$, each of its components bearing form $\mathbf{x}_i G_{ij}(\mathbf{r}, \mathbf{r}') \mathbf{x}_j$, representing the \mathbf{x}_i component of the magnetic field excited by an \mathbf{x}_j -oriented point dipole of moment $-1/j\omega\varepsilon$, the scalar function $G_{ij}(\mathbf{r}, \mathbf{r}')$ playing the role of the field propagator.

Now, let us return to the derivation. Plugging (2.24) and (2.25) into (2.9), we obtain

$$(\nabla \times \nabla \times - k^2) \int \underline{\mathbf{G}}^{\text{HM}}(\mathbf{r}, \mathbf{r}') \cdot \mathbf{M}(\mathbf{r}') d\mathbf{r}' = \int \mathbf{M}(\mathbf{r}') \delta(\mathbf{r}' - \mathbf{r}) d\mathbf{r}' , \quad (2.26)$$

which we can transform further upon noting that we can move the vector Helmholtz operator inside the field integral, provided the integral obtained so converges uniformly [66].

This is true for all observation points except ones determined by $\mathbf{r} = \mathbf{r}'$, i.e. source points. In this case, the field integral diverges because the Green's function does, which we know to be true without knowing its form explicitly since: a) any "physical" function describing interaction between sources of finite energy is exclusively a function of the space-time distance between them, b) any such function has to vanish or at least be bounded at infinity. Since sufficiently close to \mathbf{r}' , each component of the Green's dyad behaves to dominant order as the free-space scalar Green's function (in \mathbb{R}^3) (2.18), it is implied c) that it has to fall off at least as $|\mathbf{r} - \mathbf{r}'|^\alpha$, $\alpha \leq -1$. This can be seen if one recalls that a Green's function subject to general boundary conditions can be written, owing to the linearity of the Helmholtz equation and the validity of Green's theorem, as the sum of the direct contribution – the free space one, and the secondary – the waves reflected at boundaries. Then it follows that any Green's function's singularity will essentially be dominated by the singularities of the free space Green's function and its derivatives [67]. Finally, one concludes that the Green's dyadic possesses a singularity at $\mathbf{r} = \mathbf{r}'$. Hence, a problem is encountered when evaluating a field at this point, motivating one to exclude this special point in some fashion. This is the well-known problem of the **singularity of Green's functions** and has been researched extensively (see e.g. [68], [69], [70]). A way to mitigate this problem relies on a lemma on improper integrals, stating that an integral of a function containing a singular point \mathbf{r}_0

$$I = \int_V f(\mathbf{r}) d\mathbf{r}$$

converges, or exists, if the limit

$$\lim_{\delta \rightarrow 0} \int_{V-\nu} f(\mathbf{r}) d\mathbf{r} \quad (2.27)$$

exists, ν being a variable region subject to the sole restriction that it must have \mathbf{r}_0 in its interior, and that its maximum dimension does not exceed δ [68, p. 147]. In essence, one surrounds the singular point by a small volume, thereby excluding this point from the problem, but letting the maximum size of the volume approach zero. If the limit exists, the quantity defined by the integral exists, which in our case is the field.

This particular procedure applied to our case will be dealt with in detail later on, since it would obscure the present discussion, and we defer it to after we will have derived the basic equations and identities involving the dyadic Green's function, giving us better insight into the specifics of the problem. For the moment, we shall assume that our Green's function can be regularized, rendering the LHS integral (2.26) uniformly convergent which, ultimately, allows us to interchange the integration and the Helmholtz operator.

Having established the restrictions on the interchange of integral and differential operators, we move the operator inside the integral, obtaining

$$\int (\nabla \times \nabla \times - k^2) \underline{\mathbf{G}}^{\text{HM}}(\mathbf{r}, \mathbf{r}') \cdot \mathbf{M}(\mathbf{r}') d\mathbf{r}' = \int \mathbf{1} \delta(\mathbf{r}' - \mathbf{r}) \cdot \mathbf{M}(\mathbf{r}') d\mathbf{r}', \quad (2.28)$$

where $\mathbf{1}$ is the unit dyad having the property $\mathbf{1}\underline{\mathbf{A}} = \underline{\mathbf{A}}\mathbf{1} = \underline{\mathbf{A}}$, $\underline{\mathbf{A}}$ being an arbitrary dyad or vector. Comparing the LHS with the RHS, we note that in order for the equality to hold, the following differential operator equation must hold

$$(\nabla \times \nabla \times - k^2) \underline{\mathbf{G}}^{\text{HM}}(\mathbf{r}, \mathbf{r}') = \mathbf{1} \delta(\mathbf{r} - \mathbf{r}'), \quad (2.29)$$

subject to the same boundary conditions as the magnetic field itself

$$\begin{aligned} \hat{\mathbf{n}} \times (\nabla \times \underline{\mathbf{G}}^{\text{HM}}(\mathbf{r}, \mathbf{r}')) &= 0, \quad \mathbf{r} \in \Omega_{\text{PEC}} \\ \lim_{\rho \rightarrow \infty} \sqrt{\rho} (\nabla \times \underline{\mathbf{G}}^{\text{HM}}(\mathbf{r}, \mathbf{r}') + jk_t \hat{\boldsymbol{\rho}} \times \underline{\mathbf{G}}^{\text{HM}}(\mathbf{r}, \mathbf{r}')) &= 0 \end{aligned} \quad (2.30)$$

where $\hat{\mathbf{n}}$ is the PEC surface normal S of the PPW region, and k_t is the transverse wavenumber. The former condition demands that the tangential electric field produced by a magnetic current is zero at PEC plates, while the latter, known as the Sommerfeld radiation condition [57], dictates that the energy transfer is directed towards infinity and the fields fall off faster than $\rho^{-1/2}$, guaranteeing uniqueness of solution. Note that we have used the delta function symmetry property $\delta(\mathbf{r} - \mathbf{r}') = \delta(\mathbf{r}' - \mathbf{r})$ to bring (2.29) into a more familiar form. Moreover, because the RHS of (2.29) has this property, the LHS must have that same property as well. To be more precise, since the RHS is a symmetric operator under the prescribed boundary condition (2.30), the LHS is as well, hence reciprocity under the transformation $\mathbf{r} \leftrightarrow \mathbf{r}'$ of $\underline{\mathbf{G}}^{\text{HM}}$ follows.

In sum, we have simplified the field problem given by (2.9) to finding the dyadic Green's function as the solution to (2.29), and performing the integration (2.25).

There are several methods available to systematically solve (2.29), of which the most widespread is the **Ohm-Rayleigh method** [71], [72]. Its central idea is to use a dyadic analogue to the classical solution of scalar Green's function by eigenfunction-expansion. Basically, one introduces complete sets of vector wave functions, which are defined as eigenfunction solutions of the homogeneous vector Helmholtz equations

$$\nabla \times \nabla \times \mathbf{D}(\mathbf{r}) - \kappa^2 \mathbf{D}(\mathbf{r}) = 0, \quad (2.31)$$

κ being an arbitrary parameter for now. The solutions of (2.31) can be generated from solutions of the scalar Helmholtz equation

$$(\nabla^2 + \kappa^2) \begin{matrix} \psi' \\ \psi'' \end{matrix}(\mathbf{r}) = 0, \quad (2.32)$$

satisfying Neumann or Dirichlet boundary conditions at the problem boundary surface S , $\partial_n \psi'(\mathbf{r}) = 0$ and $\psi''(\mathbf{r}) = 0$, respectively. If one defines a so-called pilot vector $\hat{\mathbf{a}}$, and constructs the following functions

$$\begin{aligned} \mathbf{M}'(\mathbf{r}) &= \nabla \times \hat{\mathbf{a}} \psi'(\mathbf{r}) \quad ; \quad \mathbf{N}'(\mathbf{r}) = \frac{1}{\kappa} \nabla \times \nabla \times \hat{\mathbf{a}} \psi'(\mathbf{r}) \\ \mathbf{M}''(\mathbf{r}) &= \nabla \times \hat{\mathbf{a}} \psi''(\mathbf{r}) \quad ; \quad \mathbf{N}''(\mathbf{r}) = \frac{1}{\kappa} \nabla \times \nabla \times \hat{\mathbf{a}} \psi''(\mathbf{r}) \end{aligned} \quad (2.33)$$

one has effectively constructed a divergenceless TM/TE vector basis, the interpretation of these function being the following – the primed functions correspond to, respectively, the magnetic and electric TM field, whereas the doubly-primed functions correspond to the magnetic and the electric TE field. Note that these functions are actually nothing more than the fields obtained from Hertz-Debye potentials, mentioned in the previous subsection. These forms are valid in regions containing no more than a single, isotropic medium. If one wishes to deal with fields in multilayered, anisotropic regions, the definitions (2.33) have to be modified. This modification will be shown explicitly in one of the following sections.

Furthermore, the intention of introduction the $\frac{1}{\kappa}$ factor in the definition of \mathbf{N} functions

was solely to obtain symmetrical auxiliary relations between \mathbf{M} and \mathbf{N} functions obtainable from (2.31).

In addition to the divergenceless vector functions, one needs to specify *irrotational* vector wave functions as well. The reason for this is that one must be able to represent the static fields as well. For this purpose, the following functions are introduced:

$$\begin{pmatrix} \mathbf{L}'(\mathbf{r}) \\ \mathbf{L}''(\mathbf{r}) \end{pmatrix} = \nabla \begin{pmatrix} \psi_0'(\mathbf{r}) \\ \psi_0''(\mathbf{r}) \end{pmatrix}, \quad (2.34)$$

where ψ_0'' is the solution to the Laplace equation

$$\begin{aligned} \nabla^2 \psi_0'(\mathbf{r}) &= 0, \\ \psi_0''(\mathbf{r}) &= 0, \end{aligned} \quad (2.35)$$

satisfying $\partial_n \psi_0' = 0$, $\psi_0'' = 0$. Now, if the sets $\{\psi\}$ and $\{\psi_0\}$ are complete and orthogonal (the TM/TE superscripts are omitted for the sake of compactness), one can construct vector bases orthonormal under the scalar product

$$\langle \mathbf{f}, \mathbf{g} \rangle = \int \mathbf{f}(\mathbf{r}) \cdot \mathbf{g}(\mathbf{r})^* d\mathbf{r}, \quad (2.36)$$

the asterisk denoting the complex conjugate. These bases are not only capable of representing an arbitrary vector function, but a dyadic one as well. In other words, there exist dyadic completeness relations

$$\begin{aligned} \sum_m \mathbf{a}_m \otimes \mathbf{M}_m'(\mathbf{r}) + \mathbf{b}_m \otimes \mathbf{N}_m''(\mathbf{r}) + \mathbf{c}_m \otimes \mathbf{L}_m'(\mathbf{r}) &= \mathbf{1}\delta(\mathbf{r}-\mathbf{r}') \\ \sum_m \mathbf{d}_m \otimes \mathbf{M}_m''(\mathbf{r}) + \mathbf{e}_m \otimes \mathbf{N}_m'(\mathbf{r}) + \mathbf{f}_m \otimes \mathbf{L}_m''(\mathbf{r}) &= \mathbf{1}\delta(\mathbf{r}-\mathbf{r}') \end{aligned}, \quad (2.37)$$

\otimes indicating the dyadic product (more commonly known as the *outer product*), m indexing the terms of the series (the sum is to be interpreted as a general summation/integral operator). The reason why there are two such relations is quite simple - there are two kinds of fields - the magnetic and the electric one, satisfying different boundary conditions. Therefore, one needs two sets of functions to describe them - one for each. The first relation is related to the expansion of magnetic fields, the second one to electric fields. Performing scalar products with \mathbf{M}_m , \mathbf{N}_m and \mathbf{L}_m eigenfunctions, one obtains the completeness relations

$$\begin{aligned} \sum_m \mathbf{M}_m'(\mathbf{r}') \otimes \mathbf{M}_m'(\mathbf{r}) + \mathbf{N}_m''(\mathbf{r}') \otimes \mathbf{N}_m''(\mathbf{r}) + \mathbf{L}_m'(\mathbf{r}') \otimes \mathbf{L}_m'(\mathbf{r}) &= \mathbf{1}\delta(\mathbf{r}-\mathbf{r}') \\ \sum_m \mathbf{M}_m''(\mathbf{r}') \otimes \mathbf{M}_m''(\mathbf{r}) + \mathbf{N}_m'(\mathbf{r}') \otimes \mathbf{N}_m'(\mathbf{r}) + \mathbf{L}_m''(\mathbf{r}') \otimes \mathbf{L}_m''(\mathbf{r}) &= \mathbf{1}\delta(\mathbf{r}-\mathbf{r}') \end{aligned} \quad (2.38)$$

These relations serve as starting points in solving dyadic Green's function differential equations. In order to solve (2.29), we use the first one, relevant to the magnetic field.

Expanding the RHS of (2.29) using (2.37) and the RHS in a similar fashion, we obtain

$$\begin{aligned}
 (\nabla \times \nabla \times - k^2) \sum_m \mathbf{g}_m \otimes \mathbf{M}'_m(\mathbf{r}) + \mathbf{h}_m \otimes \mathbf{N}''_m(\mathbf{r}) + \mathbf{i}_m \otimes \mathbf{L}'_m(\mathbf{r}) = \\
 \sum_m \mathbf{a}_m \otimes \mathbf{M}'_m(\mathbf{r}) + \mathbf{b}_m \otimes \mathbf{N}''_m(\mathbf{r}) + \mathbf{c}_m \otimes \mathbf{L}'_m(\mathbf{r})
 \end{aligned} \tag{2.39}$$

This, in general, is an infinite linear system. If we recall that functions belonging to different bases are linearly independent, then the implication is that we have to match the coefficients of each m -th pair of dyadic functions, one on the LHS, one on the RHS. Moreover, interchanging the summation with the Helmholtz operator, and recalling that the unknown expansion coefficients do not depend on \mathbf{r} , we obtain

$$\begin{aligned}
 \mathbf{g}_m &= \frac{\mathbf{a}_m}{\kappa^2 - k^2} = \frac{\mathbf{M}'_m(\mathbf{r}')}{\kappa^2 - k^2} \\
 \mathbf{h}_m &= \frac{\mathbf{b}_m}{\kappa^2 - k^2} = \frac{\mathbf{N}''_m(\mathbf{r}')}{\kappa^2 - k^2} \\
 \mathbf{i}_m &= \frac{\mathbf{c}_m}{-k^2} = \frac{\mathbf{L}'_m(\mathbf{r}')}{-k^2}
 \end{aligned} \tag{2.40}$$

At this point, the role of the parameter κ should be clarified. One may ask why we did not demand (2.31) to satisfy the same equation with k . The reason is the following – if we had, the expansion coefficients (2.40) would have been undefined due to resonance, i.e. $\kappa^2 = k^2$ rendering the coefficients infinite and the expansion non-unique. In order to have a well-defined and unique Green's function, this parameter κ can be chosen arbitrarily, but must be such that $\kappa^2 \neq k^2$. More concisely, κ is a free parameter of the spectral expansion, and by means of analytic continuation [60, pp. 392–398] it can be shown that the expansion remains valid even when $\kappa^2 \rightarrow k^2$. Further manipulations leading to more useful forms depend upon the specific geometry of the problem. However, the result will not depend on this parameter, and a singular term can always be extracted, which corresponds to the well-known *source correction term*.

The advantage of this method lies in its simplicity and conceptual familiarity. The drawback is tediousness and rather involved and often abstruse extraction of discontinuous terms, which needs to be done when an MoM procedure is used, since accurate evaluation of diagonal elements of MoM matrices relies on it. It is for this reason we had decided to adhere to an alternative procedure, lacking these debilitating features.

2.2.1.3 Schwinger-Marcuvitz-Felsen Formalism

The **Schwinger-Marcuvitz-Felsen formalism**, which we adopted as our method of choice to derive dyadic Green's functions, goes all the way back to WWII to the seminal work done at the MIT Rad lab by Julian Schwinger, and was, historically, the first approach to deriving dyadic Green's functions. In fact, Morse and Feshbach's famous treatise on Green's functions [60, Ch. 7] is heavily influenced by Schwinger's work, which established the concept of the dyadic Green's function (then referred to as the *tensor Green's function*). Consequent works of Marcuvitz [73], Marcuvitz and Schwinger [63] and Felsen [74] have extended and reformulated Schwinger's work, phrasing it in terms of transmission-line terminology. The whole process relies on the scalarization of the problem, where one first decomposes the complicated dyadic operator defining the Green's function into simpler ones enabling the decomposition of the field into TE and TM contributions, derivable from two scalar potentials. Moreover, such a decomposition explicitly isolates the discontinuous terms, which will prove to be crucial in the MoM procedure.

We begin as in [75], by using the identity $\nabla \times \nabla \times = \nabla(\nabla \cdot) - \nabla^2$ to rewrite the operator differential equation (2.29) as

$$(\nabla(\nabla \cdot) - \nabla^2 - k^2) \underline{\mathbf{G}}^{\text{HM}}(\mathbf{r}, \mathbf{r}') = \mathbf{1} \delta(\mathbf{r} - \mathbf{r}') . \quad (2.41)$$

Then, we note that the LHS of the expression above contains a divergence of $\underline{\mathbf{G}}^{\text{HM}}$, which can be obtained by operating with the divergence on (2.29), yielding

$$\nabla \cdot \underline{\mathbf{G}}^{\text{HM}} = -\frac{1}{k^2} \nabla \delta(\mathbf{r} - \mathbf{r}') . \quad (2.42)$$

Using this result in (2.41), one obtains, after a simple rearrangement of terms:

$$-(\nabla^2 + k^2) \underline{\mathbf{G}}^{\text{HM}}(\mathbf{r}, \mathbf{r}') = \left(\mathbf{1} + \frac{\nabla \otimes \nabla}{k^2} \right) \delta(\mathbf{r} - \mathbf{r}') . \quad (2.43)$$

Then the general form of the Green's dyadic, using the language of operator calculus [76] is:

$$\underline{\mathbf{G}}^{\text{HM}}(\mathbf{r}, \mathbf{r}') = -(\nabla^2 + k^2)^{-1} \left(\mathbf{1} + \frac{\nabla \otimes \nabla}{k^2} \right) \delta(\mathbf{r} - \mathbf{r}') , \quad (2.44)$$

$(\nabla^2 + k^2)^{-1}$ being the inverse of the scalar Helmholtz operator which, under general boundary conditions, induces two scalar potential functions necessary to construct the complete EM field.

In the case of an unbounded, homogeneous medium, it is easily seen that $\underline{\mathbf{G}}^{\text{HM}}$ is of the form

$$\underline{\mathbf{G}}^{\text{HM}}(\mathbf{r}, \mathbf{r}') = \left(\mathbf{1} + \frac{\nabla \otimes \nabla}{k^2} \right) \mathbf{G}(\mathbf{r}, \mathbf{r}') , \quad (2.45)$$

with the scalar function $g(\mathbf{r}, \mathbf{r}')$ satisfying the differential equation

$$(\nabla^2 + k^2) \mathbf{G}(\mathbf{r}, \mathbf{r}') = -\delta(\mathbf{r} - \mathbf{r}') , \quad (2.46)$$

subject to the Sommerfeld radiation condition.

Hence, the problem has been translated to finding scalar functions satisfying

$$\mathbf{G}(\mathbf{r}, \mathbf{r}') = -(\nabla^2 + k^2)^{-1} \delta(\mathbf{r} - \mathbf{r}') , \quad (2.47)$$

and applying the dyadic operator $\mathbf{1} + \frac{\nabla \otimes \nabla}{k^2}$ (which we will denote as $\underline{\mathbf{T}}$ from now on). But, recalling the \mathbf{A}/\mathbf{F} potential derivation of the magnetic field where we had obtained the radiation integral (2.19), (which we repeat here for convenience)

$$\mathbf{H}(\mathbf{r}) = -j\omega\epsilon \left\{ \int \mathbf{G}(\mathbf{r}, \mathbf{r}') \mathbf{M}(\mathbf{r}') d\mathbf{r}' + \frac{1}{k^2} \nabla \nabla \cdot \int \mathbf{G}(\mathbf{r}, \mathbf{r}') \mathbf{M}(\mathbf{r}') d\mathbf{r}' \right\} ,$$

we note that we could have arrived at (2.45) by “extracting” this operator directly from the radiation integral. Also, by comparison, one notes that (2.46) is, in fact, the \mathbf{F} potential scalar Green's function defined by (2.15).

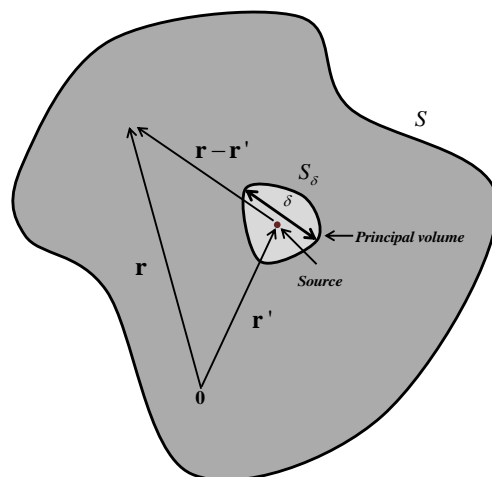
Hence, conceptually, the dyadic Green's function is nothing more than an auxiliary operator useful for formulating the radiation integral in a compact way. This general form, though elegant, does not provide any insight into the problem at hand, of course. However, it gives

better insight into the singularity problem, which we discussed a while ago and to which we now turn our attention fully.

As previously discussed, the radiation integral (2.25) becomes ill-defined when $\mathbf{r} = \mathbf{r}'$, since the Green's function becomes singular there. Not only does it possess the free-space $|\mathbf{r} - \mathbf{r}'|^{-1}$ singularity, but higher-order ones as well, owing up to the presence of spatial derivatives in \mathbf{T} , rendering the radiation integral non-uniformly convergent. Hence, one has to redefine the field integral in an improper sense, which may be done as follows. First, note that the twofold application of divergence under the integral sign results in a term of order $O(|\mathbf{r} - \mathbf{r}'|^{-3})$. Outside the source region, this creates no problems, as the integral is uniformly convergent. Therefore, one can exchange the order of integration and differentiation to her/his liking without affecting the result. However, in the source region, this term gives rise to a non-integrable singularity [77, p. 28]. Then our only chance of defining a convergent integral is if we can somehow lower the order of the singularity. This can be done if we bring the spatial derivatives outside the integral and define the field as an *improper integral*. For this purpose imagine two surfaces S and S_δ (Figure 2.4), S enclosing the problem region V , with general impedance boundary conditions specified on it, S_δ being an arbitrary surface of maximum chord δ enclosing the singular point \mathbf{r}' , subtending the volume V_δ . Now we can redefine the second term of the field integral (2.25) as [59, p. 379]

$$\begin{aligned}
 \nabla \nabla \int_V G(\mathbf{r}, \mathbf{r}') \mathbf{M}(\mathbf{r}') d\mathbf{r}' &= \lim_{\delta \rightarrow 0} \left\{ \nabla \nabla \int_{V-V_\delta} G(\mathbf{r}, \mathbf{r}') \mathbf{M}(\mathbf{r}') d\mathbf{r}' + \nabla \nabla \int_{V_\delta} G(\mathbf{r}, \mathbf{r}') \mathbf{M}(\mathbf{r}') d\mathbf{r}' \right\} \\
 &= \lim_{\delta \rightarrow 0} \left\{ \int_{V-V_\delta} \nabla \nabla G(\mathbf{r}, \mathbf{r}') \mathbf{M}(\mathbf{r}') d\mathbf{r}' + \nabla \int_{V_\delta} \nabla G(\mathbf{r}, \mathbf{r}') \mathbf{M}(\mathbf{r}') d\mathbf{r}' \right\} \\
 &= \lim_{\delta \rightarrow 0} \left\{ \int_{V-V_\delta} \nabla \nabla G(\mathbf{r}, \mathbf{r}') \mathbf{M}(\mathbf{r}') d\mathbf{r}' - \nabla \int_{V_\delta} \nabla' G(\mathbf{r}, \mathbf{r}') \mathbf{M}(\mathbf{r}') d\mathbf{r}' \right\},
 \end{aligned} \tag{2.48}$$

Figure 2.4 The principal volume geometry



where we have exchanged the order of differentiation and integration in the first RHS term because the volume $V - V_\delta$ does not contain the singular point \mathbf{r}' , therefore converging unconditionally, albeit to a value *dependent on the shape of the exclusion volume* V_δ . In the second integral, we have moved only one spatial derivative inside the integral. The reason is that a single spatial derivative acting on the Green's function increases the integrand's singularity order to $O(|\mathbf{r} - \mathbf{r}'|^{-2})$, still making it weakly singular and, therefore, integrable, which would not have been the case had we moved both derivatives inside the integral. It is important to note that the values of integrals on the RHS are both dependent on the shape of the exclusion volume. However, they add up to a unique value, corresponding to the quantity on the LHS. Moreover, using Green's theorem (partial integration), one can show that the second RHS term reduces to

$$\begin{aligned} \int_{V_\delta} \nabla' G(\mathbf{r}, \mathbf{r}') \mathbf{M}(\mathbf{r}') d\mathbf{r}' &= \int_{S_\delta} G(\mathbf{r}, \mathbf{r}') \mathbf{M}(\mathbf{r}') \cdot \hat{\mathbf{n}} dS - \int_{V_\delta} G(\mathbf{r}, \mathbf{r}') \nabla' \mathbf{M}(\mathbf{r}') d\mathbf{r}' \\ &= \int_{S_\delta} G(\mathbf{r}, \mathbf{r}') \mathbf{M}(\mathbf{r}') \cdot \hat{\mathbf{n}} dS + j\omega \int_{V_\delta} G(\mathbf{r}, \mathbf{r}') \rho_m(\mathbf{r}') d\mathbf{r}' \end{aligned} \quad (2.49)$$

where we have used the charge continuity equation to rewrite the second integral. Since the charge ρ_m is continuous, and the volume of V_δ is proportional to $|\mathbf{r} - \mathbf{r}'|^3$, it follows then that the second term of (2.49) vanishes. The first term, on the other hand, is the field in V_δ due to charge $\mathbf{M}(\mathbf{r}') \cdot \hat{\mathbf{n}} dS$ built up on the surface S_δ , and is electrostatic in nature. Hence, it satisfies the Laplace equation, which is scale invariant, i.e. the field will not vanish even in the limit $\delta \rightarrow 0$. Since in this limit this term must be linearly proportional to the current $\mathbf{M}(\mathbf{r}')$, (2.48) can be written as

$$\nabla \nabla \int_V G(\mathbf{r}, \mathbf{r}') \mathbf{M}(\mathbf{r}') d\mathbf{r}' = \lim_{\delta \rightarrow 0} \int_{V - V_\delta} \nabla \nabla G(\mathbf{r}, \mathbf{r}') \mathbf{M}(\mathbf{r}') d\mathbf{r}' - \underline{\underline{\mathbf{L}}} \cdot \mathbf{M}(\mathbf{r}'), \quad (2.50)$$

where $\underline{\underline{\mathbf{L}}}$ is the so-called *depolarizing dyad*, dependent on the shape of the exclusion volume. It has been calculated for a number of shapes of exclusion volumes, see for example [66].

Finally, using these results, one can write down the expression for the field, valid even inside the source region as

$$\mathbf{H}(\mathbf{r}) = -j\omega\epsilon \left\{ \lim_{\delta \rightarrow 0} \int_{V - V_\delta} \underline{\underline{\mathbf{G}}}^{\text{HM}}(\mathbf{r}, \mathbf{r}') \cdot \mathbf{M}(\mathbf{r}') d\mathbf{r}' + \frac{\underline{\underline{\mathbf{L}}} \cdot \mathbf{M}(\mathbf{r}')}{k^2} \right\}$$

or, more concisely

$$\mathbf{H}(\mathbf{r}) = -j\omega\epsilon \left\{ \mathcal{P.V.} \int_V \underline{\underline{\mathbf{G}}}^{\text{HM}}(\mathbf{r}, \mathbf{r}') \cdot \mathbf{M}(\mathbf{r}') d\mathbf{r}' + \frac{\underline{\underline{\mathbf{L}}} \cdot \mathbf{M}(\mathbf{r}')}{k^2} \right\}, \quad (2.51)$$

where $\mathcal{P.V.}$ denotes the principal value integral in the Cauchy sense. The intuitive interpretation of this integral is the following - when one observes the field in the source region, it is necessary to isolate the singularity by enclosing it in an artificial small volume. This "causes" charge to build up on its surface, which in turn creates an electrostatic field depending on the shape of the volume that does not vanish even in the limit of vanishing volume. Since we have thusly introduced a spurious field which was not there before we

had placed this volume, we have to kill it off to produce the correct field, and this is exactly what the depolarizing term does!

This procedure has been investigated thoroughly by a large number of authors, and has sparked quite a lot of controversy. It has been argued mostly on physical grounds (with the depolarization interpretation). However, it is very interesting to note that the whole procedure is simply an application of the very important and celebrated theorem of Sokhotski-Plemelj [78, p. 113] to vector fields over \mathbb{R}^3 ! It is even more interesting to note that, to the best of author's knowledge, no seminal paper or textbook on this topic even mentions the theorem!

To make the field integral (2.51) even more concise, we can include the depolarizing term into the definition of the Green's function

$$\underline{\mathbf{G}}^{\text{HM}}(\mathbf{r}, \mathbf{r}') = \mathcal{P.V.} \underline{\mathbf{G}}^{\text{HM}}(\mathbf{r}, \mathbf{r}') + \frac{\mathbf{L}}{k^2} \delta(\mathbf{r} - \mathbf{r}') , \quad (2.52)$$

where we have stipulated that whenever this operator is used, it should be used within the principal value framework.

Now that we have properly defined the dyadic Green's function, we are finally ready to tackle the problem at hand – the field of magnetic current sources radiating inside parallel plate waveguides. This will be the topic of the next subsection.

2.2.1.4 Dyadic Magnetic Green's Function for a Parallel Plate Waveguide

After a rather lengthy general discussion on Green's functions, we return to our original problem – given some impressed magnetic sources in a parallel plate waveguide of height h , what is total magnetic field at an arbitrary point inside it? The answer was given in the previous subsection – we can find the magnetic field using the radiation integral (2.25) upon finding the pertinent Green's dyadic. Whereas in the previous section we had found the general form of the Green's dyadic, now we have to find it for the particular case of a parallel plate waveguide (referred to from now on as *PPW*).

Referring back to Figure 2.3, which shows a PPW defined as follows - its bottom PEC plate is lying in the $z = 0$ plane, and the unit normal pointing in the z - direction, i.e. $\hat{\mathbf{n}} = \hat{\mathbf{z}}$, while the top plate lies in the $z = h$ plane, an isotropic, homogeneous dielectric medium of permittivity ε_r filling the space between plates. The structure is driven by an arbitrary magnetic current source of finite power. Our task is then clear – we must solve the operator differential equation (2.29), subject to boundary conditions

$$\begin{aligned} \hat{\mathbf{n}} \times (\nabla \times \underline{\mathbf{G}}^{\text{HM}}(\mathbf{r}, \mathbf{r}')) &= 0, \quad z \in \{0, h\} \\ \lim_{\rho \rightarrow \infty} \sqrt{\rho} (\nabla \times \underline{\mathbf{G}}^{\text{HM}}(\mathbf{r}, \mathbf{r}') + jk_r \hat{\boldsymbol{\rho}} \times \underline{\mathbf{G}}^{\text{HM}}(\mathbf{r}, \mathbf{r}')) &= 0 \end{aligned} \quad (2.53)$$

The meaning of the first condition is obvious – the tangential electric field created by a magnetic source must be zero at the PEC boundaries – bottom and top metal plates. The second one should be clear as well – the energy transfer should be towards infinity, i.e. in the transverse direction since the structure is bounded in z , i.e. the electromagnetic field should asymptotically behave as an outgoing cylindrical wave at infinity; in addition, the sources, in the words of Sommerfeld, “must be sources, not sinks of energy” [57, p. 189]. If one were to permit the addition of ingoing waves to the solution, its uniqueness would be rendered moot. Consequently, it would be of no use whatsoever. Now, we know the very general form of the Green's dyadic (2.45), from which we can clearly see that we must first

obtain the scalar Green's functions in order to derive it. Though such a form is convenient for the evaluation of the free-space Green's dyadic, where a scalar Green's function is easily obtained, it is not the case where planarly stratified media are present and the problem regions are closed by PEC boundaries. In such cases, it may be more convenient to use a representation in the basis along the stratification direction [64, Sec. 1.4], derivable by operator calculus tools. It allows the decomposition of fields into TE and TM contributions with respect to the stratification direction, simplifying the problem to finding two scalar potentials. This is the approach we adopt and here we will take a moment to flesh out its essential ideas.

We begin with an attempt to decompose the dyadic operator $\underline{\mathbf{T}}$ into transverse and longitudinal components, longitudinal meaning "in the stratification direction", i.e. in $\hat{\mathbf{z}}$ direction. For this purpose, we introduce the transverse nabla operator defined as

$\nabla_t = \nabla - \hat{\mathbf{z}}\partial_z$. First we decompose the unit dyad, our starting point being the 2-D (transverse) version of the identity $\nabla \times \nabla \times \mathbf{1} = \nabla \nabla - \nabla^2 \mathbf{1}$:

$$(\nabla \times \hat{\mathbf{z}}) \otimes (\nabla \times \hat{\mathbf{z}}) = \nabla_t \otimes \nabla_t - \nabla_t^2 \mathbf{1}, \quad (2.54)$$

from which follows

$$\nabla_t^2 \mathbf{1} = \nabla_t^2 \hat{\mathbf{z}} \otimes \hat{\mathbf{z}} + \nabla_t \otimes \nabla_t + (\nabla \times \hat{\mathbf{z}}) \otimes (\nabla \times \hat{\mathbf{z}}), \quad (2.55)$$

and, finally:

$$\mathbf{1} = \hat{\mathbf{z}} \otimes \hat{\mathbf{z}} + \frac{\nabla_t \otimes \nabla_t}{\nabla_t^2} + \frac{(\nabla \times \hat{\mathbf{z}}) \otimes (\nabla \times \hat{\mathbf{z}})}{\nabla_t^2}. \quad (2.56)$$

The inverse of the transverse Laplacian ∇_t^2 is defined as $\nabla_t^{-2} \nabla_t^2 = \nabla_t^2 \nabla_t^{-2} = \mathbf{1}$, and its explicit representation depends on the basis the functions it acts on are defined in. Now we have to decompose the $\nabla \otimes \nabla$ operator, which we can do using identities

$$\nabla \otimes \nabla = \nabla_t \otimes \nabla_t + (\nabla_t \otimes \hat{\mathbf{z}} + \hat{\mathbf{z}} \otimes \nabla_t) \partial_z + \hat{\mathbf{z}} \otimes \hat{\mathbf{z}} \partial_z^2, \quad (2.57)$$

and

$$(\nabla \times (\nabla \times \hat{\mathbf{z}})) \otimes (\nabla \times (\nabla \times \hat{\mathbf{z}})) = \nabla_t \otimes \nabla_t \partial_z^2 - (\nabla_t \otimes \hat{\mathbf{z}} + \hat{\mathbf{z}} \otimes \nabla_t) \partial_z \nabla_t^2 + \hat{\mathbf{z}} \otimes \hat{\mathbf{z}} \nabla_t^2 \nabla_t^2. \quad (2.58)$$

On multiplying (2.57) with ∇_t^2 and adding it to (2.58), one obtains

$$\nabla_t^2 \nabla \otimes \nabla = (\hat{\mathbf{z}} \otimes \hat{\mathbf{z}} \nabla_t^2 + \nabla_t \otimes \nabla_t) \nabla^2 - (\nabla \times \nabla \times \hat{\mathbf{z}}) \otimes (\nabla \times \nabla \times \hat{\mathbf{z}}), \quad (2.59)$$

and, upon "normalization" with ∇_t^2 ,

$$\nabla \otimes \nabla = \left(\hat{\mathbf{z}} \otimes \hat{\mathbf{z}} + \frac{\nabla_t \otimes \nabla_t}{\nabla_t^2} \right) \nabla^2 - \frac{(\nabla \times \nabla \times \hat{\mathbf{z}}) \otimes (\nabla \times \nabla \times \hat{\mathbf{z}})}{\nabla_t^2}. \quad (2.60)$$

Summing (2.56) and (2.60), we reexpress the $\underline{\mathbf{T}}$ operator as

$$\begin{aligned} \underline{\mathbf{T}} = \mathbf{1} + \frac{\nabla \otimes \nabla}{k^2} &= \frac{1}{k^2} \left(\hat{\mathbf{z}} \otimes \hat{\mathbf{z}} + \frac{\nabla_t \otimes \nabla_t}{\nabla_t^2} \right) (\nabla^2 + k^2) \\ &+ \left\{ \frac{(\nabla \times \hat{\mathbf{z}}) \otimes (\nabla \times \hat{\mathbf{z}})}{\nabla_t^2} - \frac{1}{k^2} \frac{(\nabla \times \nabla \times \hat{\mathbf{z}}) \otimes (\nabla \times \nabla \times \hat{\mathbf{z}})}{\nabla_t^2} \right\} \end{aligned} \quad (2.61)$$

Then, plugging (2.61) into (2.44), and applying boundary conditions (2.53), we deduce that in order for (2.44) to be a valid solution to (2.29), we need *two* scalar Green's functions, which we denote as G' and G'' , satisfying $\partial_n G' = 0|_{z=0,h}$ and $G'' = 0|_{z=0,h}$. The introduction of these functions is possible due to the fact that the operator $-(\nabla^2 + k^2)^{-1} \delta(\mathbf{r} - \mathbf{r}')$ has a "duplicity", i.e. one can construct it in two bases, each of the vectors spanning the bases satisfying either Dirichlet or Neumann boundary conditions, providing this degree of freedom. Therefore, the full form of the Green's dyadic is:

$$\begin{aligned} \underline{\mathbf{G}}^{\text{HM}}(\mathbf{r}, \mathbf{r}') &= -\frac{1}{k^2} \left(\hat{\mathbf{z}} \otimes \hat{\mathbf{z}} + \frac{\nabla_t \otimes \nabla_t}{\nabla_t^2} \right) \delta(\mathbf{r} - \mathbf{r}') \\ &- \frac{(\nabla \times \hat{\mathbf{z}}) \otimes (\nabla \times \hat{\mathbf{z}})}{\nabla_t^2} G'(\mathbf{r}, \mathbf{r}') - \frac{1}{k^2} \frac{(\nabla \times \nabla \times \hat{\mathbf{z}}) \otimes (\nabla \times \nabla \times \hat{\mathbf{z}})}{\nabla_t^2} G''(\mathbf{r}, \mathbf{r}'), \end{aligned} \quad (2.62)$$

(note that we used $\nabla = -\nabla'$) which, on introducing auxiliary potentials

$$\mathcal{S}(\mathbf{r}, \mathbf{r}') = \frac{G(\mathbf{r}, \mathbf{r}')}{-\nabla_t^2}, \quad (2.63)$$

subject to $\partial_n \mathcal{S}' = 0|_{z=0,h}$ and $\mathcal{S}'' = 0|_{z=0,h}$ (inherited from scalar Green's functions), becomes

$$\begin{aligned} \underline{\mathbf{G}}^{\text{HM}}(\mathbf{r}, \mathbf{r}') &= -\frac{1}{k^2} \left(\hat{\mathbf{z}} \otimes \hat{\mathbf{z}} + \frac{\nabla_t \otimes \nabla_t}{\nabla_t^2} \right) \delta(\mathbf{r} - \mathbf{r}') \\ &+ (\nabla \times \hat{\mathbf{z}}) \otimes (\nabla \times \hat{\mathbf{z}}) \mathcal{S}'(\mathbf{r}, \mathbf{r}') + \frac{1}{k^2} (\nabla \times \nabla \times \hat{\mathbf{z}}) \otimes (\nabla \times \nabla \times \hat{\mathbf{z}}) \mathcal{S}''(\mathbf{r}, \mathbf{r}') \end{aligned} \quad (2.64)$$

This form is valid in homogeneous, isotropic media, possibly closed by PEC boundaries, being our present case. Later we shall show how to obtain the Green's dyadic for inhomogeneous media, specializing it to the case of planar-stratified, piecewise-constant media.

Two remarkable facts about representation (2.64) should be noted – the delta term, taking into account the discontinuities of the Green's dyadic, naturally comes out of the inverse operator formalism. The longitudinal part corresponds to the depolarizing dyad obtained for a pillbox-shaped principal volume, as obtained in [66]. The transverse part, on the other hand, regularizes the Green's dyadic further, cancelling the spurious delta term coming from the differentiation of \mathcal{S}'' , as will be shown later on. Hence, this explicit decomposition has an upper hand with respect to other Green's dyadic representations, where this spurious transverse term is "hidden" and may be easily overlooked (see [79]).

To sum it all up, this representation allows one to scalarize the problem – one needs to find scalar Green's functions (2.63) which, upon applying pertinent dyadic differential operators on them, yield the Green's dyadic. These functions may be obtained in a multitude of ways,

but we opt for the transmission-line approach of Felsen and Marcuvitz, since it is the most intuitive, familiar and physical. Here we will present only its essentials necessary to derive the aforementioned scalar Green's functions, deferring the details to appendices as necessary, and referring the interested reader to [64, Ch. 2]

2.2.1.5 Transmission-line Rephrasing of the Problem

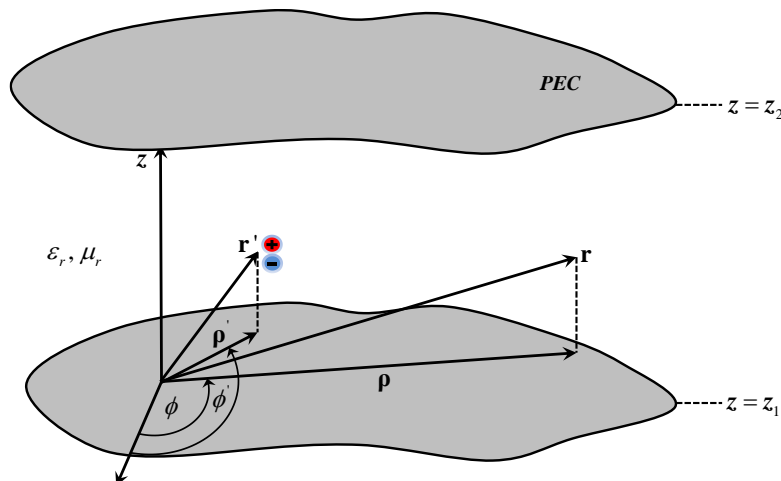
The transmission line formalism [80], championed in the microwave community for decades, rests on a simple premise – there is a “dominant” direction of energy transfer or change of geometrical and material parameters, as in closed microwave devices, so in the open antenna problems. From a mathematical perspective, the transmission-line formalism is nothing more than a prescribed set of recipes for solving ordinary differential equations, which are obtained from wave equations when coordinate separability of solutions applies, and phrased in terms of physical concepts. Since the guide cross-section does not usually vary, a modal representation is often possible to describe the functional dependence over the cross-section, whereas the longitudinal dependence problem may be advantageously formulated in terms of transmission-line concepts. In conjunction with the method of characteristic Green's functions [81], [73], it becomes a powerful framework for construction of solutions in the presence of sources. We note here that we try to adhere to Felsen's notation as best as possible all throughout this and the following subsections.

Our problem setup is as follows – a PPW can be considered as a cylindrical region of infinite extent in the transverse direction, closed by PEC boundaries at coordinates $z = z_1, z_2$, as shown in the following figure.

We begin the derivation by explicitly separating the transverse and longitudinal field dependence, effected by firstly reexpressing the curl Maxwell equations using $\nabla = \nabla_t + \hat{\mathbf{z}}\partial_z$ and $\mathbf{E} = \mathbf{E}_t + \mathbf{E}_z$, and then by scalarly pre-multiplying and post-cross-multiplying them by $\hat{\mathbf{z}}$, yielding:

$$\begin{aligned} \nabla_t (\mathbf{E}_t \times \hat{\mathbf{z}}) &= -j\omega\mu H_z - \mathbf{M}_z \\ \nabla_t (\mathbf{H}_t \times \hat{\mathbf{z}}) &= j\omega\varepsilon E_z + \mathbf{J}_z \\ -\partial_z \mathbf{E}_t + \nabla_t E_z &= j\omega\mu (\mathbf{H}_t \times \hat{\mathbf{z}}) + \mathbf{M}_t \times \hat{\mathbf{z}} \\ -\partial_z \mathbf{H}_t + \nabla_t H_z &= -j\omega\varepsilon (\mathbf{E}_t \times \hat{\mathbf{z}}) - \mathbf{J}_t \times \hat{\mathbf{z}} . \end{aligned} \tag{2.65}$$

Figure 2.5 Transversely unbounded, vertically parallel-plate bounded region



Then, one notes that z -components can be eliminated from the latter two equations, reexpressing them in terms of transverse ones using the first two equations:

$$\begin{aligned} -\partial_z \mathbf{E}_t &= j\omega\mu \left(\mathbf{1} + \frac{\nabla_t \nabla_t}{k^2} \right) (\mathbf{H}_t \times \hat{\mathbf{z}}) + \mathbf{M}_t \times \hat{\mathbf{z}} \\ -\partial_z \mathbf{H}_t &= j\omega\varepsilon \left(\mathbf{1} + \frac{\nabla_t \nabla_t}{k^2} \right) (\hat{\mathbf{z}} \times \mathbf{E}_t) + \hat{\mathbf{z}} \times \mathbf{J}_t . \end{aligned} \quad (2.66)$$

Hence, we can focus solely on transverse components, longitudinal ones being obtainable from the first pair of equations (2.65). A further simplification, in the form of separation of cross-sectional and longitudinal dependence of transverse fields, can be accomplished by introducing sets of suitable orthogonal vector eigenfunctions of the operator $\nabla_t \nabla_t$, which satisfy proper boundary conditions on the sidewall. They are defined as

$$\begin{aligned} \mathbf{e}'_i(\boldsymbol{\rho}) &= -\frac{\nabla_t \phi_i(\boldsymbol{\rho})}{k_{ii}'} , \mathbf{h}'_i(\boldsymbol{\rho}) = \hat{\mathbf{z}} \times \mathbf{e}'_i(\boldsymbol{\rho}) ; \\ (\nabla_t \nabla_t - k_{ii}'^2) \mathbf{e}'_i(\boldsymbol{\rho}) &= 0 , \nabla_t \nabla_t \mathbf{h}'_i(\boldsymbol{\rho}) = 0 ; \\ (\nabla_t^2 + k_{ii}'^2) \phi_i(\boldsymbol{\rho}) &= 0 , \phi_i(\boldsymbol{\rho}) = 0 , \boldsymbol{\rho} \in S \text{ if } k_{ii}' \neq 0 , \\ (\nabla_t^2 + k_{ii}'^2) \phi_i(\boldsymbol{\rho}) &= 0 , \partial_\nu \phi_i(\boldsymbol{\rho}) = 0 , \boldsymbol{\rho} \in S \text{ if } k_{ii}' = 0 , \end{aligned} \quad (2.67)$$

where from the first pair of equations (2.65) it is obvious that functions defined so will not contribute a magnetic field z -component ; hence they belong to the TM_z set. Moreover, these functions satisfy the following orthonormality relations

$$\int \mathbf{e}'_i(\boldsymbol{\rho}) \cdot \mathbf{e}'_j(\boldsymbol{\rho}) dS = \delta_{ij} \quad ; \quad \int \mathbf{h}'_i(\boldsymbol{\rho}) \cdot \mathbf{h}'_j(\boldsymbol{\rho}) dS = \delta_{ij} , \quad (2.68)$$

where the latter follows from the first one along with the rotational invariance of the scalar product. In addition, as a consequence of (2.68), the following power normalization holds for the entire set:

$$\int \mathbf{e}'_i(\boldsymbol{\rho}) \times \mathbf{h}'_j(\boldsymbol{\rho}) \cdot \hat{\mathbf{z}} dS = \delta_{ij} . \quad (2.69)$$

Analogously, one defines sets

$$\begin{aligned} \mathbf{h}''_i(\boldsymbol{\rho}) &= -\frac{\nabla_t \psi_i(\boldsymbol{\rho})}{k_{ii}''} , \mathbf{e}''_i(\boldsymbol{\rho}) = \mathbf{h}''_i(\boldsymbol{\rho}) \times \hat{\mathbf{z}} ; \\ (\nabla_t \nabla_t - k_{ii}''^2) \mathbf{h}''_i(\boldsymbol{\rho}) &= 0 , \nabla_t \nabla_t \mathbf{e}''_i(\boldsymbol{\rho}) = 0 ; \\ (\nabla_t^2 + k_{ii}''^2) \psi_i(\boldsymbol{\rho}) &= 0 , \partial_\nu \psi_i(\boldsymbol{\rho}) = 0 , \boldsymbol{\rho} \in S , \end{aligned} \quad (2.70)$$

which correspond to TE_z fields and satisfy analogous orthonormality relations. Then, it is possible to reexpress the transverse fields as

$$\begin{aligned} \mathbf{E}_t &= \sum_i V_i'(z) \mathbf{e}'_i(\boldsymbol{\rho}) + \sum_i V_i''(z) \mathbf{e}''_i(\boldsymbol{\rho}) , \\ \mathbf{H}_t &= \sum_i I_i'(z) \mathbf{h}'_i(\boldsymbol{\rho}) + \sum_i I_i''(z) \mathbf{h}''_i(\boldsymbol{\rho}) , \end{aligned} \quad (2.71)$$

the z -dependent modal voltages and currents being obtainable by a simple projection

$$A_i(z) = \int \mathbf{B}_i(\mathbf{r}) \cdot \mathbf{c}_i^*(\boldsymbol{\rho}) dS, \quad (2.72)$$

A_i being the modal quantity of interest (superscripts denoting the TM or TE set have been dropped for the sake of clarity), \mathbf{B}_i the transverse field or current of interest and \mathbf{c}_i^* the complex-conjugate (or more generally, adjoint) vector eigenfunction. If there are no discontinuities in the guide and it is of uniform cross-section, inserting the expansion (2.71) into (2.66) yields an infinite system of ordinary differential equations:

$$-d_z V_i = j\kappa_i Z_i I_i + v_i, \quad -d_z I_i = j\kappa_i Y_i V_i + i_i, \quad (2.73)$$

which are recognized as transmission-line equations, expressed in a suggestive form enabling the identification of transmission-line quantities such as the modal voltage V_i and current I_i , the propagation constant κ_i and modal impedance and admittance, Z_i and Y_i , respectively, given by

$$\kappa_i'' = \sqrt{k^2 - k_i''^2}, \quad Z_i' = \frac{\kappa_i'}{\omega\epsilon}, \quad Y_i' = \frac{\omega\mu}{\kappa_i'}. \quad (2.74)$$

Now our task is to relate the modal voltages and currents with sources. The linearity of equations (2.73) allows us to conjecture

$$\begin{aligned} V(z) &= -\int Z(z, z') i(z') dz' - \int T^V(z, z') v(z') dz', \\ I(z) &= -\int T^I(z, z') i(z') dz' - \int Y(z, z') v(z') dz', \end{aligned} \quad (2.75)$$

where the integral kernels are readily interpreted as follows - $Z(z, z')$ is the voltage at z due to a unit current generator located at z' , $T^V(z, z')$ is the voltage at z due to a unit voltage generator at z' , whereas $T^I(z, z')$ and $Y(z, z')$ are the corresponding currents due to the same excitations. The equations defining these quantities may be obtained by superposition - if one first considers the special excitations $i(z') = 0, v(z') = -\delta(z - z')$ in (2.75), and inserts the resulting voltages and currents into the transmission line equations, the following defining equations are obtained:

$$\begin{aligned} -d_z T^V(z, z') &= j\kappa ZY(z, z') - \delta(z - z'), \\ -d_z Y(z, z') &= j\kappa Y T^V(z, z'), \end{aligned} \quad (2.76)$$

whereas the equations for dual quantities may be obtained upon imposing the excitations $i(z') = -\delta(z - z'), v(z') = 0$:

$$\begin{aligned} -d_z T^I(z, z') &= j\kappa YZ(z, z') - \delta(z - z'), \\ -d_z Z(z, z') &= j\kappa Z T^I(z, z'). \end{aligned} \quad (2.77)$$

It should be stressed that the boundary conditions have not yet been stipulated, so these forms apply to general boundary conditions, and this formalism applies equally whether material parameters do or do not vary with z . In addition, it can be shown by classical methods that these functions satisfy the following useful reciprocity relations

$$\begin{aligned}
 Z(z, z') &= Z(z', z) , \\
 Y(z, z') &= Y(z', z) , \\
 T^V(z, z') &= -T^I(z, z') .
 \end{aligned} \tag{2.78}$$

Having established the basis for the transmission-line formalism, our task is now to apply it to derive the scalar Green's functions. For this purpose, we have to express them in terms of transmission-line quantities. This is readily accomplished in the following manner – we interchange the summation and differentiation operators in the modal expansions (2.71), obtaining formally

$$\begin{aligned}
 \mathbf{E}_t(\mathbf{r}) &= -\nabla_t V'(\mathbf{r}) - \nabla_t V''(\mathbf{r}) \times \hat{\mathbf{z}} , \\
 \mathbf{H}_t(\mathbf{r}) \times \hat{\mathbf{z}} &= -\nabla_t I'(\mathbf{r}) - \nabla_t I''(\mathbf{r}) \times \hat{\mathbf{z}} ,
 \end{aligned} \tag{2.79}$$

where the scalar functions are defined as

$$\begin{aligned}
 I'_i(\mathbf{r}) &= \sum_i \frac{I'_i(z) \phi_i(\boldsymbol{\rho})}{k_{ii}'}, & V'_i(\mathbf{r}) &= \sum_i \frac{V'_i(z) \phi_i(\boldsymbol{\rho})}{k_{ii}'}; \\
 I''_i(\mathbf{r}) &= \sum_i \frac{I''_i(z) \psi_i(\boldsymbol{\rho})}{k_{ii}''}, & V''_i(\mathbf{r}) &= \sum_i \frac{V''_i(z) \psi_i(\boldsymbol{\rho})}{k_{ii}''},
 \end{aligned} \tag{2.80}$$

which, in conjunction with (2.65), may be used to obtain the following field expressions

$$\begin{aligned}
 \mathbf{E}(\mathbf{r}) &= \frac{1}{j\omega\epsilon} \nabla \times \nabla \times (\hat{\mathbf{z}} I'(\mathbf{r})) - \nabla \times (\hat{\mathbf{z}} V''(\mathbf{r})) , \\
 \mathbf{H}(\mathbf{r}) &= \nabla \times (\hat{\mathbf{z}} I'(\mathbf{r})) + \frac{1}{j\omega\mu} \nabla \times \nabla \times (\hat{\mathbf{z}} V''(\mathbf{r})) ,
 \end{aligned} \tag{2.81}$$

demonstrating that only two scalar functions are needed to construct an arbitrary Maxwell field [53, Ch. 3] and, upon introducing substitutions $\pi'(\mathbf{r}) = I'(\mathbf{r}) / j\omega\epsilon$ and $\pi''(\mathbf{r}) = I''(\mathbf{r}) / j\omega\mu$, lead to the well-known Debye-Hertz potential field expressions [82, p. 32]

$$\begin{aligned}
 \mathbf{E}(\mathbf{r}) &= \nabla \times \nabla \times (\hat{\mathbf{z}} \pi'(\mathbf{r})) - j\omega\mu \nabla \times (\hat{\mathbf{z}} \pi''(\mathbf{r})) , \\
 \mathbf{H}(\mathbf{r}) &= j\omega\epsilon \nabla \times (\hat{\mathbf{z}} \pi'(\mathbf{r})) + \nabla \times \nabla \times (\hat{\mathbf{z}} \pi''(\mathbf{r})) .
 \end{aligned} \tag{2.82}$$

To connect the fields to sources in an explicit manner, we consider fields due to following point sources:

$$\mathbf{J} = \mathbf{J}_0 \delta(\mathbf{r} - \mathbf{r}') , \quad \mathbf{M} = \mathbf{M}_0 \delta(\mathbf{r} - \mathbf{r}') , \tag{2.83}$$

from which the modal source current and voltage amplitudes, necessary for the formulation of transmission-line problems (2.76) and (2.77) can be calculated as

$$\begin{aligned}
 v_i(z') &= \int \mathbf{M}(\mathbf{r}') \cdot \mathbf{h}_i^*(\boldsymbol{\rho}') dS + Z_i^* \int \mathbf{J}(\mathbf{r}') \cdot \mathbf{e}_{zi}^*(\boldsymbol{\rho}') dS , \\
 i_i(z') &= \int \mathbf{J}(\mathbf{r}') \cdot \mathbf{e}_i^*(\boldsymbol{\rho}') dS + Y_i^* \int \mathbf{M}(\mathbf{r}') \cdot \mathbf{h}_{zi}^*(\boldsymbol{\rho}') dS .
 \end{aligned} \tag{2.84}$$

If the modal source amplitudes are then inserted into (2.75), the following equations expressing the TM modal current and TE modal voltage are obtained, which on further simplification by using reciprocity relations (2.78) are given by

$$\begin{aligned}
 I_i'(z, z') &= -\left(v_i'(z') + \frac{1}{j\omega\epsilon} i_i'(z') d_z \right) Y_i'(z, z'), \\
 V_i''(z, z') &= -\left(i_i''(z') + \frac{1}{j\omega\mu} v_i''(z') d_z \right) Z_i''(z, z'),
 \end{aligned} \tag{2.85}$$

which, upon inserting (2.84) and exhibiting the vector transverse functions in full form as in (2.67) and (2.70), and then inserting into (2.80) finally yields

$$\begin{aligned}
 I_i'(\mathbf{r}, \mathbf{r}') &= \nabla' \times \nabla' \times \hat{\mathbf{z}} \mathcal{S}'(\mathbf{r}, \mathbf{r}') \cdot \mathbf{J}_0 - j\omega\epsilon \nabla' \times \hat{\mathbf{z}} \mathcal{S}'(\mathbf{r}, \mathbf{r}') \cdot \mathbf{M}_0, \\
 V_i''(\mathbf{r}, \mathbf{r}') &= j\omega\mu \nabla' \times \hat{\mathbf{z}} \mathcal{S}''(\mathbf{r}, \mathbf{r}') \cdot \mathbf{J}_0 + \nabla' \times \nabla' \times \hat{\mathbf{z}} \mathcal{S}''(\mathbf{r}, \mathbf{r}') \cdot \mathbf{M}_0,
 \end{aligned} \tag{2.86}$$

the \mathcal{S} potentials being

$$\begin{aligned}
 \mathcal{S}'(\mathbf{r}, \mathbf{r}') &= j\omega\epsilon \sum_i \frac{\phi_i(\boldsymbol{\rho}) \phi_i(\boldsymbol{\rho}')}{k_{ii}^2} Y_i'(z, z'), \\
 \mathcal{S}''(\mathbf{r}, \mathbf{r}') &= j\omega\mu \sum_i \frac{\psi_i(\boldsymbol{\rho}) \psi_i(\boldsymbol{\rho}')}{k_{ii}^2} Z_i''(z, z').
 \end{aligned} \tag{2.87}$$

It should be noted that the expansions in (2.87) are valid only if $k_{ii} \neq 0$, whereas the TEM mode should be treated separately and added to the S' expansion. Moreover, note that the **summation and differentiation may not necessarily commute**, as was implied in the derivation of (2.86). This behavior is usually the case when an integral representation of potentials is necessary, e.g. when the guide cross-section is unbounded, and impacts the definition of potentials and, consequently, fields, since one will have to keep the differentiation inside the spectral integrals to render them convergent, or explicitly isolate and discard the offending singularity.

Now, using these results in (2.81) and adding the source-region delta terms, we arrive at exactly (2.64)! Here we then note that the modal transmission-line TM current and TE voltage Green's functions are related to longitudinal scalar modal Green's functions as

$$g_{zi}'(z, z') = \frac{1}{j\omega\epsilon} Y_i'(z, z'), \quad g_{zi}''(z, z') = \frac{1}{j\omega\mu} Z_i''(z, z'). \tag{2.88}$$

Though one may be surprised why we had chosen to take the round trip to the dyadic magnetic Green's function expression by way of transmission-line formalism, when we had already obtained it by direct inverse operator formalism, it should be clear that by doing so we obtained explicit expressions from which one readily constructs the required scalar potentials. Moreover, the transmission-line phrasing provides a clear physical interpretation of quantities involved, favorable over the more abstract formalism and terminology of ordinary differential equations, since it makes the boundary conditions of scalar functions evident and provides a systematic way of field construction when stratified media are present.

To summarize, employing the transmission-line formalism, we reduced the problem of finding the scalar Green's functions to finding sets of orthonormal scalar eigenfunctions in the cross-section coordinates, and scalar transmission-line Green's functions in the longitudinal coordinates, which is the topic of the next subsection

2.2.1.6 Scalar Green's functions

Though there are several approaches to deriving scalar Green's functions, a particular one, chosen here, carries significant advantage with respect to alternative ones. The approach is the one of **characteristic Green's functions** [81], championed by Marcuvitz and his followers. It offers a powerful and general framework for deriving Green's functions and associated alternative representations in a straightforward way, along with the ability to derive normalized eigenfunctions in situations where the alternative frameworks do not make clear how to do so, particularly in open or semi-open problems when continuous spectrum is present. In this subsection we will lay out the basic theory behind this approach and apply it to derivation of required scalar Green's functions.

Firstly, we repeat the problem at hand – given a cylindrical region of infinite transverse extent and bounded by infinite PEC planes at $z = z_1, z_2$, find two functions G' and G'' , defined by

$$(\nabla^2 + k^2) \begin{matrix} G' \\ G'' \end{matrix}(\mathbf{r}, \mathbf{r}') = -\delta(\mathbf{r} - \mathbf{r}') ,$$

satisfying $\partial_z G' = 0$ and $G'' = 0$ at $z = z_1, z_2$, Sommerfeld radiation conditions as $\rho \rightarrow \infty$, and $\delta(\mathbf{r} - \mathbf{r}')$ can be “factored” as $\delta(\boldsymbol{\rho} - \boldsymbol{\rho}')\delta(z - z')$. Since we have shown that separability of transverse and longitudinal coordinate dependence applies in our case, we can introduce auxiliary Green's functions satisfying the following inhomogeneous Sturm-Liouville problems

$$\begin{aligned} (\nabla_t^2 + \lambda_t) g_t(\boldsymbol{\rho}, \boldsymbol{\rho}'; \sqrt{\lambda_t}) &= -\delta(\boldsymbol{\rho} - \boldsymbol{\rho}') , \\ (d_z^2 + \lambda_z) g_z(z, z'; \sqrt{\lambda_z}) &= -\delta(z - z') , \end{aligned} \quad (2.89)$$

where spectral parameters λ_t and λ_z are yet unspecified, but satisfy $k^2 = \lambda_t + \lambda_z$. These functions are then termed *characteristic Green's functions*. Knowledge of these functions and their singularities allows one to construct the 3-D Green's functions by appropriate contour integration, by virtue of the following theorem [82, Sec. 2.6]

$$\begin{aligned} G(\mathbf{r}, \mathbf{r}') &= -\frac{j}{2\pi} \oint_{C_{\lambda_z}} g_t(\boldsymbol{\rho}, \boldsymbol{\rho}'; \sqrt{k^2 - \lambda_z}) g_z(z, z'; \sqrt{\lambda_z}) d\lambda_z \\ &= -\frac{j}{2\pi} \oint_{C_{\lambda_t}} g_t(\boldsymbol{\rho}, \boldsymbol{\rho}'; \sqrt{\lambda_t}) g_z(z, z'; \sqrt{k^2 - \lambda_t}) \lambda_t d\lambda_t , \end{aligned} \quad (2.90)$$

where C_λ is a positively oriented curve enclosing the singularities of just one of the characteristic Green's functions in the respective spectral plane of choice, but no other. This relation is easily verified on insertion into the 3-D Green's function's defining equation and applying the residue theorem. Therefore, we are concerned with seeking the respective characteristic Green's functions. First, we focus on the transverse one. Since both TM and TE Green's functions obey the same boundary conditions at transverse infinity, they will necessarily be of the same form, easily expressed in closed form as [64, p. 447]

$$g_t(\boldsymbol{\rho}, \boldsymbol{\rho}'; \sqrt{\lambda_t}) = \frac{1}{4j} \sum_{n=-\infty}^{\infty} e^{-jn(\phi - \phi')} J_n(\sqrt{\lambda_t} \rho_<) H_n^{(2)}(\sqrt{\lambda_t} \rho_>) , \quad (2.91)$$

where J_n and $H_n^{(2)}$ are Bessel functions of order n , and Hankel functions of second kind and order n respectively, where the latter represent outgoing cylindrical waves dying off at infinity, chosen so due to the particular choice of time-dependence ($e^{j\omega t}$); $\rho_{>/<} = \max / \min \{\rho, \rho'\}$. The particular form (2.91) can be reexpressed in a succinct way using the Gegenbauer addition theorem (see [83]) as

$$g_t(\boldsymbol{\rho}, \boldsymbol{\rho}'; \sqrt{\lambda_t}) = \frac{1}{4j} H_0^{(2)}(\sqrt{\lambda_t} |\boldsymbol{\rho} - \boldsymbol{\rho}'|) . \quad (2.92)$$

The longitudinal characteristic Green's functions, on the other hand, are expressible in two equivalent forms, and we shall demonstrate both of them, since one or the other may be advantageous in a given situation. First, without reference to a specific boundary condition, a one-dimensional Green's function may be constructed if one is in possession of a complete, orthonormal eigenfunction set, i.e. each function satisfying the Sturm-Liouville eigenvalue problem $(d_z^2 + \lambda_{zi})f_i(z) = 0$ [77, Ch. 5], along with the orthonormality condition

$$\int f_i(\sqrt{\lambda_i}z) f_j(\sqrt{\lambda_j}z) w(z) dz = \delta_{ij} , \quad (2.93)$$

where $w(z)$ is the weight of the Sturm-Liouville problem and δ_{ij} being the Kronecker delta, or a standard delta function if the problem region is open or semi-open. If one then assumes that the Green's function can be expanded in terms of so-defined eigenfunctions, simple manipulations lead to the following well-known form

$$g_z(z, z'; \lambda_z) = -\sum_i \frac{f_i(\sqrt{\lambda_{zi}z}) f_i(\sqrt{\lambda_{zi}z'})}{\lambda_z - \lambda_{zi}} . \quad (2.94)$$

However, due to this function being divergent at $\lambda_z = \lambda_{zi}$, one might wonder if it represents a *unique solution*, and rightly so. Essentially, it will be a unique solution if the complex parameter λ_z is restricted as $\lambda_z \neq \lambda_{zi}$, since the contrary would imply the addition of a homogeneous solution to the Green's function, any number of which can be added to it while still satisfying the pertinent differential equation [82, Sec. 2.5]. Fortunately, one can still use this eigenfunction form while maintaining uniqueness of solution using analytic continuation as it applies to meromorphic functions (i.e. functions possessing *simple poles*) as well (which is our case), which enables us to show that uniqueness hold even in the limit $\lambda_z \rightarrow \lambda_{zi}$. This, finally, enables us to apply the residue theorem (or branch cut integration in case of open or semi-open problems) in (2.90). It is easily seen that this form of the characteristic Green's function might be convenient if the problem region is closed, leading to a discrete spectrum and, consequently, straight-forward normalization of eigenfunctions. Otherwise, an alternative method may be used, convenient when normalization may not be so obvious or simple (especially when continuous spectrum is allowed by the problem), which relies on the construction of the Green's function from linearly independent solutions of the homogeneous 1-D Sturm-Liouville equation (denoted as "SLE" from here on)

$$\left[d_z p(z) d_z + q(z) - \lambda w(z) \right] \varphi(z) = 0, \quad (2.95)$$

$p(z)$, $q(z)$ and $w(z)$ depending on whether TM currents or TE voltages are considered. From the observation that the Green's function must satisfy the homogeneous SLE for $z \neq z'$, we note that

$$g_z(z, z'; \lambda_z) = \begin{cases} A\varphi_1(\sqrt{\lambda_z}z), & z > z' \\ B\varphi_2(\sqrt{\lambda_z}z), & z < z' \end{cases}, \quad (2.96)$$

where the solutions φ_1 and φ_2 satisfy the proper boundary conditions at endpoints of the region. From the requirements of reciprocity, continuity at z' and the jump condition $p d_z g_z \Big|_{z'}^{\dot{z}'} = -1$, obtained by integrating the inhomogeneous SLE around z' , we obtain the following form of the characteristic Green's function

$$g_z(z, z'; \lambda_z) = \frac{\varphi_1(\sqrt{\lambda_z}z)\varphi_2(\sqrt{\lambda_z}z')}{-p(z')W(z')}, \quad (2.97)$$

$W(z')$ being the Wronskian determinant [82, p. 65] defined as

$$W(z') = (\varphi_1 d_z \varphi_2 - \varphi_2 d_z \varphi_1). \quad (2.98)$$

The product $p(z')W(z')$ can be shown to be independent of z' , but depends on λ_z in such a way that (2.97) will have simple poles in the λ_z plane coinciding with the poles of (2.94). It is remarkable that although the forms (2.97) and (2.94) are different, they are completely equivalent. This method of deriving the characteristic Green's function is particularly powerful, since it enables one to easily find normalized eigenfunctions when the normalization procedure is difficult or arcane, by the relation

$$-\frac{j}{2\pi} \oint_{C_{\lambda_z}} g_z(z, z'; \sqrt{\lambda_z}) d\lambda_z = \sum_i f_i(\sqrt{\lambda_{zi}}z) f_i(\sqrt{\lambda_{zi}}z') = \frac{\delta(z-z')}{w(z')}. \quad (2.99)$$

However, when using this form of Green's function in (2.90) to construct the 3-D Green's function, the denominator, in general, is a complicated function of λ_z . For example, when the problem possesses a discrete spectrum, one can evaluate the Green's function by residue theorem. To do so, one usually expands the denominator in a Taylor series around simple poles, which requires the knowledge of the derivative of the denominator, which can be a tedious task prone to errors, requiring consequently the use of symbolic software tools such as Mathematica or MATLAB if they are to be avoided. On the other hand, form (2.94) is more easily obtained in closed-domain problems, since a straightforward numerical normalization routine requiring nothing more than simple closed-form integrals can be easily implemented. Unfortunately, in order to find the positions of simple poles in the spectral plane, one has to solve a transcendental dispersion equation, regardless of which method is used. Since the internal problem, as we have defined it, always involves regions closed by PEC boundary conditions, we opted for the form (2.94).

We start with the TM longitudinal Green's function. The quantity of interest, in this case, is the admittance $Y'(z, z')$, its defining equation easily found from (2.76) to be

$$(d_z^2 + \kappa'^2)Y'(z, z') = -j\kappa'Y'\delta(z-z'), \quad (2.100)$$

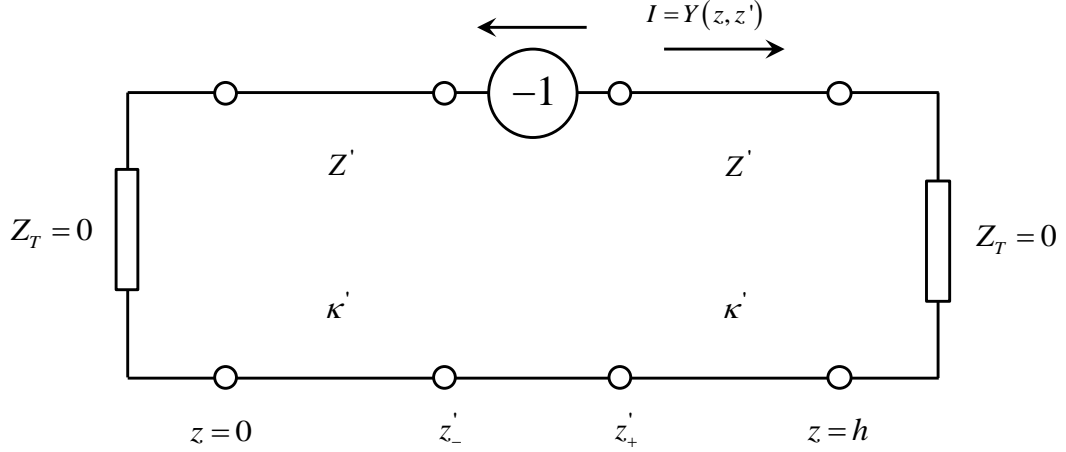
$\kappa'Y'$ equal to $\omega\varepsilon$, permittivity being the one of the medium at the observation point z .

Then, by defining $g_z(z, z'; \lambda_z) = \frac{1}{j\omega\varepsilon} Y'(z, z'; \lambda_z)$ we obtain the classical Green's function differential equation

$$(d_z^2 + \lambda_z') g_z'(z, z'; \lambda_z') = -\delta(z - z'), \quad (2.101)$$

g_z' readily interpretable from transmission-line equations as the current at a point z on a transmission line defined by the characteristic impedance Z' and propagation constant $\kappa' = \sqrt{\lambda_z'}$, due to a negative unit series voltage at z' , the scheme of which is given in Figure 2.6

Figure 2.6 Network scheme for the TM admittance Green's function calculation



Then it is obvious that the boundary conditions are such that $d_z g_z' \Big|_{z=z_1, z_2} = 0$, $z_1 = 0$ and $z_2 = h$, the particular end points chosen so for convenience and simplicity. Following the recipe of the first method, we first find normalized eigenfunctions of the operator $L_z \equiv d_z^2$, defined by

$$(d_z^2 + \lambda_{z_i}') f_i'(z) = 0, \quad (2.102)$$

satisfying the same boundary conditions as the Green's function itself. These are easily found to be

$$f_i'(z) = \sqrt{\frac{\varepsilon_i}{h}} \cos(\sqrt{\lambda_{z_i}'} z), \quad \lambda_{z_i}' = \frac{i\pi}{h}, \quad i \in \mathbb{Z}, \quad (2.103)$$

ε_i being the Neumann number defined as $\varepsilon_i = 1$ if $i = 0$, and $\varepsilon_i = 2$ otherwise. Substituting these eigenfunctions into the Green's function general expression (2.94), and subsequently into the construction contour integral (2.90), it is easily shown by virtue of the residue theorem (since the integration contour is such that it captures all the poles of the longitudinal Green's function, shown in Figure 2.7) that the 3-D spatial TM Green's function is given by the modal sum

$$G'(\mathbf{r}, \mathbf{r}') = \sum_{i=0}^{\infty} \frac{1}{4j} H_0^{(2)}(k_{z_i}' |\boldsymbol{\rho} - \boldsymbol{\rho}'|) \sqrt{\frac{\varepsilon_i}{h}} \cos(k_{z_i}' z) \sqrt{\frac{\varepsilon_i}{h}} \cos(k_{z_i}' z'), \quad (2.104)$$

from which it is evident that it will converge fast when the height of the waveguide is such that higher-order modes are in cut-off, due to the exponential convergence of the Hankel zero-order function for imaginary arguments, i.e.

$$H_0^{(2)}(k_{ii}'|\boldsymbol{\rho}-\boldsymbol{\rho}'|) \approx \sqrt{\frac{-2}{\pi j \alpha_{ii}'|\boldsymbol{\rho}-\boldsymbol{\rho}'|}} \exp\left(-\alpha_{ii}'|\boldsymbol{\rho}-\boldsymbol{\rho}'| + j\frac{\pi}{4}\right). \quad (2.105)$$

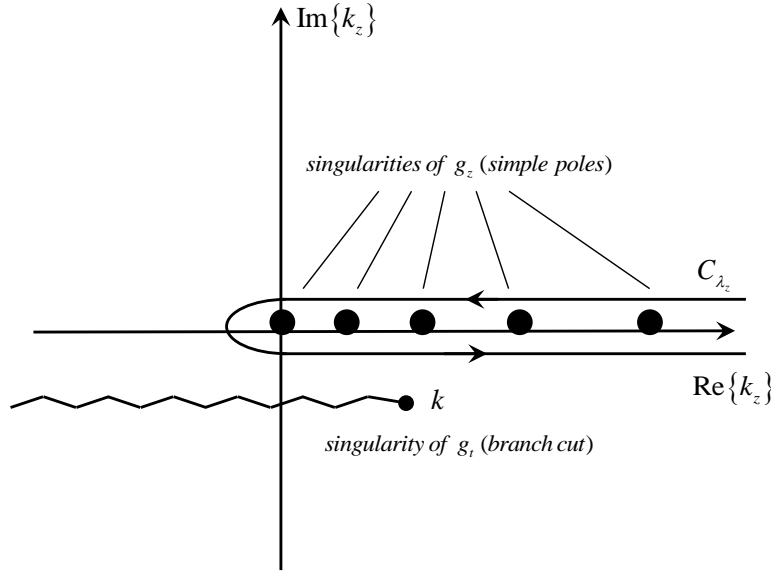
Another major advantage of this form is that it is expressed in terms of cylindrical functions, naturally conforming to cylindrical boundaries, and expressible in any shifted coordinate system by virtue of the Gegenbauer addition theorem, which will prove to be a crucial property in solving the problem of scattering off of cylinders in a PPW.

Finally, we can find the scalar potential necessary to construct the TM part of the Green's dyadic by $\mathcal{S}'(\mathbf{r}, \mathbf{r}') = -\frac{1}{\nabla_t^2} \mathbf{G}'(\mathbf{r}, \mathbf{r}')$, which one can attempt to obtain using the Green's

function construction integral over the contour capturing solely the singularities of the longitudinal GF (Figure 2.7), but now in the transverse wavenumber spectral plane where the integration contour avoids the Hankel function's logarithmic branch cut.

$$\begin{aligned} \mathcal{S}'(\mathbf{r}, \mathbf{r}') &= -\frac{1}{\nabla_t^2} \frac{-j}{2\pi} \oint_{C_{\lambda_i}} g_t(\boldsymbol{\rho}, \boldsymbol{\rho}'; \sqrt{\lambda_i}) g_z(z, z'; \sqrt{k^2 - \lambda_i}) \sqrt{\lambda_i} d\lambda_i \\ &= \frac{-j}{2\pi} \oint_{C_{\lambda_i}} \frac{1}{\lambda_i} g_t(\boldsymbol{\rho}, \boldsymbol{\rho}'; \sqrt{\lambda_i}) g_z(z, z'; \sqrt{k^2 - \lambda_i}) \sqrt{\lambda_i} d\lambda_i, \end{aligned} \quad (2.106)$$

Figure 2.7 Topology of the Green's function singularities in the plane



However, this direct spectral approach tacitly assumes the validity of interchange of integration and differentiation, which relies on the ability to regularize the integral, i.e. removing the offending $k_t \rightarrow 0$ singularity which makes the integral intractable. We show that this is not feasible in a straightforward way in appendix A. An alternative approach, based on the spectral theory of operators [84, p. 262], offers an unambiguous way to consistently define the odd-looking $-1/\nabla_t^2$ operator, relying on the possibility of finding an orthonormal, complete set of eigenfunctions of the operator ∇_t^2 .

Hence, let us assume we are in possession of a set $\{f_n\}$, each function in this set having compact support over the interval (ρ_1, ρ_2) and satisfying the transverse wave-equation under impedance-type boundary conditions, i.e.

$$(\nabla_t^2 + k_m^2) f_n(\boldsymbol{\rho}) = 0, \quad f_n + \gamma_{1,2} \partial_\rho f_n = 0 \Big|_{|\boldsymbol{\rho}|=\rho_1, \rho_2}. \quad (2.107)$$

Furthermore, let each function f_n be a member of the Hilbert space of square-integrable functions, i.e. $f_n \in H_{L_2}$, such that there exists a completeness relation

$$\langle f_n, f_m \rangle = \int_D f_n(\boldsymbol{\rho}) f_m^*(\boldsymbol{\rho}) d\boldsymbol{\rho} = \delta_{nm}, \quad (2.108)$$

induced by the complex-conjugate scalar product over the common support of the functions involved, denoted by D . Then by classical arguments of Fourier analysis it follows that this set may be used to construct an arbitrary function as

$$F(\boldsymbol{\rho}) = \sum_{n=1}^N a_n f_n(\boldsymbol{\rho}), \quad (2.109)$$

where the index n runs, in general, to infinity, and the expansion coefficients are obtained as

$$a_n = \int_D F(\boldsymbol{\rho}) f_n^*(\boldsymbol{\rho}) d\boldsymbol{\rho}. \quad (2.110)$$

Acting on an arbitrary function with ∇_t^2 , in view of the eigenfunction equation (2.107), yields

$$\nabla_t^2 F(\boldsymbol{\rho}) = - \sum_{n=1}^N k_m^2 a_n f_n(\boldsymbol{\rho}), \quad (2.111)$$

which can easily be represented in matrix form, due to the operator being diagonal in this basis, as

$$\nabla_t^2 F(\boldsymbol{\rho}) = \begin{pmatrix} -k_{t1}^2 & 0 & \cdot & \cdot & \cdot & 0 \\ 0 & -k_{t2}^2 & 0 & \cdot & \cdot & 0 \\ \cdot & 0 & \cdot & \cdot & \cdot & \cdot \\ \cdot & \cdot & \cdot & \cdot & \cdot & \cdot \\ \cdot & \cdot & \cdot & \cdot & \cdot & 0 \\ 0 & 0 & \cdot & \cdot & \cdot & -k_{tN}^2 \end{pmatrix} \begin{pmatrix} a_1 f_1 \\ a_2 f_2 \\ \cdot \\ \cdot \\ \cdot \\ a_N f_N \end{pmatrix}. \quad (2.112)$$

Now, since the operator $1/\nabla_t^2$ is defined by the relation $\frac{1}{\nabla_t^2} \nabla_t^2 = \mathbf{1}$, it follows that it can be represented as the matrix inverse to ∇_t^2

$$\frac{1}{\nabla_t^2} = \begin{pmatrix} \frac{1}{-k_{t1}^2} & 0 & \cdot & \cdot & \cdot & 0 \\ 0 & \frac{1}{-k_{t2}^2} & 0 & \cdot & \cdot & 0 \\ \cdot & 0 & \cdot & \cdot & \cdot & \cdot \\ \cdot & \cdot & \cdot & \cdot & \cdot & \cdot \\ \cdot & \cdot & \cdot & \cdot & \cdot & 0 \\ 0 & 0 & \cdot & \cdot & \cdot & \frac{1}{-k_{tN}^2} \end{pmatrix} \quad (2.113)$$

By induction one easily generalizes this result to $N \rightarrow \infty$, which is the commonly encountered scenario.

In our case, all of the above assumptions hold due to the self-adjointness of the ∇_t^2 operator, and since the transverse Green's function is representable in terms of its eigenfunctions, of the form $J_n(k_t \rho) e^{-jn\phi}$, $H_n^{(2)}(k_t \rho) e^{-jn\phi}$, as can be seen from (2.91). Hence, operationally, we obtain the S-potentials simply by dividing each term of the Green's function modal expansion by the square of the respective mode's transverse wavenumber! According to this method, the general form of the S-potential is

$$\mathcal{S}'(\mathbf{r}, \mathbf{r}') = \sum_{i=0}^{\infty} \frac{1}{4j} \frac{H_0^{(2)}(k_{ti} |\mathbf{p} - \mathbf{p}'|)}{k_{ti}^2} \sqrt{\frac{\epsilon_i}{h}} \cos(k_{zi} z) \sqrt{\frac{\epsilon_i}{h}} \cos(k_{zi} z'). \quad (2.114)$$

Here we point out a possible source of error, where the incorrect definition of the inverse Laplace operator results in an extra logarithmic term, as can be obtained by, e.g., formal derivation in the vein of Felsen and Marcuvitz [64, Sec. 1.4]. Doing so leads to a potential unbounded at infinity. Consequently, the slot admittance derived in terms of scalar potentials also diverges, unless a special gauge is used to keep all logarithmic terms zero. However, this leads to conceptual difficulties and should be avoided. Later on we shall demonstrate how to derive the slot admittance consistently (see Appendix A, pp. 140).

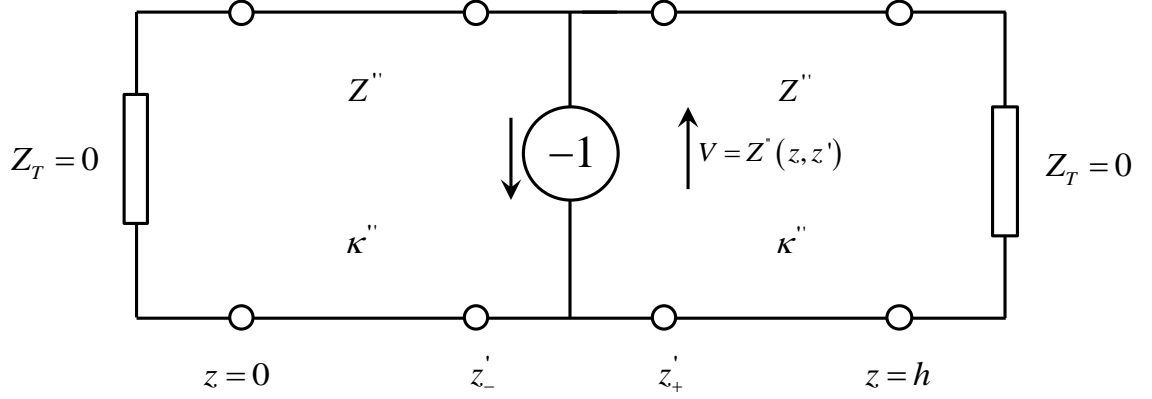
Analogously, we solve the TE problem by forming a transmission-line problem, this time deriving the TE impedance function $Z''(z, z')$, defined by

$$(d_z^2 + \kappa''^2) Z''(z, z') = -j\kappa'' Z'' \delta(z - z'), \quad (2.115)$$

$\kappa'' Z''$ equal to $\omega\mu$. Again, defining $g_z''(z, z'; \lambda_z'') = Z''(z, z'; \lambda_z'') / j\omega\mu$, we obtain the Green's function equation, where g_z'' is interpreted as the voltage on a transmission line at z due to a shunt negative unit current generator at z' , the scheme of which is shown in Figure 2.8. It satisfies $g_z''|_{z=z_1, z_2} = 0$, and again, in order to derive it, we must first solve the eigenvalue problem

$$(d_z^2 + \lambda_{zi}''^2) f_i''(z) = 0, \quad (2.116)$$

Figure 2.8 Network scheme for the TE impedance Green's function calculation



where the eigenfunctions are now found to be

$$f_i''(z) = \sqrt{\frac{2}{h}} \sin(\sqrt{\lambda_i''} z), \quad \lambda_i'' = \frac{i\pi}{h}, \quad i \in \mathbb{Z} / \{0\}. \quad (2.117)$$

Repeating the same steps as for the TM Green's function, we obtain

$$G''(\mathbf{r}, \mathbf{r}') = \sum_{i=1}^{\infty} \frac{1}{4j} H_0^{(2)}(k_{ii}'' |\boldsymbol{\rho} - \boldsymbol{\rho}'|) \sqrt{\frac{2}{h}} \sin(k_{zi}'' z) \sqrt{\frac{2}{h}} \sin(k_{zi}'' z'), \quad (2.118)$$

and, subsequently,

$$\mathcal{S}''(\mathbf{r}, \mathbf{r}') = -\frac{1}{\nabla_t^2} G''(\mathbf{r}, \mathbf{r}') = \sum_{i=1}^{\infty} \frac{1}{4j} \frac{H_0^{(2)}(k_{ii}'' |\boldsymbol{\rho} - \boldsymbol{\rho}'|)}{k_{ii}''^2} \sqrt{\frac{2}{h}} \sin(k_{zi}'' z) \sqrt{\frac{2}{h}} \sin(k_{zi}'' z'). \quad (2.119)$$

It should be noted that the TE modal sum runs from the first mode to infinity, whereas the TM modal sum runs from zeroth mode. This is due to the TM mode spectrum allowing the existence of a no-cutoff mode with no dependence on the longitudinal coordinate, i.e. a TEM mode. Even though in the general case one needs to define the TEM problem separately, here it was not necessary since the poles of both the TM and TE Green's function include the zeroth mode, but it contributes solely to the scalar TM potential because of its cosine dependence in z , whereas it is formally present in the TE potential but its contribution is zero due to sine dependence in z .

With the scalar potential functions known, it is possible to derive the field due to an arbitrary magnetic current source radiating into a PPW by (2.64). This serves as the starting point in the hybrid method, since it not only allows the calculation of the source field impinging on a cylinder embedded inside a PPW, but in case of presence of radiating slots on metal plates, also allows one to formulate an integral equation leading to an MoM problem.

2.2.1.7 What If the Medium Is Stratified?

Several recently proposed designs, including an LTCC slot array [30], an air-gap RLSA [85], to name a few, rely on the inclusion of multilayered dielectrics inside PPWs, thereby taking advantage of peculiar dispersion characteristics of such structures to broaden the operational band or of loss reduction by focusing the field away from conducting boundaries. Though largely in its experimental phase, such devices show promising features previously unobtainable by classical single-layer design. Therefore, it is of interest to include the effects of such loading into the general analysis of SIW structures.

In order to do so, we must rederive the PPW Green's function to apply to stratified media. Here we shall consider only longitudinally stratified media, since it is the most commonly encountered in practice. First we will give an extension of the field expressions derived in previous sections based on Maxwell's equations for an inhomogeneous medium, followed by comments on the differences between the single- and multi-layer case.

The problem, shown in Figure 2.9, consists of a number of stacked dielectric layers of varying thickness, stratified in the longitudinal direction. Each layer has constant permittivity and permeability within a layer, but may change abruptly from one to the other, and a source may be located in any layer or even span several, if not all, layers. In other words, layer material parameters are considered piecewise-constant. We shall keep this in mind since care must be exercised in order to define a consistent mathematical problem.

As can be noted already, trouble may arise at layer junctions, since there the derivatives of discontinuous material parameters, present in Maxwell's equations, give rise to terms containing delta functions and its derivatives which cannot be handled in a consistent manner. Therefore, one formulates a so-called "weak" Sturm-Liouville problem [77, Sec. 5.2], where one approaches the layer junction point in a limiting procedure, "artificially" stipulating the continuity of fields. This then bypasses the problems associated with discontinuous derivatives. However, we are getting ahead of ourselves here.

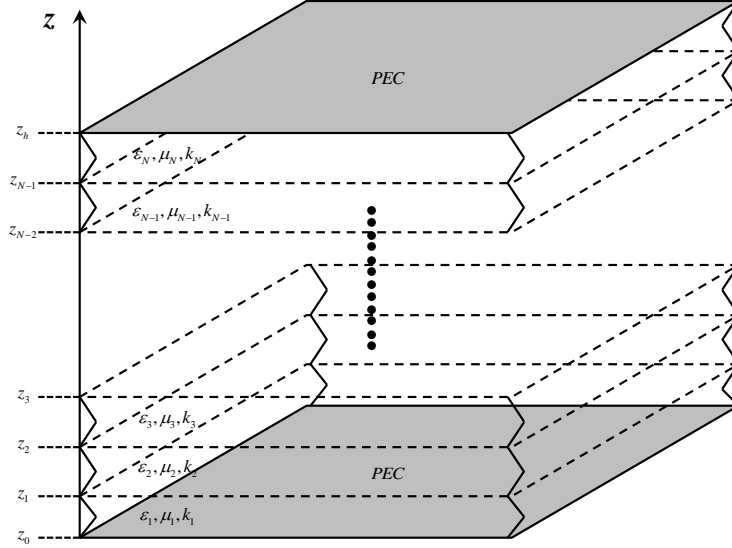
First, we observe that the whole procedure of decomposing the field dependence on transverse and longitudinal coordinates, contained in (2.65) through (2.78), holds for inhomogeneous media as well. The major complication in the general inhomogeneous case is the possible variability of the guide's cross-section shape, the difficulty there being the representation of a field's transverse functional dependence, which may become difficult, or even intractable. Now, after one introduces scalar potentials $I(\mathbf{r})$ and $V(\mathbf{r})$, the field expressions at source-free points (2.81) should be modified to read

$$\begin{aligned}\mathbf{E}(\mathbf{r}) &= j\omega\epsilon(z)\nabla\times\nabla\times(\hat{\mathbf{z}}I'(\mathbf{r})) - \nabla\times(\hat{\mathbf{z}}V''(\mathbf{r})), \\ \mathbf{H}(\mathbf{r}) &= \nabla\times(\hat{\mathbf{z}}I'(\mathbf{r})) + j\omega\mu(z)\nabla\times\nabla\times(\hat{\mathbf{z}}V''(\mathbf{r})),\end{aligned}\tag{2.120}$$

where the dependence of material parameters on the longitudinal coordinate is explicitly exhibited. Then, to connect the fields to sources, we repeat the same procedure as outlined in the previous section – we explicitly derive transmission-line currents and voltages due to a delta-source $I'(z, z')$, $V''(z, z')$ as follows. First, to find the TM current, we consider the special "concentrated" sources (2.83), which, after projecting them onto the modal basis, lead to a network representation in terms of negative unit voltage source $v_i'(z) = v_i'(z')\delta(z - z')$ connected in series to a z – transmission line, and a negative unit shunt current $i_i'(z) = i_i'(z')\delta(z - z')$, the line itself characterized by a z – dependent

propagation constant $\kappa'(z)$ and the associated characteristic impedance $Z'(z) = \kappa'(z) / \omega\mathcal{E}(z)$.

Figure 2.9 A PPW filled with a longitudinally stratified dielectric



From equations (2.75), still valid in the inhomogeneous case, one can relate, by linearity, the transmission-line current to transmission-line source voltage and current as

$$I_i'(z, z') = -Y_i'(z, z')v_i'(z') - T_i^{\text{I}'}(z, z')i_i'(z') . \quad (2.121)$$

Now, to simplify this relation, we use the symmetry property of TL Green's function $T_i^{\text{I}'}$

$$\begin{aligned} T_i^{\text{I}'}(z, z') &= -T_i^{\text{V}'}(z', z) \\ &= \frac{1}{j\kappa_i'(z')Y_i'(z')} d_z Y_i'(z', z) \\ &= \frac{1}{j\omega\mathcal{E}(z')} d_z Y_i'(z, z'), \end{aligned} \quad (2.122)$$

whereby we have reexpressed $T_i^{\text{I}'}$ in terms of Y_i' . Note that, as opposed to the single-layer case, the factor in front of the derivative of the admittance Green's function depends on the source coordinate. Then, inserting (2.122) into (2.121) yields

$$I_i'(z, z') = -\left(v_i'(z') + i_i'(z') \frac{1}{j\omega\mathcal{E}(z')} d_z \right) Y_i'(z, z') , \quad (2.123)$$

reducing our effort to finding solely the TM admittance Green's function. The TE voltage, obtained either by duality from (2.123) or straightforward derivation from (2.75), is obtained as

$$V_i''(z, z') = - \left(i_i''(z') + v_i''(z') \frac{1}{j\omega\mu(z')} d_z \right) Z_i''(z, z'). \quad (2.124)$$

Therefore, all we need to do now to express the field in terms of the assumed modal expansion is to explicitly express the source modal coefficients i_i and v_i by projection (2.84) onto the transverse field basis. The TM current, after expressing the vector modal functions explicitly and some relatively straightforward vector algebra, is expressed as

$$\begin{aligned} I'(\mathbf{r}, \mathbf{r}') &= \sum_i \frac{1}{j\omega\epsilon(z')} \nabla' \times \nabla' \times \hat{\mathbf{z}} \frac{\phi_i(\boldsymbol{\rho})\phi_i(\boldsymbol{\rho}')}{k_{ii}^2} Y_i'(z, z') \cdot \mathbf{J}_0 \\ &\quad - \sum_i \nabla' \times \hat{\mathbf{z}} \frac{\phi_i(\boldsymbol{\rho})\phi_i(\boldsymbol{\rho}')}{k_{ii}^2} Y_i'(z, z') \cdot \mathbf{M}_0, \end{aligned} \quad (2.125)$$

where, upon introducing a function

$$\mathcal{S}'(\mathbf{r}, \mathbf{r}') = \frac{1}{j\omega\epsilon(z')} \sum_i \frac{\phi_i(\boldsymbol{\rho})\phi_i(\boldsymbol{\rho}')}{k_{ii}^2} Y_i'(z, z'), \quad (2.126)$$

and assuming its uniform convergence, enabling the interchange of summation and differential operators, (2.125) can be expressed more concisely as

$$I'(\mathbf{r}, \mathbf{r}') = (\nabla' \times \nabla' \times \hat{\mathbf{z}} S'(\mathbf{r}, \mathbf{r}')) \cdot \mathbf{J}_0 - j\omega\epsilon(z') (\nabla' \times \hat{\mathbf{z}} S'(\mathbf{r}, \mathbf{r}')) \cdot \mathbf{M}_0, \quad (2.127)$$

while the TE voltage function can be similarly expressed as

$$V''(\mathbf{r}, \mathbf{r}') = (\nabla' \times \nabla' \times \hat{\mathbf{z}} S''(\mathbf{r}, \mathbf{r}')) \cdot \mathbf{M}_0 + j\omega\mu(z') (\nabla' \times \hat{\mathbf{z}} S''(\mathbf{r}, \mathbf{r}')) \cdot \mathbf{J}_0, \quad (2.128)$$

with

$$\mathcal{S}''(\mathbf{r}, \mathbf{r}') = \frac{1}{j\omega\mu(z')} \sum_i \frac{\psi_i(\boldsymbol{\rho})\psi_i(\boldsymbol{\rho}')}{k_{ii}^2} Z_i''(z, z'). \quad (2.129)$$

On inserting (2.127) and (2.128) into (2.120), with \mathbf{J}_0 being a zero-vector and assuming a piecewise-continuous medium, we obtain expressions for fields due to an arbitrarily oriented point magnetic current

$$\begin{aligned} \mathbf{H}(\mathbf{r}, \mathbf{r}') &= -j\omega\epsilon(z') (\nabla \times \hat{\mathbf{z}}) \otimes (\nabla \times \hat{\mathbf{z}}) S'(\mathbf{r}, \mathbf{r}') \cdot \mathbf{M}_0 \\ &\quad + \frac{1}{j\omega\mu(z')} (\nabla \times \nabla \times \hat{\mathbf{z}}) \otimes (\nabla \times \nabla \times \hat{\mathbf{z}}) S''(\mathbf{r}, \mathbf{r}') \cdot \mathbf{M}_0, \end{aligned} \quad (2.130)$$

from which the magnetic Green's dyadic is defined as

$$\begin{aligned} \underline{\mathbf{G}}^{\text{HM}}(\mathbf{r}, \mathbf{r}') &= (\nabla \times \hat{\mathbf{z}}) \otimes (\nabla \times \hat{\mathbf{z}}) \mathcal{S}'(\mathbf{r}, \mathbf{r}') \\ &\quad + \frac{1}{\omega^2 \epsilon(z') \mu(z')} (\nabla \times \nabla \times \hat{\mathbf{z}}) \otimes (\nabla \times \nabla \times \hat{\mathbf{z}}) \mathcal{S}''(\mathbf{r}, \mathbf{r}'). \end{aligned} \quad (2.131)$$

This form, resembling the single-layer form, bears no extra complexities with respect to the single-layer case. In essence, one only needs to find the appropriate modal TL Green's

functions, still expressible in closed form, albeit finding modal propagation constants requires a numerical or graphical procedure, as will be explained shortly.

Now we turn to the general solution to (2.131). It is clear that we need to find the scalar potentials, which can be accomplished by finding TM and TE Green's functions first. We use here the same formalism as the one applied in the previous section for the single-layer case, with slight modifications to render the analysis simpler and clearer. We begin by noting that the scalar Green's function can still be constructed from knowledge of characteristic Green's functions. Since the boundary conditions at transverse infinity are not affected by the medium stratification, and if the field is to be continuous, it has to have the same form in each layer, leading to the exact same form of solution as for the single-layer case (2.92), again both for TE and TM fields. However, the characteristic longitudinal Green's function complicates, since now one has to define it for all distinct source and observation point combinations. First, we need to obtain the differential equations for Green's functions of interest. This can be done as for the single-layer case, by virtue of transmission-line equations (2.76) and (2.77) from which one derives

$$\begin{aligned} \left(\varepsilon(z) d_z \frac{1}{\varepsilon(z)} d_z + \lambda'_z \right) Y'(z, z'; \lambda'_z) &= -j\omega \varepsilon(z') \delta(z - z') , \\ \left(\mu(z) d_z \frac{1}{\mu(z)} d_z + \lambda''_z \right) Z''(z, z'; \lambda''_z) &= -j\omega \mu(z') \delta(z - z') , \end{aligned} \quad (2.132)$$

Then, upon defining $Y' = j\omega \varepsilon(z') g'_z(z, z'; \lambda'_z)$ and $Z'' = j\omega \mu(z') g''_z(z, z'; \lambda''_z)$, the longitudinal characteristic Green's functions can be shown to satisfy

$$\left(\frac{1}{w(z)} d_z w(z) d_z + \lambda_z \right) g_z(z, z'; \lambda_z) = -\delta(z - z') \quad , \quad (2.133)$$

the weighting function $w(z)$ being $\varepsilon(z)$ for TM functions and $\mu(z)$ for TE functions, while λ_z is the spectral parameter of the layer containing the observation point, satisfying $\lambda_z = k_n^2 - \lambda_i$ (n denoting the observation layer). Here it is worth mentioning that the presence of discontinuous material boundaries does not affect the self-adjointness of the operator $L_z \equiv \frac{1}{w(z)} d_z w(z) d_z$, hence preserving the orthogonality property of its eigenfunction set, now under the *weighted* scalar product

$$\langle f, h \rangle_w = \int_a^b f(z) h(z) w(z) dz . \quad (2.134)$$

With the problem so defined, one can easily show that the characteristic longitudinal Green's function is of the form

$$g_z(z, z'; \lambda_z) = -w(z') \sum_i \frac{f_i(z) f_i(z')}{\lambda - \lambda_i} , \quad (2.135)$$

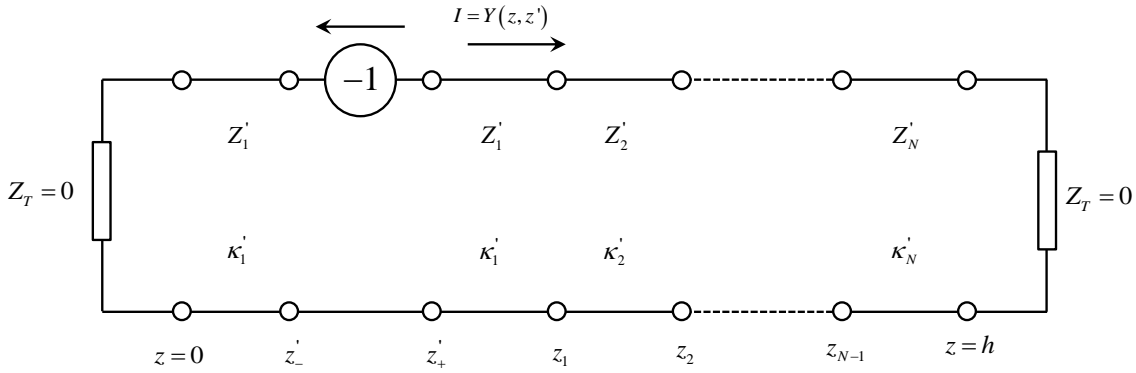
After this preliminary discussion, we shall solve the TM problem first. To this end, we seek the admittance Green's function, defined by

$$\left(\varepsilon(z) d_z \frac{1}{\varepsilon(z)} d_z + \lambda'_z \right) g'_z(z, z'; \lambda'_z) = -\delta(z - z'),$$

$$d_z g'_z(z, z'; \lambda'_z) = 0 \Big|_{z=0, h}, \quad [g'_z(z, z'; \lambda'_z)]_{d_n - \Delta}^{d_n + \Delta} = 0, \quad \left[\frac{1}{\varepsilon(z)} d_z g'_z(z, z'; \lambda'_z) \right]_{d_n - \Delta}^{d_n + \Delta} = 0,$$
(2.136)

where square brackets denote the difference between the value of the bracketed quantity just above and just below a layer junction, the adverb “just” meaning “infinitesimally”. Again, this problem can be formulated as a network problem, an exemplary scheme of which is given in Figure 2.10.

Figure 2.10 Network scheme of a TM problem in a longitudinally stratified, piecewise-continuous medium



In order to construct the Green’s function, we first construct the eigenfunction basis by solving the eigenfunction problem

$$\left(\varepsilon(z) d_z \frac{1}{\varepsilon(z)} d_z + \lambda'_{z_i, n} \right) f'_i(z) = 0, \quad d_z f'_i(z) = 0 \Big|_{z=0, h},$$

$$[f'_i(z)]_{d_n - \Delta}^{d_n + \Delta} = 0, \quad \left[\frac{1}{\varepsilon(z)} d_z f'_i(z) \right]_{d_n - \Delta}^{d_n + \Delta} = 0,$$
(2.137)

the eigenfunctions satisfying the same boundary conditions as the Green’s function itself. From the boundary conditions at PEC boundaries, it is clear that in layers adjacent to them the eigenfunctions must be of the form

$$f'_i(z) = \begin{cases} c_1 \cos(\kappa'_{i,1} z), & 0 \leq z < d_1 \\ c_N \cos(\kappa'_{i,N} (h - z)), & d_{N-1} \leq z \leq h \end{cases},$$
(2.138)

$\kappa'_{i,n} = \sqrt{\lambda'_{z_i, n}}$, while in the intermediate layers they must be of general form, hence

$$f'_i(z) = c_{i,n} \cos(\kappa'_{i,n} z) + s_{i,n} \sin(\kappa'_{i,n} z), \quad d_1 \leq z < d_{N-1},$$
(2.139)

n denoting the number of the layer containing the observation point, and $\lambda'_{i,n} = k_n^2 - \lambda'_i$. The continuity requirements on f'_i , interpreted as the current supported by the transmission line in the absence of sources, and the associated “voltage” r'_i , defined as

$$r_i' = -\frac{1}{j\kappa_i Y_i} d_z f_i' , \quad (2.140)$$

then enable one to express the coefficients c_n and s_n in terms of either c_1 or c_N .

Once all the coefficients of the eigenfunction are expressed in terms of a single-one, whichever one may choose, the eigenfunction can be normalised under the scalar product

$$\langle f_i', f_j' \rangle = \int_0^h f_i'(z) f_j'(z) \frac{1}{\varepsilon(z)} dz = \delta_{ij} . \quad (2.141)$$

In addition, the enforcement of boundary conditions leads to a linear system in unknown coefficients, the determinant of which leads to the dispersion equation relating the propagation constants in different layers. Unfortunately, since the unknown of this equation appears as the argument of products of irrational and trigonometric functions, it renders the equation transcendental, hence requiring a numerical solution. Once the propagation constants of eigenfunctions are known, one constructs the longitudinal characteristic Green's function as before, and uses it in the construction integral to finally obtain the 3D-Green's function, exhibiting the exact same general form as the single-layer scalar Green's function.

The TE problem is obtained by duality from the TM solution, or straightforward derivation analogous to the TM case. In particular, now we seek the impedance Green's function, defined by

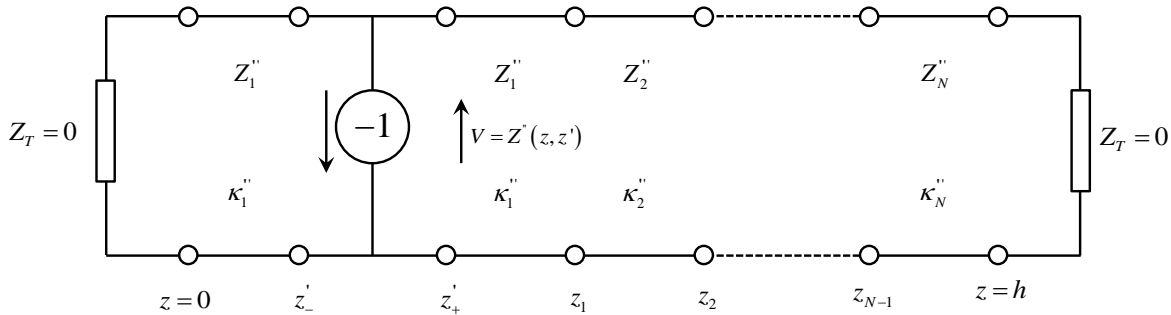
$$\begin{aligned} & \left(\mu(z) d_z \frac{1}{\mu(z)} d_z + \lambda_z'' \right) g_z''(z, z'; \lambda_z'') = -\delta(z - z') , \\ g_z''(z, z'; \lambda_z'') = 0 \Big|_{z=0, h} , & \left[g_z''(z, z'; \lambda_z'') \right]_{d_n - \Delta}^{d_n + \Delta} = 0 , \left[\frac{1}{\mu(z)} d_z g_z''(z, z'; \lambda_z'') \right]_{d_n - \Delta}^{d_n + \Delta} = 0 , \end{aligned} \quad (2.142)$$

the boundary conditions derived from (2.53), and its (exemplary) network scheme given in Figure 2.11. Again, we seek an eigenfunction basis from which we can construct the solution to (2.142), obtainable upon solving the general eigenvalue problem

$$\begin{aligned} & \left(\mu(z) d_z \frac{1}{\mu(z)} d_z + \lambda_{z_i}'' \right) f_i''(z) = 0 , f_i''(z) = 0 \Big|_{z=0, h} , \\ & \left[f_i''(z) \right]_{d_n - \Delta}^{d_n + \Delta} = 0 , \left[\frac{1}{\mu(z)} d_z f_i''(z) \right]_{d_n - \Delta}^{d_n + \Delta} = 0 , \end{aligned} \quad (2.143)$$

whose general solution is

$$f_i''(z) = \begin{cases} s_1 \sin(\kappa_{i,1}'' z) , & 0 \leq z < d_1 \\ s_n \sin(\kappa_{i,n}'' z) + c_n \cos(\kappa_{i,n}'' z) , & d_1 \leq z < d_{N-1} \\ s_N \sin(\kappa_{i,N}'' (h - z)) , & d_{N-1} \leq z \leq h \end{cases} . \quad (2.144)$$

Figure 2.11 Network scheme of a TE problem in a longitudinally stratified, piecewise-continuous medium


The eigenfunctions, so obtained, are then normalized under the scalar product

$$\langle f_i'', f_j'' \rangle = \int_0^h f_i''(z) f_j''(z) \frac{1}{\mu(z)} dz = \delta_{ij} \quad , \quad (2.145)$$

and their respective eigenvalues are found from the pertinent dispersion equation, depending on the specific geometric parameters of the loaded waveguide. From the eigenfunction basis one constructs the Green's function as in the TM case.

Example

To give a concrete example of a multilayered medium Green's function, we shall demonstrate its derivation for a PPW loaded with a two-layer medium, i.e. a medium composed of two planar slabs of differing permittivity, joined at $z = d$. First, according to the recipe laid out a moment ago, we solve the eigenvalue problems to find the general forms of eigenfunctions (with slight abuse of notation) as

$$f_i'(z) = \begin{cases} c_{i,1} \cos(\kappa'_{i,1} z) , & 0 \leq z < d \\ c_{i,2} \cos(\kappa'_{i,2} (h - z)) , & d \leq z \leq h \end{cases} , \quad (2.146)$$

$$f_i''(z) = \begin{cases} s_{i,1} \sin(\kappa'_{i,1} z) , & 0 \leq z < d \\ s_{i,2} \sin(\kappa'_{i,2} (h - z)) , & d \leq z \leq h \end{cases} .$$

Then the continuity requirements at $z = d$ enable us to connect the unknown coefficients of the respective eigenfunctions to give

$$c_{i,2} = c_{i,1} \frac{\cos(\kappa'_{i,1} d)}{\cos(\kappa'_{i,2} (h - d))} , \quad s_{i,2} = s_{i,1} \frac{\sin(\kappa'_{i,1} d)}{\sin(\kappa'_{i,2} (h - d))} , \quad (2.147)$$

and give the TM and TE dispersion equations, respectively

$$Z'_{i,1} \sin(\kappa'_{i,1} t_1) \cos(\kappa'_{i,2} t_2) + Z'_{i,2} \cos(\kappa'_{i,1} t_1) \sin(\kappa'_{i,2} t_2) = 0 , \quad (2.148)$$

$$Y''_1 \cos(\kappa''_{i,1} t_1) \sin(\kappa''_{i,2} t_2) + Y''_2 \sin(\kappa''_{i,1} t_1) \cos(\kappa''_{i,2} t_2) = 0 ,$$

their solutions determining the eigenvalues of the problem, obtained either graphically (see for example FELSEN, 1973., p. 292) or numerically by a root-finding algorithm. Here the parameters t denotes the thickness of each layer. Though these equations may seem a bit inconspicuous, if we rewrite them as

$$\begin{aligned} Z'_{i,1} \operatorname{tg}(\kappa'_{i,1} t_1) + Z'_{i,2} \operatorname{tg}(\kappa'_{i,2} t_2) &= 0, \\ Y''_{i,1} \operatorname{ctg}(\kappa''_{i,1} t_1) + Y''_{i,2} \operatorname{ctg}(\kappa''_{i,2} t_2) &= 0, \end{aligned} \quad (2.149)$$

we can give their interpretation immediately as the sum of terminal impedances/admittances at the bottom and the top (from the “left” and “right” as commonly said in the microwave community) of the structure at the layer junction, which is zero, implying a resonance, i.e. (2.149) is the *transmission-line resonance condition*.

Now, since one needs a *normalized* set of eigenfunctions to construct the characteristic Green's function, we normalize it under the weighted scalar product which yields

$$\begin{aligned} c_{i,1} \equiv c'_i &= \left\{ \frac{1}{\varepsilon_1} \left(\frac{\sin(\kappa'_{i1} d) \cos(\kappa'_{i1} d)}{2\kappa'_{i1}} + \frac{1}{2} d \right) \right. \\ &\quad \left. + \frac{1}{\varepsilon_2} \left(\frac{\cos(\kappa'_{i1} d)}{\cos(\kappa'_{i2} (h-d))} \right)^2 \left(\frac{\sin(\kappa'_{i2} (h-d)) \cos(\kappa'_{i2} (h-d))}{2\kappa'_{i2}} + \frac{1}{2} (h-d) \right) \right\}^{-1/2}, \\ s_{i,1} \equiv c''_i &= \left\{ \frac{1}{\mu_1} \left(-\frac{\sin(\kappa''_{i1} d) \cos(\kappa''_{i1} d)}{2\kappa''_{i1}} + \frac{1}{2} d \right) \right. \\ &\quad \left. + \frac{1}{\mu_2} \left(\frac{\sin(\kappa''_{i1} d)}{\sin(\kappa''_{i2} (h-d))} \right)^2 \left(-\frac{\sin(\kappa''_{i2} (h-d)) \cos(\kappa''_{i2} (h-d))}{2\kappa''_{i2}} + \frac{1}{2} (h-d) \right) \right\}^{-1/2}. \end{aligned} \quad (2.150)$$

Finally, the Green's functions, obtained by the construction integral (2.90) are

$$\begin{aligned} G'(\mathbf{r}, \mathbf{r}') &= \sum_i \frac{1}{4j} H_0^{(2)}(k'_i |\mathbf{p} - \mathbf{p}'|) \left\{ \begin{aligned} &\frac{1}{\varepsilon_1} c'_i \cos(\sqrt{\lambda'_{i1}} z) c'_i \cos(\sqrt{\lambda'_{i1}} z'), & 0 \leq \{z, z'\} < d \\ &\frac{1}{\varepsilon_1} c'_i \xi'_i \cos(\sqrt{\lambda'_{i2}} (h-z)) c'_i \cos(\sqrt{\lambda'_{i1}} z'), & d \leq z \leq h, 0 \leq z' < d \\ &\frac{1}{\varepsilon_2} c'_i \cos(\sqrt{\lambda'_{i1}} z) c'_i \xi'_i \cos(\sqrt{\lambda'_{i2}} (h-z')), & 0 \leq z < d, d \leq z' \leq h \\ &\frac{1}{\varepsilon_2} c'_i \xi'_i \cos(\sqrt{\lambda'_{i2}} (h-z)) c'_i \xi'_i \cos(\sqrt{\lambda'_{i2}} (h-z')), & d \leq \{z, z'\} \leq h \end{aligned} \right. \\ G''(\mathbf{r}, \mathbf{r}') &= \sum_i \frac{1}{4j} H_0^{(2)}(k''_i |\mathbf{p} - \mathbf{p}'|) \left\{ \begin{aligned} &\frac{1}{\mu_1} c''_i \sin(\sqrt{\lambda''_{i1}} z) c''_i \sin(\sqrt{\lambda''_{i1}} z'), & 0 \leq \{z, z'\} < d \\ &\frac{1}{\mu_1} c''_i \xi''_i \sin(\sqrt{\lambda''_{i2}} (h-z)) c''_i \sin(\sqrt{\lambda''_{i1}} z'), & d \leq z \leq h, 0 \leq z' < d \\ &\frac{1}{\mu_2} c''_i \sin(\sqrt{\lambda''_{i1}} z) c''_i \xi''_i \sin(\sqrt{\lambda''_{i2}} (h-z')), & 0 \leq z < d, d \leq z' \leq h \\ &\frac{1}{\mu_2} c''_i \xi''_i \cos(\sqrt{\lambda''_{i2}} (h-z)) c''_i \xi''_i \cos(\sqrt{\lambda''_{i2}} (h-z')), & d \leq \{z, z'\} \leq h \end{aligned} \right. \end{aligned} \quad (2.151)$$

where $\xi_i = f_{i1} / f_{i2}|_{z=d}$. We note here that the Green's functions, so defined, satisfy the following reciprocity property

$$\frac{1}{w(\mathbf{r}')}G(\mathbf{r},\mathbf{r}') = \frac{1}{w(\mathbf{r})}G(\mathbf{r}',\mathbf{r}), \quad (2.152)$$

rendering their derivation easier, since the knowledge of a Green's function for one source/observation point combination implies the knowledge of the converse combination.

It is now clear where the main complication with respect to the single-layer case lies – the necessity of defining the Green's function for each source/observation point combination. Though tedious, the derivation of Green's functions in layered media may be automated using the T-matrix formalism, as already mentioned, whereby a linear relation is established between the voltages and currents (to be thought of in a generalized sense) at two different points on a transmission line by

$$\begin{pmatrix} V_2 \\ I_2 \end{pmatrix} = \begin{pmatrix} A & B \\ C & D \end{pmatrix} \begin{pmatrix} V_1 \\ I_1 \end{pmatrix}, \quad (2.153)$$

the linear operator usually denoted by $\underline{\mathbf{T}}$. Now, in our case it is convenient to relate the voltage and current of a given mode in one medium to the ones in another medium. The T-matrix relating the voltages and currents at two points in a *given medium* (or, to use the transmission-line terminology, transmission-line section) is [86]

$$\underline{\mathbf{T}} = \begin{pmatrix} \cos(\kappa_{i,n}\Delta z) & jZ_{i,n} \sin(\kappa_{i,n}\Delta z) \\ j\frac{1}{Z_{i,n}} \sin(\kappa_{i,n}\Delta z) & \cos(\kappa_{i,n}\Delta z) \end{pmatrix}, \quad (2.154)$$

index i denoting the mode under consideration, and n the medium (layer), whereas $\Delta z = z_2 - z_1$. The major advantage of using this formalism is the simple handling of a large number of different sections by merely *cascading* the T-matrices of each section. To be more specific, one relates the voltage-current vector at a point in the transmission-line by *propagating* it towards the point of interest using the T-matrix of each section we are propagating it through, i.e.

$$\begin{pmatrix} V_n \\ I_n \end{pmatrix} = \prod_{j=1}^n \underline{\mathbf{T}}_j \begin{pmatrix} V_1 \\ I_1 \end{pmatrix}. \quad (2.155)$$

This allows straightforward construction of eigenfunctions from the voltages and currents in one of the extremal layers.

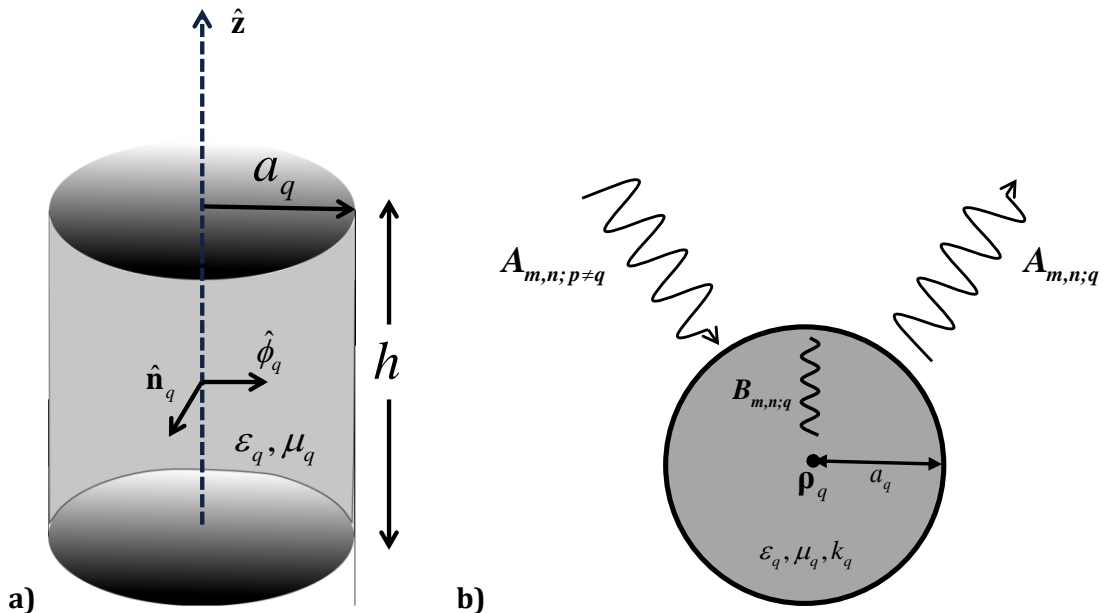
Though at this point it may not be obvious why this particular approach to deriving dyadic Green's functions (abbreviated as "DGF" from here on) is more convenient than the alternatives (e.g. [87], [88]), it will become apparent in the following sections dealing with the formulation of method-of-moments problems. For now it should be stressed that the SMF formalism provides an explicit procedure for construction of DGFs due to the straightforward isolation of singular terms inherent in the inverse operator approach used. Moreover, it enables one to deal primarily with scalar quantities, as opposed to vector or dyadic ones in other common approaches. In addition, the recasting of the problem in transmission-line terminology gives a conceptually familiar, intuitive physical picture of the abstract mathematical manipulations involved. The use of the characteristic GF approach enables recipe-like construction of normalized eigenfunctions, even in situations where the normalization procedure is not at all obvious.

2.2.1.8 Scattering by Cylindrical Posts

With the DGF derived, we can find the field due to an arbitrary, well-behaved magnetic current. Now we turn to the problem of scattering off cylindrical posts, ever-present in SIW devices. The approach adopted here is based on works by [89], [41]. We will show how to model the field scattered off a post, and how to find the field scattered by a number of posts by solving a reduced linear system which represents the approximate self-consistency condition when the boundary conditions on posts are enforced. In addition, we provide a rule-of-thumb criterion for choosing the number of modes sufficient to accurately describe the electromagnetic interaction in a typical SIW problem, and discuss the orthogonality of modes scattered by posts. Firstly, let us consider a general, cylindrical post of circular cross-section, running from the bottom to the top plate of a PPW, as shown in Figure 2.12. It can have any radius and might be made either from metal or a dielectric material. The only restriction we place upon it is that it is not multilayered, i.e. not stratified in the $\hat{\rho}$ - direction, which is the unit vector of the displacement vector spanning from the cylinder axis to an arbitrary observation point. Though an interesting case, we neglect it since it is, to the author's knowledge, not commonly present in practical SIW devices. The field incident on such a cylinder may have an arbitrary functional dependence, and will induce currents on it, of polarization or conduction kind. From the results in the previous subsection, it is evident that the exciting field will assume a form of a modal sum. Hence, it is only natural to expect that the field scattered of a cylinder will have a similar form in the same basis, since in source-free regions both fields satisfy the same differential equations

$$\begin{pmatrix} \nabla \times \nabla \times - k^2 \\ \mathbf{H}(\mathbf{r}) \end{pmatrix} = 0 \quad , \quad (2.156)$$

Figure 2.12 a) Geometry of a typical SIW post ; b) Typical post-scattering problem



and same boundary conditions on metal plates and, possibly, at material junctions if inhomogeneous materials exist within the PPW. In addition, these fields will be decomposable into TE and TM parts. Therefore, it will be possible to express a general scattered field as

$$\mathbf{H}_q^s(\mathbf{r}, \mathbf{r}_q) = \sum_{m,n} A_{m,n}^e \mathbf{M}_{m,n}^e(\mathbf{r}, \mathbf{r}_q) + \sum_{m,n} A_{m,n}^h \mathbf{N}_{m,n}^h(\mathbf{r}, \mathbf{r}_q), \quad (2.157)$$

index q denoting the q -th cylinder, vector functions \mathbf{M} and \mathbf{N} being conveniently normalized functions representing the TM and TE modal field, respectively, with coefficients $A_{m,n}$ being their amplitudes, independent of \mathbf{r}, \mathbf{r}_q . Indexes m and n enumerate the longitudinal and azimuthal mode in question, respectively, since, in order to fully describe the field, one must allow a general variation in z , ρ and ϕ . It should be stressed that there is a certain amount of freedom in choosing the form of modal fields, reflected in the choice of the normalization and radial field dependence. To find the most convenient one, we ask the following question – given a known impressed magnetic current, how does the field inside the PPW look like? Though it may sound offbeat, it will lead us to the consideration of the general form of *modes* excited in the PPW. Using the results of previous subsections, first for the single-layer case (which will serve as the conceptual basis for later extension to stratified media), we can express the impressed field succinctly as

$$\begin{aligned} \mathbf{H}_{imp}(\mathbf{r}) = & -j\omega\epsilon \int \left((\nabla \times \hat{\mathbf{z}}) \otimes (\nabla' \times \hat{\mathbf{z}}) \sum_m \frac{g_{t,m}'(\boldsymbol{\rho}, \boldsymbol{\rho}')}{-\nabla_t'^2} i_m'(z) i_m'(z') \right. \\ & \left. + \frac{1}{k^2} (\nabla \times \nabla \times \hat{\mathbf{z}}) \otimes (\nabla' \times \nabla' \times \hat{\mathbf{z}}) \sum_m \frac{g_{t,m}''(\boldsymbol{\rho}, \boldsymbol{\rho}')}{-\nabla_t'^2} v_m''(z) v_m''(z') \right) \cdot \mathbf{M}(\mathbf{r}') d\mathbf{r}', \end{aligned} \quad (2.158)$$

where i_m' and v_m'' are normalized TM and TE longitudinal mode functions. We discarded the source corrections appearing in (2.64) since we naturally assume that no cylinder overlaps with the source region, therefore $\mathbf{r} \neq \mathbf{r}'$. Now, the ultimate goal here is to separate out the observation and source-coordinate functional dependence, leading to a form resembling the natural cavity modes. From (2.158) it is apparent that the longitudinal part is already separated. However, the transverse part has $\boldsymbol{\rho}$ and $\boldsymbol{\rho}'$ tangled (see (2.159)). In order to mitigate this, we recall that ultimately we have to find the field impinging on the surface of the post (possibly penetrating its interior if it is dielectric) to construct a boundary problem. In a global coordinate system, this becomes nigh intractable, since a parametrization of the cylinder's surface must be found, and for each one that is not centered in the origin of this global system, it presents an ordeal. Hence, we shall reexpress the impinging field in the coordinate system *centered on the cylinder's axis at $\boldsymbol{\rho}_q$* . This is facilitated by a standard trick – one uses the Gegenbauer addition theorem, whereby the transverse GF is transformed as

$$\begin{aligned} g_{t,m} &= \frac{1}{4j} H_0^{(2)}(k_{t,m} |\boldsymbol{\rho} - \boldsymbol{\rho}'|) = \frac{1}{4j} H_0^{(2)}(k_{t,m} |\boldsymbol{\rho}' - \boldsymbol{\rho}|) = \frac{1}{4j} H_0^{(2)}\left(k_{t,m} \left| (\boldsymbol{\rho}' - \boldsymbol{\rho}_q) - (\boldsymbol{\rho} - \boldsymbol{\rho}_q) \right| \right) \\ &= \frac{1}{4j} \sum_{n=-\infty}^{+\infty} J_n(k_{t,m} R_q^<) H_n^{(2)}(k_{t,m} R_q^>) e^{-jn(\phi_s - \phi_c)}, \end{aligned} \quad (2.159)$$

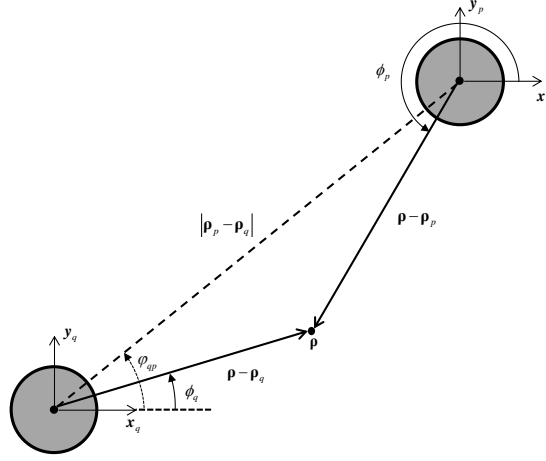
the pertinent coordinates given in Figure 2.13. Now we can integrate out the source-coordinate dependence in (2.158) since

$$\mathbf{H}(\mathbf{r}) = -j\omega\varepsilon \int \left\{ D_1 \otimes D_1' \sum_m \frac{1}{-\nabla_t'^2} \left(\frac{1}{4j} \sum_{n=-\infty}^{+\infty} J_n(k_{t,m}' R_q^<) H_n^{(2)}(k_{t,m}' R_q^>) e^{-jn(\phi_s - \phi_c)} \right) i_m'(z) i_m'(z') \right. \\ \left. + \frac{1}{k^2} D_2 \otimes D_2' \sum_m \frac{1}{-\nabla_t'^2} \left(\frac{1}{4j} \sum_{n=-\infty}^{+\infty} J_n(k_{t,m}'' R_q^<) H_n^{(2)}(k_{t,m}'' R_q^>) e^{-jn(\phi_s - \phi_c)} \right) v_m''(z) v_m''(z') \right\} \cdot \mathbf{M}(\mathbf{r}') d\mathbf{r}', \quad (2.160)$$

where $D_1 = \nabla \times \hat{\mathbf{z}}$, $D_2 = \nabla \times \nabla \times \hat{\mathbf{z}}$ (primed operators denote action on functions dependant on source coordinates).

If now we assume $R_q^< = |\boldsymbol{\rho}' - \boldsymbol{\rho}_q|$, thus “forcing” the outgoing wave representation, we finally arrive to the field representation of source-excited, incoming waves in the global coordinate system by *outgoing waves in the cylinder system*

Figure 2.13 Geometrical parameters related to the Gegenbauer addition theorem



$$\mathbf{H}(\mathbf{r}) = -j\omega\varepsilon \sum_m \frac{1}{4j} \sum_n D_1 \frac{H_n^{(2)}(k_{t,m}' |\boldsymbol{\rho} - \boldsymbol{\rho}_q|) e^{-jn\phi_q}}{k_{t,m}'^2} i_m'(z) \int \left(D_1' J_n(k_{t,m}' |\boldsymbol{\rho}' - \boldsymbol{\rho}_q|) e^{jn\phi_q'} i_m'(z') \right) \cdot \mathbf{M}(\mathbf{r}') d\mathbf{r}' \\ - j\omega\varepsilon \frac{1}{k^2} \sum_m \frac{1}{4j} \sum_n D_2 \frac{H_n^{(2)}(k_{t,m}'' |\boldsymbol{\rho} - \boldsymbol{\rho}_q|) e^{-jn\phi_q}}{k_{t,m}''^2} v_m''(z) \int \left(D_2' J_n(k_{t,m}'' |\boldsymbol{\rho}' - \boldsymbol{\rho}_q|) e^{jn\phi_q'} v_m''(z') \right) \cdot \mathbf{M}(\mathbf{r}') d\mathbf{r}'. \quad (2.161)$$

From this expression, it becomes clear how to express the field scattered by cylinders in the most convenient form – by using the exact same functional form in the observation coordinate as the impinging field itself! This enables simpler expression of boundary conditions since both the impinging and scattered field are treated on the same footing. Therefore, we choose

$$\mathbf{M}_{m,n}'(\mathbf{r}) = \nabla \times \hat{\mathbf{z}} H_n^{(2)}(k_{t,m}' |\boldsymbol{\rho} - \boldsymbol{\rho}_q|) e^{-jn\phi_q} i_m'(z), \\ \mathbf{N}_{m,n}''(\mathbf{r}) = \frac{1}{k} \nabla \times \nabla \times \hat{\mathbf{z}} H_n^{(2)}(k_{t,m}'' |\boldsymbol{\rho} - \boldsymbol{\rho}_q|) e^{-jn\phi_q} v_m''(z), \quad |\boldsymbol{\rho} - \boldsymbol{\rho}_q| \geq a_q \quad (2.162)$$

if the cylinder in question is a PEC, or if it is dielectric

$$\begin{aligned}
 \mathbf{M}'_{m,n}(\boldsymbol{\rho}, \boldsymbol{\rho}_p; z) &= \begin{cases} \nabla \times \hat{\mathbf{z}} H_n^{(2)}(k'_{t,m} |\boldsymbol{\rho} - \boldsymbol{\rho}_q|) e^{-jn\phi_q} i'_m(z), & |\boldsymbol{\rho} - \boldsymbol{\rho}_q| \geq a_q \\ \nabla \times \hat{\mathbf{z}} J_n(k'_{t,m} |\boldsymbol{\rho} - \boldsymbol{\rho}_q|) e^{-jn\phi_q} i'_m(z), & |\boldsymbol{\rho} - \boldsymbol{\rho}_q| \leq a_q, \end{cases} \\
 \mathbf{N}''_{m,n}(\boldsymbol{\rho}, \boldsymbol{\rho}_p; z) &= \begin{cases} \frac{1}{k} \nabla \times \nabla \times \hat{\mathbf{z}} H_n^{(2)}(k''_{t,m} |\boldsymbol{\rho} - \boldsymbol{\rho}_q|) e^{-jn\phi_q} v''_m(z), & |\boldsymbol{\rho} - \boldsymbol{\rho}_q| \geq a_q \\ \frac{1}{k_q} \nabla \times \nabla \times \hat{\mathbf{z}} J_n(k''_{t,m,q} |\boldsymbol{\rho} - \boldsymbol{\rho}_q|) e^{-jn\phi_q} v''_m(z), & |\boldsymbol{\rho} - \boldsymbol{\rho}_q| \leq a_q, \end{cases}
 \end{aligned} \tag{2.163}$$

which can be easily verified to satisfy the vector Helmholtz equation. Note that for the dielectric cylinder (which we shall refer to as a “post” from now on) problem we asserted the same vertical dependence in both the post and the surrounding medium, anticipating the continuity of tangential field components across the boundary. Moreover, the factor $1/k$ appearing in the definition of TE functions was added just for convenience, as will be shown shortly. The basis, shown in (2.162) and (2.163), is the well-known Hansen-type basis [52, Ch. 4], used by a number of authors not only to represent the scattered field, but as a basis for construction of dyadic GFs, as mentioned in the previous subsections. However, a number of problems are associated with the latter, since the spurious singularities are difficult to exhibit explicitly using this approach. Nonetheless, no detriments are associated with the scattered field representation.

In sum, with the scattered field basis chosen in this manner, we are ready to tackle the general problem of scattering from multiple posts embedded in a PPW. First, we shall derive the general case of an arbitrary number of dielectric/PEC posts.

For this reason, consider a dielectric-loaded PPW of height h , permittivity ε_r , with N posts, $N = N_d + N_p$ being the sum of the numbers of dielectric and metal posts. A general source \mathbf{M} excites the waveguide, the kind of which is not important as long as it injects a finite amount of power into it. Our goal then is to derive an explicit expression for the total field in the PPW, and in doing so we shall adhere to the notation used in [45] and [46].

We start by writing down the total field as the sum of the impressed and scattered field

$$\mathbf{H}(\mathbf{r}) = \mathbf{H}_{imp}(\mathbf{r}) + \sum_p \mathbf{H}_p^s(\mathbf{r}, \mathbf{r}_p), \tag{2.164}$$

where the sum in the second term runs over all the posts, denoted by q . Now, it is clear that the impressed field is readily found by (2.158). On the other hand, we do not know the amplitudes of the scattered fields. In order to find them, we must solve the boundary problem *at each post*, which depends on the material the post is made from.

First we consider a **PEC post**, for which the boundary condition is stated as: *the tangential components of the sum of the impressed electric field, the electric field scattered by post q and the electric field scattered towards q by all the other posts must be zero at the boundary surface of post q* , i.e.

$$\hat{\mathbf{n}}_q \times \left(\mathbf{E}_{imp} + \sum_{p \neq q} \mathbf{E}_p + \mathbf{E}_q \right) = 0 \Big|_{\partial R_q}, \tag{2.165}$$

where $\hat{\mathbf{n}}_q$ is the post q unit surface normal, expressed as $\hat{\mathbf{n}}_q = (\boldsymbol{\rho} - \boldsymbol{\rho}_q) / |\boldsymbol{\rho} - \boldsymbol{\rho}_q|$ and ∂R_q denotes the bounding surface. As demonstrated at the beginning of this subsection, the most

elegant way to enforce the boundary conditions on a post is to reexpress the fields in its local coordinate system centred on its axis. To get there, we shall first have to express the pertinent electric fields from magnetic fields using the Maxwell curl equation for H as

$$\hat{\mathbf{n}}_q \times \frac{\nabla}{j\omega\epsilon} \times \left(\mathbf{H}_{imp} + \sum_{p \neq q} \mathbf{H}_p + \mathbf{H}_q \right) = 0 \Big|_{\partial R_q}. \quad (2.166)$$

The impressed field impinging on the post q is already given by (2.161), whereas the field scattered toward q by all the remaining posts is given by

$$\begin{aligned} \sum_{p \neq q} \mathbf{H}_p &= \sum_{p \neq q, m, n} A'_{m,n} \mathbf{M}'_{m,n}(\boldsymbol{\rho}, \boldsymbol{\rho}_p; z) + \sum_{p \neq q, m, n} A''_{m,n} \mathbf{N}''_{m,n}(\boldsymbol{\rho}, \boldsymbol{\rho}_p; z) \\ &= \sum_{p \neq q, m, n} A'_{m,n} \nabla \times \hat{\mathbf{z}} H_n^{(2)}(k'_{t,m} |\boldsymbol{\rho} - \boldsymbol{\rho}_p|) e^{-jn\phi_p} \mathbf{i}'_m(z) \\ &\quad + \sum_{p \neq q, m, n} A''_{m,n} \frac{1}{k} \nabla \times \nabla \times \hat{\mathbf{z}} H_n^{(2)}(k''_{t,m} |\boldsymbol{\rho} - \boldsymbol{\rho}_p|) e^{-jn\phi_p} \mathbf{v}''_m(z), \end{aligned} \quad (2.167)$$

where the terms are centered on the axes of scattering posts. However, using the Gegenbauer addition theorem again, now applied to Hankel functions of positive-integer order as

$$\begin{aligned} H_n^{(2)}(k'_{t,m} |\boldsymbol{\rho} - \boldsymbol{\rho}_p|) e^{-jn\phi_p} &= H_n^{(2)}(k'_{t,m} |\boldsymbol{\rho}_p - \boldsymbol{\rho}|) e^{-jn\phi_p} = H_n^{(2)}(k'_{t,m} |(\boldsymbol{\rho}_p - \boldsymbol{\rho}_q) - (\boldsymbol{\rho} - \boldsymbol{\rho}_q)|) e^{-jn\phi_p} \\ &= \sum_{r=-\infty}^{+\infty} (-1)^{n-r} J_r(k'_{t,m} |\boldsymbol{\rho} - \boldsymbol{\rho}_q|) H_{n-r}^{(2)}(k'_{t,m} |\boldsymbol{\rho}_p - \boldsymbol{\rho}_q|) e^{-jr\phi_q} e^{-j(n-r)\phi_{qp}}, \end{aligned} \quad (2.168)$$

we shift the scattered fields reference points onto post q axis, obtaining

$$\begin{aligned} \sum_{p \neq q} \mathbf{H}_p &= \sum_{p \neq q, m, n} A'_{m,n,p} \nabla \times \hat{\mathbf{z}} \left(\sum_{r=-\infty}^{+\infty} (-1)^{n-r} J_n(k'_{t,m} |\boldsymbol{\rho} - \boldsymbol{\rho}_q|) H_{n-r}^{(2)}(k'_{t,m} |\boldsymbol{\rho}_p - \boldsymbol{\rho}_q|) e^{-jr\phi_q} e^{-j(n-r)\phi_{qp}} \mathbf{i}'_m(z) \right) \\ &\quad + \sum_{p \neq q, m, n} A''_{m,n,p} \frac{1}{k} \nabla \times \nabla \times \hat{\mathbf{z}} \left(\sum_{r=-\infty}^{+\infty} (-1)^{n-r} J_n(k''_{t,m} |\boldsymbol{\rho} - \boldsymbol{\rho}_q|) H_{n-r}^{(2)}(k''_{t,m} |\boldsymbol{\rho}_p - \boldsymbol{\rho}_q|) e^{-jr\phi_q} e^{-j(n-r)\phi_{qp}} \mathbf{v}''_m(z) \right). \end{aligned} \quad (2.169)$$

Then, upon using identities $\nabla \times \mathbf{M}'_{m,n} = k \mathbf{N}'_{m,n}$ and $\nabla \times \mathbf{N}''_{m,n} = k \mathbf{M}''_{m,n}$, derivable from Helmholtz equations of respective quantities, the electric field scattered toward q is finally obtained as

$$\begin{aligned} \sum_{p \neq q} \mathbf{E}_p &= \sum_{p \neq q, m, n} A'_{m,n,p} \frac{\nabla \times \nabla \times \hat{\mathbf{z}}}{j\omega\epsilon} \left(\sum_{r=-\infty}^{+\infty} (-1)^{n-r} J_n(k'_{t,m} |\boldsymbol{\rho} - \boldsymbol{\rho}_q|) H_{n-r}^{(2)}(k'_{t,m} |\boldsymbol{\rho}_p - \boldsymbol{\rho}_q|) e^{-jr\phi_q} e^{-j(n-r)\phi_{qp}} \mathbf{i}'_m(z) \right) \\ &\quad + \sum_{p \neq q, m, n} A''_{m,n,p} \frac{\nabla \times \hat{\mathbf{z}}}{j\omega\epsilon / k} \left(\sum_{r=-\infty}^{+\infty} (-1)^{n-r} J_n(k''_{t,m} |\boldsymbol{\rho} - \boldsymbol{\rho}_q|) H_{n-r}^{(2)}(k''_{t,m} |\boldsymbol{\rho}_p - \boldsymbol{\rho}_q|) e^{-jr\phi_q} e^{-j(n-r)\phi_{qp}} \mathbf{v}''_m(z) \right). \end{aligned} \quad (2.170)$$

Applying the same reasoning for the impressed field, we express it in the q system as

$$\begin{aligned}
 \mathbf{E}_{imp}(\mathbf{r}) = & -j\omega\epsilon \sum_m \frac{1}{4j} \sum_n \frac{\nabla \times \nabla \times \hat{\mathbf{z}}}{j\omega\epsilon} \frac{J_n(k'_{t,m} |\boldsymbol{\rho} - \boldsymbol{\rho}_q|) e^{-jn\phi_q}}{k'^2_{t,m}} i'_m(z) \int (D_1 H_n^{(2)}(k'_{t,m} |\boldsymbol{\rho}' - \boldsymbol{\rho}_q|) e^{jn\phi'_q} i'_m(z')) \cdot \mathbf{M}(\mathbf{r}') d\mathbf{r}' \\
 & - j\omega\epsilon \frac{1}{k^2} \sum_m \frac{1}{4j} \sum_n \frac{\nabla \times \hat{\mathbf{z}}}{j\omega\epsilon/k} \frac{J_n(k''_{t,m} |\boldsymbol{\rho} - \boldsymbol{\rho}_q|) e^{-jn\phi_q}}{k''^2_{t,m}} v''_m(z) \int (D_2 H_n^{(2)}(k''_{t,m} |\boldsymbol{\rho}' - \boldsymbol{\rho}_q|) e^{jn\phi'_q} v''_m(z')) \cdot \mathbf{M}(\mathbf{r}') d\mathbf{r}'.
 \end{aligned} \tag{2.171}$$

The field scattered by post q is simply expressed using the same expansion as for fields scattered by other posts

$$\begin{aligned}
 \mathbf{E}_q = & \sum_{m,n} A'_{m,n,q} \frac{\nabla \times \nabla \times \hat{\mathbf{z}}}{j\omega\epsilon} \left(\sum_{n=-\infty}^{+\infty} H_n^{(2)}(k'_{t,m} |\boldsymbol{\rho} - \boldsymbol{\rho}_q|) e^{-jn\phi_q} i'_m(z) \right) \\
 & + \sum_{m,n} A''_{m,n,q} \frac{\nabla \times \hat{\mathbf{z}}}{j\omega\epsilon/k} \left(\sum_{n=-\infty}^{+\infty} H_n^{(2)}(k''_{t,m} |\boldsymbol{\rho} - \boldsymbol{\rho}_q|) e^{-jn\phi_q} v''_m(z) \right).
 \end{aligned} \tag{2.172}$$

with all the partial fields expressed in the post's local system, we can setup a boundary problem simply by inserting the obtained fields into (2.165), leading to the so-called *self-consistency conditions* (as commonly used in multiple-scattering theory), for TM and TE fields independently. This is possible because posts run from the top to the bottom plate, and their surface impedance is zero; hence the currents excited on posts will maintain the form of the modal fields incident on them and will not couple TM and TE modes. In other words, TM and TE fields satisfy the PEC boundary conditions on posts independently, in the following way

$$\begin{aligned}
 \hat{\mathbf{n}}_q \times \left(-j\omega\epsilon \sum_{m,n} \frac{1}{4j} \sum_n \frac{\nabla \times \nabla \times \hat{\mathbf{z}}}{j\omega\epsilon} \frac{J_n(k'_{t,m} |\boldsymbol{\rho} - \boldsymbol{\rho}_q|) e^{-jn\phi_q}}{k'^2_{t,m}} i'_m(z) \int (D_1 H_n^{(2)}(k'_{t,m} |\boldsymbol{\rho}' - \boldsymbol{\rho}_q|) e^{jn\phi'_q} i'_m(z')) \cdot \mathbf{M}(\mathbf{r}') d\mathbf{r}' \right. \\
 + \sum_{p \neq q, m, n, r} A'_{m,n,p} \frac{\nabla \times \nabla \times \hat{\mathbf{z}}}{j\omega\epsilon} (-1)^{n-r} J_n(k'_{t,m} |\boldsymbol{\rho} - \boldsymbol{\rho}_q|) H_{n-r}^{(2)}(k'_{t,m} |\boldsymbol{\rho}_p - \boldsymbol{\rho}_q|) e^{-jr\phi_q} e^{-j(n-r)\phi_{qp}} i'_m(z) \\
 \left. + \sum_{m,n} A'_{m,n,q} \frac{\nabla \times \nabla \times \hat{\mathbf{z}}}{j\omega\epsilon} H_n^{(2)}(k'_{t,m} |\boldsymbol{\rho} - \boldsymbol{\rho}_q|) e^{-jn\phi_q} i'_m(z) \right) = 0 \Big|_{|\boldsymbol{\rho} - \boldsymbol{\rho}_q| = a_q},
 \end{aligned} \tag{2.173}$$

for TM fields, and

$$\begin{aligned}
 \hat{\mathbf{n}}_q \times \left(-j\omega\epsilon \frac{1}{k^2} \sum_m \frac{1}{4j} \sum_r \frac{\nabla \times \hat{\mathbf{z}}}{j\omega\epsilon/k} \frac{J_r(k''_{t,m} |\boldsymbol{\rho} - \boldsymbol{\rho}_q|) e^{-jr\phi_q}}{k''^2_{t,m}} v''_m(z) \int (D_2 H_r^{(2)}(k''_{t,m} |\boldsymbol{\rho}' - \boldsymbol{\rho}_q|) e^{jr\phi'_q} v''_m(z')) \cdot \mathbf{M}(\mathbf{r}') d\mathbf{r}' \right. \\
 + \sum_{p \neq q, m, n, r} A''_{m,n,p} \frac{\nabla \times \hat{\mathbf{z}}}{j\omega\epsilon/k} (-1)^{n-r} J_n(k''_{t,m} |\boldsymbol{\rho} - \boldsymbol{\rho}_q|) H_{n-r}^{(2)}(k''_{t,m} |\boldsymbol{\rho}_p - \boldsymbol{\rho}_q|) e^{-jr\phi_q} e^{-j(n-r)\phi_{qp}} v''_m(z) \\
 \left. + \sum_{m,n} A''_{m,n,q} \frac{\nabla \times \hat{\mathbf{z}}}{j\omega\epsilon/k} H_n^{(2)}(k''_{t,m} |\boldsymbol{\rho} - \boldsymbol{\rho}_q|) e^{-jn\phi_q} v''_m(z) \right) = 0 \Big|_{|\boldsymbol{\rho} - \boldsymbol{\rho}_q| = a_q},
 \end{aligned} \tag{2.174}$$

for TE fields. These equations constitute infinite linear systems; hence a general analytical solution is intractable. Nevertheless, in practical problems only a small number of modes contribute to the overall field (i.e. few modes will suffice to approximate EM fields well, the sufficient number of which leads to satisfactory accuracy we will discuss shortly). This is mostly so because the PPWs in question operate in the dominant-mode regime, and posts are predominantly small compared to the wavelength. Then the solution, albeit an

approximate one, to (2.173) and (2.174) is tractable using truncated forms of the respective self-consistency conditions. Rigorously speaking, we are representing the field as a series of eigenvectors of a compact, self-adjoint operator over the space of L^2 functions defined on \mathbb{R}^3 . Since the collection of all its eigenvectors forms a complete base, it follows that it is possible to expand a sufficiently well-behaved function in terms of a weighted sum of the aforementioned eigenvectors; the weights being the expansion coefficients. Moreover, since the sum converges, it is implied that the expansion coefficients of terms of order $N \geq M$ tend to zero as the order of the partial sum, denoted by N , is increased to infinity. Hence, we may approximate the true solution sufficiently well by truncating the sum at finite order. Therefore, we consider N_m longitudinal modes and N_ϕ azimuthal harmonics in the following analysis, although we could, in principle, consider an infinity of modes.

Firstly, to facilitate manipulation of the equations, we introduce the following notation

$$\begin{aligned}
 v'_{q,m,r} &= -j\omega\varepsilon \frac{1}{4j} \frac{1}{k'^2} \int \left(D_1' H_r^{(2)}(k'_{t,m} |\boldsymbol{\rho}' - \boldsymbol{\rho}_q|) e^{jr\phi'_q} i'_m(z') \right) \cdot \mathbf{M}(\mathbf{r}') d\mathbf{r}' \\
 v''_{q,m,r} &= -j\omega\varepsilon \frac{1}{k^2} \frac{1}{4j} \frac{1}{k''^2} \int \left(D_2' H_r^{(2)}(k''_{t,m} |\boldsymbol{\rho}' - \boldsymbol{\rho}_q|) e^{jr\phi'_q} v''_m(z') \right) \cdot \mathbf{M}(\mathbf{r}') d\mathbf{r}' \\
 \Phi'_{imp,m,r} &= J_r(k'_{t,m} |\boldsymbol{\rho} - \boldsymbol{\rho}_q|) e^{-jr\phi'_q} i'_m(z) \\
 \Phi''_{imp,m,r} &= J_r(k''_{t,m} |\boldsymbol{\rho} - \boldsymbol{\rho}_q|) e^{-jr\phi'_q} v''_m(z) \\
 \Phi'_{p \neq q, m, n} &= (-1)^{n-r} J_n(k'_{t,m} |\boldsymbol{\rho} - \boldsymbol{\rho}_q|) H_{n-r}^{(2)}(k'_{t,m} |\boldsymbol{\rho}_p - \boldsymbol{\rho}_q|) e^{-jr\phi'_q} e^{-j(n-r)\phi_{qp}} i'_m(z) \\
 \Phi''_{p \neq q, m, n} &= (-1)^{n-r} J_n(k''_{t,m} |\boldsymbol{\rho} - \boldsymbol{\rho}_q|) H_{n-r}^{(2)}(k''_{t,m} |\boldsymbol{\rho}_p - \boldsymbol{\rho}_q|) e^{-jr\phi'_q} e^{-j(n-r)\phi_{qp}} v''_m(z) \\
 \Phi'_{q, m, n} &= H_n^{(2)}(k'_{t,m} |\boldsymbol{\rho} - \boldsymbol{\rho}_q|) e^{-jn\phi'_q} i'_m(z) \\
 \Phi''_{q, m, n} &= H_n^{(2)}(k''_{t,m} |\boldsymbol{\rho} - \boldsymbol{\rho}_q|) e^{-jn\phi'_q} v''_m(z)
 \end{aligned} \tag{2.175}$$

v denoting the impressed field excitation amplitudes, whereas Φ denote the scalar potentials.

Then, one notes that the summands in each of the sums, enumerated by the index pair $\{m, n\}$, are linearly independent. In addition, terms with either differing m or n are **orthogonal**. This property, as mentioned before, implies that modes used in the expansion of fields are not coupled – there is not only no coupling between TM and TE modes, but between individual modes of TM or TE sets! It turns out that this property singularly contributes to the efficiency of the method, owing to a smaller number of non-zero terms in the interaction matrices of linear systems one has to consider. For example, if the modes are not orthogonal, as is the case in e.g. PPWs with poorly conducting metal plates, then one needs to compute the cross-coupling amplitudes describing the energy transfer between two modes belonging to different sets, whereas this is not the case when the modes are orthogonal. Whether the modes are orthogonal or not depends on the properties of the

Helmholtz operator defining the problem. If the operator is self-adjoint, the modes will be orthogonal, whereas if it is non-self-adjoint this will, generally, not be the case.

Continuing further, we inspect the constraints the scalar potentials must fulfil if the self-consistency conditions (referred to from here on as *SCC*) are to be satisfied, beginning with TM fields.

Since each term in (2.173) has the form $\hat{\mathbf{n}}_q \times \nabla \times \nabla \times \hat{\mathbf{z}} \Phi'(|\boldsymbol{\rho} - \boldsymbol{\rho}_q|, z)$, using the identity $\nabla \times \nabla \times \hat{\mathbf{z}} = \partial_z \nabla_t - \nabla_t^2 \hat{\mathbf{z}}$, along with the fact that this operator transforms as a vector (since it is constructed as the cross product of a vector and a pseudovector), we arrive to the conclusion that $\Phi'(|\boldsymbol{\rho} - \boldsymbol{\rho}_q|, z) = 0|_{|\boldsymbol{\rho} - \boldsymbol{\rho}_q| = a_q}$.

As for the TE equation (2.174), all terms are of the form $\hat{\mathbf{n}}_q \times \nabla \times \hat{\mathbf{z}} \Phi''(|\boldsymbol{\rho} - \boldsymbol{\rho}_q|, z)$, which, upon reexpressing the operator acting on the scalar function as $\hat{\mathbf{n}}_q \times \nabla \times \hat{\mathbf{z}} = -(\hat{\mathbf{n}}_q \cdot \nabla) \hat{\mathbf{z}} = -\partial_{n_q} \hat{\mathbf{z}}$, implies that in order to satisfy the SCC, each scalar function has to satisfy $\partial_{n_q} \Phi''(|\boldsymbol{\rho} - \boldsymbol{\rho}_q|, z) = 0|_{|\boldsymbol{\rho} - \boldsymbol{\rho}_q| = a_q}$.

Hence, using the obtained constraints, along with scalarly multiplying (2.173) by $i'_m(z)$ and (2.174) with $v''_m(z)$, using the scalar product

$$\langle u_m, u_n \rangle = \int_{z_1}^{z_2} w(z) u_m(z) u_n(z) dz,$$

$$w(z) = \begin{cases} 1, & n_{\text{layers}} = 1 \\ \varepsilon(z) \left(d_z u = 0|_{z=z_{1,2}} \right); \mu(z) \left(u = 0|_{z=z_{1,2}} \right), & n_{\text{layers}} > 1 \end{cases}$$

yields, in view of the orthonormality of longitudinal functions, for each m

$$\sum_r v'_{m,q,r} \Phi'_{\text{imp},m,q,r}(|\boldsymbol{\rho} - \boldsymbol{\rho}_q|) + \sum_{p \neq q, n, r} A'_{m,n,p} \Phi'_{m,p \neq q,r}(|\boldsymbol{\rho} - \boldsymbol{\rho}_q|) + \sum_n A'_{m,n,q} \Phi'_{m,q,r}(|\boldsymbol{\rho} - \boldsymbol{\rho}_q|) = 0|_{|\boldsymbol{\rho} - \boldsymbol{\rho}_q| = a_q}$$

$$\sum_r v''_{m,q,r} \partial_{n_q} \Phi'_{\text{imp},m,q,r}(|\boldsymbol{\rho} - \boldsymbol{\rho}_q|) + \sum_{p \neq q, n, r} A'_{m,p,n} \partial_{n_q} \Phi'_{m,p \neq q,r}(|\boldsymbol{\rho} - \boldsymbol{\rho}_q|) + \sum_n A'_{m,q,r} \partial_{n_q} \Phi'_{m,q,r}(|\boldsymbol{\rho} - \boldsymbol{\rho}_q|) = 0|_{|\boldsymbol{\rho} - \boldsymbol{\rho}_q| = a_q},$$

(2.176)

where the scalar functions have no z – dependence anymore, since it was integrated out. It is clear that now we have equations relating modes with a fixed longitudinal dependence, but having different azimuthal dependence. However, noting that the set of azimuthal harmonics $\{e^{-jr\phi_q}\}$ is orthogonal, we conclude that self-consistency conditions can be formulated for each n -th harmonic, which can be formally accomplished by scalarly multiplying the last two equations by $e^{-jr\phi_q}$ (note that the complex-conjugate scalar product is used, and that r has the same span as n , implying they are interchangeable), giving

$$v'_{m,q,r} J_r(k'_{t,m} a_q) + \sum_{p \neq q, n} A'_{m,p,n} (-1)^{n-r} J_r(k'_{t,m} a_q) H_{n-r}^{(2)}(k'_{t,m} |\boldsymbol{\rho}_p - \boldsymbol{\rho}_q|) e^{-j(n-r)\phi_{qp}} + A'_{m,q,r} H_n^{(2)}(k'_{t,m} a_q) = 0,$$

$$v''_{m,q,r} J_r(k'_{t,m} a_q) + \sum_{p \neq q, n} A'_{m,p,n} (-1)^{n-r} J_r(k'_{t,m} a_q) H_{n-r}^{(2)}(k'_{t,m} |\boldsymbol{\rho}_p - \boldsymbol{\rho}_q|) e^{-j(n-r)\phi_{qp}} + A'_{m,q,r} H_n^{(2)}(k'_{t,m} a_q) = 0$$

(2.177)

from which, by dividing both sides of the TM SCC by $H_n^{(2)}(k'_{t,m}a_q)$, the TE SCC by $H_n^{(2)}(k''_{t,m}a_q)$, and rearranging, we obtain

$$\begin{aligned} \sum_{p \neq q, n} A'_{m,n,p} T'_{m,r,n,q,p} + A'_{m,r,q} &= \Omega'_{m,r,q} & \sum_{p \neq q, n} A''_{m,n,p} T''_{m,r,n,q,p} + A''_{m,r,q} &= \Omega''_{m,r,q} \\ T'_{m,r,n,q,p} &= (-1)^{n-r} \frac{J_r(k'_{t,m}a_q)}{H_r^{(2)}(k'_{t,m}a_q)} H_{n-r}^{(2)}(k'_{t,m}|\boldsymbol{\rho}_p - \boldsymbol{\rho}_q|) e^{-j(n-r)\varphi_{pq}} & T''_{m,r,n,q,p} &= (-1)^{n-r} \frac{J_r(k''_{t,m}a_q)}{H_r^{(2)}(k''_{t,m}a_q)} H_{n-r}^{(2)}(k''_{t,m}|\boldsymbol{\rho}_p - \boldsymbol{\rho}_q|) e^{-j(n-r)\varphi_{pq}}, \\ \Omega'_{m,r,q} &= \frac{J_r(k'_{t,m}a_q)}{H_r^{(2)}(k'_{t,m}a_q)} V_{q,m,r} & \Omega''_{m,r,q} &= \frac{J_r(k''_{t,m}a_q)}{H_r^{(2)}(k''_{t,m}a_q)} V_{q,m,r} \end{aligned} \quad (2.178)$$

the prime on cylindrical functions pertaining to TE fields denoting the derivative with respect to their respective arguments. Coefficients T'^n are interpreted as the amplitude of the modal field, characterized by indexes m, r , which is incident on post q when a unit amplitude modal field, characterized by indexes m, n is scattered off the post p . Analogously, coefficients $\Omega'_{m,r,q}$ are interpreted as the amplitude of the modal field, characterized by indexes m, r , which is incident on post q when an impressed magnetic current radiates inside the guide.

Writing down the self-consistency conditions for the remaining posts, we obtain a linear system having the following form:

$$\underline{\underline{\mathbf{T}}}_m \underline{\underline{\mathbf{A}}}_m = \underline{\underline{\Omega}}_m \quad ,$$

which, more explicitly, has the following structure:

$$\begin{pmatrix} T_{m,1,1,1,1} & T_{m,1,2,1,1} & \cdots & T_{m,1,N_\phi,1,1} & T_{m,1,1,2,1} & \cdots & T_{m,1,1,N_\phi,2,1} & \cdots & T_{m,1,1,N_\phi,N_\phi,1} \\ T_{m,2,1,1,1} & T_{m,2,2,1,1} & \cdots & T_{m,2,N_\phi,1,1} & T_{m,2,1,2,1} & \cdots & T_{m,1,N_\phi,2,1} & \cdots & T_{m,2,2,N_\phi,N_\phi,1} \\ \cdot & \cdot \\ T_{m,N_\phi,1,1,1} & T_{m,N_\phi,2,1,1} & \cdots & T_{m,N_\phi,N_\phi,1,1} & T_{m,N_\phi,1,2,1} & \cdots & T_{m,N_\phi,N_\phi,2,1} & \cdots & T_{m,N_\phi,N_\phi,N_\phi,1} \\ T_{m,1,1,1,2} & T_{m,1,2,1,2} & \cdots & T_{m,1,N_\phi,1,2} & T_{m,1,1,2,2} & \cdots & T_{m,1,N_\phi,2,2} & \cdots & T_{m,1,1,N_\phi,N_\phi,2} \\ T_{m,2,1,1,2} & T_{m,2,2,1,2} & \cdots & T_{m,2,N_\phi,1,2} & T_{m,2,1,2,2} & \cdots & T_{m,1,N_\phi,2,2} & \cdots & T_{m,2,2,N_\phi,N_\phi,2} \\ \cdot & \cdot \\ T_{m,N_\phi,1,1,2} & T_{m,N_\phi,2,1,2} & \cdots & T_{m,N_\phi,N_\phi,1,2} & T_{m,N_\phi,1,2,2} & \cdots & T_{m,N_\phi,N_\phi,2,2} & \cdots & T_{m,N_\phi,N_\phi,N_\phi,2} \\ \cdot & \cdot \\ T_{m,N_\phi,1,1,N_\phi} & T_{m,N_\phi,2,1,N_\phi} & \cdots & T_{m,N_\phi,N_\phi,1,N_\phi} & T_{m,N_\phi,1,2,N_\phi} & \cdots & T_{m,N_\phi,N_\phi,2,N_\phi} & \cdots & T_{m,N_\phi,N_\phi,N_\phi,N_\phi} \end{pmatrix} \begin{pmatrix} A_{m,1,1} \\ A_{m,2,1} \\ \cdot \\ \cdot \\ A_{m,N_\phi,1} \\ A_{m,1,2} \\ \cdot \\ A_{m,N_\phi,2} \\ \cdot \\ A_{m,N_\phi,N_\phi} \end{pmatrix} = \begin{pmatrix} \Omega_{m,1,1} \\ \Omega_{m,2,1} \\ \cdot \\ \cdot \\ \Omega_{m,N_\phi,1} \\ \Omega_{m,1,2} \\ \cdot \\ \Omega_{m,N_\phi,2} \\ \cdot \\ \Omega_{m,N_\phi,N_\phi} \end{pmatrix} \quad (2.179)$$

As we have assumed the presence of exclusively PEC posts for the present moment, the dimensions of the matrix $\underline{\underline{\mathbf{T}}}_m$ will be $N_{posts}N_\phi \times N_{posts}N_\phi$, whereas the unknown scattering amplitudes vector $\underline{\underline{\mathbf{A}}}_m$ will be of length $N_{posts}N_\phi$. This makes it clear that one needs to solve $2 \times N_m$ such problems to find the EM field to a given degree of accuracy, stipulated by the choice of the number of vertical and azimuthal harmonics used.

Now, if one wishes to consider **scattering off of dielectric posts**, one sets up a problem in which the fields inside and outside the cylinders must be matched in such a fashion that the tangential components of EM fields are continuous across the surrounding medium/post boundary. As already hinted at the beginning of this subsection, we require a different scattered-field representation now, since we need to model the fields in the interior as well as in the exterior of posts. Keeping in mind the scattered fields representation of (2.163), we first set-up a boundary problem for a generic dielectric post as

$$\begin{aligned} \hat{\mathbf{n}}_q \times \left(\mathbf{E}_{imp} + \sum_{p \neq q} \mathbf{E}_p + \mathbf{E}_q^s \right) &= \hat{\mathbf{n}}_q \times \mathbf{E}_q^{int} \Big|_{\partial R_q} \\ \hat{\mathbf{n}}_q \times \left(\mathbf{H}_{imp} + \sum_{p \neq q} \mathbf{H}_p + \mathbf{H}_q^s \right) &= \hat{\mathbf{n}}_q \times \mathbf{H}_q^{int} \Big|_{\partial R_q} . \end{aligned} \quad (2.180)$$

The new terms with respect to the PEC case are the internal fields \mathbf{E}_{int}^q and \mathbf{H}_{int}^q , defined as

$$\begin{aligned} \mathbf{H}_{int}^q &= \sum_{m,n} B_{m,n}' \nabla \times \hat{\mathbf{z}} J_n \left(k_{t,m,q}' |\boldsymbol{\rho} - \boldsymbol{\rho}_q| \right) e^{-jn\phi_q} i_m'(z) \\ &\quad + \sum_{m,n} B_{m,n}'' \frac{1}{k_q} \nabla \times \nabla \times \hat{\mathbf{z}} J_n \left(k_{t,m,q}'' |\boldsymbol{\rho} - \boldsymbol{\rho}_q| \right) e^{-jn\phi_q} v_m''(z), \\ \mathbf{E}_{int}^q &= \sum_{m,n} B_{m,n}' \frac{\nabla \times \nabla \times \hat{\mathbf{z}}}{j\omega\epsilon} J_n \left(k_{t,m,q}' |\boldsymbol{\rho} - \boldsymbol{\rho}_q| \right) e^{-jn\phi_q} i_m'(z) \\ &\quad + \sum_{m,n} B_{m,n}'' \frac{\nabla \times \hat{\mathbf{z}}}{j\omega\epsilon / k_q} J_n \left(k_{t,m,q}'' |\boldsymbol{\rho} - \boldsymbol{\rho}_q| \right) e^{-jn\phi_q} v_m''(z), \end{aligned} \quad (2.181)$$

where it should be noted that we have stipulated the same azimuthal and longitudinal dependence of fields outside and inside the cylinders in anticipation of the tangential fields continuity requirement. To tackle this problem, we employ the same methods as for the PEC case but, unfortunately, the TM and TE fields are not decoupled any more! This is a consequence of transverse inhomogeneity, causing the currents induced on the cylinder to destroy the pure TM or TE character of the field, even though impressed fields may be composed of only a single type of modes. This is not true only if the sole excited mode in the cavity is the $m=0$ wave, since it is the only mode constant in the longitudinal direction, implying that no TE modes can be produced by its scattering since there exists no TE mode with constant longitudinal dependence. Otherwise, the computational burden increases, as already explained, since then one has to calculate cross-coupling amplitudes.

Here we shall be dealing with the scattering of an $m=0$ mode, since in most practical cases it is the only one propagating, and carrying out the analysis under the assumption that it is the only mode scattering off a dielectric post in the cavity yields accurate results (of course, provided the height of the PPW and permittivity of the loading medium are such that higher-order modes are sufficiently suppressed at the frequency of interest). For the case when modes $m>0$ are propagating, the analysis is more complex due to the aforementioned mode coupling, and is addressed in detail in Appendix B.

We assume that only the $m=0$ mode is injected into the cavity, as would be, e.g., the case if we were to use a standard coaxial transition to fire-up the PPW. In addition, *both* PEC and dielectric posts cohabit the PPW. Then, enforcing the continuity of tangential H-fields, we can write down the system

$$\begin{aligned}
 \hat{\mathbf{n}}_q \times & \left(-j\omega\varepsilon \sum_n \frac{1}{4j} \nabla \times \hat{\mathbf{z}} \frac{H_n^{(2)}(k'_{t,0} |\boldsymbol{\rho} - \boldsymbol{\rho}_q|) e^{-jn\phi_q}}{k'_{t,0}{}^2} i'_0(z) \int \left(D_1 J_n(k'_{t,0} |\boldsymbol{\rho}' - \boldsymbol{\rho}_q|) e^{jn\phi'_q} i'_0(z') \right) \cdot \mathbf{M}(\mathbf{r}') d\mathbf{r}' \right. \\
 & + \sum_{p \neq q, n} A'_{0,n,p} \nabla \times \hat{\mathbf{z}} \left(\sum_{r=-\infty}^{+\infty} (-1)^{n-r} J_n(k'_{t,0} |\boldsymbol{\rho} - \boldsymbol{\rho}_q|) H_{n-r}^{(2)}(k'_{t,0} |\boldsymbol{\rho}_p - \boldsymbol{\rho}_q|) e^{-jr\phi_q} e^{-j(n-r)\phi_{qp}} i'_0(z) \right) \\
 & \left. + \sum_{0,r} A'_{0,r,q} \nabla \times \hat{\mathbf{z}} H_n^{(2)}(k'_{t,0} |\boldsymbol{\rho} - \boldsymbol{\rho}_q|) e^{-jr\phi_q} i'_0(z) \right) \\
 & = \hat{\mathbf{n}}_q \times \left(\sum_{0,r} B'_{0,r} \nabla \times \hat{\mathbf{z}} J_n(k'_{t,0,q} |\boldsymbol{\rho} - \boldsymbol{\rho}_q|) e^{-jr\phi_q} i'_0(z) \right) \Big|_{|\boldsymbol{\rho} - \boldsymbol{\rho}_q| = a_q} .
 \end{aligned} \tag{2.182}$$

To reduce the system further, we use the identity $\hat{\mathbf{n}}_q \times \nabla \times \hat{\mathbf{z}} = -(\hat{\mathbf{n}}_q \cdot \nabla) \hat{\mathbf{z}} = -\partial_{n_q} \hat{\mathbf{z}}$ and the orthogonality of azimuthal as well as longitudinal harmonics to obtain

$$-j\omega\varepsilon \frac{1}{4j} \partial_{n_q} \Phi'_{0,r,q}{}^{imp} \nu_{0,r,q} + \sum_{p \neq q, n} A'_{0,n,p} \partial_{n_q} \Phi'_{0,r,p,q}{}^s + A'_{0,r,q} \partial_{n_q} \Phi'_{0,r,q}{}^s = B'_{0,r,q} \partial_{n_q} \Phi'_{0,r,p,q}{}^{int} , \tag{2.183}$$

where

$$\begin{aligned}
 \Phi'_{0,r,q}{}^{imp} &= H_r^{(2)}(k'_{t,0} a_q) , \\
 \nu_{0,r,q} &= \frac{1}{k'_{t,0}{}^2} \int \left(D_1 J_r(k'_{t,0} |\boldsymbol{\rho}' - \boldsymbol{\rho}_q|) e^{jr\phi'_q} i'_0(z') \right) \cdot \mathbf{M}(\mathbf{r}') d\mathbf{r}' , \\
 \Phi'_{0,n,p,q}{}^s &= (-1)^{n-r} J_n(k'_{t,0} a_q) H_{n-r}^{(2)}(k'_{t,0} |\boldsymbol{\rho}_p - \boldsymbol{\rho}_q|) e^{-j(n-r)\phi_{qp}} , \\
 \Phi'_{0,r,q}{}^s &= H_r^{(2)}(k'_{t,0} a_q) , \\
 \Phi'_{0,r,q}{}^{int} &= J_r(k'_{t,0,q} a_q) .
 \end{aligned}$$

Note that the “only” difference between the PEC and the dielectric post case is the presence of the scattered term, which becomes identically zero when $\varepsilon \rightarrow -\infty$, as expected.

It is a simple matter of dividing (2.183) by $H_r^{(2)}(k'_{t,0} a_q)$ in transiting to the final form of the scattering linear system obtained from the tangential H-field continuity:

$$\sum_{p \neq q, n} A'_{0,n,p} R'_{0,r,n,p,q}{}^{(1)} + A'_{0,r,q} - B'_{0,r,q} T'_{0,r,q}{}^{(1)} = \Omega'_{0,r,q}{}^{(1)} , \tag{2.184}$$

with the coefficients defined as

$$\begin{aligned}
 R'_{0,r,n,p,q}{}^{(1)} &= (-1)^{n-r} \frac{J_r(k'_{t,0} a_q)}{H_r^{(2)}(k'_{t,0} a_q)} H_{n-r}^{(2)}(k'_{t,0} |\boldsymbol{\rho}_p - \boldsymbol{\rho}_q|) e^{-j(n-r)\phi_{qp}} , \\
 T'_{0,r,q}{}^{(1)} &= \frac{k'_{t,0,q}}{k'_{t,0}} \frac{J_r(k'_{t,0,q} a_q)}{H_r^{(2)}(k'_{t,0} a_q)} , \\
 \Omega'_{0,r,q}{}^{(1)} &= j\omega\varepsilon \frac{1}{4j} \frac{J_r(k'_{t,0} a_q)}{H_r^{(2)}(k'_{t,0} a_q)} \nu_{0,r,q} .
 \end{aligned} \tag{2.185}$$

Alternatively, we could have enforced the electric field continuity, which would result in the system

$$\sum_{p \neq q, n} A'_{0,n,p} R'_{0,r,n,p,q}{}^{(2)} + A'_{0,r,q} - B'_{0,r,q} T'_{0,r,q}{}^{(2)} = \Omega'_{0,r,q}{}^{(2)} \quad , \quad (2.186)$$

with

$$R'_{0,r,n,p,q}{}^{(2)} = (-1)^{n-r} \frac{J_r(k'_{t,0} a_q)}{H_r^{(2)}(k'_{t,0} a_q)} H_{n-r}^{(2)}(k'_{t,0} |\boldsymbol{\rho}_p - \boldsymbol{\rho}_q|) e^{-j(n-r)\phi_{qp}} \quad ,$$

$$T'_{0,r,q}{}^{(2)} = \frac{\varepsilon'_q k'_{t,0,q}{}^2}{\varepsilon'_q k'_{t,0}{}^2} \frac{J_r(k'_{t,0,q} a_q)}{H_r^{(2)}(k'_{t,0,q} a_q)} \quad ,$$

$$\Omega'_{0,r,q}{}^{(2)} = j\omega\varepsilon \frac{1}{4j} \frac{J_r(k'_{t,0} a_q)}{H_r^{(2)}(k'_{t,0} a_q)} V_{0,r,q} \quad . \quad (2.187)$$

In fact, we opt for the latter system, since its particular form involves the calculation of cylindrical functions, as opposed to their derivatives in (2.185), since calculating derivatives implies, in view of the cylindrical functions recurrence relation

$$d_w Z_n(w) = \frac{1}{2} (Z_{n-1}(w) - Z_{n+1}(w)) \quad , \quad (2.188)$$

differences of two Bessel/Hankel functions. Hence, writing down the self-consistency conditions for all the posts, both PEC and dielectric ones, we can cast the complete linear system into a matrix representation

$$\underline{\underline{\mathbf{T}}}'_m (\underline{\mathbf{A}}'_m, \underline{\mathbf{B}}'_m) = \underline{\underline{\Omega}}'_m \quad , \quad (2.189)$$

the vector $(\underline{\mathbf{A}}'_m, \underline{\mathbf{B}}'_m)$ containing both the scattering and absorption coefficients (the term “absorption” indicating trapping of the field inside a dielectric post).

Therefore, for sufficient accuracy in cases when dielectric posts are present, it is enough to consider only the dielectric-post scattering of the $m=0$ mode, whereas the higher-order modes may be considered only in the PEC post scattering. However, if the geometry is such that higher-order modes are propagating, or have significant amplitudes, then the modal coupling must be properly taken into account. Since the procedure is extremely tedious and rarely necessary in practice, we shall not discuss it further.

Layered medium post-scattering

If now we are interested in post-scattering when the PPW is loaded with a **layered dielectric**, we have to start over from the boundary condition on posts, and modify both the Green’s dyadic to (2.131), as well as the scattered fields, which should read

$$\mathbf{M}'_{m,n}(\boldsymbol{\rho}, \boldsymbol{\rho}_p; z) = \nabla \times \hat{\mathbf{z}} H_n^{(2)}(k'_{t,m} |\boldsymbol{\rho} - \boldsymbol{\rho}_q|) e^{-jn\phi_q} i'_m(z) \quad ,$$

$$\mathbf{N}''_{m,n}(\boldsymbol{\rho}, \boldsymbol{\rho}_p; z) = \frac{1}{j\omega\mu(z)} \nabla \times \nabla \times \hat{\mathbf{z}} H_n^{(2)}(k''_{t,m} |\boldsymbol{\rho} - \boldsymbol{\rho}_q|) e^{-jn\phi_q} v''_m(z) \quad , \quad |\boldsymbol{\rho} - \boldsymbol{\rho}_q| \geq a_q \quad , \quad (2.190)$$

for fields scattered off a PEC post, and

$$\begin{aligned}
 \mathbf{M}'_{m,n}(\boldsymbol{\rho}, \boldsymbol{\rho}_p; z) &= \begin{cases} \nabla \times \hat{\mathbf{z}} H_n^{(2)}(k'_{t,m} |\boldsymbol{\rho} - \boldsymbol{\rho}_q|) e^{-jn\phi_q} i'_m(z), & |\boldsymbol{\rho} - \boldsymbol{\rho}_q| \geq a_q \\ \nabla \times \hat{\mathbf{z}} J_n(k'_{t,m} |\boldsymbol{\rho} - \boldsymbol{\rho}_q|) e^{-jn\phi_q} i'_m(z), & |\boldsymbol{\rho} - \boldsymbol{\rho}_q| \leq a_q, \end{cases} \\
 \mathbf{N}''_{m,n}(\boldsymbol{\rho}, \boldsymbol{\rho}_p; z) &= \begin{cases} \frac{1}{j\omega\mu(z)} \nabla \times \nabla \times \hat{\mathbf{z}} H_n^{(2)}(k''_{t,m} |\boldsymbol{\rho} - \boldsymbol{\rho}_q|) e^{-jn\phi_q} v''_m(z), & |\boldsymbol{\rho} - \boldsymbol{\rho}_q| \geq a_q \\ \frac{1}{j\omega\mu(z_q)} \nabla \times \nabla \times \hat{\mathbf{z}} J_n(k''_{t,m,q} |\boldsymbol{\rho} - \boldsymbol{\rho}_q|) e^{-jn\phi_q} v''_m(z), & |\boldsymbol{\rho} - \boldsymbol{\rho}_q| \leq a_q, \end{cases}
 \end{aligned} \tag{2.191}$$

for fields scattered off a dielectric post. Note that now the TE modes have a $1/j\omega\mu(z)$ factor instead of $1/k^2$. This was chosen so to enable simpler application of the longitudinal functions orthogonality in the derivation of the scattering-amplitude linear system, which holds under the weighted scalar product. As will be evident shortly, this choice is rather natural having in mind the general form of the impressed TE field

$$\begin{aligned}
 \mathbf{H}_{imp}''(\mathbf{r}) &= -j\omega\varepsilon(z') \int \frac{1}{\omega^2\varepsilon(z')\mu(z)} (\nabla \times \nabla \times \hat{\mathbf{z}}) \otimes (\nabla' \times \nabla' \times \hat{\mathbf{z}}) \mathcal{S}''(\mathbf{r}, \mathbf{r}') \cdot \mathbf{M}(\mathbf{r}') d\mathbf{r}' \\
 &= \frac{1}{j\omega\mu(z)} \int (\nabla \times \nabla \times \hat{\mathbf{z}}) \otimes (\nabla' \times \nabla' \times \hat{\mathbf{z}}) \mathcal{S}''(\mathbf{r}, \mathbf{r}') \cdot \mathbf{M}(\mathbf{r}') d\mathbf{r}',
 \end{aligned} \tag{2.192}$$

where upon applying the Gegenbauer addition theorem to the scalar potential, one obtains

$$\begin{aligned}
 \mathbf{H}_{imp}''(\mathbf{r}) &= \frac{1}{j\omega\mu(z)} \sum_m \frac{1}{4j} \sum_n D_2 \frac{H_n^{(2)}(k''_{t,m} |\boldsymbol{\rho} - \boldsymbol{\rho}_q|) e^{-jn\phi_q}}{k''_{t,m}{}^2} v''_m(z) \\
 &\quad \times \int \left(D_2 J_n(k''_{t,m} |\boldsymbol{\rho}' - \boldsymbol{\rho}_q|) e^{jn\phi_q} v''_m(z') \right) \cdot \mathbf{M}(\mathbf{r}') d\mathbf{r}'.
 \end{aligned} \tag{2.193}$$

Hence, as before, the most convenient choice of the scattered-field representation is the exact same functional form of the impressed field. One can easily show the scattered fields (2.190) and (2.191) satisfy the Helmholtz vector equations and, in addition, the following useful relations

$$\begin{aligned}
 \mathbf{N}'' &= \frac{1}{j\omega\mu(z)} \nabla \times \nabla \times \hat{\mathbf{z}} \Phi'', \quad \mathbf{M}'' = \nabla \times \hat{\mathbf{z}} \Phi'' \\
 &\Rightarrow \nabla \times \mathbf{N}'' = -j\omega\varepsilon(z) \mathbf{M}'' .
 \end{aligned} \tag{2.194}$$

Then, repeating the steps followed in the derivation of the single-layer linear systems, we arrive at systems of the same form as (2.179)

$$\begin{aligned}
 \sum_{p \neq q, n} A'_{m,n,p} \Gamma'_{m,r,n,q,p} + A'_{m,r,q} &= \Omega'_{m,r,q}, \\
 \Gamma'_{m,r,n,q,p} &= (-1)^{n-r} \frac{J_r(k'_{t,m} a_q)}{H_r^{(2)}(k'_{t,m} a_q)} H_{n-r}^{(2)}(k'_{t,m} |\boldsymbol{\rho}_p - \boldsymbol{\rho}_q|) e^{-j(n-r)\phi_{qp}},
 \end{aligned}$$

$$\Omega'_{m,r,q} = \frac{J_r(k'_{t,m} a_q)}{H_r^{(2)}(k'_{t,m} a_q)} V'_{q,m,r}$$

$$V'_{q,m,r} = -j\omega\epsilon(z') \frac{1}{4j} \frac{1}{k'_{t,m}{}^2} \int \left(D_1' \frac{1}{\epsilon(z')} H_r^{(2)}(k'_{t,m} |\boldsymbol{\rho}' - \boldsymbol{\rho}_q|) e^{j r \phi'_q} i'_m(z') \right) \cdot \mathbf{M}(\mathbf{r}') d\mathbf{r}' ,$$
(2.195)

for TM fields, and for TE fields

$$\sum_{p \neq q, n} A''_{m,n,p} T''_{m,r,n,q,p} + A''_{m,r,q} = \Omega''_{m,r,q} ,$$

$$T''_{m,r,n,q,p} = (-1)^{n-r} \frac{J_r(k''_{t,m} a_q)}{H_r^{(2)}(k''_{t,m} a_q)} H_{n-r}^{(2)}(k''_{t,m} |\boldsymbol{\rho}_p - \boldsymbol{\rho}_q|) e^{-j(n-r)\phi_{qp}} ,$$

$$\Omega''_{m,r,q} = \frac{J_r(k''_{t,m} a_q)}{H_r^{(2)}(k''_{t,m} a_q)} V''_{q,m,r} ,$$

$$V''_{q,m,r} = \frac{1}{4j} \frac{1}{k''_{t,m}{}^2} \int \left(D_2' \frac{1}{\mu(z')} H_r^{(2)}(k''_{t,m} |\boldsymbol{\rho}' - \boldsymbol{\rho}_q|) e^{j r \phi'_q} v''_m(z') \right) \cdot \mathbf{M}(\mathbf{r}') d\mathbf{r}' .$$
(2.196)

It should be noted that the complexity of the self-consistency conditions does not increase in comparison to single-layer SIW devices, if layered media are present.

Unfortunately, dielectric-post scattering complicates the analysis tremendously due to mode-coupling induced by longitudinal inhomogeneity. More precisely, a general dielectric post may be composed of an arbitrary number of layers of arbitrary thickness. Hence, the longitudinal dependence of fields inside such a post will generally be drastically different than the one of fields outside, with the implication that even though the field impinging on such a post may be a pure mode m , *all modes* will be scattered back. The extent to which a given mode t will be excited is determined primarily by the scalar product between the longitudinal functions outside and inside a post. Of course, a well-designed device will prevent the propagation of such modes, but the phase-shift and scattering amplitude of a dielectric post are now not easily controllable due to the complexity of its field distribution; these kinds of devices are, to the author's knowledge, not used in practice.

2.2.2 Let there be light - exciting the siw

While exposing the formalism used to evaluate electromagnetic fields in internal regions of an SIW-type device, we have been constantly referring to the fields due to impressed sources. However, we have not referred to any specific excitation, for which we amend in this subsection. We will deal with the most common excitations, their mathematical models and the extent of their validity, focusing primarily on the calculation of excitation amplitudes. The discussion on the extraction of port parameters from fields is relegated to after we will have discussed the slot admittance calculation in subsection 2.5

Now, as is evident from the vast body of work on SIW devices, the most common feeds used to inject power are the coaxial transition (usually of SMA kind), horn antennas/waveguides, and slot transitions. This should come as no surprise since the operational band, power-handling capabilities, and ease of manufacturing of said feeds are superb. Additionally, microstrip lines can be used as feeds as well, since the guided field profile matches well the one guided in an SIW [1], resulting in respectable matching.

Hence, if the analysis is to be of any practical use, realistic models of feeds have to be included, and the port parameters easily obtainable. With this in mind, we opt for the waveguide-port model of feeds, choosing to approximate our feeds as equivalent magnetic currents existing over a surface corresponding to the feed aperture. Such models lead to unambiguous definition of port-parameters and hold over a wide range of frequencies, as opposed to lumped or discrete port models. Firstly we shall apply this principle to the coaxial transition.

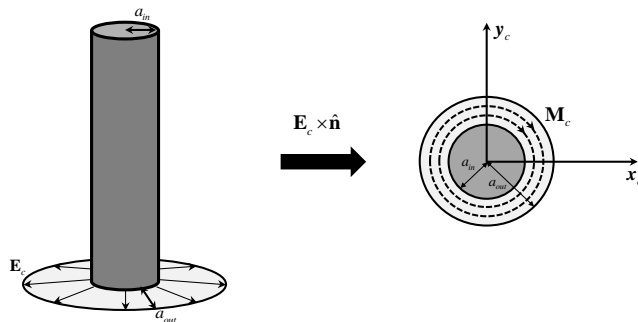
Coaxial port

Figure 2.14 shows the layout of a generic coaxial port model. It consists of a central conductor of radius a_{in} protruding through a plate, usually the bottom one, and is surrounded by an annulus of negative unit-amplitude magnetic current flowing in the ϕ_c direction, and extending from a_{in} to a_{out} . Essentially, stipulating so enforces that a unit magnetic current excites the guide regardless of the frequency, the current being related to the fundamental mode of the coaxial line as

$$\begin{aligned} \mathbf{M}_{coax}(\mathbf{r}') &= \mathbf{E}_{coax}(\mathbf{r}') \times \hat{\mathbf{n}} \\ &= -\frac{V_0 \delta(z - z_{plate}^+)}{|\boldsymbol{\rho}' - \boldsymbol{\rho}_c| \ln\left(\frac{a_{in}}{a_{out}}\right)} \hat{\phi}_c. \end{aligned} \quad (2.197)$$

This approximation will hold well as long as the operating frequency is sufficiently below the cut-off frequency of the second mode of the coaxial line. Since the current is rotationally invariant, and is concentrated just above or below a metal plate, one expects that the field launched into a PPW will also possess rotational invariance; hence, it will not contain any TE modes.

Figure 2.14 Coaxial port model used in the analysis



The analytic, closed-form expression for the field excitation amplitude is

$$\Omega'_{q,r,m} = \begin{cases} \frac{J_r(k'_{tm} a_q)}{H_r^{(2)}(k'_{tm} a_q)} \\ \frac{J_r(k'_{tm} a_q)}{H_r^{(2)}(k'_{tm} a_q)} \end{cases} \gamma'_{m,-r},$$

$$\gamma'_{m,-r} = \begin{cases} H_{-r}^{(2)}(k'_{t_m} | \boldsymbol{\rho}_c - \boldsymbol{\rho}_q |) \frac{e^{jr\phi_{qlc}} 2\pi V_0}{\ln(a_{out}/a_{in})} (J_0(k'_{t_m} a_{out}) - J_0(k'_{t_m} a_{in})) i'_m(z_{plate}) , & \boldsymbol{\rho}_c \neq \boldsymbol{\rho}_q \\ \frac{2\pi V_0}{\ln(a_{out}/a_{in})} (H_0^{(2)}(k'_{t_m} a_{out}) - H_0^{(2)}(k'_{t_m} a_{in})) i'_m(z_{plate}) , & \boldsymbol{\rho}_c = \boldsymbol{\rho}_q \\ 0 , & \text{otherwise .} \end{cases} \quad (2.198)$$

Additionally, it can be easily shown that $\Omega_{q,r,m}^* = 0$. Another benefit of having chosen the current distribution as in (2.197) is that the self-admittance of a coaxial port can be expressed in closed form, the admittance between ports being defined as

$$Y_{P_i, P_j} = \frac{I_{P_i}}{V_{P_j}} \Big|_{V_{P_k}=0, k \neq j} = -\frac{1}{V_i V_j} \int \mathbf{M}_{P_i}(\mathbf{r}') \cdot \mathbf{H}_{P_j}(\mathbf{r}') d\mathbf{r}' . \quad (2.199)$$

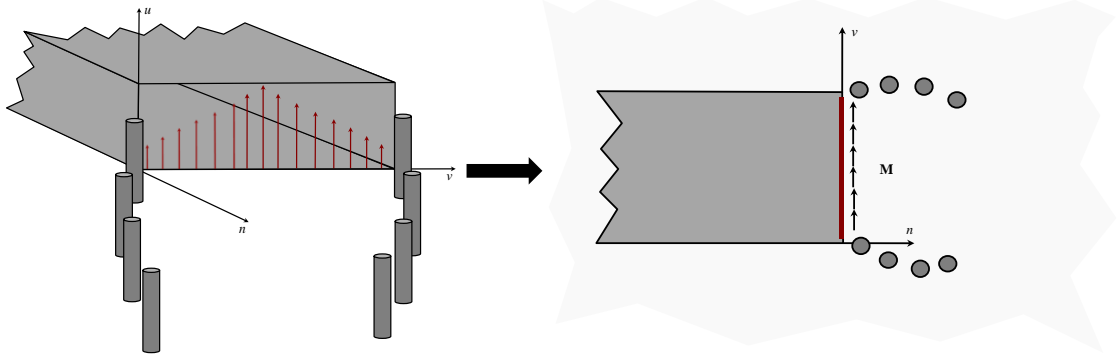
Then, the self-admittance is

$$\begin{aligned} Y_{P_i, P_i} = & \sum_m \frac{\chi'_m}{k'_{t_m}{}^2} \left\{ \frac{2j}{\pi} \ln \left(\frac{a_{P_i, out}}{a_{P_i, in}} \right) + J_0(k'_{t_m} a_{P_i, in}) [H_0^{(2)}(k'_{t_m} a_{P_i, out}) - H_0^{(2)}(k'_{t_m} a_{P_i, in})] \right. \\ & \left. - H_0^{(2)}(k'_{t_m} a_{P_i, out}) [J_0(k'_{t_m} a_{P_i, out}) - J_0(k'_{t_m} a_{P_i, in})] \right\} \\ & + \sum_{p,m,n} A'_{i;m,n,p} H_n^{(2)}(k'_{t_m} | \boldsymbol{\rho}_{P_i} - \boldsymbol{\rho}_p |) e^{jn\phi_{pP_i}} \frac{-2\pi}{V_i \ln \left(\frac{a_{P_i, out}}{a_{P_i, in}} \right)} (J_0(k'_{t_m} a_{P_i, out}) - J_0(k'_{t_m} a_{P_i, in})) \\ & + \sum_m A'_{i;m,0,P_i} \frac{-2\pi}{V_i \ln \left(\frac{a_{P_i, out}}{a_{P_i, in}} \right)} (H_0^{(2)}(k'_{t_m} a_{P_i, out}) - H_0^{(2)}(k'_{t_m} a_{P_i, in})) , \end{aligned} \quad (2.200)$$

χ'_m being the m -th mode coefficient depending on the stratification and coaxial current magnitude. The first term describes the direct PPW-wave self-interaction, while the second and third terms describe the post-scattering self-interaction.

Waveguide port

The second common type of excitation used to inject power into SIW devices is the waveguide transition, or as we shall refer to it here, **the waveguide port**. Due to its ability to handle large power and provide good matching, it is the excitation of choice for many an application. Now, the standard procedure for modelling such a port relies on the use of the equivalence principle, and is quite similar to the one used to model the coaxial port. To be more specific, consider the junction between the feeding rectangular guide and the SIW guide, as shown in the following figure.

Figure 2.15 Junction between a rectangular and an SIW guide


Firstly, we enforce the dominant TE_{01} mode to impinge onto the junction, since in practice this is the most common case. Its form is given in the local coordinate system of the port by [80]

$$\mathbf{e}^{TE_{01}}(\mathbf{r}) = C_e \sin\left(\frac{\pi}{W}v\right)\hat{\mathbf{u}}, \quad \mathbf{h}^{TE_{01}}(\mathbf{r}) = C_h \sin\left(\frac{\pi}{W}v\right)(-\hat{\mathbf{v}}), \quad (2.201)$$

and is normalized to carry unit power as

$$\int_P \mathbf{e}^{TE_{01}}(\mathbf{r}) \times \mathbf{h}^{TE_{01}}(\mathbf{r})^* \cdot \hat{\mathbf{n}} dS = 1. \quad (2.202)$$

Now, as is done, e.g., in problems pertaining to aperture radiation into free space, one could apply the equivalence principle, and envelop the guide by an enclosing surface, subsequently placing distributing magnetic and electric currents *all over it*, if one wishes to rigorously take into account the diffraction at the guide termination. However, in practice the guide is designed so as to minimize this diffraction, and the SIW confines the field strongly, further preventing backscattering. Hence, neglecting the diffraction/backscattering does not introduce significant errors. Then, whenever these assumptions hold, we can apply the equivalence principle approximately, as shown in Figure 2.15, and close the guide aperture by a PEC plate, shorting out the equivalent electric current, and leaving solely the magnetic ones. We should have, in principle, placed a PEC plate extending across the whole plane in which the aperture lies, but since the post fences keep the field focused in the guide, we may use a truncated plate, implying we do not have to consider any scattering phenomena outside the SIW guide. Hence, the equivalent magnetic current may be simply related to the feeding electric field as

$$\mathbf{M}_{wg}(\mathbf{r}) = 2\mathbf{e}^{TE_{01}}(\mathbf{r}) \times \hat{\mathbf{n}} = C \sin\left(\frac{\pi}{W}v\right)\hat{\mathbf{v}}, \quad (2.203)$$

where the constant C can be chosen to make the current unit in amplitude. However, the PEC lid used does not conform to the cylindrical coordinate system, which is used, and this might significantly complicate the analysis. For example, when calculating field impressed by the waveguide port, one should include the effect of scattering from the PEC lid. As its geometry is most naturally expressed in rectangular coordinates, and the Green's function is expressed in cylindrical coordinates, an awkward procedure must be effected where the lid is first discretized and the scattering problem numerically solved. However, a trick, devised by Arneri and Amendola [15], can be applied, whereby one replaces the lid by a fence of tightly spaced small vertical posts of radius smaller than, say, $0.05\lambda_g$. This

arrangement effectively emulates the continuous metallization of a PEC lid, and the scattering problem is dramatically easier to solve.

2.2.3 The exterior problem

So far, we have discussed the internal problem – scattering inside a PPW, possibly in the presence of PEC or dielectric posts. However, as mentioned in the introductory subsections of this chapter, a large portion of SIW devices belong to the class of antennas; these are, most commonly, in the subclass of slot arrays. It is why the analysis then must include radiation and scattering in open half-spaces if one wishes to be able to consider such scenarios. As will be shown in following sections, slots can be analyzed successfully and accurately using the MoM formalism (see for example [90], [91] etc.), whereby the effect of slots is modelled using the equivalent currents concept. The slots connecting a PPW and a half-space will then be modelled as magnetic currents radiating above PEC plates of infinite extent. To find the field they generate in the half-space, it is obvious that one must have in possession the pertinent Green's function.

It is easily found upon recalling that our preferred “flavour” of choice for the equivalence principle stipulates that slots, if present, are to be filled with the same material the plate in which they are excavated is made from. The slots are then replaced by equivalent magnetic and electric currents, but since the plate is a PEC, it will short out the electric currents, leaving only the magnetic ones. A simple application of PEC boundary conditions then leads to the conclusion that the tangential magnetic fields must have a maximum (or a minimum) at the surface of the PEC, whereas the normal ones must be shorted out there (otherwise their presence at the boundary would imply the existence of tangential electric fields). This observation, in conjunction with the plate's infinite extent, stipulates that the effect of magnetic currents is doubled. In effect, the Green's dyadic then has the same functional dependence as the free-space one, save for the additional factor of 2 which comes from the above considerations, and is given by

$$\underline{\mathbf{G}}^{HM}(\mathbf{r}, \mathbf{r}') = \left(\mathbf{1} + \frac{\nabla \otimes \nabla}{k^2} \right) \frac{e^{jk|\mathbf{r}-\mathbf{r}'|}}{2\pi|\mathbf{r}-\mathbf{r}'|} . \quad (2.204)$$

Of course, this form lends itself to useful approximations, e.g. the far-field approximation, or multipole expansion, but as far as the external problem is concerned, this completes the analytical part. If scatterers are present in the half-space, they too can be modelled within the MoM framework, or if high-frequency regime conditions apply, physical theory of diffraction [92] or the geometrical theory of diffraction [93] may be applied in various forms. Moreover, if the plate is made from a material having finite conductivity, it can still be modelled analytically using the concept of effective magnetic currents as proposed in [18] and analytic Green's functions for such cases are available. However, the finite conductivity case is outside the scope of this thesis and will not be discussed further.

2.3 The slot thickens – mixing mode matching and the method of moments

Up to this point, we have covered a fair amount of ground, having established the methods to be used in analysis of SIW devices, along with the range of structures that can be successfully tackled using these methods. Here we shall weave in the final patch in the tapestry that is the hybrid mode-matching/MoM, by actually adding the “MoM” into it.

First, we shall repeat the formulation of the slot-problem with emphasis on, leading to a system of coupled integral equations. Then, we will discuss how to discretize them and turn into linear systems using the well-known framework of the method of moments, at the same time adopting a bird’s eye view of the sub-problems (post-scattered fields, impressed fields, slot-scattered fields) and an ant-view of each sub-problem with focus on the crucial details. After this exposition, we shall comment on the properties of said linear systems in connection with the problem geometry, which will lead us to the appropriate choice of algorithm for the solution. Finally, we will discuss the approximations used in MoM matrix filling which render the analysis computationally efficient, and present some rule-of-thumb criteria for choosing the sufficient number of basis functions and range of interactions necessary for a given accuracy.

2.3.1 From slots to equivalent currents

In the introductory section of this chapter, we discussed how to reexpress the fairly complex problem of finding the EM fields in a stacked-PPWs geometry as a “simpler” one where formally decoupled regions are connected by equivalent currents. At this point, we repeat the most important results.

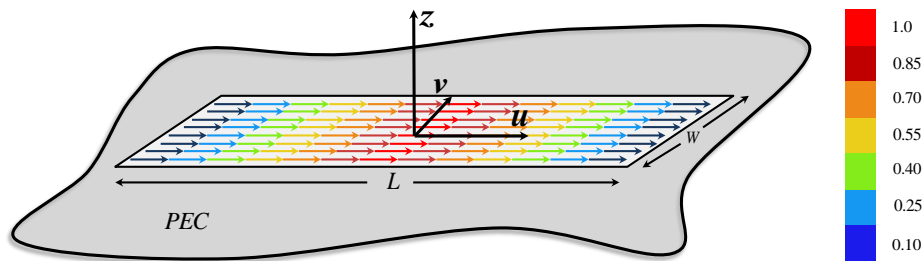
Firstly, upon applying the equivalence principle, each slot is replaced by two equivalent currents – one above the slot, flowing in the direction of its largest dimension, the second one being of the exact same amplitude and functional form, but of opposite direction; this will guarantee the continuity of tangential electric fields. As mentioned before, we consider the slots as thin, meaning one of their dimensions is smaller than 0.1λ . This is the most common case in practice because they are significantly easier to control than wide ones, as their radiation pattern and coupling properties are well-researched (see, e.g., [94]). If wide slots are present, one must then include the functional dependence in the “other” direction.

Now comes the question of how to model the current functional dependence. Over the years, a large number of basis functions have been devised, ranging from triangular [95], quadrilateral, piecewise-continuous, edge-singular [96] etc., each suitable to a specific problem, some more flexible than the others. In our case, the currents will be distributed on a rectangular surface, flowing along the direction of the maximum chord, i.e. the slot length, which we shall refer to as the *longitudinal direction*. As the restriction to thin slots dictates that the change of the current in the transverse direction (along the width) is negligible, i.e. can be considered constant, we can use basis functions having dependence solely in the longitudinal direction. For instance, we might use piecewise-constant functions, or even pulse basis functions. However, owing to their discontinuity, they do not satisfy the charge-current conservation, potentially introducing spurious charges and currents, and lead to more cumbersome expressions for slot admittance, as will be evident later on. Hence, we shall adopt entire-domain functions of sine dependence in a slot’s local coordinate system, given by

$$\mathbf{b}_{q,n}(u, v) = \hat{\mathbf{u}}_q \frac{1}{W_q} \sin\left(\frac{n\pi}{L_q}\left(u + \frac{L_q}{2}\right)\right), \quad (2.205)$$

$$-\frac{L_q}{2} \leq u \leq \frac{L_q}{2}; \quad -\frac{W_q}{2} \leq v \leq \frac{W_q}{2}$$

Figure 2.16 Slot coordinates and characteristic lengths; a colour plot of the first-order basis function current distribution (The amplitude is normalized with respect to the maximum; the warmest colour denotes the largest amplitude)



W_q, L_q being the width and length of slot q , respectively. The current, then, is represented as

$$\mathbf{M}_q = \sum_n V_{q,n} \mathbf{b}_{q,n}(u_q, v_q). \quad (2.206)$$

It may seem this choice is a bit out-of-the-blue, but the motivation behind is quite simple – the magnetic currents are related to the electric fields, generated at obstacles, as simple rotations with respect to the obstacle normal, i.e. $\mathbf{M}_i(\mathbf{r}) = \mathbf{E}_i(\mathbf{r}) \times \hat{\mathbf{n}}$. In practice, when slots are used as radiators or couplers, one attempts to excite the slots into resonance, the lowest one occurring when the slots are approximately half-wavelength long. It is then reasonable to expect that the electric field across the slot will be almost sinusoidal (this can be also reasoned if one thinks of a slot as a narrow rectangular waveguide). Hence, a basis having the same functional form as the cross-sectional TE_{0n} modes of a waveguide having the same dimensions as the slot (n denoting the order of the harmonic in u), is very convenient. Moreover, the analytic properties of this particular basis facilitates the admittance calculation, since two out of four integrals involved in its expression can be evaluated analytically [97]. In addition, the magnetic dipole moment, if needed, can be simply expressed in closed form upon integrating the current over the slot surface as

$$\mathbf{m}_q = \sum_n V_{q,n} L_q \frac{1 - (-1)^n}{n\pi}. \quad (2.207)$$

Equipped with a ready basis for current representation, we can tackle the slot-problem. Firstly, we shall reformulate the boundary conditions as a set of coupled integral equations. Since the tangential magnetic field has to be continuous across each slot, i.e.

$$\hat{\mathbf{n}} \times \mathbf{H}_w^{\text{Total}}(\mathbf{r}_q) \times \hat{\mathbf{n}} = \hat{\mathbf{n}} \times \mathbf{H}_{w+1}^{\text{Total}}(\mathbf{r}_q) \times \hat{\mathbf{n}}, \quad (2.208)$$

implying that the total tangential magnetic field across each point of the surface of slot q , created by both impressed sources as well as secondary ones (scatterers), in the region

denoted by index w , being either a PPW or a half-space, has to be equal to the total tangential magnetic field across each point of the surface of slot q in the region $w+1$. Now, the total field in a given region is the sum of several contributions

$$\begin{aligned} \mathbf{H}_w^{Total} = \mathbf{H}_w^{imp} + \mathbf{H}_w^{scattered} = & -\sum_i j\omega\epsilon_w \underline{\mathbf{G}}_w^{HM} * \mathbf{M}_{w,i} \\ & + \sum_p A'_{w,p,m,n} \mathbf{M}'_{w,p,m,n} + A''_{w,p,m,n} \mathbf{N}'_{w,p,m,n} \\ & - \sum_q j\omega\epsilon_w \underline{\mathbf{G}}_w^{HM} * \mathbf{M}_{w,q} , \end{aligned} \quad (2.209)$$

where the latter two terms are, respectively, the post-scattered and slot-scattered fields. Of course, if the region is a half-space, there are no post-scattered fields, though there may exist fields scattered from an obstacle. As the post-scattered field is approximated by a finite number of modes, so will the slot-scattered field be approximated as the contribution from a finite number of current basis functions. In order to find the slot-scattering amplitudes, i.e. the unknown current expansion coefficients, (2.208) can be converted to a linear system. This idea goes a long way back to works of Kontorovich, Krylov, Akilov and Hilbert, among many others, whereas its specific application to electromagnetic problems is credited to Harrington [98]. It rests on the premise that by projecting a system such as (2.208) onto a basis of choice using a suitably defined scalar product, one effectively “knocks out” the functional dependence of all the partial fields involved across the region where a condition such as (2.208) holds. In other words, by such a procedure, one transits from an equation which should hold at infinitely many points to an “averaged” equation which holds in either approximate or exact sense over the problem domain. To put this on a firmer mathematical basis, let us first define the following linear operator

$$\mathbf{L}^{(k)}[\mathbf{M}] = -j\omega\epsilon_k \int \underline{\mathbf{G}}_k^{SW}(\mathbf{r}, \mathbf{r}') \mathbf{M}(\mathbf{r}') d\mathbf{r}' ,$$

which acts on a magnetic current \mathbf{M} to produce the magnetic field in the waveguide k . Here the kernel of this transformation is not the no-posts PPW dyadic Green’s function we sought and derived in the previous section, but includes the effect of scattering off of posts as well. The current may be either an impressed one, or an induced one. Our geometry consists of waveguides stacked on top of each other, a waveguide indexed n being bounded from below by a plate indexed k and from above by a plate indexed $k+1$. The convention for indexing currents and fields is the following – a magnetic field existing in the waveguide/region k is indexed by k . A current existing on the lower plate of the waveguide k is denoted by index k , whereas if a current is localized to the upper plate of the waveguide k , it is denoted by index $k+1$. Then, by explicitly separating the fields into impressed ones and induced ones (induced at slots, in our case), we can rewrite the boundary condition (2.208) on the plate k as

$$\hat{\mathbf{z}} \times \left\{ \mathbf{L}^{(k+1)}[\mathbf{M}^{(k+1)}] - \mathbf{L}^{(k+1)}[\mathbf{M}^{(k)}] - \mathbf{L}^{(k)}[\mathbf{M}^{(k)}] + \mathbf{L}^{(k)}[\mathbf{M}^{(k-1)}] \right\} \times \hat{\mathbf{z}} = \hat{\mathbf{z}} \times \left\{ \mathbf{H}_{imp}^{(k)} - \mathbf{H}_{imp}^{(k+1)} \right\} \times \hat{\mathbf{z}} . \quad (2.210)$$

Unknown currents at each slot are expanded as (2.206) and plugged into (2.210), enforced across each slot. This constitutes a set of coupled integral equations with current amplitudes $V_{q,n}$ as unknowns. To transit to a system of *linear equations*, we can choose a set of so-called *test functions*, their spatial support being a part or the whole domain of the problem. The testing functions should cover the domains of all basis functions, lest one ends with an underspecified linear system, as will be obvious in a few moments. Then, we perform a

scalar product of the system (2.210) with each function in this set, the scalar product, in our case, being defined as the complex-conjugate product

$$\langle \mathbf{f}, \mathbf{g} \rangle = \int_S \mathbf{f}(\mathbf{r}) \cdot \mathbf{g}(\mathbf{r})^* d\mathbf{r} . \quad (2.211)$$

Doing so leads to linear system of the general form

$$\underline{\mathbf{Y}}\mathbf{V} = \mathbf{I} , \quad (2.212)$$

with the $\underline{\mathbf{Y}}$ being the admittance matrix, a general entry of which has the form

$$\begin{aligned} Y_{l,s} = & \int_S \mathbf{w}_l(\mathbf{r}) \cdot \left[-j\omega\varepsilon_k \int_{S'} \underline{\mathbf{G}}_k \cdot \mathbf{b}_s(\mathbf{r}') d\mathbf{r}' \right] d\mathbf{r} , \\ & + \int_S \mathbf{w}_l(\mathbf{r}) \cdot \left[-j\omega\varepsilon_{k+1} \int_{S'} \underline{\mathbf{G}}_{k+1} \cdot \mathbf{b}_s(\mathbf{r}') d\mathbf{r}' \right] d\mathbf{r} \end{aligned} \quad (2.213)$$

where the weighting function \mathbf{w} is defined over a slot, and the Green's dyadics include the effect of post-scattering. The admittance itself can be interpreted as the reaction [99], interaction "energy" between two unit-strength magnetic currents [100], [101], or as a weighted projection between the basis functions, where the Green's function plays the role of the weighting function.

Different choices of testing functions lead to different accuracy, convergence of solution and computational effort, which are almost always in trade-off – one can have at most two satisfactory properties. Therefore, a discussion of bases is absolutely necessary to justify our choice.

The simplest choice of testing functions is the point-pulse basis , whereby one performs scalar products with a train of weighted Dirac delta functions $w_q = \hat{\mathbf{u}}_q \sum_i a_i \delta(\mathbf{r}_q - \mathbf{r}_i)$.

Intuitively, this has the effect of relaxing the boundary condition in such a way that it holds at finitely many points over the given problem region. The basis has the advantage of making the scalar product implied in (2.213) trivial, lifting the computational burden of having to use numerical integration schemes in the MoM matrix filling, which is usually the bottleneck of the method. However, the point-matching scheme's greatest strength is also its greatest weakness because it rests on relaxing the boundary conditions, which usually leads to poorer accuracy compared to results obtained with other bases. Other options include a plethora of basis functions such as piecewise-constant, piecewise sinusoidal, triangular etc., which we will not delve on too exhaustively now, but an interested reader may refer to Gibson [50] for a concise summary of the most common ones.

The triangular base offers flexibility since it can effectively be used to model shapes of large variety. However, it leads to a heavier admittance calculation due to subdivision of the region where it is applied, and requires a routine for generating this subdivision. It is very convenient for geometries having a more complex/irregular layout.

The piecewise-sine base has the ability to reconstruct the current distributions with only a few subsections over the slot, provided the slots are excited around resonance. In addition, its analytic properties allow simplifications in calculating the admittance matrix entries. Though by its nature it is a piecewise expansion, the subsectional basis functions and their derivatives are continuous, which is of paramount importance in evaluating the admittance matrix entries.

where a generic sub-matrix $\underline{\underline{Y}}_{q,r}^{(p)}$ collects admittances between the slots on interface q (“interface” denoting the metal plate where the slots are situated) and interface r , the interactions taking place in region p . The grand admittance matrix has a tridiagonal structure owing up to the interactions taking place only between adjacent interfaces; the diagonal sub-matrices $\left(\underline{\underline{Y}}_{k,k}^{(k-1)} + \underline{\underline{Y}}_{k,k}^{(k)}\right)$ collect admittances of slots on the same interface but due to interactions mediated in different regions, whereas the off-diagonal sub-matrices $-\underline{\underline{Y}}_{v,w}^{(u)}$ collect the negative of admittances between slots on adjacent interfaces v, w due to wave interaction in the region u . Hence, the only possible combinations of sub-matrix indexes are $(k, k), (k+1, k), (k, k+1), (k+1, k+1)$. It should be noted that $\underline{\underline{Y}}_{1,1}^{(0)}$ and $\underline{\underline{Y}}_{N+1,N+1}^{(N+1)}$ contain half-space admittances of the form

$$\underline{\underline{Y}}_{l,s} = \int_S \mathbf{b}_l(\mathbf{r}) \left[-j\omega\epsilon_k \int_S \underline{\underline{G}}_k^{\text{HS}} \mathbf{b}_s(\mathbf{r}') d\mathbf{r}' \right] d\mathbf{r} = \underline{\underline{Y}}_{l,s}^{(k)}, \quad (2.217)$$

where the Green’s dyadic is of the form (2.204).

In sum, if one wishes to effectively analyze slots in metal plates, the method-of-moments formalism can be applied in a straightforward manner to SIW-type problems – the slots can be filled by the same material the plates in which they are excavated are made from, and equivalent magnetic currents can be placed on their respective surfaces. Then the continuity of tangential electric and magnetic fields is stipulated across each slot; the continuity of the electric field leads to the currents, placed above and below each slot, being equal in magnitude and functional dependence, but opposite in direction. The continuity of the magnetic field leads to a system of coupled integral equations, which can be approximately solved by discretization. First, the unknown currents are chosen to be represented in an entire-domain sine basis. Then, following the method of Petrov and Galerkin, the system of integral equations is projected onto that very same basis the currents are expanded in with the aid of a suitably chosen scalar product. This results in a symmetric linear system relating the vector containing unknown currents amplitudes and the so-called excitation vector by a linear transformation, effected by the generalized admittance matrix, which collects the reactions (in the sense of Rumsey) between all the basis functions. In a typical problem, such a matrix contains a large number of entries (on the order of 10^4), and the calculation of each entry usually requires a numerical integration. Hence, the filling of this matrix will be the bottleneck of the method, its efficiency singularly depending on one’s ability to compute the entries in an efficient manner. This paramount problem is dealt with in the next subsection.

2.3.2 Admittance calculation

The admittances defined in (2.214) and (2.217) can be computed using a variety of methods, e.g. using spectral-domain integration, both numerically by suitably deforming the Fourier inverse contours and sampling, and using the steepest-descent-path integration. On the other hand, integration in spatial domain can be convenient in some cases where higher precision is necessary (for example, when calculating the admittance of closely-spaced slots), mainly resting on one of the many variants of the Gaussian quadrature [103]. In addition, one has to evaluate the self-admittances (the interaction of a basis function with itself), which are singular integrals due to the singularity of the Green’s functions involved. There one needs to be quite careful since improper handling of such integrals may lead to inaccurate and plain nonsensical results.

In this subsection we shall deal with all the peculiarities of calculating the admittances, proposing the most elegant, efficient, or straight-forward way of doing so.

A. SIW ADMITTANCE

The most common entry in the admittance matrix is the internal-problem admittance, defined by the integral

$$Y_{l,s} = \int_S \mathbf{b}_l(\mathbf{r}) \left[-j\omega\epsilon_k \int_{S'} \underline{\mathbf{G}}_k^{SIW} \cdot \mathbf{b}_s(\mathbf{r}') d\mathbf{r}' \right] d\mathbf{r} = Y_{l,s}^{(k)}, \quad (2.218)$$

which, as mentioned before, contains both the direct PPW interaction, and the post-scattered wave interaction, and therefore can be reexpressed as

$$Y_{l,s} = \int_S \mathbf{b}_l(\mathbf{r}) \cdot \mathbf{H}^{SIW,s}(\mathbf{r}) d\mathbf{r} = \int_S \mathbf{b}_l(\mathbf{r}) \cdot (\mathbf{H}^{PPW,s}(\mathbf{r}) + \mathbf{H}^{Posts,s}(\mathbf{r})) d\mathbf{r} = Y_{l,s}^{PPW} + Y_{l,s}^{Posts}. \quad (2.219)$$

In order to calculate the direct PPW admittance, given by

$$Y_{l,s}^{PPW} = \int_S \mathbf{b}_l(u,v) \left(-j\omega\epsilon \int_S \underline{\mathbf{G}}^{PPW}(\mathbf{r},\mathbf{r}') \cdot \mathbf{b}_s(u',v') du'dv' \right) dudv, \quad (2.220)$$

we resort to the procedure used by Albani in [104], whereby a significant analytical simplification is obtained upon using the following facts: the currents are transverse, $\hat{\mathbf{u}}$ -directed, and $\nabla = -\nabla'$ since the admittance depends on the distance between the slots through the Green's dyadic, making it possible to express the complicated derivatives in the Green's dyadic as derivatives in u/u' . Moreover, a two-fold application of the one-dimensional Green's first theorem (i.e. partial integration) moves the derivatives from the Green's function onto basis functions, simplifying the integral to

$$Y_{l,s}^{PPW} = \frac{-1}{j\omega\mu} \iint_{\text{slots}} \iint_{\text{slots}} \left(\mathbf{b}_l(u,v) \mathbf{b}_s(u',v') k^2 \hat{\mathbf{u}} \cdot \hat{\mathbf{u}}' \mathcal{G}'(\mathbf{r},\mathbf{r}') \right. \\ \left. + \partial_u \mathbf{b}_l(u,v) \partial_{u'} \mathbf{b}_s(u',v') \left[\partial_z \partial_{z'} \mathcal{S}''(\mathbf{r},\mathbf{r}') + \frac{1}{\nabla_t^2} \delta(\mathbf{r}-\mathbf{r}') - k^2 \mathcal{S}'(\mathbf{r},\mathbf{r}') \right] \right) dudvdu'dv', \quad (2.221)$$

where the first term, dependent on the scalar product between the current unit vectors, corresponds to the admittance due to magnetic current interaction, akin to Friis formula, where the mismatch due to the tilt between the respective radiation maxima is taken into account. The second term can be interpreted as the interaction between magnetic charges, or a first-order correction to the admittance involving the derivatives of the currents. Note that (2.221) is expressed solely in scalar form (save for the $\hat{\mathbf{u}}\hat{\mathbf{u}}'$ scalar product in the first term), alleviating the need to perform tedious scalar products and differentiating the dyadic Green's function directly, dyad by dyad. However, the second term contains uncommon terms, the most "suspicious" one being the inverse-Laplacian delta term. Fortunately, (2.221) can be simplified further upon taking a closer look to the double derivative of the TE S-potential $\partial_z \partial_{z'} \mathcal{S}''$ which, upon exhibiting it in Fourier series-integral form [64, Sec. 5.2 b)]

$$\partial_{zz'}^2 \mathcal{S}''(\mathbf{r}, \mathbf{r}') = \partial_{zz'}^2 \frac{-1}{\nabla_t^2} \frac{1}{4\pi} \sum_n e^{-jn(\phi-\phi')} \cdot \int_{\infty e^{-j\pi}}^{\infty} J_n(k_t \rho_{<}) H_n^{(2)}(k_t \rho_{>}) g_z''(z, z'; \lambda_z) k_t dk_t, \quad (2.222)$$

($e^{-j\pi}$ in the lower integration limit indicating we bypass the logarithmic branch cut singularity at $k_t = 0$ below the real line) and interchanging the differential and integral operators, can be expressed as

$$\partial_{zz'}^2 \mathcal{S}''(\mathbf{r}, \mathbf{r}') = \frac{-1}{\nabla_t^2} \frac{1}{4\pi} \sum_n e^{-jn(\phi-\phi')} \int_{\infty e^{-j\pi}}^{\infty} J_n(k_t \rho_{<}) H_n^{(2)}(k_t \rho_{>}) d_z d_{z'} g_z''(z, z'; \lambda_z) k_t dk_t. \quad (2.223)$$

Now, from the above discussion it should be clear that in order to find a more explicit form of double derivative term (2.222), one needs an explicit expression for the double derivative of the longitudinal transmission-line Green's function g_{zi}'' . This can be obtained using the symmetry relations (2.78) in the defining equation (2.76), yielding

$$d_z d_{z'} g_z''(z, z') = \lambda_z \tilde{g}_z''(z, z') + \delta(z - z'), \quad (2.224)$$

where \tilde{g}_z'' is the “dual” TE Green's function – it is related to the TE admittance Green's function $Y''(z, z')$ as

$$\tilde{g}_z''(z, z') = -j \frac{\omega \mu}{\lambda_z} Y''(z, z'), \quad (2.225)$$

and interpreted as the transmission-line modal current at z due to a voltage of moment $j\lambda_{zi}/(\omega\mu)$ at z' , satisfying $d_z \tilde{g}_z'' = 0|_{z=0,h}$. Then, using (2.224) in (2.223), along with the fact that $\tilde{S}'' = S'$ in the single-layer case, the PPW admittance simplifies greatly to

$$Y_{l,s}^{PPW} = \frac{-1}{j\omega\mu} \iint \iint_{\text{test base}} (k^2 \hat{\mathbf{u}} \cdot \hat{\mathbf{u}}' - \partial_u \partial_{u'}) (b_l(u, v) b_s(u', v')) G'(\mathbf{r}, \mathbf{r}') du dv du' dv', \quad (2.226)$$

where the u/u' differential operator acts on basis functions (by virtue of partial integration). Hence, we have an expression involving only one scalar Green's function, additionally relieving the computational burden since there is no need to compute the TE scalar potentials as in (2.221).

In the **stratified medium case**, however, a simplified expression akin to (2.226) cannot be obtained since the spectrum of the dual TE Green's function and the TM Green's function do not coincide any more, and a more complicated expression replaces the admittance. The derivation proceeds along the same lines as for the single-layer case, though care must be exercised due to appearance of position-dependent material parameters.

First, reexpressing the derivatives present in Green's dyadic in terms of derivatives in u/u' and applying a two-fold partial integration, we arrive at the starting expression

$$\begin{aligned} \mathbf{Y}_{l,s}^{PPW} = & -j\omega\epsilon(z') \iint_{\text{test base}} \iint \partial_u b_l(u,v) \left[-\mathcal{S}'(\mathbf{r},\mathbf{r}') + k(z')^{-2} \frac{\mu(z')}{\mu(z)} \partial_z \partial_{z'} \mathcal{S}''(\mathbf{r},\mathbf{r}') + k(z')^{-2} \frac{1}{\nabla_t^2} \delta(\mathbf{r}-\mathbf{r}') \right] \\ & \times \partial_u b_s(u',v') dudvdu' dv' \\ & - j\omega\epsilon(z') \iint_{\text{test base}} \iint b_l(u,v) \hat{\mathbf{u}} \cdot \hat{\mathbf{u}}' \mathbf{G}'(\mathbf{r},\mathbf{r}') b_s(u',v') dudvdu' dv' . \end{aligned} \quad (2.227)$$

Again, we have to reexpress the TE potential double derivative in terms of other related functions using symmetry relations and transmission-line equations, amounting to (see the appendix for a detailed derivation)

$$\partial_z \partial_{z'} \mathcal{S}''(\mathbf{r},\mathbf{r}') = k(z')^2 \frac{\mu(z)}{\mu(z')} \tilde{\mathcal{S}}''(\mathbf{r},\mathbf{r}') - \frac{\mu(z)}{\mu(z')} \tilde{\mathbf{G}}''(\mathbf{r},\mathbf{r}') - \frac{\mu(z)}{\mu(z')} \frac{1}{\nabla_t^2} \delta(\mathbf{r}-\mathbf{r}'), \quad (2.228)$$

where the dual TE potential can be derived in the same manner as the "regular" potentials, and is given by

$$\tilde{\mathcal{S}}''(\mathbf{r},\mathbf{r}') = \sum_i \frac{\mu(z')}{\kappa_i''(z')^2} \frac{1}{4j} \frac{H_0^{(2)}(k_i'' R)}{k_i''^2} i_i''(z) i_i''(z'). \quad (2.229)$$

The longitudinal modal "currents" i_i'' satisfy $d_z i_i'' = 0|_{z=z_{PEC}}$ at PEC boundaries and continuity requirements across layer junctions

$$i_{i,n}'' = i_{i,n+1}'' , \quad \frac{-1}{j\kappa_{i,n}''(z) Y_{i,n}''(z)} d_z i_{i,n}'' = \frac{-1}{j\kappa_{i,n+1}''(z) Y_{i,n+1}''(z)} d_z i_{i,n+1}'' \Big|_{z=d_n} ,$$

n indexing the junction across which the continuity is enforced and $Y_{i,n}''$ being the modal TE admittance in the layer n . The spectrum of this function coincides with the TE modal spectrum, which is beneficial from the computational point of view since one needs not find the pertinent propagation constants, being the same as for the TE modes.

It should be noted that the last term of (2.228) cancels the corresponding delta-term in the charge-coupling integral of (2.227), leading to the regularized expression

$$\begin{aligned} \mathbf{Y}_{l,s}^{PPW} = & -j\omega\epsilon(z') \iint_{\text{test base}} \iint \partial_u b_l(u,v) \left[-\mathcal{S}'(\mathbf{r},\mathbf{r}') + \tilde{\mathcal{S}}''(\mathbf{r},\mathbf{r}') - k(z')^{-2} \tilde{\mathbf{G}}''(\mathbf{r},\mathbf{r}') \right] \partial_u b_s(u',v') dudvdu' dv' \\ & - j\omega\epsilon(z') (\hat{\mathbf{u}} \cdot \hat{\mathbf{u}}') \iint_{\text{test base}} \iint b_l(u,v) \mathbf{G}'(\mathbf{r},\mathbf{r}') b_s(u',v') dudvdu' dv' . \end{aligned} \quad (2.230)$$

It is evident the admittance calculation in this case is computationally more demanding than the single-layer case, since the dual functions must be calculated in addition to the ordinary potentials.

Regardless, the power of the Schwinger-Marcuvitz-Felsen approach is finally evident – the admittance expressions contain only scalar functions, easily constructed by the characteristic Green's function method, both in single-layer and stratified-layer scenarios. Moreover, the potentials possess integrable logarithmic singularities, owing up to the representation in terms of Hankel functions. This fact facilitates the self-admittance calculation significantly, since the singular integrals can be simply cast into a numerically convenient form by simple change of variables; the singularities are "pushed" towards the

lower limits of integrals, which are then calculated by Gaussian quadrature. Remarkably, the SMF formalism, in addition to providing a conceptually familiar framework based on the transmission-line formalism, is self-consistent as well – the inverse-operator formalism, applied to the derivation of the Green's dyadic, facilitates the identification and cancellation of discontinuous terms, a characteristic not inherent to alternative approaches (see e.g. [105] for a discussion on the discontinuities of DGFs). This renders any MoM method using the SMF Green's dyadics transparent and simpler.

B. SLOT-POST ADMITTANCE

In addition to the direct PPW interaction between a pair of slots/basis functions, the energy transfer due to scattering off of posts takes place in an SIW-type device. The admittance due to this interaction can be generally expressed as

$$\mathbf{Y}_{l,s}^{Posts} = \int \mathbf{b}_l(\mathbf{r}) \cdot \mathbf{H}_s^{Posts}(\mathbf{r}) d\mathbf{r} , \quad (2.231)$$

\mathbf{H}_s^{Posts} being the magnetic field created when the field generated by the current \mathbf{b}_s scatters off of all the posts toward some point \mathbf{r} . But, this is just the field one can find using the methods presented in the subsection 2.2.1.8., its form being

$$\mathbf{H}_s^{Posts}(\mathbf{r}) = \sum_{q,m,n} A'_{s;q,m,n} \mathbf{M}'_{m,n}(\boldsymbol{\rho}, \boldsymbol{\rho}_q; z) + \sum_{q,m,n} A''_{s;q,m,n} \mathbf{N}''_{m,n}(\boldsymbol{\rho}, \boldsymbol{\rho}_q; z) , \quad (2.232)$$

scattering amplitudes A'' being solutions to linear systems $\underline{\underline{T}}_m' \mathbf{A}'_m = \boldsymbol{\Omega}'_m$, $\underline{\underline{T}}_m'' \mathbf{A}''_m = \boldsymbol{\Omega}''_m$. In more detail, for each mode m the matrix $\underline{\underline{T}}_m$ is constructed, and is common to $N_{slots} N_b$ linear systems, $N_{slots} N_b$ being the total number of basis functions assigned to all the slots of a given PPW. These systems will differ in the excitation vector, which collects the amplitudes of the modes (m, n) excited by a slot basis function

$$\Omega'_{s;m,r,q} = \chi'_{m,r,q} \frac{J_r(k'_{t_m} a_q)}{H_r^{(2)}(k'_{t_m} a_q)} I'_{s;m,r,q} , \quad I'_{s;m,r,q} = \int \mathbf{M}'_{r,m}(\boldsymbol{\rho}' - \boldsymbol{\rho}_q; z') \cdot \mathbf{b}_s(\mathbf{r}') d\mathbf{r}' ; \quad (2.233)$$

$$\Omega''_{s;m,r,q} = \chi''_{m,r,q} \frac{J_r(k''_{t_m} a_q)}{H_r^{(2)}(k''_{t_m} a_q)} I''_{s;m,r,q} , \quad I''_{s;m,r,q} = \int \mathbf{N}''_{r,m}(\boldsymbol{\rho}' - \boldsymbol{\rho}_q; z') \cdot \mathbf{b}_s(\mathbf{r}') d\mathbf{r}' ,$$

the coefficients χ being the modal coefficients of the pertinent Green's dyadic. Therefore, they can be solved in parallel, significantly speeding-up the analysis.

Once the amplitudes A'' are known, the slot-post admittance can be calculated by

$$\begin{aligned} \mathbf{Y}_{l,s}^{Posts} &= \int \mathbf{b}_l(\mathbf{r}) \cdot \left(\sum_{q,m,n} A'_{s;q,m,n} \mathbf{M}'_{m,n}(\boldsymbol{\rho}, \boldsymbol{\rho}_q; z) + \sum_{q,m,n} A''_{s;q,m,n} \mathbf{N}''_{m,n}(\boldsymbol{\rho}, \boldsymbol{\rho}_q; z) \right) d\mathbf{r} \\ &= \sum_{q,m,n} A'_{s;q,m,n} \int \mathbf{b}_l(\mathbf{r}) \cdot \mathbf{M}'_{m,n}(\boldsymbol{\rho}, \boldsymbol{\rho}_q; z) d\mathbf{r} + \sum_{q,m,n} A''_{s;q,m,n} \int \mathbf{b}_l(\mathbf{r}) \cdot \mathbf{N}''_{m,n}(\boldsymbol{\rho}, \boldsymbol{\rho}_q; z) d\mathbf{r} , \end{aligned} \quad (2.234)$$

where the scalar product between the basis functions and field modes have to be performed. However, these integrals were performed in the process of finding the amplitudes A'' and,

in fact, are exactly the $I'_{f;m,r,q}$ coefficients! Therefore, the slot-post admittance can be elegantly calculated as

$$Y_{l,s}^{Posts} = \sum_{q,n} \left[A'_{s;q,0,n} I'_{l;q,0,n} + \sum_{m>0} \left(A'_{s;q,m,n} I'_{l;q,m,n} + A''_{s;q,m,n} I''_{l;q,m,n} \right) \right]. \quad (2.235)$$

C. HALF-SPACE ADMITTANCE

If the SIW device of interest radiates into a half-space bounded by the uppermost/lowermost PEC plate closing the device, slot radiators will interact by half-space radiation, and at the radiating interface an additional admittance term accounting for it will appear

$$Y_{l,s}^{HS} = \int \mathbf{b}_l(u, v) \left(\int \underline{\mathbf{G}}^{HS}(\mathbf{r}, \mathbf{r}') \mathbf{b}_l(u', v') du' dv' \right) du dv, \quad (2.236)$$

the Green's dyadic being the one of the pertinent half-space, defined by (2.204). As such, it is amenable to various well-known approximate but efficient methods based on either the far-field approximation of the scalar Green's function, or a plethora of spectral integration methods, numerical or closed form based on the steepest-descent-path integration (see e.g. [102]). Hence, we shall not discuss it further since it would not add any new insight.

2.3.3 The excitation vector of the MoM system

The elements of the excitation vector, defined by(2.215), can be conveniently calculated by a procedure analogous to the one we used to calculate the slot admittance. First, we recall that a generic element of the excitation vector is composed of sub-elements

$$\begin{aligned} i_l &= \int \mathbf{b}_l(\mathbf{r}) \cdot \mathbf{H}_{imp}^i(\mathbf{r}) d\mathbf{r} \\ &= \int \mathbf{b}_l(\mathbf{r}) \cdot \left(\mathbf{H}_{imp}^{i;PPW}(\mathbf{r}) + \mathbf{H}_{imp}^{i;Posts}(\mathbf{r}) \right) d\mathbf{r} \\ &= i_l^{PPW} + i_l^{Posts}, \end{aligned} \quad (2.237)$$

the PPW contribution being

$$i_l^{PPW} = \int \mathbf{b}_l(\mathbf{r}) \left(\int \underline{\mathbf{G}}^{PPW}(\mathbf{r}, \mathbf{r}') \mathbf{M}_i(\mathbf{r}') d\mathbf{r}' \right) d\mathbf{r}, \quad (2.238)$$

and the posts-contribution is

$$i_l^{Posts} = \int \mathbf{b}_l(\mathbf{r}) \cdot \mathbf{H}_{imp}^{i;Posts}(\mathbf{r}) d\mathbf{r}. \quad (2.239)$$

(Note that the subscripts denoting the region where the fields are calculated are dropped.) $\mathbf{H}_{imp}^{i;Posts}$ is found in the same way as the (2.232), the only difference being in the driving terms which are, in this case

$$\begin{aligned} I'_{i;m,r,q} &= \int \mathbf{M}'_{r,m}(\boldsymbol{\rho}' - \boldsymbol{\rho}_q; z') \cdot \mathbf{M}_i(\mathbf{r}') d\mathbf{r}', \\ I''_{i;m,r,q} &= \int \mathbf{N}'_{r,m}(\boldsymbol{\rho}' - \boldsymbol{\rho}_q; z') \cdot \mathbf{M}_i(\mathbf{r}') d\mathbf{r}'. \end{aligned} \quad (2.240)$$

Therefore, similar to the slot-post admittance (2.235), the i_l^{Posts} can be calculated as

$$\dot{i}_l^{Posts} = \sum_{q,n} \left[A'_{l;q,0,n} I'_{i;q,0,n} + \sum_{m>0} \left(A'_{l;q,m,n} I'_{i;q,m,n} + A''_{l;q,m,n} I''_{i;q,m,n} \right) \right]. \quad (2.241)$$

2.3.4 Calculating the input/output parameters

A poor antenna engineer, struck by the terrible misfortune of having to use an ad-hoc electromagnetic code, is not interested in all the fancy mathematics behind it or the optimal algorithms used. Of primary concern to him is whether the antenna/device in question has acceptable return loss, and whether the realized gain of, say, an SIW slot array is large enough. We have already presented how to compute the port admittances in the absence of slots. Here we present the most convenient ways to do so when they are present, within the framework used to compute the fields.

The admittance between ports i and j is defined, as per usual, by the projection integral

$$\mathbf{Y}_{j,i}^{Port} = \frac{-1}{V_i V_j} \int \mathbf{M}_j(\mathbf{r}) \cdot \mathbf{H}_i^{Port} d\mathbf{r} = \frac{I_j}{V_i} \Big|_{V_{j,i}=0}.$$

The port i magnetic field has two canonical contributions – the SIW-wave in the absence of slots, and the slot-scattered field, i.e. $\mathbf{H}_i^{Port} = \mathbf{H}_i^{Port;SIW} + \mathbf{H}_i^{Port;Slots}$. Therefore, the admittance can be decomposed in the same manner. The SIW field $\mathbf{H}_i^{Port;SIW}$ is composed of the direct PPW-wave due to port i and the post-scattered waves found by methods presented in section 2.2.1. It will be different from zero only if the ports are located in the same waveguide. The slot-scattered field is the field scattered by slots towards port j when port i is excited and all the other are shorted. It is composed of the sum of partial fields radiated by all the basis functions on slots in the waveguide where the port j is located

$$\mathbf{H}_i^{Port;Slots} = \sum_s v_s^{Port i} \mathbf{H}_s^{SIW}, \quad (2.242)$$

The excitation amplitude of each basis function is denoted by $v_s^{Port i}$, obtained as the solution of the MoM problem when port i is excited and the rest are shorted. The field \mathbf{H}_s^{SIW} , on the other hand, is given by $\mathbf{H}_s^{SIW} = \mathbf{H}_s^{PPW} + \mathbf{H}_s^{Posts}$, where the first term gives rise to the admittance $\mathbf{Y}_j^{s;PPW}$, of the same form as $\mathbf{Y}_{j,i}^{PPW}$ but with the basis function \mathbf{b}_s as the exciting current instead of the current of port i . The field \mathbf{H}_s^{Posts} has already been computed, and if its form is plugged into the above admittance expression, we finally obtain the slot-post admittance

$$\mathbf{Y}_{j,i}^{Slots-Posts} = -\frac{1}{V_i V_j} \sum_s v_s^{Port i} \sum_{p,n} \left[A'_{s;0,n,p} I'_{j;0,n,p} + \sum_{m>0} \left(A'_{s;m,n,p} I'_{j;m,n,p} + A''_{s;m,n,p} I''_{j;m,n,p} \right) \right], \quad (2.243)$$

the total admittance being

$$\mathbf{Y}_{j,i}^{Port} = \mathbf{Y}_{j,i}^{SIW} + \sum_s v_s^{Port i} \left(\mathbf{Y}_{j,i}^{s;SIW} + \mathbf{Y}_{j,i}^{s;Slots-Posts} \right), \quad (2.244)$$

with the understanding that $Y_{j,i}^{SW}$ is zero if ports are located in different waveguides.

From the above mentioned quantities, one can retrieve the input impedance, S -parameters, the impedance matrix etc. However, in radiating problems involving slots, in addition to input parameters, one is interested in directivity, gain, cross-polarization levels and other quantities associated to the radiation pattern. The radiation pattern itself is easily calculated, once the magnetic current amplitudes of all the slots radiating into a given half-space are known, by the radiation integral

$$\mathbf{E}(\mathbf{r}) = -\nabla \times \int \underline{\mathbf{G}}^{\text{HS}}(\mathbf{r}, \mathbf{r}') \cdot \mathbf{M}(\mathbf{r}') d\mathbf{r}' = -\nabla \times \int \underline{\mathbf{G}}^{\text{HS}}(\mathbf{r}, \mathbf{r}') \cdot \sum_n V_n \mathbf{b}_n(\mathbf{r}') d\mathbf{r}', \quad (2.245)$$

where

$$\underline{\mathbf{G}}^{\text{HS}}(\mathbf{r}, \mathbf{r}') = \left(\mathbf{1} + \frac{\nabla \nabla}{k^2} \right) \frac{e^{-jkR}}{2\pi R} \quad (2.246)$$

is the half-space Green's dyadic (R being the distance between the source and the observation point). In general, (2.245) is intractable in closed form, but can be significantly simplified upon observing that in the far zone the second term of (2.246) is of the order $O(R^{-3})$ and hence can be neglected without sacrificing accuracy in a notable manner. In addition, the scalar half-space Green's function can be accurately approximated in the standard way [26, p. 286] as

$$G^{\text{HS}}(\mathbf{r}, \mathbf{r}') = \frac{e^{-jkR}}{2\pi R} \approx \frac{e^{-jk(r-r'\cos\psi)}}{2\pi r}, \quad (2.247)$$

where $r = |\mathbf{r}|$, $r' = |\mathbf{r}'|$, and ψ is the angle between \mathbf{r} and \mathbf{r}' . Now, in calculating the directivity and the associated quantities, such as the realized gain, it is necessary to compute the total radiated power, which can be calculated in a number of ways. The straightforward and, consequently, the most laborious way would be to create a dense mesh of points on a sphere in the far field and numerically integrate the power density (per solid angle), given in terms of the far-zone electric field components as

$$P(\theta, \varphi) = \frac{1}{2\eta} (\mathbf{E}_\theta^2 + \mathbf{E}_\varphi^2), \quad (2.248)$$

where θ and φ are the elevation and azimuth defined in an arbitrarily appointed spherical coordinate system (but usually taken to have its origin in the geometrical center of the considered antenna system). However, there is a much simpler and faster way utilizing quantities already computed during the MoM procedure. It relies on the very definition of the rate of change of energy in a charge-field system composed of impressed currents radiating into a given medium [82, p. 11]

$$U = - \int \mathbf{M}(\mathbf{r}) \cdot \mathbf{H}^*(\mathbf{r}) d\mathbf{r}, \quad (2.249)$$

whose real part is, to quote Collin, interpreted as "the work done by an impressed current source against the radiation reaction field, and accounts for the power loss in the medium and the transport of power across the surface S' " (the surface S is any surface enveloping the impressed sources). Of course, care should be exercised with such statements, since the possibility of such a general interpretation of this expression for arbitrary media is questionable. Now, in order to connect the impressed work (2.249) to the previously obtained quantities, we write it out fully

$$\begin{aligned}
 U &= - \int \mathbf{M}(\mathbf{r}) \cdot \mathbf{H}^*(\mathbf{r}) \, d\mathbf{r} = - \int \mathbf{M}(\mathbf{r}) \cdot \left(\int \underline{\mathbf{G}}(\mathbf{r}, \mathbf{r}') \cdot \mathbf{M}(\mathbf{r}') \, d\mathbf{r}' \right)^* \, d\mathbf{r} \\
 &= - \int \sum_n V_n \mathbf{b}_n(\mathbf{r}) \cdot \left(\int \underline{\mathbf{G}}(\mathbf{r}, \mathbf{r}') \cdot \sum_{n'} V_{n'} \mathbf{b}_{n'}(\mathbf{r}') \, d\mathbf{r}' \right)^* \, d\mathbf{r} \\
 &= - \sum_n V_n \int \mathbf{b}_n(\mathbf{r}) \cdot \left(\sum_{n'} V_{n'} \int \underline{\mathbf{G}}(\mathbf{r}, \mathbf{r}') \cdot \mathbf{b}_{n'}(\mathbf{r}') \, d\mathbf{r}' \right)^* \, d\mathbf{r} \\
 &= - \sum_n \sum_{n'} V_n V_{n'}^* \int \mathbf{b}_n(\mathbf{r}) \cdot \left(\int \underline{\mathbf{G}}(\mathbf{r}, \mathbf{r}') \cdot \mathbf{b}_{n'}(\mathbf{r}') \, d\mathbf{r}' \right)^* \, d\mathbf{r} \\
 &= - \sum_n \sum_{n'} V_n V_{n'}^* \int \mathbf{b}_n(\mathbf{r}) \cdot \left(\int \underline{\mathbf{G}}^*(\mathbf{r}, \mathbf{r}') \cdot \mathbf{b}_{n'}(\mathbf{r}') \, d\mathbf{r}' \right) \, d\mathbf{r} \\
 &= - \sum_n \sum_{n'} V_n V_{n'}^* \left(\int \mathbf{b}_n(\mathbf{r}) \cdot \left(\int \underline{\mathbf{G}}(\mathbf{r}, \mathbf{r}') \cdot \mathbf{b}_{n'}(\mathbf{r}') \, d\mathbf{r}' \right) \, d\mathbf{r} \right)^* \\
 &= - \sum_n \sum_{n'} V_n V_{n'}^* Y_{nn'}^* = - \sum_n \sum_{n'} V_n (V_{n'} Y_{nn'})^* = - \sum_n V_n I_n^* ,
 \end{aligned} \tag{2.250}$$

where use has been made of the fact that vector basis functions are real, i.e. $\mathbf{b}_n = \mathbf{b}_n^*$. Hence, the power supplied to the half-space can be quickly computed using the magnetic current amplitude vector and the admittance matrix. Since we are dealing with time-harmonic fields, it makes sense to average the supplied work over a period of oscillation

$$\langle U \rangle_t = - \frac{1}{2} \sum_n V_n I_n^* , \tag{2.251}$$

and since the medium is assumed to have no losses, taking the real part of (2.251) finally yields the *total radiated power*.

2.4 Fast is not fast enough – speeding up the method even further

Up to this point, we have been dealing with the exposition of the formalism used, touching only lightly on the subject of efficiency the method provides. Here we shall consider the common symmetries and approximations, valid and applicable to a wide class of SIW-type structures, granting significant reduction of the overall computation time. Moreover, we shall reiterate several pragmatic, rule-of-thumb criteria for choosing the sufficient number of modes/basis functions guaranteeing good accuracy, while keeping the computation time reasonable. In addition, we shall recap the speed-up strategies mentioned in previous sections, along with recommended known algorithms for matrix inversion and numerical integration giving best results.

All commercial solvers, such as HFSS, CST Microwave Studio, FEKO etc. rely on the discretization of the problem domain in question, i.e. the scatterers are represented by suitable functions existing over a part of the scatterer which approximate the true layout. Depending on the type of solver, either the current or the geometry itself is discretized. In our case, we “discretize” the currents, but since the geometry of a generic SIW consists of canonical cylindrical and rectangular shapes, we use entire-domain functions “covering” the whole objects to approximate the fields/currents. On the other hand, an MoM-based solver

such as FEKO meshes the surface of each cylinder and slot first using triangular patches, then distributing a current over each such patch. Therefore, our approach is inherently more efficient. Note that if the geometries considered were irregular, our approach would not be capable to account for the irregularity, whereas commercial solvers shine through in such scenarios (unless, of course, the problem is too big to be handled by the respective method).

The second forte of the method is based on the fact that integral equations which appear in it are solved by the Galerkin method, i.e. the testing and the basis functions belong to the same set. As already mentioned, this gives rise to symmetric interaction matrices, reducing the effort of filling the whole matrix from N^2 operations (numerical integrations) to $N^2 / 2 + N / 2$. It should be noted that the application of the Galerkin method is not sufficient to yield symmetric interaction matrices, but the original field problem expressed by the H-field vector differential equation must be phrased in terms of a complex-symmetric operator relating the field and the current [106], i.e. the Lorentz reciprocity principle must hold.

In connection to the first point, related to the discretization, the used field representation in terms of the angular-mode radial transmission-line representation [64, Sec. 3.3] is advantageous on several levels. The first and foremost advantage is the fast convergence of fields already at moderate distances from the source, if the device being investigated has a moderate electrical longitudinal size (as is almost always the case in practice). Phrased more rigorously, a small number of longitudinal modes are necessary to accurately describe the longitudinal field variation in the SIW; the transverse field variation, given by Hankel functions of second kind, has exponential decay for imaginary transverse wavenumbers, which is the common case for higher-order modes. An empirical criterion presented in [45] gives the number of longitudinal modes sufficient for good accuracy as $N_m = \text{number of propagating modes} + 2$, though in many cases only the lowest two modes are necessary; the first one accounting for the majority of interactions, long- and close-range, the second one being a higher-order refinement accounting for the near-field interaction between closely-spaced scatterers. In fact, one can go a step further and adopt an adaptive longitudinal-mode number selection strategy [46]. Since a realistic PPW will be of small height, only the lowest-order mode will propagate, while the higher-order modes are suppressed. The geometrical spreading of the higher-order modes, which are assumed to have large imaginary wavenumbers ($k_{t_m} = -j\alpha_m$), is asymptotically

$$\left| H_n^{(2)}(-j\alpha_m R) \right| \approx \sqrt{\frac{2}{\pi\alpha_m R}} e^{-\alpha_m R}. \quad (2.252)$$

From this expression it is obvious the higher-order modes have a short range, and any interaction matrix of these modes will have a large number of entries of very small value. Instead of explicitly determining these, one can set them to zero according to some cut-off criterion. The simplest one is attained upon first defining the reciprocal distance $1/\tau_m = \alpha_m$ where the exponential drops to $1/e$. This will serve as the “meter” for the area around the element where the mode m will be postulated to have a significant enough amplitude. Outside this area, its amplitude will be considered negligible (identically zero). For example, defining a “significance range” of $3\tau_m$ around an element stipulates that the mode can be considered to be zero in the region where its exponential part drops below 5 %. In our numerical tests, we have used the $4\tau_m$ range, roughly corresponding to up to 1 % of the original amplitude. Now it becomes clear how to simplify our problem – for a given element, and for a given mode, find all the elements which are in the significance range around it, and

set up a boundary condition problem involving only those elements, while setting the modal scattering amplitudes of all the other elements to zero. This gives rise to much smaller and more stable linear systems for higher-order modes, reducing the computation time significantly and lifting the requirement of handling severely sparse matrices.

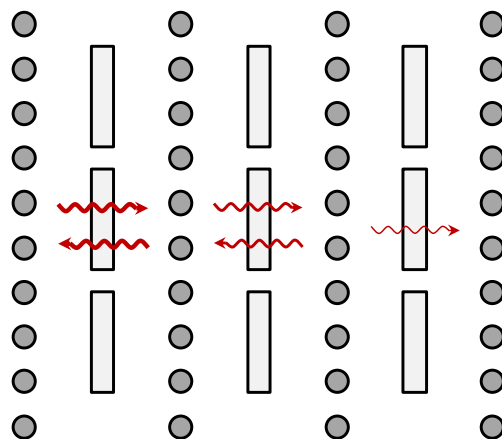
In a wide range of problems, the azimuthal variation can be efficiently described by a small number of azimuthal harmonics, due to the fact that a large number of SIW devices make use of posts of radii small compared to the wavelength. As such, the current induced on them will not vary significantly across their respective circumferences. The empirical criterion for choosing the sufficient number of azimuthal harmonics to be used in the analysis was presented in subsection 2.2.1.8, but we repeat it here for convenience:

$$N_{\phi} = \lfloor 2\pi a_{\max} / \lambda_{\min} + 1.5 \rfloor.$$

A typical-sized post is on the order of approximately 0.3λ , which leads to 3 azimuthal modes necessary for accurate field representation according to the above criterion. But, it should be noted that this criterion is *global*, i.e. applies to each and every post, regardless of its actual radius. An adaptive scheme can be easily applied where *each* post has its own necessary number of azimuthal harmonics, according to $N_{\phi, \text{post}} = \lfloor 2\pi a_{\text{post}} / \lambda_{\min} + 1.5 \rfloor$. This leads to an even lesser number of unknowns.

Now, in general one should rigorously consider the PPW-wave interaction between all posts and slots. But, consider a structure shown in the following figure. Such structures are commonplace since the most natural way of designing a corporate-fed SIW device is to feed several waveguides at once. The guides share common walls while the interaction between them can be tuned by changing the wall-post period p . Usually, the period is less than a fifth of the guided wavelength, providing tight field confinement. It is then reasonable to expect that posts and slots belonging to different waveguides will in general interact negligibly, which results in small-value entries in admittance/post-interaction matrices. Again, setting these entries to zero spares us the effort of actually calculating them. But, a prudent criterion must be devised in order to take into account such interaction, while preserving the accuracy of the more rigorous solution obtained by consideration of all the interactions.

Figure 2.17 Wave interaction in a multi-waveguide SIW device



A conservative and a well-known one is to use the “nearest-neighbour approximation” – only the PPW-wave interactions between elements comprising or belonging to neighbouring guides are taken into account, while the rest are set to zero. If $\mathbf{Y}_{l,k}^{PPW}$ and

$\mathbf{Y}_{l,k}^{Posts}$ represent vectors collecting all the direct-PPW and post-interaction amplitudes between guides l and k , our criterion then demands that

$$\mathbf{Y}_{l,k}^{PPW} + \mathbf{Y}_{l,k}^{Posts} = \mathbf{0}, |l-k| > 1. \quad (2.253)$$

This constitutes an ad-hoc approach and therefore cannot be used in the analysis of general SIW devices.

An additional computational burden reduction can be obtained if there is a repeating pattern of slots, as e.g. in [107]. Then the slot-admittances calculated for the group of slots constituting the “unit cell” can be used to fill the admittance matrix entries of other groups having the same pattern. To illustrate the idea better, consider an array of N columns of M slots, each column having the same geometrical parameters. If one computes all the admittances blindly, there will be a total of $2 \times (NMN_b) \times (NMN_b)$ integrals. The factor 2 comes from the fact that the total admittance of each slot pair is composed of either a sum of two PPW admittances, or one PPW and a half-space admittance. N_b refers to the number of basis functions used to model the current on each slot. Then, by calculating admittances between the slots of a single column, one automatically has the admittances pertaining to all the other columns. Therefore, the number of integrals to be computed is reduced by a factor of N , which can be significant in large arrays. It should be stressed that this procedure is possible if the PPW pertaining to the slots is translationally invariant.

2.5 Conclusion and future development

A number of methods for the efficient analysis of planar SIW structures have been devised and applied over the years. In this thesis, a hybrid method merging the method of moments and mode-matching is presented, which builds upon the aforementioned methods, extending them to handle fairly general planar SIW problems. These include the presence of several stacked planar SIW waveguides connected via narrow coupling slots, guides loaded by media composed of an arbitrary number of planar dielectric layers, closed as well as radiating SIW devices.

In comparison to other similar methods, our carries the key advantage of scalarization – in order to find the pertinent dyadic Green’s function, the mentioned methods rely on what is known as the Ohm-Rayleigh procedure. Essentially, one first finds complete sets of *vector* functions satisfying the Maxwell-Heaviside equations. These are obtained by differentiation from scalar functions (corresponding to characteristic modes of the boundary value problem in question). From there one proceeds to expanding the dyadic Green’s function in terms of the obtained vector “eigenfunctions”, leading to a spectral representation; an inverse Fourier transform is then effected, yielding the desired spatial representation. However, one should be extremely careful in performing the inverse transform since it will yield singularities which must be taken into account in a potential subsequent self-admittance (or self-impedance) evaluation. In addition, the procedure is quite tedious due to a series of function expansions and spectral integrations, in conjunction with abstruse regularization which must be applied to render the integrals convergent. Another, more conceptual than technical, difficulty is the relative lack of intuitiveness (i.e. it does not lend itself to simple physical interpretation) with respect to the method of Schwinger-Marcuvitz-Felsen we applied.

On the other hand, we demonstrate how to construct the necessary dyadic Green’s function from scalar potentials, which we derive in what we believe to be an elegant manner – conceptually clear, physically interpretable and mathematically consistent. We show how the Green’s dyadic for PPWs loaded with piecewise-continuous dielectric media is

constructed and regularized, the regularization being of utmost importance in the subsequent application of the Petrov-Galerkin method.

A numerical method is ultimately judged by its efficiency – the ability to yield sufficiently accurate results within an acceptable time period. In our case, the key concept enabling the construction of an efficient method is the use of the radial transmission line field representation – the functions representing the field are expressed as products of Bessel or Hankel functions with azimuthal harmonics (complex exponentials periodic in the angular variable). Since most guided-wave devices of practical interest support the propagation of a single mode (usually the lowest-order one), higher-order modes will be in cutoff. Hence, the Hankel functions, used to encode the radial dependence of fields, will be exponentially dampened. From this it follows that only a small number of modes will be necessary to accurately represent the total field. Similar arguments apply to azimuthal modes describing the angular variation of currents and fields – if designed well, an SIW device will contain posts of circumference small compared to the dominant transverse wavenumber. Hence, a small number of azimuthal functions will be able to reconstruct the angular variation of pertinent fields and currents.

In conclusion, using this field representation enables us to efficiently represent both the fields due to impressed sources, and the scattered field.

This allows the construction of linear systems whose solution yields the amplitudes of fields scattered by posts; both dielectric and metal posts are considered.

Furthermore, we show how to numerically evaluate the fields in stacked devices consisting of a number of SIW guides connected by rectangular slots. This is done within the framework of the method of moments, which we formulate both for closed and open structures. We show how to construct linear method-of-moment systems using quantities already computed in the mode-matching analysis, thereby avoiding recomputation and, consequently, lowering the execution time. Various ad-hoc methods of lowering the number of unknowns and operations are presented, which result in significant time saving of the order of N , where N is the number of unit cells of a cascaded device (i.e., consisting of a number of identical guides, radiating or otherwise). Unfortunately, at present we do not have an automatized procedure which could be capable of autonomously recognizing the repetition patterns and symmetries of a general device. This might be an interesting direction to take in future research.

Although we present the results of the numerical experiments testing the efficiency of our code in the following chapter, we shall nevertheless spill a couple of spoilers here. From extensive experiments conducted against a commercial, well-known and well-tested EM solver, we demonstrate the significant advantage of our method over the commercial solver. The accuracy, which we define as the agreement between relevant quantities evaluated on a series of structures, using both the commercial solver and a MATLAB code based on our method, is excellent for all considered structures. Minor discrepancies exist, though they are the most pronounced in radiation patterns below the -20 dB mark, and can be considered less significant. As pertains the S -parameters, the agreement is excellent as well, even for multilayer-loaded SIW devices, as long as the ports used are not driven outside the single-mode regime. An extension of the method, covering the case of multiple-mode driven ports has been recently devised by professors Casaletti and Valerio, and will be featured in an up-coming article. In terms of computation time, our method is significantly faster than the commercial solver, being from 4 to roughly 20 times faster (depending on the considered device). In addition, the memory usage of our code is severely lower due to a significantly smaller number of unknowns and applied speed-up methods. This is, in fact, what limits the applicability of the commercial solver to the analysis of large structures – at a certain point, the number of unknowns becomes so vast that even high-end

computers are not able to store all the necessary matrices. In such cases, our method can be reliably applied.

A summary of the most important results of the thesis is given below:

- I.** The extension of the Schwinger-Marcuvitz-Felsen formalism to PPWs loaded with planar multilayer dielectric media.
- II.** Consistent removal of spurious singularities of the Green's dyadic.
- III.** The application of the above formalism to planar SIW problems containing narrow rectangular slots.
- IV.** Generalized expressions for slot admittance in planar multilayer-dielectric SIW devices.
- V.** Significant reduction in computational time and memory usage with respect to standard EM solvers, with preserved accuracy.

Though the method presented in this thesis can be applied to a wide variety of SIW devices, it lacks several important features which would make it a complete analysis tool fit to handle practical scenarios. The first and foremost such feature is the handling of metal and dielectric losses. Though most devices are designed to minimize the said losses, and in some cases they might even be neglected, it is imperative to be able to predict them. This would require a different field representation, depending on the conductivity of metal boundaries. To be more specific, the presence of lossy metal surfaces, if their conductivity is high enough, could be taken into account by Leontovich boundary conditions [17], whereby they are represented by surface impedances. In general, this will lead to the description of the field by mutually non-orthogonal TM and TE sets, i.e. lossy surfaces cause mode-coupling. This approach in accounting for metal losses in SIW/SIW-like geometries has been applied in, e.g., [18], [19] and [20], to name a few, though no attempts to generalize to the case of a multilayer-dielectric-loaded PPW have been made. If, on the other hand, the considered conductivity is low, metal objects become penetrable and can be modelled, for example, as lossy dielectrics. This then leads to a more difficult problem, since the spectrum, in general, becomes continuous (although the discrete spectrum will most likely be present as well).

As described in section 2.2.1, the method assumes metal plates of infinite extent. In most practical cases, even for narrow slotted arrays, the truncation does not produce significant edge effects, i.e. spurious maxima in the radiation pattern due to edge diffraction. However, it might be beneficial to include corrections due to diffraction, for completeness' sake, since it is not always prudent to neglect them. This can be done using an appropriate variant of the theory of diffraction (see e.g. [21]).

3 RESULTS

Having presented the theoretical background of the hybrid method, along with numerical considerations involving the various truncation criteria, problem complexity, issues with numerical stability, and recommended techniques to handle specific parts of the analysis, we now arrive to the testing ground, where all the previously employed theorems, mathematical representations and rigour appear before the stern judgment of the experiment, and are sentenced according to the answer they provide to the most important question– do they work? This chapter answers that question systematically, starting from basic mode-matching problems involving no aperture radiation. There the post-scattering due to posts is put to the test, and the approximations and rule-of-thumb criteria for simplifying the analysis are justified. Both single- and multiple-layer dielectric media are considered, the limitations of the mathematical representations being established from considering extreme cases of thin dielectric layers. From there we proceed to radiation problems in the form of slot array analysis. Radiation patterns are compared to the ones obtained by the High Frequency Structural Simulator® [108], again both for single- and multiple-layer dielectric loaded antennas. In addition, runtime and CPU-load comparisons are put before the reader to demonstrate the relative reduction in both with respect to more general solvers.

3.1 Post-scattering in closed SIW structures

Closed SIW structures comprise the majority of devices realized in SIW technology. By “closed” we refer to devices not intended for generation of radiation, be it by continuous leakage from the narrow wall, or aperture radiation from broad walls; put more simply, we refer to devices having negligible leakage losses of any form. We will compare both single-layer dielectric structures and their multi-layered counterparts against the FEM-based commercial solver HFSS.

3.1.1 Waveguide resonator

Figure 3.1 depicts an SIW waveguide resonator, consisting of a rectangular arrangement of metal posts, embedded in a dielectric substrate of relative permittivity $\epsilon_r = 2.2$. At each end of the resonator, approximately at $0.25\lambda_g$ away from the back wall, a coaxial transition is placed, launching a TEM mode. The geometrical parameters are shown in Table 3.1. The scattering parameters were then calculated over a wide frequency range, both with our homebrewn MATLAB code and HFSS. This particular structure was chosen as a benchmark since a) it represents a commonly used geometry, b) contains a common excitation, and c) it serves as the milestone towards more complicated structures since it establishes the validity of mode-matching in a simple scenario. As pertains the analysis, the following table summarizes both the number of basis functions and the mesh used, in the code and HFSS, respectively. In addition, computational times are listed as well to show the

relative merit of using one method over the other. This will be the template for all the other results that follow.

Figure 3.1 Closed resonator SIW structure fed by coaxial ports

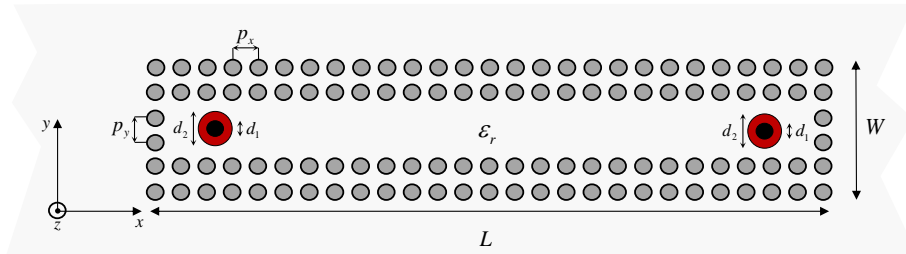


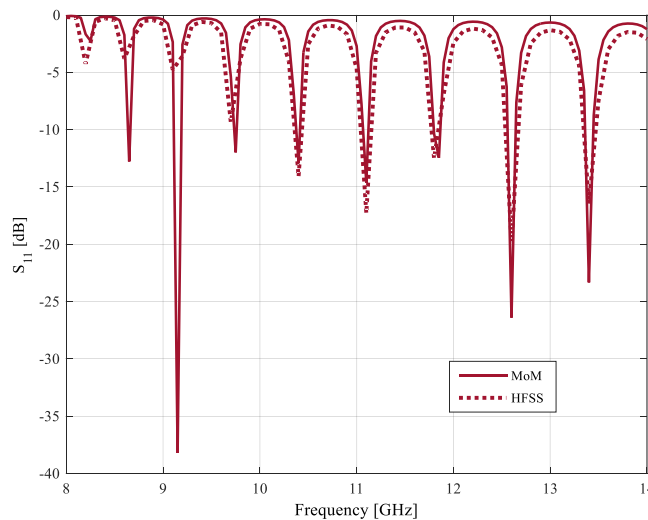
Table 3.1 Geometrical parameters of the closed resonator SIW structure

Cylinders	N=114; a=0.2 mm ; p_x= p_y=4.6 mm
Frequency range	[8, 14] GHz
Dimensions	119.6 mm × 23 mm × 3.2 mm (L × W × h)
ϵ_r	2.2
Feeds	2 coaxial ports - $d_2 = 4d_1 = 4a = 0.8$ mm

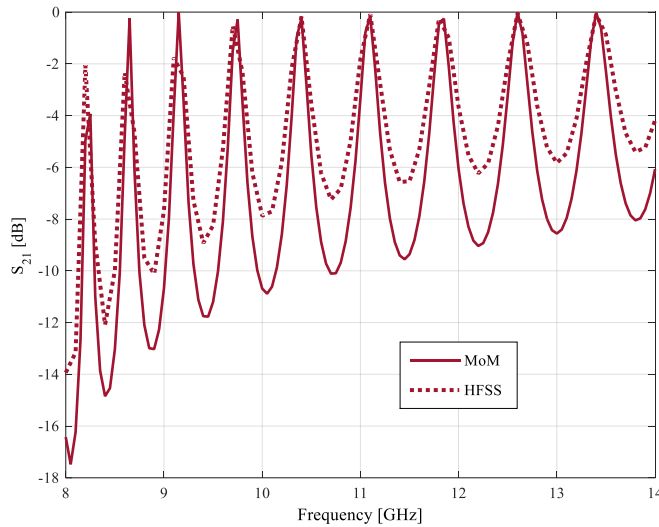
It is to be noted the code and HFSS agree very well on S_{11} , less so on S_{21} . As the frequency increases, the results diverge, which is due to the precision of HFSS results, limited by the mesh coarseness. In this example, we did not wish to exaggerate on the mesh cell size in HFSS, but keep it at a level which provides sufficiently accurate results at a reasonable computational time. The example which follows will amend for this “lack” in precision.

Figure 3.2 S-parameters of the closed SIW resonator; a) S_{11} , b) S_{21}

a)



b)

**Table 3.2 Mesh properties and runtimes for the SIW closed resonator**

Configuration	Intel i7-4790, 3.6 GHz, 8 GB RAM	
Solver	MoM	HFSS
# unknowns	$N_z(5) \times N_\phi(7) \times N_{posts}(114) = 3990$	56 149
Runtime	2.45 min	31.45 min
RAM (max)	46 MB	849 MB

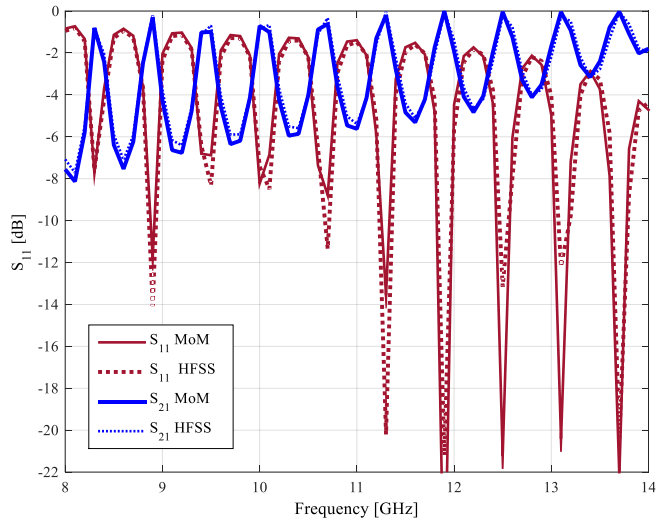
It should be emphasized here that we compare the performance of the methods in terms of the number of unknowns as well. Although the penultimate measure of performance is the total runtime and memory consumption, the number of unknowns crudely informs one of the complexity, and its trend of growth with the electrical size of the problem. Hence, it should not be considered a definite measure, but as more of an informative one describing the discretization nature of the respective method. On inspection of the respective runtimes, it is obvious that the hybrid method executes in considerably lesser time; a speed-up factor of approximately 13 is gained. Moreover, reducing the number of longitudinal harmonics used to mere two and azimuthal harmonics to five hardly decreases the accuracy while reducing the time by a further factor of roughly 3.

To verify the **multilayered** formalism, as it applies to closed structures, we simulated the very same closed resonator, but with a two-layer dielectric instead of a single-layer one. The bottom layer is 1.6 mm thick and has permittivity $\epsilon_{r1} = 2.2$, while the top one has $\epsilon_{r1} = 6.6$ and is 1.6 mm thick as well. These values were chosen randomly, referring to no realistic structure, but in such a way to put the formalism to test properly – the layer thicknesses are comparable while the permittivity contrast is large, presenting a truly multi-layered scenario. Again, using both methods we computed the S parameters, the results obtained shown in the next figure. HFSS meshed the structure in a total of 42 546 tetrahedra and triangles, taking roughly 9 times the time the hybrid code took to perform the full sweep. On the other hand, the hybrid code was ran with only two longitudinal harmonics and 5 azimuthal harmonics considered, yielding truly excellent accuracy, save for the phase of the

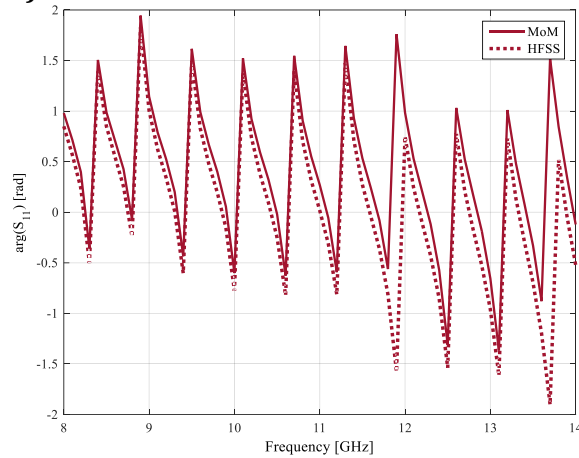
S-parameters, for which the agreement is modest. The runtimes, shown in the following table, serve to emphasize the considerable advantage of using the hybrid code.

Figure 3.3 S-parameters of the two-layer dielectric loaded slot array: a) magnitude, b) S_{11} , c) S_{21} phase

a)



b)



c)

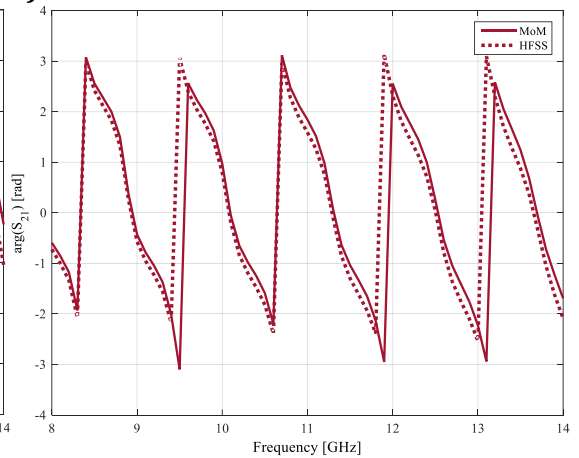


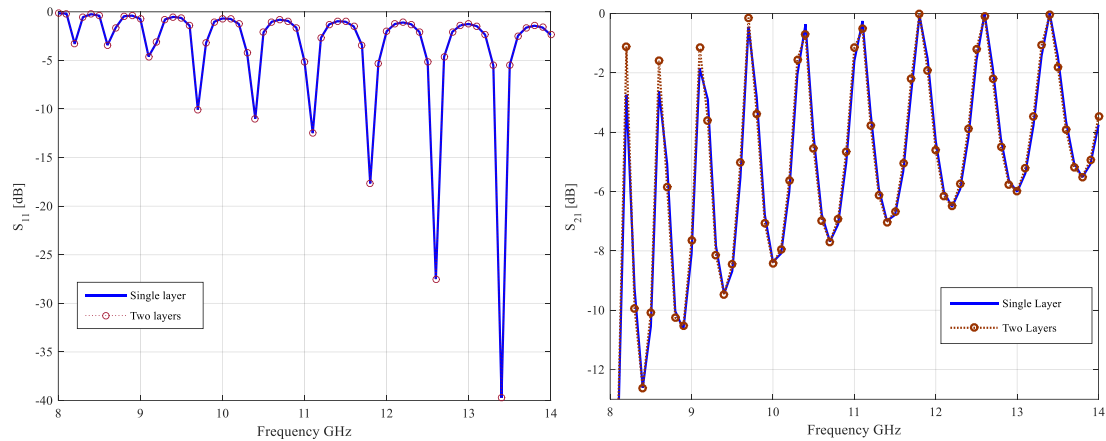
Table 3.3 Mesh properties and runtimes for the SIW closed resonator loaded with a layered dielectric

Configuration	Intel i7-4790, 3.6 GHz, 8 GB RAM	
Solver	MoM	HFSS
# unknowns	$N_z(2) \times N_\phi(5) \times N_{posts}(114) = 1140$	42 546
Runtime	1.62 min	10.26 min
RAM (max)	79 MB	380 MB

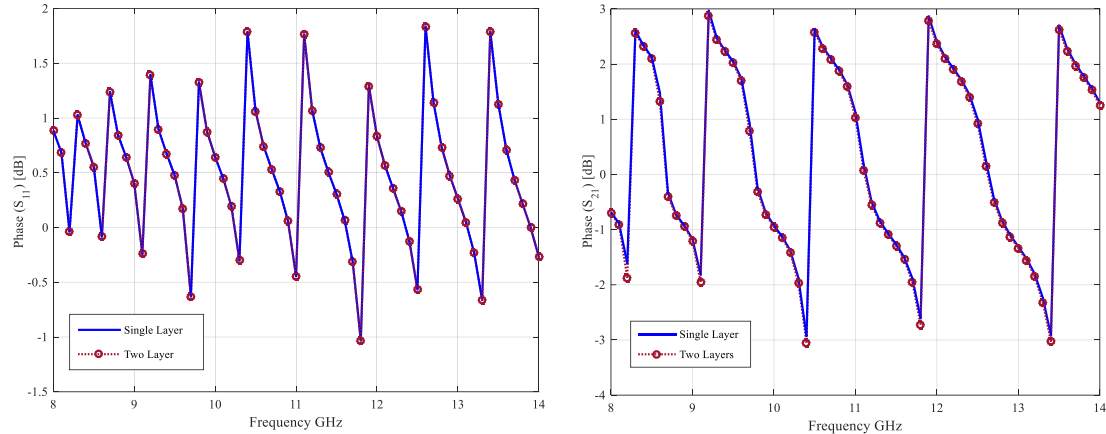
An additional test of the multilayered formalism was performed, where the permittivities of a two-layer loaded closed resonator were chosen very close to each other, i.e. $\epsilon_{r,1} = 2.2, \epsilon_{r,2} = 2.21$, and the S -parameters computed. These were then compared to the S -parameters of the single-layer resonator, revealing a better-than 1 % agreement (on average over the whole testing frequency band); these are shown in the following figures.

Figure 3.4 S -parameters of the single-layer dielectric loaded resonator versus the “almost” single-layer resonator: a) magnitude; b) phase

a)



b)



It can be seen that noticeable discrepancies in S -parameters are the ones between S_{21} of the respective devices, being present at peaks of the respective curves, i.e. resonances; this particular behaviour can be attributed to the small frequency shift induced by the dielectric contrast, and the coarseness of the frequency mesh used in the simulation. However, the overall agreement is truly excellent.

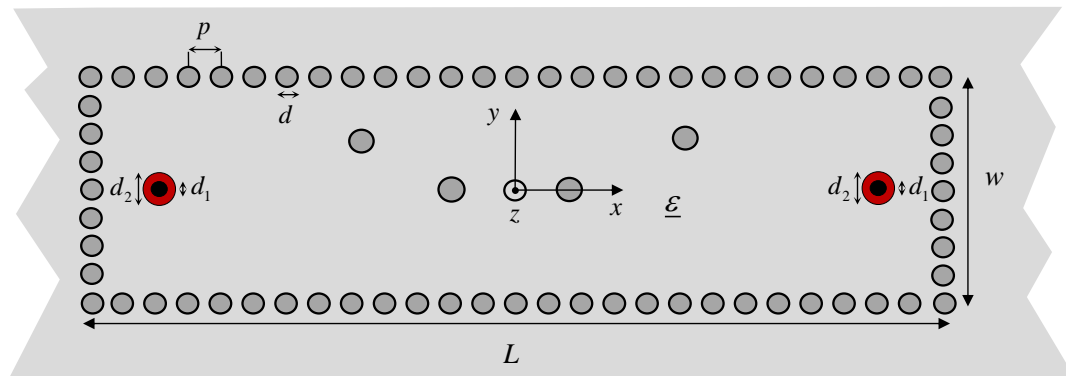
Thus, it was shown the multilayer formalism numerically reduces to the single-layer formalism when the dielectric contrast is sufficiently small, i.e. $\Delta\epsilon = |\epsilon_{r,1} - \epsilon_{r,2}| / \epsilon_{r,1} \leq 1\%$. This fact serves to reinforce the validity of both the single and multilayer formalism.

Based on the results so far, our method, as it appears at this moment, may be safely applied to the design of dielectric-loaded closed structures, provided the excitation port is not driven outside its operating band (where its model is valid). Further examples, as will be shown, serve to support this claim.

3.1.2 SIW waveguide filter

The previous two examples served as demonstrations of the hybrid method’s basic capabilities concerning simple, straightforward waveguide devices. As was shown, the method holds quite well against the industry standard solver and, presumably, against a plethora of alternative methods for solving SIW waveguide problems, described in section 1.3. However, the examples to follow pertain to more complex and, consequently, more interesting scenarios; the first one being a multilayered modification of a waveguide filter, originally presented in [109]. Its layout is depicted in the following figure.

Figure 3.5 Layout of the SIW multilayered, three-pole Chebyshev filter



The filter itself consists of a short SIW waveguide section with a pair of identical coaxial ports, located at approximately $\lambda_x / 4$ away from respective end-walls (λ_x at the central frequency $f = 27$ GHz in our case, $f = 28$ GHz in the original case). The ports launch exciting fields onto an array of inductive posts, whose radii and offsets in the transverse direction (y -direction) have been originally tuned to realize a three-pole Chebyshev filter with the central frequency at 26.5 GHz. Our modification consists solely of replacing the single-layered dielectric slab in the original device with a multilayered one, in order to investigate the effects of its presence on the bandwidth of the filter. The exact geometrical parameters of the filter are summarized in the table below.

Table 3.4 Geometrical parameters of the multilayered SIW filter

Parameter	Value
W	5.565 mm
L	3.5 cm
h	0.787 mm
d	0.3875 mm
p_x	1.525 mm
p_y	1.4 mm
d_1	0.3875 mm
d_2	1.55 mm

We performed a set of simulations against HFSS, for a series of different dielectric profiles, from which S -parameters were extracted. The dielectric profiles were chosen in such a way to test both the accuracy of the hybrid method, and to investigate the consequences of wave

propagation through a multilayered slab. The results of the investigation are shown in the following set of figures.

Figure 3.6 S-parameters of the multilayered SIW filter with $\epsilon_r = (2.2, 3.3)$, $t = (0.5, 0.5) \times h$

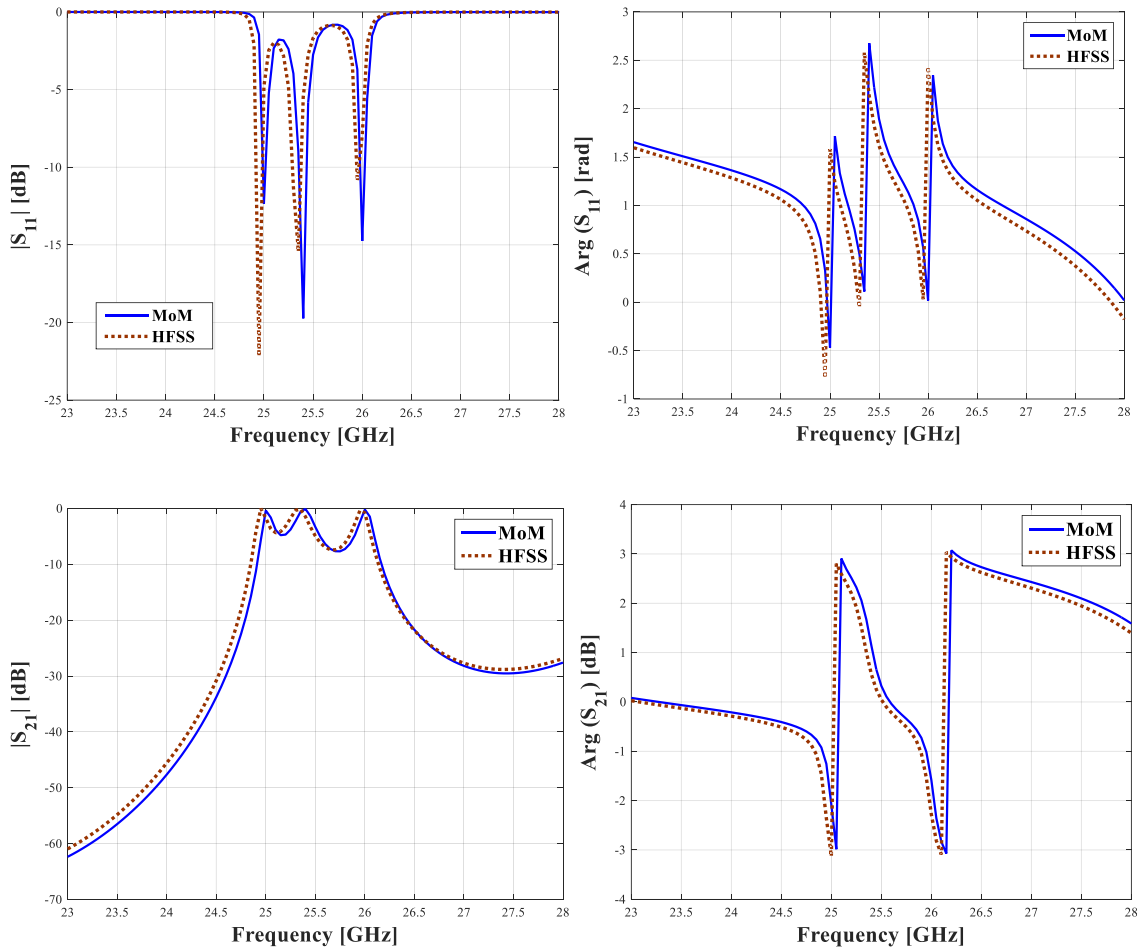
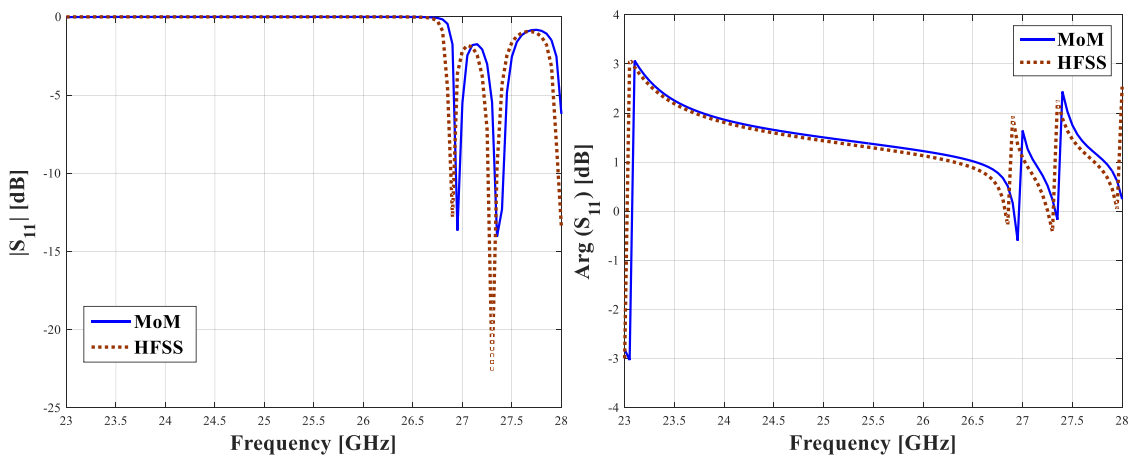


Figure 3.7 S-parameters of the multilayered SIW filter with $\epsilon_r = (2.2, 3.3)$, $t = (0.9, 0.1) \times h$



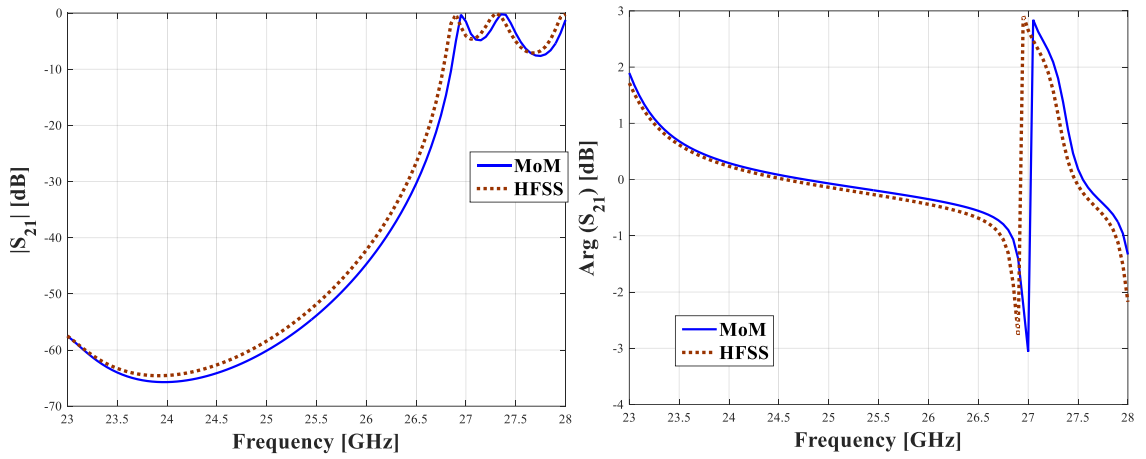


Figure 3.8 S-parameters of the multilayered SIW filter with $\epsilon_r = (2.2, 6.15)$, $t = (0.5, 0.5) \times h$

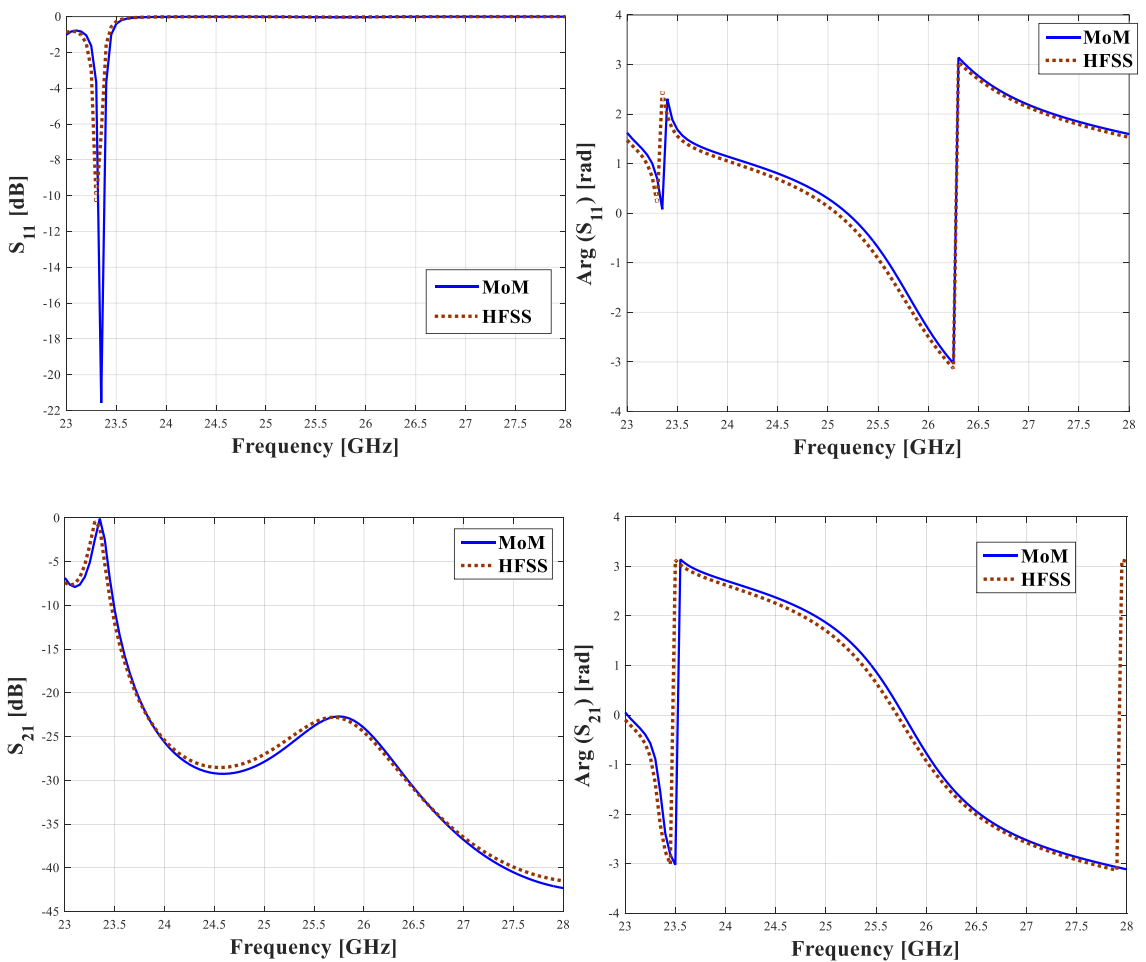
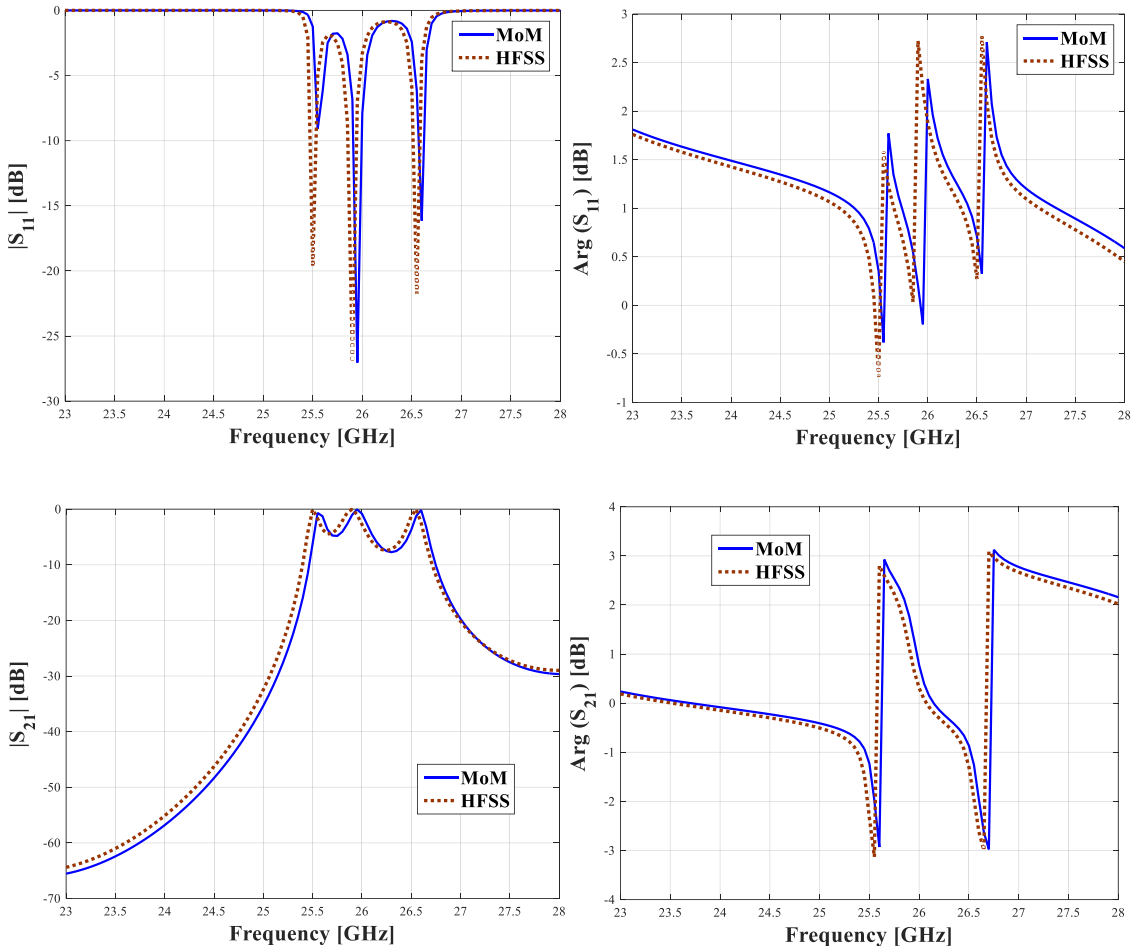
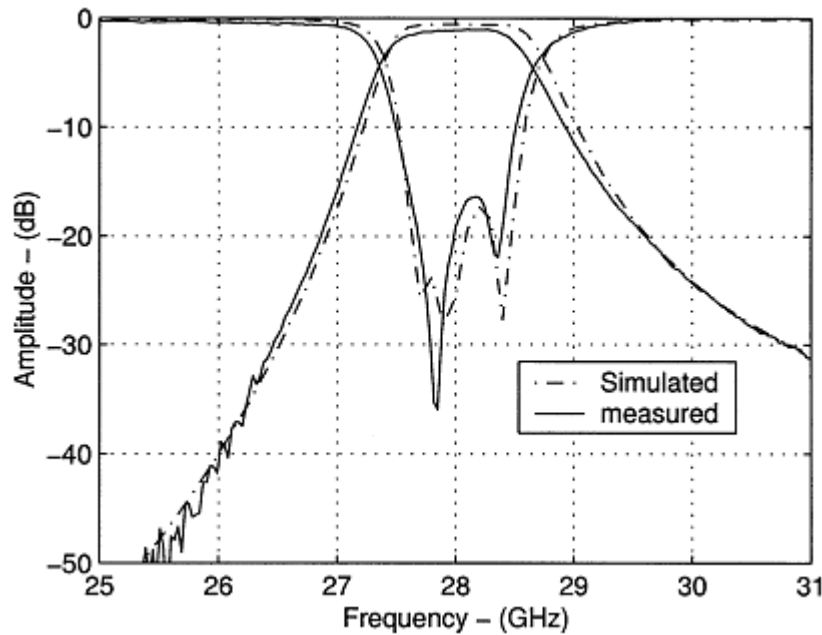


Figure 3.9 S-parameters of the multilayered SIW filter with $\epsilon_r = (2.2, 6.15)$, $t = (0.8, 0.2) \times h$



As can be seen in the figures above, the agreement is excellent throughout the whole considered band ($f = [23, 28]$ GHz), save for a frequency shift of roughly 50 MHz; such a shift is commonplace in comparisons of results obtained with electromagnetic solvers employing disparate solution methods. As for results themselves, they clearly demonstrate an unsurprising effect – the passbands of the respective variants are shifted toward higher frequencies with respect to the original structure whose S -parameters are shown in the figure below (Figure 3.10). The original one contains a dielectric slab of permittivity $\epsilon_r = 2.2$, whereas all the simulated ones contain two-layer slabs with one of the layers having permittivity larger than 2.2. Hence, the added dielectric volume of higher permittivity shifts the modal propagation constants higher up. In addition, it decreases and distorts the magnitude of S_{11} throughout the entire passband, since the presence of an additional layer makes the impulse response of the filter less stationary within the passband, leading to reduced forward scattering and ripples in the magnitude. Unfortunately, this precludes the use of layered dielectrics as means to bandwidth enlargement, as originally envisioned. However, the addition of thin layers on the top and bottom of a central dielectric layer (i.e. sandwiching) still might lead to decreased losses, although the exact effect of this modification on the dispersion is yet to be investigated.

Figure 3.10 S-parameters of the original SIW three-pole Chebyshev filter [109]

3.2 Radiating structures

Having demonstrated the accuracy of our method by numerical experiments involving closed structures, we move onto the more demanding class – radiating SIW structures. These are typically realized by etching narrow slots on the broad wall of a SIW waveguide. Here we present the results of analysis performed on a series of radiating SIW devices of increasing complexity.

To facilitate navigation through the rest of this subsection, we define here the notation pertaining to radiating devices, as follows:

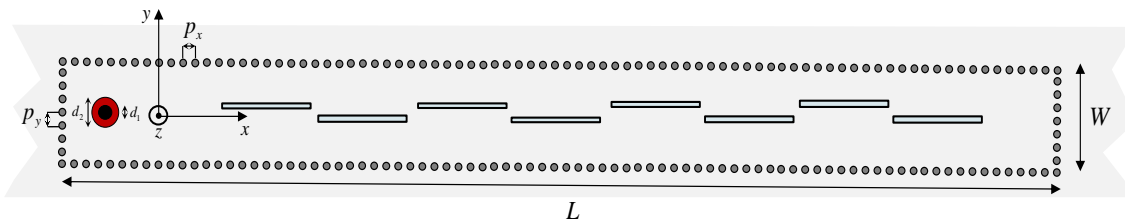
- h is the waveguide height, expressed in millimeters (as are all the other dimensions).
- t denotes the dielectric slab thickness; in case of multi-layered devices, this is a vector containing all the slab thicknesses, ordered in such a way that the thickness of the lowermost layer (i.e. having the lowest z -coordinate) is its first entry, all the subsequent ones placed after in the order of increasing z -coordinate.
- ε_r denotes the relative permittivity of the dielectric slabs present in the device; as t , it is a vector and ordered in the exact same way.
- p_x and p_y denote the period between posts in the x -direction (which we take to be the direction parallel to the device's largest chord) and y -direction, respectively.
- L denotes the length (span in x), while W denotes the width (span in y) of the waveguide/device.

In addition, since the devices analysed in the following subsections have similar geometries, it seems appropriate here to illustrate the waveguide layout of a generic radiating device, shown in the following figure.

Figure 3.11 Layered-dielectric loaded waveguide cross-section (no posts shown for clarity)


3.2.1 Waveguide slot array

The next structure we simulate is shown in the following figure. It is a standard rectangular-guide slot array implemented in SIW technology, consisting of a vertical post fence embedded in a substrate of permittivity ϵ_r , mimicking a rectangular guide. A coaxial transition, protruding through the bottom metal plane, located at approximately $0.25\lambda_g$ away from the backing wall, launches a TM-only field towards the slots etched in the upper metal plane. These are optimized for broadside radiation, the central frequency being 24.15 GHz.

Figure 3.12 SIW 8-slot array; a coaxial port feed is used


First, we simulate an array loaded with a single-layer dielectric. The device parameters are summarized in the following table (Table 3.5). The radiation pattern was computed at several frequencies within the 23.15 to 25.15 GHz band, both using the MoM code and HFSS, in order to test the accuracy of the MoM formulation. In this specific case, the waveguide-to-free-space coupling was tested before proceeding to the more general and complex case of waveguide-to-waveguide-to-free-space coupling. The results are shown in the following figures (Figure 3.13, Figure 3.14)

Table 3.5 Geometrical parameters of the SIW 8-slot array

Cylinders	$N=183$; $a=0.2$ mm ; $p_x=0.8$ mm; $p_y=0.7$ mm
Frequency range	[23.15, 25.15] GHz
Dimensions	66.4 mm \times 5.6 mm \times 0.508 mm ($L \times W \times h$)
Slot dimensions	$L_{slot} = [5.151, 5.163, 5.224, 5.25, 5.25, 5.224, 5.163, 5.151]$ mm, $W_{slot} = 0.2$ mm
ϵ_r	2.2
Feed	Coaxial port - $d_2 = 4d_1 = 4a = 0.8$ mm

As can be seen, the agreement is excellent for $\phi = 0^\circ$, being near-perfect within the main-lobe angular range, and deteriorating slightly towards $\theta = \pm 90^\circ$, but with side-lobe number and their respective maxima predicted accurately. The $\phi = 90^\circ$ radiation patterns, on the other hand, tend to agree less favorably, although the predicted field amplitudes differ less than 0.75 dB at worst.

Though the patterns shown here were computed at only two frequencies, good agreement between the methods holds throughout the whole tested frequency range. In addition, the computational performance of the MoM code is by far superior to that of HFSS, as can be seen from the following table (Table 3.6).

Figure 3.13 SIW 8-slot array radiation pattern at 23.15 GHz; a) $\phi = 0^\circ$ plane, b) $\phi = 90^\circ$ plane

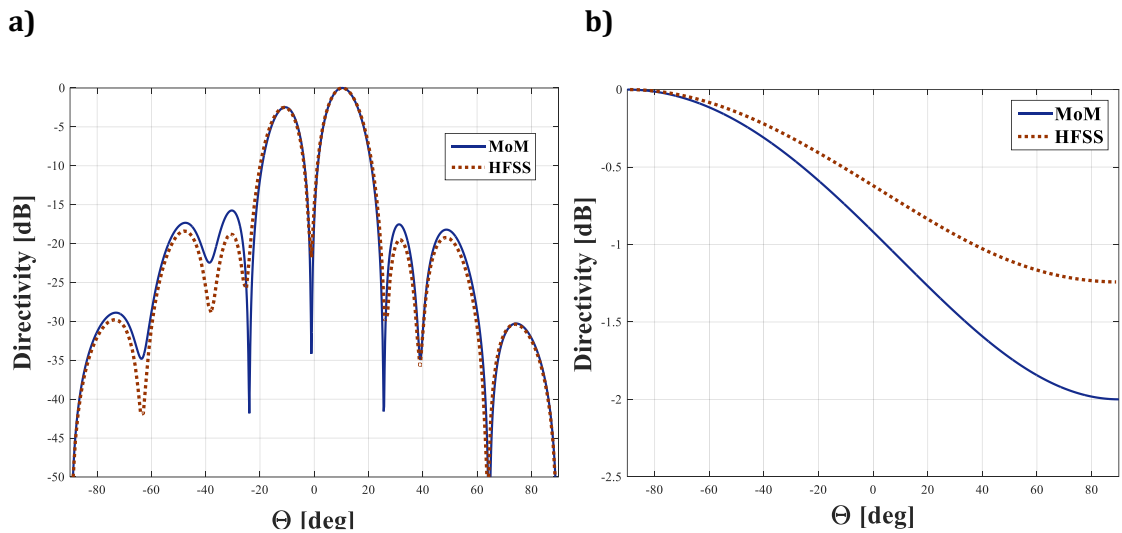


Figure 3.14 SIW 8-slot array radiation pattern at 25.15 GHz; a) $\phi = 0^\circ$ plane, a) $\phi = 90^\circ$ plane

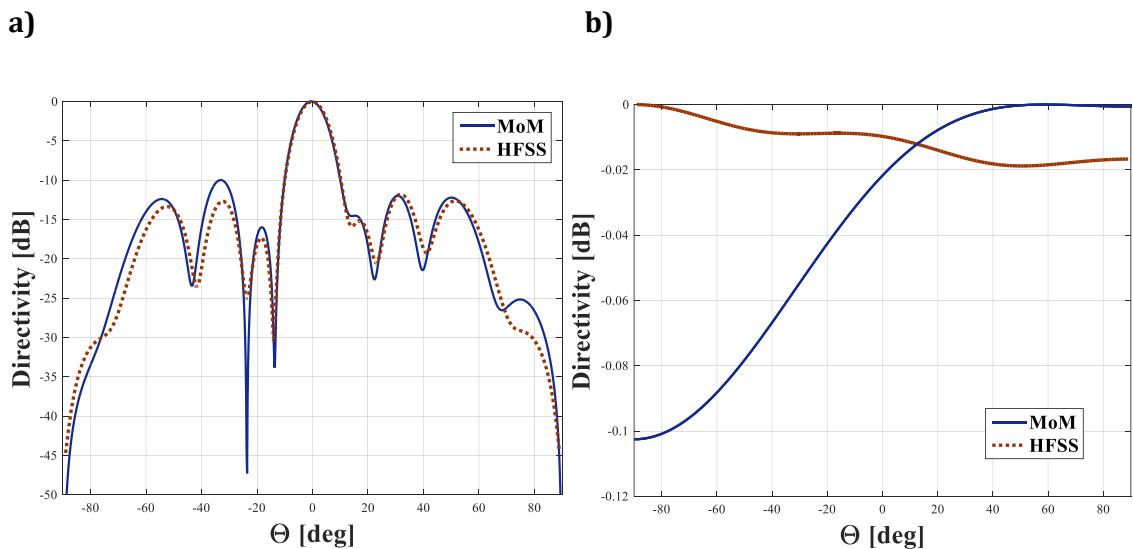
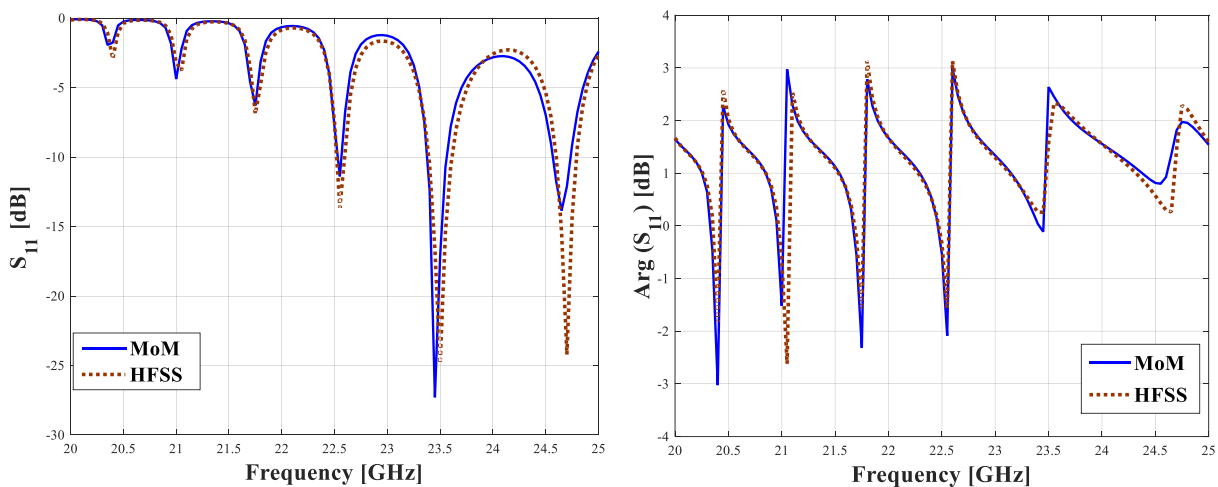


Table 3.6 Mesh properties and runtimes for the SIW 8-slot array

Configuration	Intel i7-4790, 3.6 GHz, 8 GB RAM	
Solver	MoM	HFSS
# unknowns	$N_z(2) \times N_\phi(5) \times N_{posts}(183) + N_{basis\ functions}(24) = 1854$	81 718
Runtime	1.32 min	8.78 min
RAM (max)	79 MB	2.63 GB

To ascertain the accuracy of port parameters calculation, S_{11} was computed and compared, the results shown in the following figure (**Figure 3.15**). The agreement is satisfactory, the greatest discord being roughly 1 dB at the first resonance in the considered frequency range, with the overall agreement tending to improve with frequency. Hence, we argue that, judging by the code performance so far, one can use the formulation with confidence for radiating planar-SIW problems involving slots; that is, for guides loaded with single-layer dielectrics. Whether it can be used when multi-layered dielectrics are present is tested in the following numerical experiment.

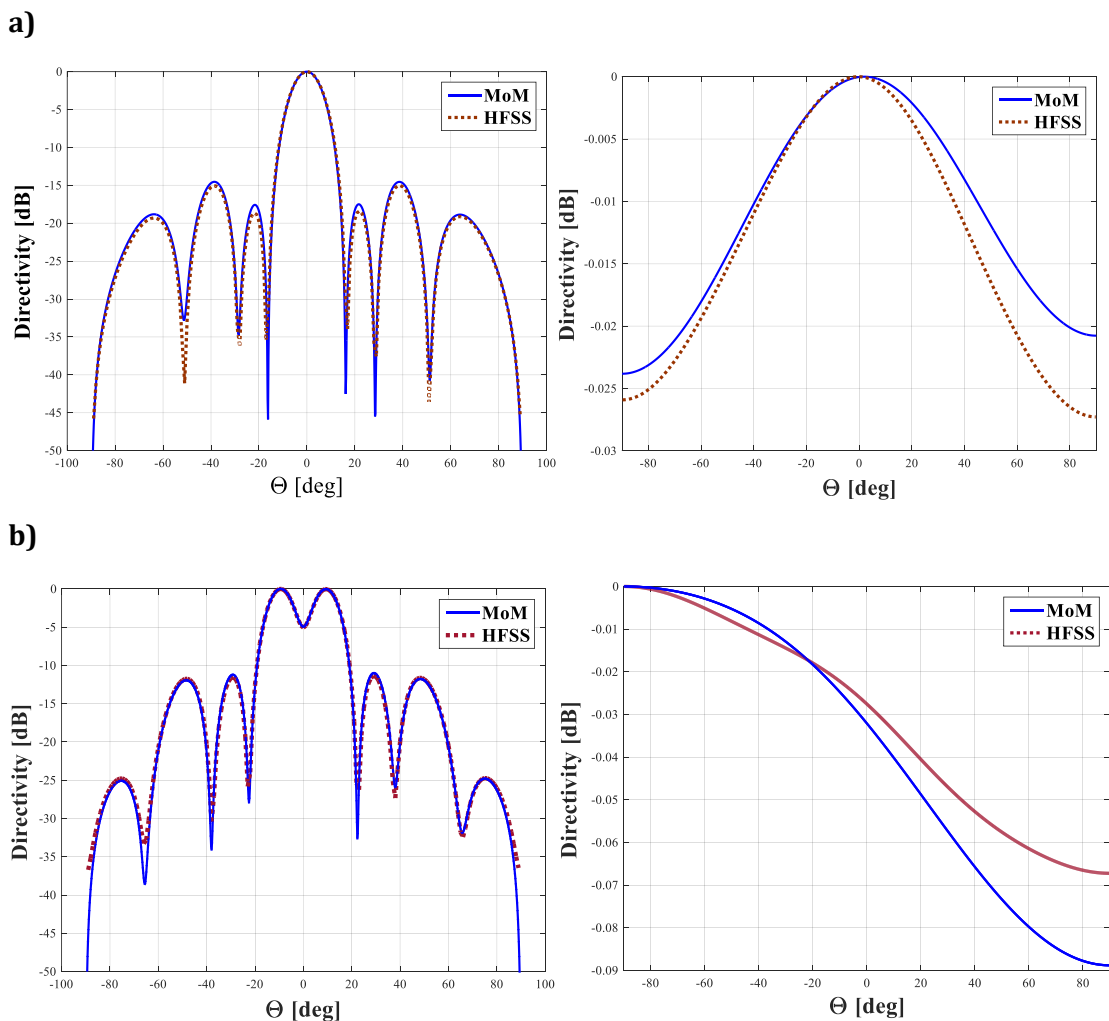
Figure 3.15 S_{11} magnitude and phase of the single-layer dielectric-loaded slot array

3.2.2 Two-layer dielectric loaded slot array

This particular device is analogous to the previously shown single-layer loaded slot array. The “only” difference is that this one is loaded with a two-layer dielectric structure. The dispersion in such a case is dramatically different than in a single-layer PPW type case, since no TEM modes exists, even when the difference in relative permittivity or the thickness of a given layer is small. It is for this reason the present example was chosen to test both the validity and limitations of the multilayer formalism presented earlier in the thesis. All the parameters are exactly the same as for the single-layer slot array, save for the permittivity profile, which in this case is as follows – the bottom layer is 0.25 mm thick (half the total height) with $\epsilon_{r1} = 2.2$, while the top layer is 0.25 mm thick as well, with $\epsilon_{r2} = 4.3$

. The normalized directivity thusly obtained are shown below (Figure 3.16). It can be seen that the agreement is excellent, especially in the main-lobe angular range. The sidelobes diverge, especially for wide observation angles near $\theta = \pm \pi / 2$. However, the agreement is very good all the way down to roughly -35 dB, and the number of lobes is predicted to be the same by both methods, leading one to conclude that the multilayer formalism may be safely used to compute radiation patterns of arrays loaded with multilayer dielectrics. Though one should be inclined to compare two similar methods (in our case, a hybrid MoM with a reliable, well-tested MoM, e.g. FEKO) in terms of performance, it is remarkable that our hybrid MoM agrees quite well with the FEM of HFSS. However, we reiterate here that caution must be exercised when setting up the simulation in HFSS in order to ensure proper convergence. As a general rule of thumb, one should compare relatively well-matched radiating structures (though it is not imperative), and the airbox used to define where the equivalent currents are computed should be well-meshed (below $0.1\lambda_{fs}$, where λ_{fs} is the free-space wavelength). The solution data, containing the number of unknowns, runtimes and RAM usage is shown in the following table (Table 3.7).

Figure 3.16 Two-layer slot array normalized directivity at: a) $\phi = [0, 90]^\circ$ planes, 21.6 GHz; b) $\phi = [0, 90]^\circ$ planes, 22.6 GHz



As can be noted, the increase in computation time and memory usage is almost negligible with respect to the single-layer case, both the one of our method and the one of HFSS.

Essentially, the multi-layered scenario does not demand significantly higher computational resources than the single-layer case.

However, as the permittivities increase, HFSS increases the mesh drastically, whereas the increase in the number of unknowns in our method is significantly lower; for most scenarios encountered in practice, it is sufficient to consider no more than two lowest-order longitudinal modes, three to five azimuthal modes on each post, and five to seven slot basis functions.

Table 3.7 Mesh properties and runtimes for the SIW two-layer slot array

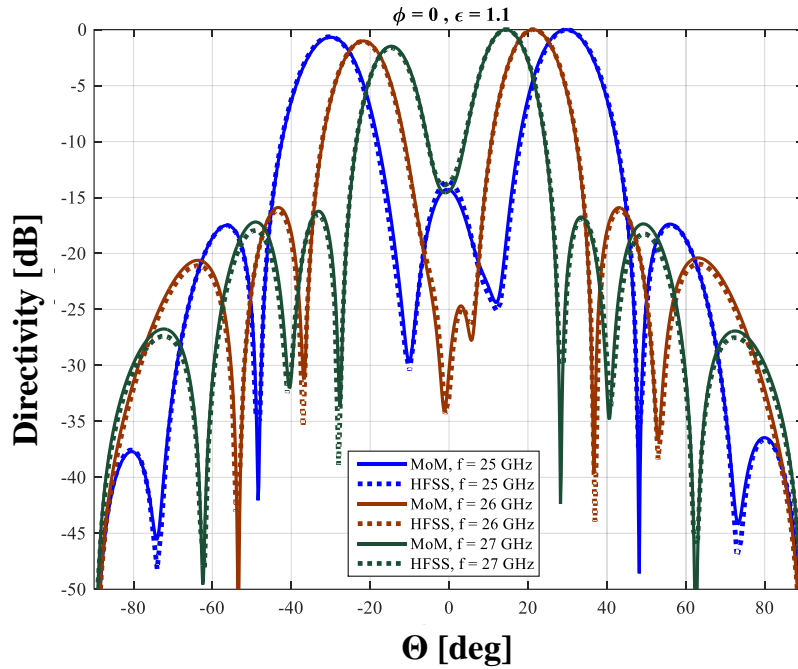
Configuration	Intel i7-4790, 3.6 GHz, 8 GB RAM	
Solver	MoM	HFSS
# unknowns	$N_z(2) \times N_\phi(5) \times N_{posts}(183) + N_{basis\ functions}(24) = 1854$	221 258
Runtime	1.57 min	9.3 min
RAM (max)	89 MB	2.93 GB

It is then expected that, for cases when higher-permittivity dielectrics are used (e.g. $\epsilon_r > 10$), our method shines through. At this point it is expedient to consider a number of different dielectric profiles if one is to attest the generality and accuracy of the proposed analysis approach. Namely, we wish to inspect whether the approach provides stable and accurate results over a relatively wide frequency range when different scenarios are considered. For this purpose, as before, we performed a set of simulations of the two-layer loaded slot array over the frequency region $f = [25, 27]$ GHz, the thicknesses of layers having been set equal, but the relative permittivities of respective layers were varied. Both the S_{11} parameter and far fields in two orthogonal planes were computed, and are shown in the following set of figures; in order to avoid clutter, we show the computed far fields at three distinct frequency points on a single figure – the endpoints and the midpoint of the chosen range. The permittivities were chosen in such a way that they take values close to commonly used dielectric materials; the permittivity of the bottom layer is kept fixed at $\epsilon_r = 2.2$, whereas the ones of the top layer were $\epsilon_r = (1.1, 5.5, 8.8)$, in the order of the following presentation. The far fields obtained with the MATLAB code and HFSS, corresponding to the same frequency are marked by the same colour.

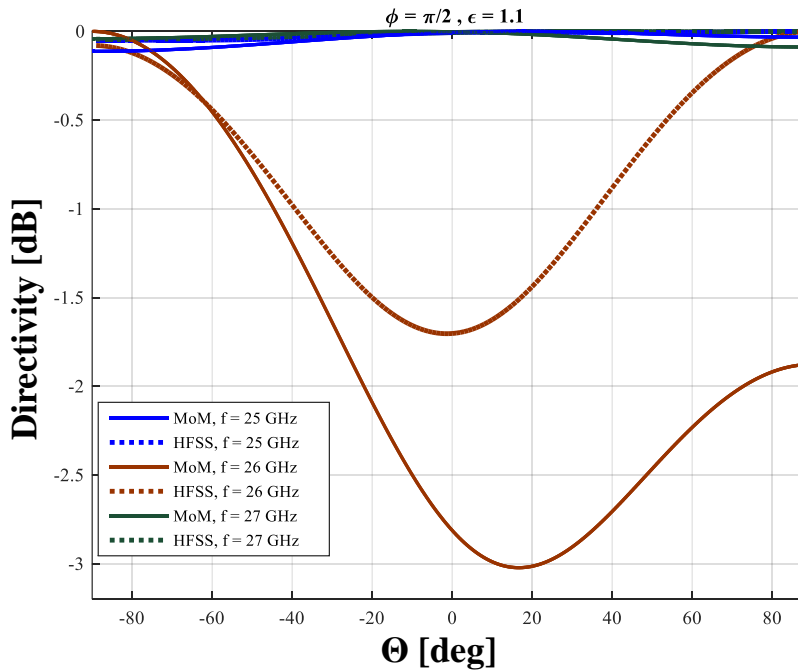
The first simulated case, shown in Figure 3.17, demonstrates the effect of the presence of two dielectric media of relatively small dielectric contrast, the bottom layer being of larger permittivity than the top one ($\epsilon_r = (2.2, 1.1)$, to be precise). With respect to the single-layer dielectric loaded slot array, containing a slab of permittivity $\epsilon_r = 2.2$, one expects a decrease of the modal cut-off frequencies; indeed, this is evidenced on comparison of the frequency dependence of modal wavenumbers of the respective slot arrays. In addition, numerical tests confirm that the longitudinal profile of propagating modes, supported by the structure, is such that there exists a standing wave in the slab of higher permittivity, whereas an evanescent wave, decaying in the positive longitudinal direction (i.e. in the $+z$ direction), exists in the slab of lower permittivity. This should be taken into account when designing radiating devices, since the field of lower-order modes will tend to be confined more strongly in the slab of higher permittivity [110, p. 15]. Of course, this caveat is to be taken as a heuristic, since the radiating elements themselves will significantly affect the total field distribution.

Figure 3.17 Two-layer slot array with $\epsilon_r = (2.2, 1.1)$: a) normalized directivity in the $\phi = 0^\circ$ plane, b) normalized directivity in the $\phi = 90^\circ$ plane, c) S_{11}

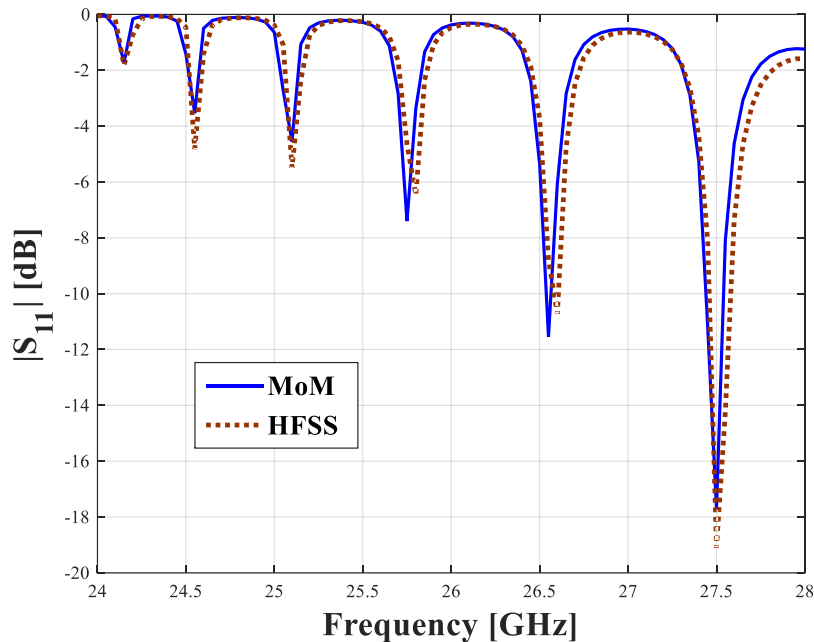
a)



b)



c)



The S_{11} parameters, obtained by both the code and HFSS, shown in Figure 3.17 c), agree well, with a slight frequency shift present, as seen in the analysis of closed structures; this is a common phenomenon present when two differing methods of analysis are used (see e.g. [111, Ch. 21]). Naturally, the agreement depends on the degree of equivalence of respective port models, convergence and accuracy of methods applied, amongst others.

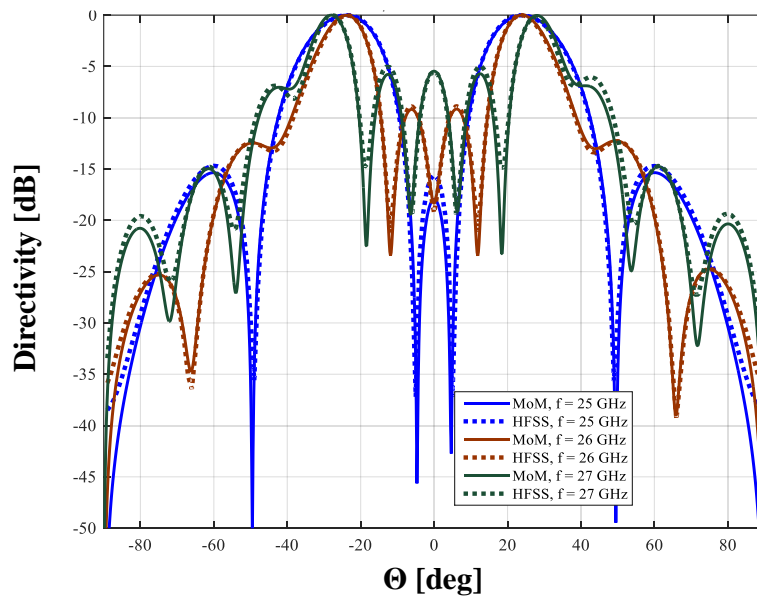
As for the radiation patterns, the agreement is excellent over the whole angular range in the $\phi = 0^\circ$ plane (i.e. H-plane), throughout the entire considered frequency range. On the other hand, the $\phi = 90^\circ$ (E-plane) radiation patterns do not agree well in general, which can be attributed to the limited size of the radiation surface used in HFSS; the computational limitation imposed by the RAM available on the test configuration (8 GB RAM) dictated a radiation surface of modest size (a rectangular box enclosing the array of height 0.5λ), and the pertinent mesh had been chosen fine enough to give accurate results in the H-plane (the maximum cell size was set to 0.05λ). On the other hand, MATLAB simulations were performed using $(N_z, N_\phi, N_{\text{MoM}}) = (3, 5, 7)$ modes/basis functions.

Concerning the remaining two cases, the far fields agree very well for the $\varepsilon_r = (2.2, 5.5)$ case (Figure 3.18), and the S_{11} agree relatively well, if one takes into account that the structure is very poorly matched over the whole frequency range (the minimum occurring at roughly -0.21 dB, for both the MATLAB code and HFSS). Unfortunately, the agreement deteriorates slightly for the $\varepsilon_r = (2.2, 8.8)$ case (Figure 3.19); the discrepancy is most noticeable between the sidelobes, up to 3 dB. The S_{11} curves differ significantly in the $f = [26, 27]$ GHz range, with a prominent frequency shift of roughly 0.1 GHz, and a large maximum discrepancy of 5 dB. Although we have not been able to identify decisively the source of disagreement, we partially traced this problem to the convergence of the HFSS model. Namely, varying the mesh cell size of both the feeding coaxial port and the radiation boundary, we noticed a lack of definite convergence, most prominently in the radiation patterns. On the other hand, the said figures of merit remain stable with increasing order of basis functions used in the MoM/mode-matching code. That this is so should not be

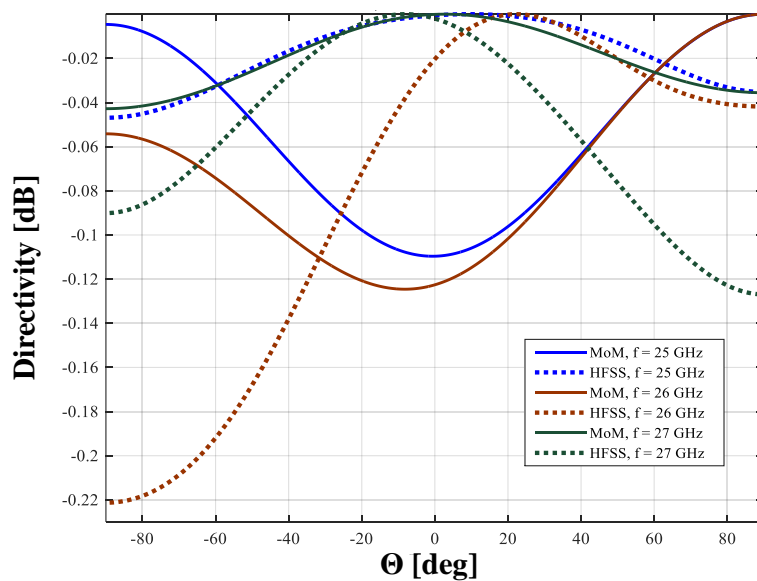
surprising – since HFSS' convergence is directly tied to the convergence of S -parameters, it is possible, and often the case, that the computed radiated fields and quantities derived therefrom may be inaccurate. The accuracy of the fields computed in mesh cells on and close to the ports will affect overall accuracy most significantly, with the implication that the accuracy with which the fields are computed on mesh cells on the radiating elements/radiation boundaries may be reduced.

Figure 3.18 Two-layer slot array with $\epsilon_r = (2.2, 5.5)$: a) normalized directivity in the $\phi = 0^\circ$ plane, b) normalized directivity in the $\phi = 90^\circ$ plane, c) S_{11}

a)



b)



c)

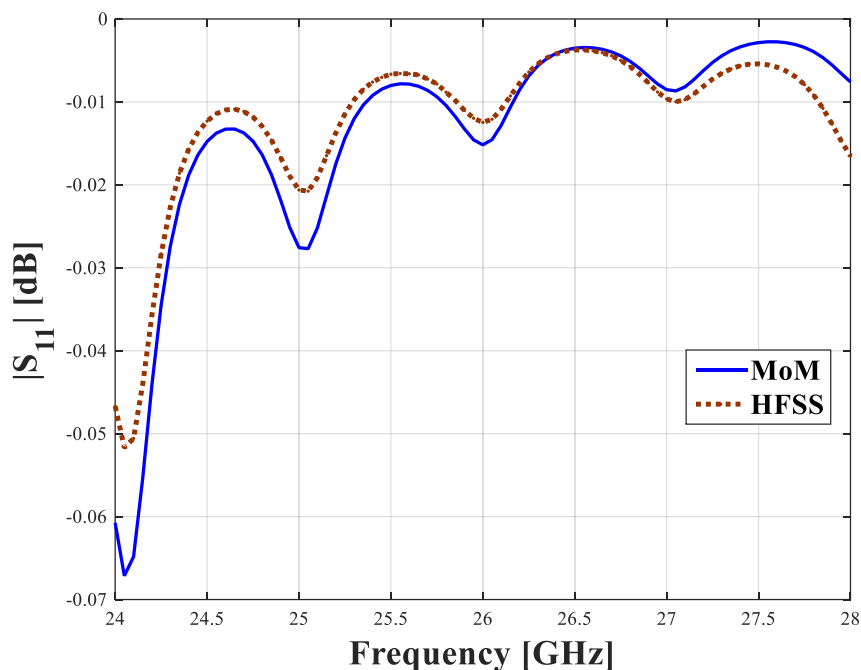
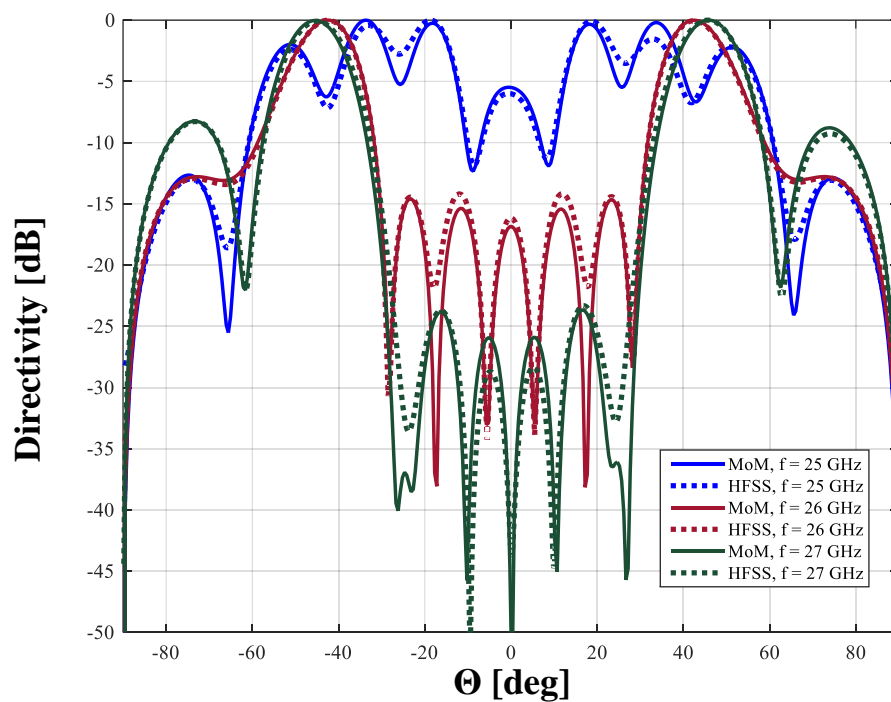
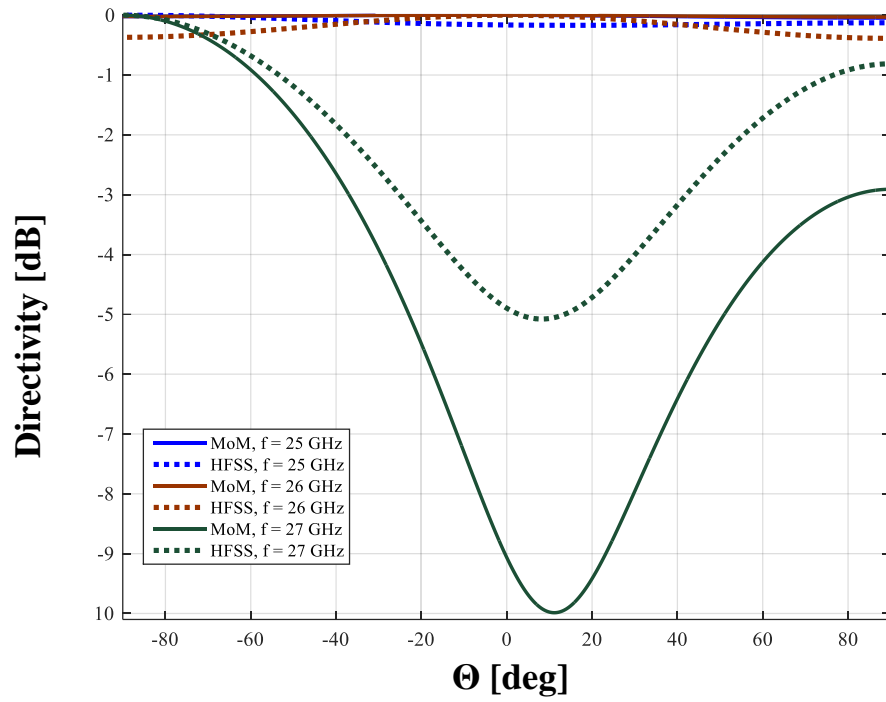


Figure 3.19 Two-layer slot array with $\epsilon_r = (2.2, 8.8)$: a) normalized radiation pattern in the $\phi = 0^\circ$ plane, b) normalized radiation pattern in the $\phi = 90^\circ$ plane, c) S_{11}

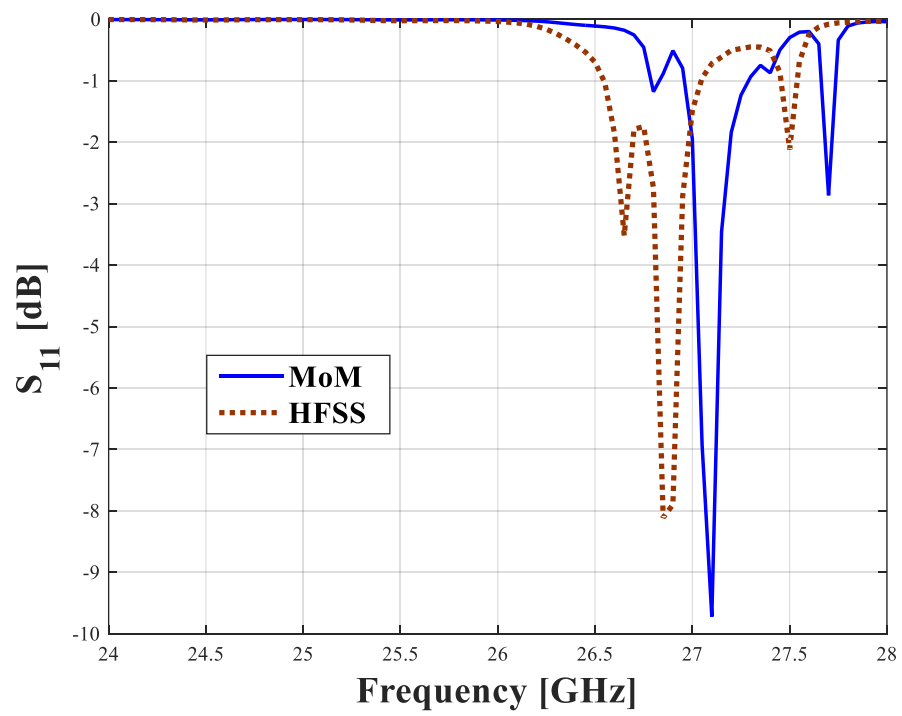
a)



b)



c)

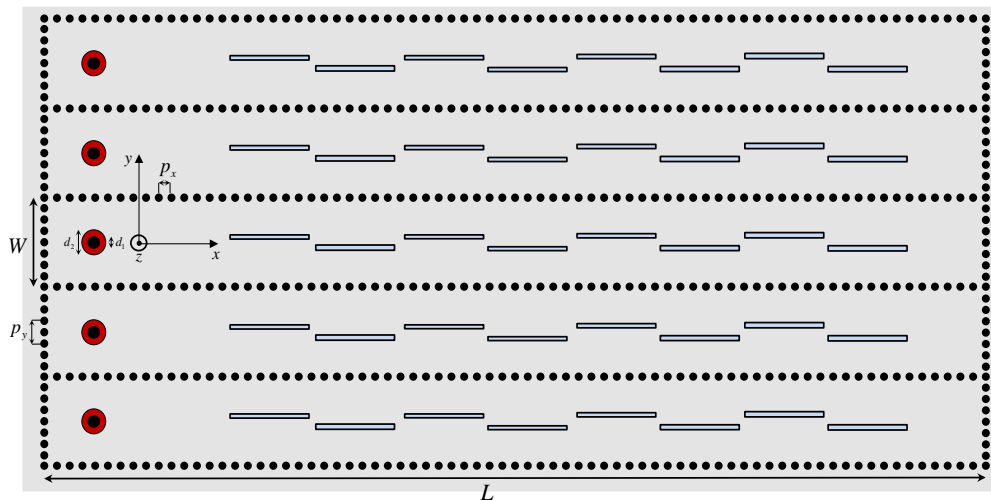


3.2.3 Five-waveguide slot array

Though the previous examples served well to emphasize the relative merits of our hybrid formulation with respect to commonplace commercial EM solvers, they were concerned with relatively simple devices containing a modest number of elements – around a hundred metal posts, maybe few or no slots and coaxial ports. If the true power of this approach is to be demonstrated, a demanding structure should be chosen as the benchmark. The first in a series of such devices is the five-waveguide slot array shown in the following figure.

It is nothing more than a cascade of five slotted waveguides from the previous two tests, set side-by-side, with all ports fired simultaneously. However, the qualifier “nothing more” might be misleading, since this structure contains roughly three times the number of pins of a single-waveguide array, and five times more slots. It should be clear that the number of interactions which must be taken into account is roughly ten times larger than in the single-waveguide case.

Figure 3.20 Five-waveguide SIW slot array



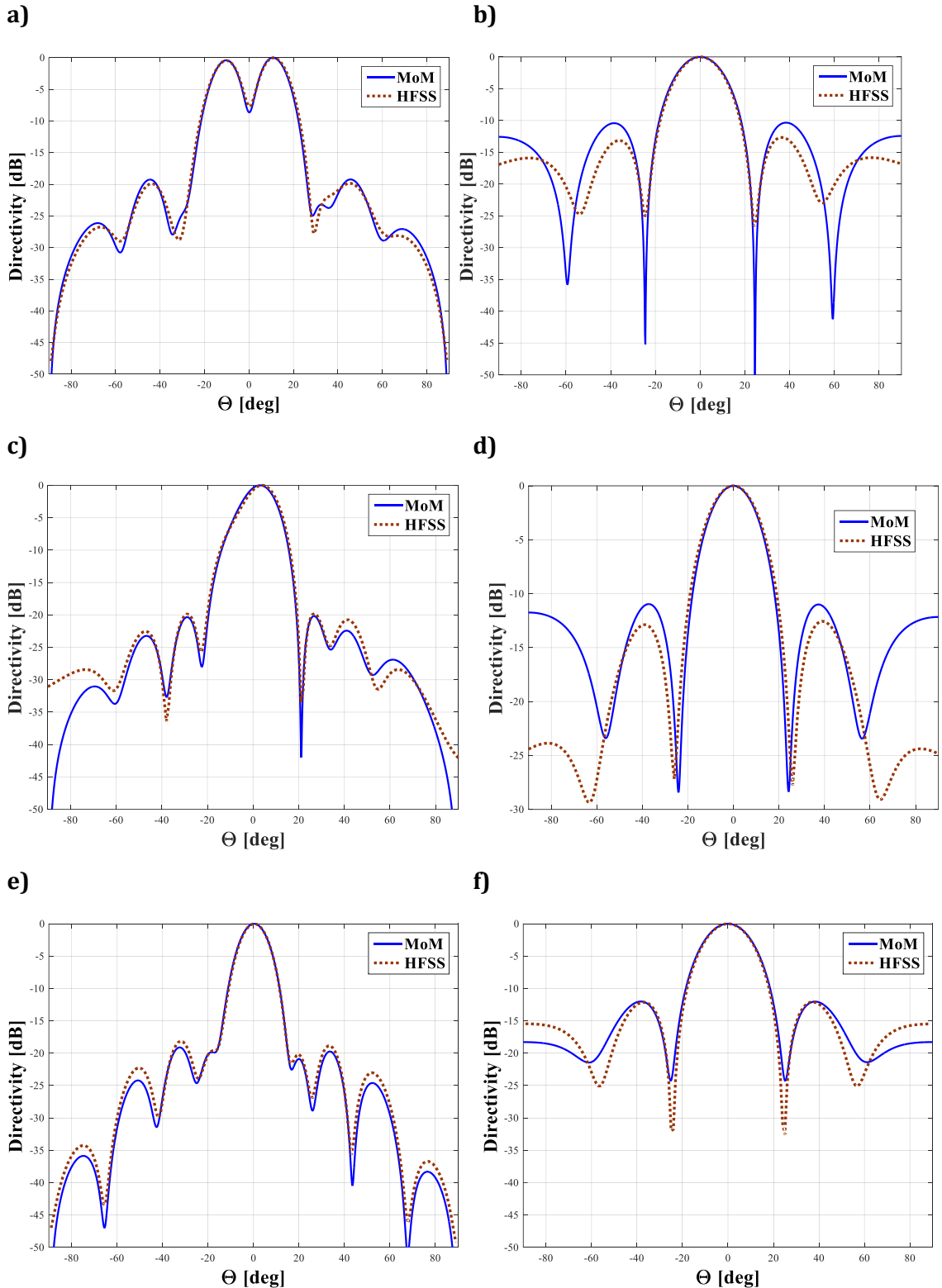
Hence, it represents a significantly more demanding test case than the previous ones. The geometrical and simulation parameters are summarized in the following table.

Table 3.8 Geometrical parameters of the five-waveguide SIW slot array

Cylinders	$N=579$; $a=0.2\text{mm}$; $p_x=0.8\text{mm}$; $p_y=0.7\text{mm}$
Frequency range	$[24.1, 26.1]$ GHz
Unit Cell Dimensions	$66.4\text{ mm} \times 5.6\text{ mm} \times 0.508\text{ mm}$ ($L \times W \times h$)
Slot Dimensions	$L_{slot} = [5.151, 5.163, 5.224, 5.25, 5.25, 5.224, 5.163, 5.151]$ mm, $W_{slot} = 0.2\text{ mm}$
Layer thicknesses	$(0.9, 0.1)h$
ϵ_r	$(2.2, 1)$
Feed	Coaxial port - $d_2 = 4d_1 = 4a = 0.8\text{ mm}$

As before, we calculated the H-plane radiation pattern of the device over several frequencies; the results are shown in the following figures.

Figure 3.21 Two-layer dielectric, five waveguide slot array radiation pattern at - a) 24.1 GHz, $\phi = 0^\circ$ plane, b) 24.1 GHz, $\phi = 90^\circ$ plane, c) 25.1 GHz, $\phi = 0^\circ$ plane, d) 25.1 GHz, $\phi = 90^\circ$ plane, e) 26.1 GHz, $\phi = 0^\circ$ plane, f) 26.1 GHz, $\phi = 90^\circ$ plane



The agreement between the methods is, as up until now, excellent for fields in the $\phi = 0^\circ$ plane despite the markedly higher complexity of this structure compared to the previous ones. Minor discrepancies exist outside the main lobe angular range, though below the -18 dB mark. Unfortunately, the $\phi = 0^\circ$ plane fields agree well only within the main lobe angular range. In terms of the computation time, this example demonstrates the relative merit of using our method – as the electrical size and complexity increase, the commercial solver becomes increasingly greedy, requiring excessive amounts of time not only to properly mesh the structure in question, but to adaptively compute the field, where the mesh is refined between iterations.

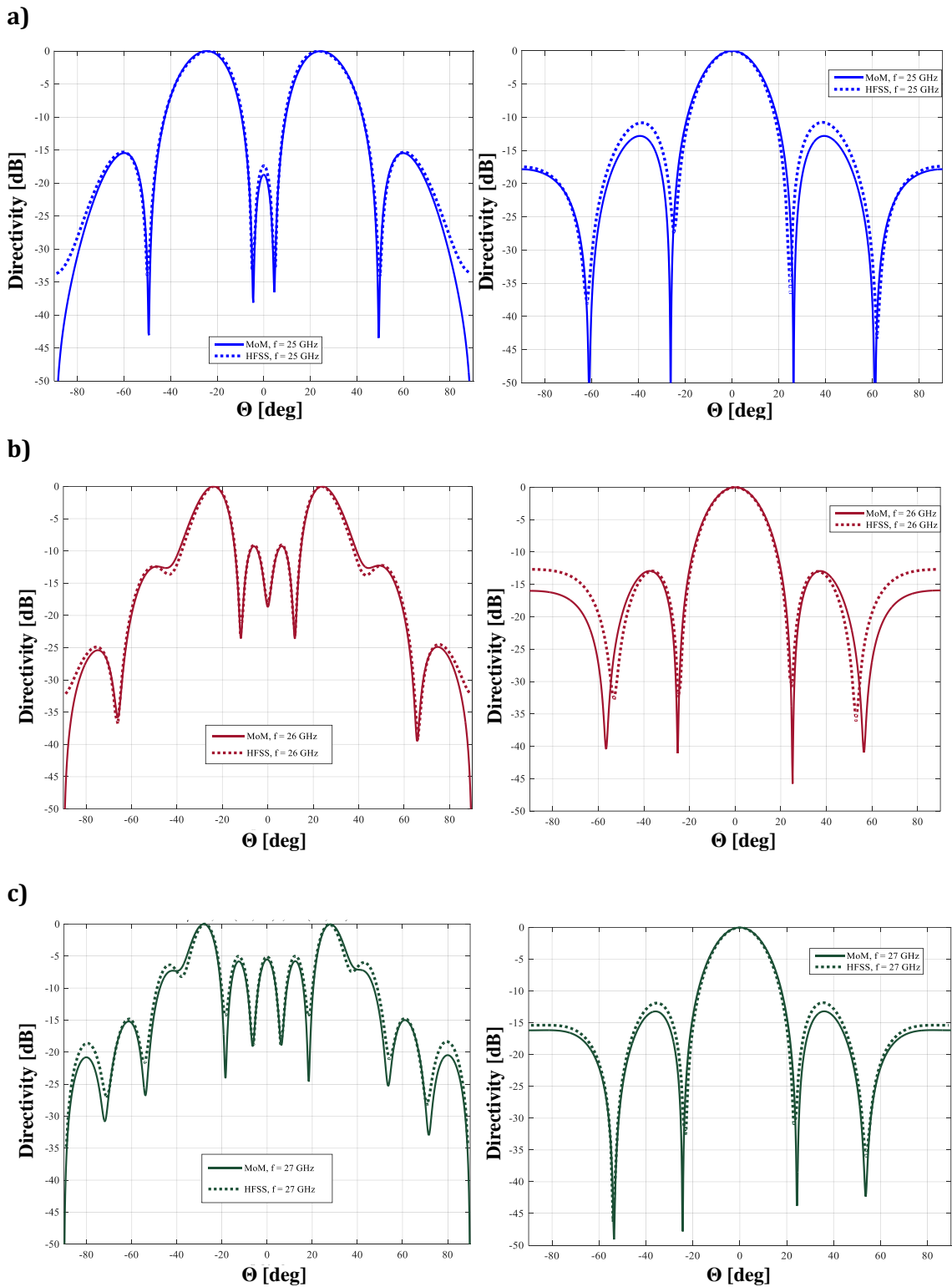
The solution data, shown in Table 3.9, clearly shows that the increase in the computation time in going from the single-waveguide to five-waveguide case is by a factor of roughly 27 for HFSS. On the other hand, our method required roughly ten times the time it took for the single-waveguide case. Thus, one can safely state that our method is immensely advantageous in comparison to the commercial solver, inasmuch that even a simulation as demanding as this one can be run on a medium-range laptop.

Table 3.9 Solution data for the five-waveguide, two-layer slot array with $t = (0.9, 0.1)h$, $\varepsilon_r = (2.2, 1)$

Configuration	Intel i7-4790, 3.6 GHz, 8 GB RAM	
Solver	MoM	HFSS
# unknowns	$N_z(2) \times N_\phi(2) \times N_{posts}(579) + N_{basis\ functions}(200) = 2516$	703 431
Runtime	11.6 min	278.7 min
RAM (max)	2.6 GB	7.31 GB

Again, we performed a series of simulations using different dielectric profiles. For the sake of brevity, we show here the case when a dielectric comprising two layers of equal thickness and permittivities $\varepsilon_r = (2.2, 5.5)$. The simulation setup here, however, differs from the single-waveguide test case due to limitations in available dynamic memory – we used $(N_z, N_\phi, N_{MoM}) = (2, 5, 5)$ in the hybrid code (compared to $(N_z, N_\phi, N_{MoM}) = (3, 5, 7)$ in the former test scenario), while the solution frequency of HFSS was set to 30 GHz, with the radiation surface meshed using elements of maximum size $l_{max} = 0.1\lambda_{mesh}$, where λ_{mesh} is the free-space wavelength at 32 GHz (chosen so as to ensure relatively accurate radiation patterns). Moreover, the order of basis functions used by HFSS' FEM solver was demoted from mixed-order to first order. The following results summarize the behaviour of respective methods in this more “stressful” scenario.

Figure 3.22 Radiation patterns of the five-waveguide slot array with $t = (0.5, 0.5)h$, $\epsilon_r = (2.2, 5.5)$: a) 25 GHz, b) 26 GHz, c) 27 GHz



Evidently, the hybrid code produces results close to the one of HFSS, even with reduced precision (dictated by the number of basis functions used). Although the agreement is good in the $\phi = 0^\circ$ plane, what is especially interesting that the agreement is significantly better

in the $\phi = 90^\circ$ plane compared to the previous test cases. Extensive testing of both the single-layer and multilayer hybrid code versions indicates that the agreement in the $\phi = 90^\circ$ plane will generally be good provided the pattern is narrow, i.e. there exists a pronounced single main lobe, although we have not determined the bounds on the angular extent thereof. Unfortunately, as stated already, we were not able to conclusively trace this phenomenon back to a specific characteristic of either of the methods used; it still remains to determine the source of discrepancy.

Regarding the computational resources used, the following table summarizes the demands and gains in the given scenario.

Table 3.10 Solution data for the five-waveguide, two-layer slot array with $t = (0.5, 0.5)h$, $\varepsilon_r = (2.2, 5.5)$

Configuration	Intel i7-4790, 3.6 GHz, 8 GB RAM	
	MoM	HFSS
Solver		
# unknowns	$N_z(2) \times N_\phi(5) \times N_{posts}(579) + N_{basis\ functions}(200) = 5990$	606 043
Runtime	68.52 min	218 min
RAM (max)	3.7 GB	7.39 GB

Even though the memory demands on HFSS have remained almost the same as in the previous case (albeit a coarser mesh was used in this one), while the computational time has reduced, the in-house MATLAB code still compares favourably with a computational time smaller by a factor of roughly 3, and the RAM consumption half the one of HFSS. In light of solid agreement between the respective results, one has here yet another confirmation of the accuracy and efficiency of our hybrid method.

Though the former test cases make a solid argument for the reliability of our home-brewn MoM/mode-matching code, due to its accuracy in scenarios with largely differing permittivity profiles, one could raise a reasonable concern whether it holds over a wide range of thickness profiles as well. In fact, it being based on a semi-analytical scheme, rooted in the use of closed-form, exact Green's functions for multi-layered media, should make it valid for arbitrary thickness/dielectric profiles. Moreover, a similar approach [87] (and one of the more successful ones) dealt with two dielectric layers of comparable thickness (equal, to be more exact) and of small permittivity contrast ($\varepsilon_r = (3.2, 4.3)$), representing an "almost" single-layer scenario. Hence, it would be both interesting and necessary to inspect the behaviour of truly multi-layered devices, i.e. ones with *both* a larger dielectric contrast and thickness difference between the layers.

For this purpose, we simulated the behaviour of the five-waveguide, multi-layer dielectric loaded array with a fixed dielectric profile and varying thickness. In more detail, the permittivities were chosen to be $\varepsilon_r = (2.2, 6.15)$ (the latter corresponding to the one of Rogers Duroid 6006 laminate), and a parametric study was performed by varying the thicknesses from $t = (0.1, 0.9)$ to $t = (0.9, 0.1)$ and computing the radiation patterns and S-parameters over the [26, 27] GHz range. For the sake of brevity, only the said extreme cases are shown below.

The first scenario, involving a bottom layer of thickness $0.1h$ and permittivity 2.2, and the upper layer of thickness $0.9h$ and permittivity 6.15, is a more challenging one, since the presence of a thick layer having relatively higher permittivity will contribute to a larger dispersion throughout the considered frequency range. To be more precise, the propagation constant of the dominant mode will increase more rapidly with frequency, compared to the second scenario ($t=(0.9,0.1)h$, $\epsilon_r=(2.2,6.15)$). This will, in turn, lead to less predictable behaviour of the radiation pattern. Moreover, such a scenario will be more demanding to simulate using HFSS' FEM, due to a larger number of mesh cells required to accurately handle the thick slab of higher permittivity.

Figure 3.23 $\phi=0^\circ$ plane radiation patterns of the five-waveguide slot array in the with $t=(0.1,0.9)h$, $\epsilon_r=(2.2,6.15)$ at (26, 27) GHz

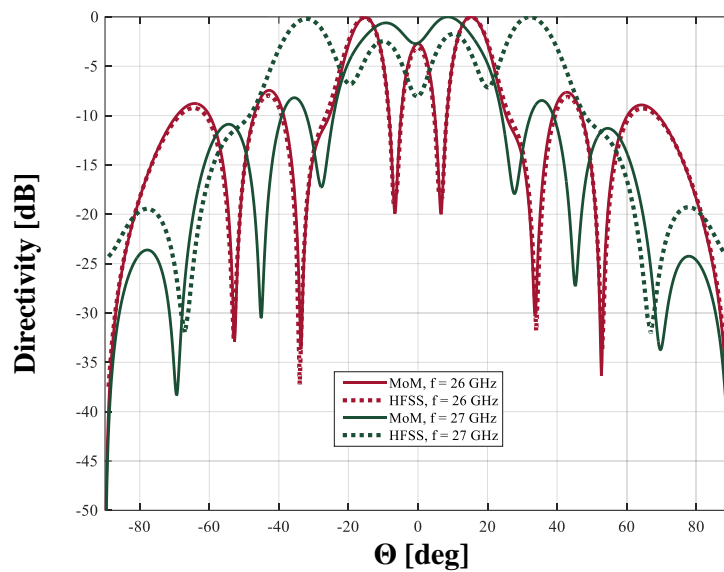
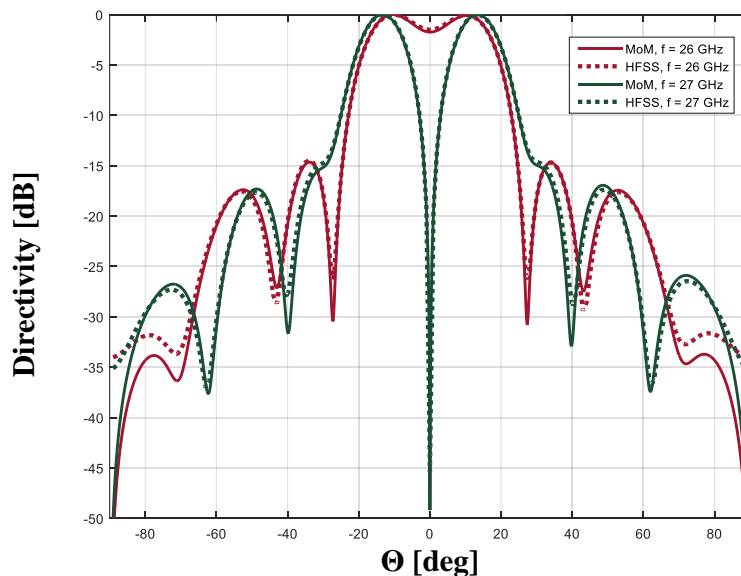


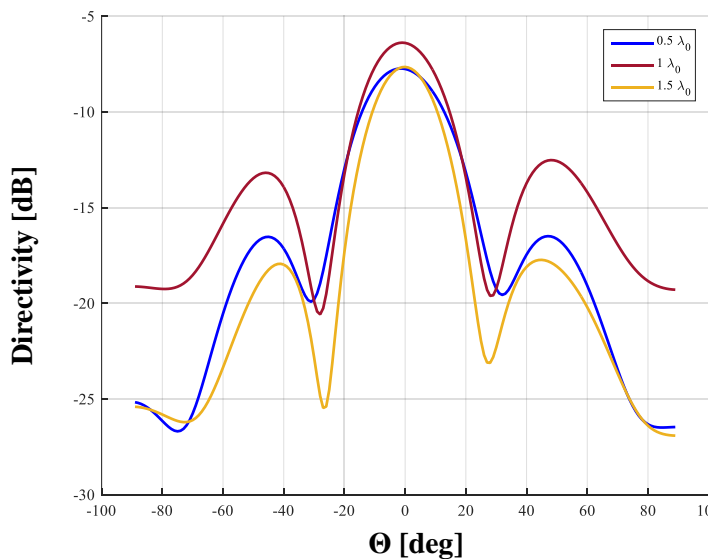
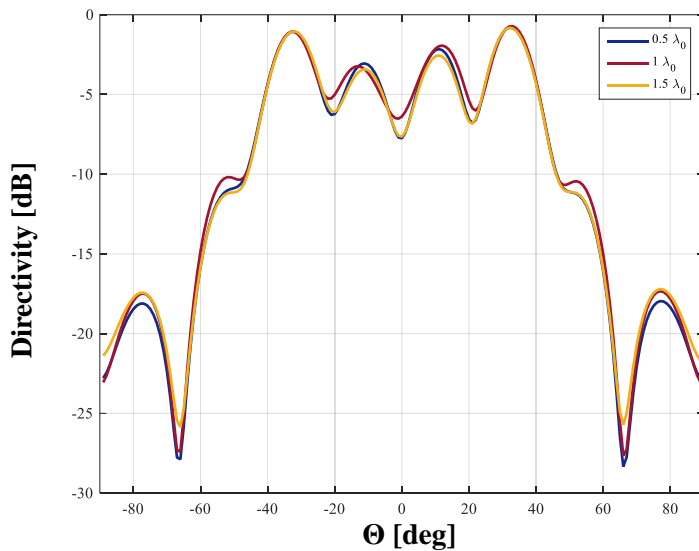
Figure 3.24 $\phi=0^\circ$ plane radiation patterns of the five-waveguide slot array in the with $t=(0.9,0.1)h$, $\epsilon_r=(2.2,6.15)$ at (26, 27) GHz



At 26 GHz, the agreement is very good, even in the grazing angle range (Figure 3.23). However, already at 27 GHz the agreement deteriorates – not only do the respective methods deviate significantly in the predicted field levels, but in the predicted number of lobes as well! This behaviour is indicative of a problem with the model – the HFSS simulation took a considerable amount of time to converge to a solution with the maximum change in the S -parameters between iterations taken to be 2 %. The radiation pattern convergence with respect to the height of the radiation box (chosen to be multiples of $\lambda_0 / 2$; λ_0 being the free-space wavelength at 24 GHz), shown in the following pair of figures (Figure 3.25), in conjunction with the poor matching of the antenna, leads one to conclude that industry solvers should be used with precaution; since one is never fully in control of the method used, nor is its implementation transparent, there is no guarantee that it will provide accurate estimates of relevant quantities for all considered devices.

Figure 3.25 Realized gain convergence with respect to the radiation box height (for the two-layer, five waveguide slot array); a) $\phi = 0^\circ$ plane, b) $\phi = 90^\circ$ plane

a)



b)

Opposed to the first one, the second scenario ($t = (0.9, 0.1)h$, $\epsilon_r = (2.2, 6.15)$) does not suffer from the aforementioned problems. As can be noted in Figure 3.24, the agreement is excellent at both frequencies (in fact, in the whole range), which can be attributed to it being a better-matched structure, and the radiation pattern is more focused towards broadside, compared to the previous case.

Hence, it is implied that care must be exercised when considering “pathological” cases since they require a more meticulous simulation setup.

3.2.4 Corporate-fed stacked waveguide slot array

At this point, the validity and accuracy of the formulation proposed in the thesis, especially the part pertaining to multi-layered scenarios, has been demonstrated over several typical cases – closed and radiating problems, single-dielectric and multi-layered problems, in varying degrees of complexity. However, it still remains to be seen whether the method retains its advantages in extreme cases – applied to devices of great complexity and electrical size. An adequate benchmark is then necessary, which embodies all, or at least most of the characteristics of actual SIW devices. For this purpose, a corporate-fed, stacked-waveguide slot array, devised by Tekkouk et al. [34], and shown in the following figure, was chosen and modified since it:

- A. consists of a large number of elements,
- B. is electrically large,
- C. is composed of several stacked waveguides, and
- D. is an example of a complex radiating device (slots being the radiating elements).

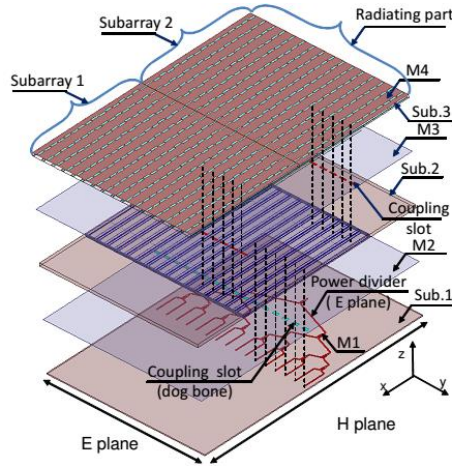
The original array, as described by Tekkouk et al., comprises three main planar waveguides, stacked on top of each other. The intermediate waveguide is partitioned into 16 distinct smaller ones by metal post fences running along the length of the structure, while the topmost guide is partitioned into 32 smaller guides by additional transverse fences. The bottom waveguide provides exciting fields by way of a 1:16 microstrip-type power divider, each of its branches running all the way to a respective coupling slot which is located on the metal plane common to the bottom and intermediate guide. The field coupled to the intermediate guide is then passed down to slots equally removed from the bottom coupling slot, which serve to relay the energy to the topmost guide, comprised of 32 identical slot arrays. These slots are located in the middle of each subguide/slot array, feeding them in phase, and thusly increasing the bandwidth of the total array.

In the following simulations we have replaced the microstrip power divider with feeding waveguides, since the hybrid code cannot yet analyse hybrid microstrip/SIW structures. However, this does not impact the operation of the array significantly with respect to the original layout – the matching bandwidth of the feed is predominantly dictated by the coupling slot resonance, whereas the feeding waveguide and the microstrip line have a wider, less sensitive matching frequency dependence in the considered band. Hence, no significant loss of fidelity is encountered in passing from the original to the tweaked structure. The exact number of elements and array dimensions are summarized in the following table.

As in previous examples showcasing radiating SIW devices, we calculated the radiation patterns at several frequencies using HFSS and the in-house hybrid code; the results are shown below. Figure 3.27 shows the radiation patterns of a single unit cell of the corporate-fed slot array at two distinct frequencies. At 14.1 GHz, the global maxima are located at roughly $\pm 45^\circ$, with a number of smaller maxima in between (the next-to-largest one being approximately 14 dB below the global one).

Figure 3.26 Corporate-fed slot array layout: a) exploded view, b) sideview schematic (taken from Tekkouk et al. [34])

a)



b)

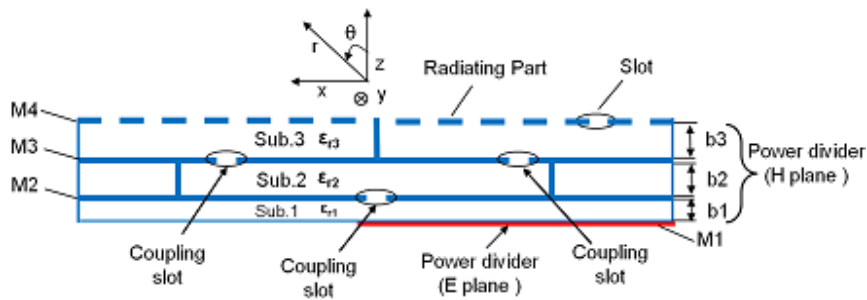


Table 3.11 Unit-cell geometrical parameters of the corporate-fed, stacked waveguide array

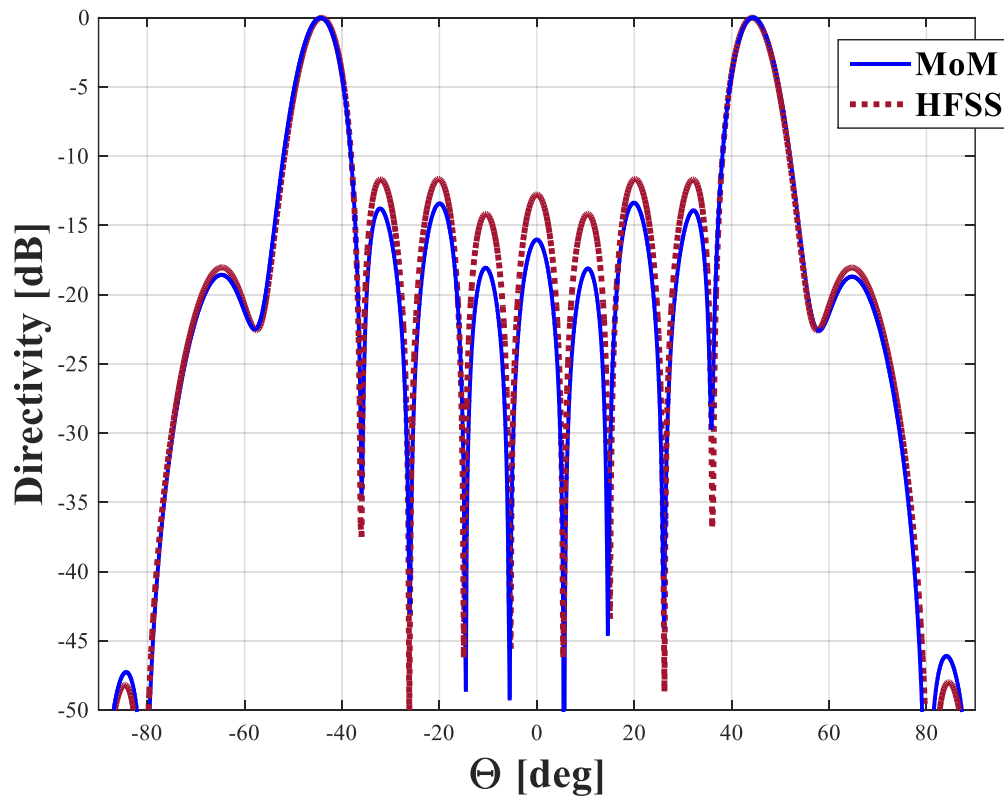
Cylinders	$N=715$; $a=0.3$ mm; $p_x=1.2$ mm; $p_y=0.94$mm
Frequency range	[14.1, 15.1] GHz ($f_0 = 14.25$ GHz)
Unit Cell Dimensions	$b_1 = 0.305$ mm, $b_2 = b_3 = 1.524$ mm ; $L \times W = 26$ cm \times 19 cm ($12.35 \lambda_0 \times 9.03 \lambda_0 @ f_0$)
Layer thicknesses	(0.7, 0.3)h
ϵ_r	[3.55, 2.2/1]
Slot dimensions	Coupling slot - $l_{slot} = 7.1$ mm, $w_{slot} = 0.3$ mm ; Radiating slots - $l_{slot} = 6.4 - 7.195$ mm, $w_{slot} = 0.15 - 0.25$ mm ;
Feed	Waveguide port

The agreement between the in-house code and HFSS is excellent all the way from the zeros preceding the main lobes up to $\pm 90^\circ$, whereas it is less than stellar between the aforementioned zeros, though the positions of maxima and zeros agree quite well; the average difference in the normalized amplitudes is more than 3 dB.

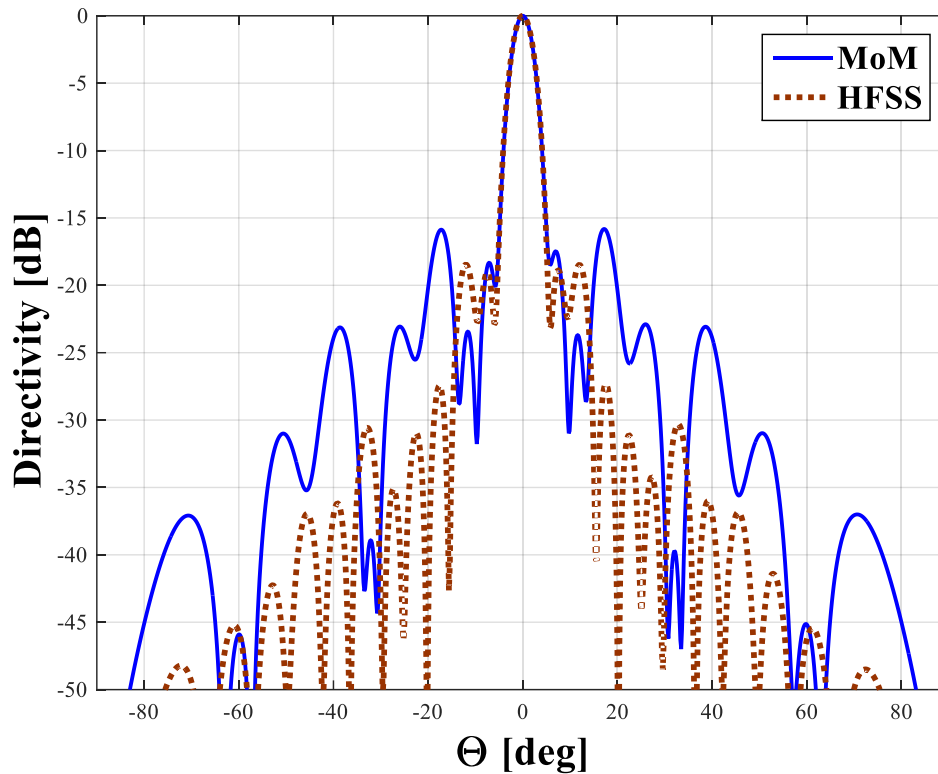
Although the secondary maxima are of amplitude below -14 dB, this reveals a significant discord between the methods, which is only further pronounced at 15.1 GHz (Figure 3.27 b)). At this frequency, the radiation is manifestly broadside, and the main lobes predicted by the code and HFSS agree quite well all the way to -18 dB. However, the side lobes are, once again, off – the first two sidelobes agree in position, whereas the amplitude is off by more than 5 dB. A reasonable guess why this happens is that the matrices involved with such a large problem become ill-conditioned and cannot be accurately handled by linear system solver routines used; this hypothesis is still under examination. Regardless, it can be safely stated that the code based on the hybrid method can be reliably used to predict the global radiation maxima even in SIW slot array radiation problems of greater complexity, such as the one considered.

Figure 3.27 Normalized directivity of the corporate-fed slot array in the $\phi = 0^\circ$ plane at a) 14.1 GHz and b) 15.1 GHz

a)



b)



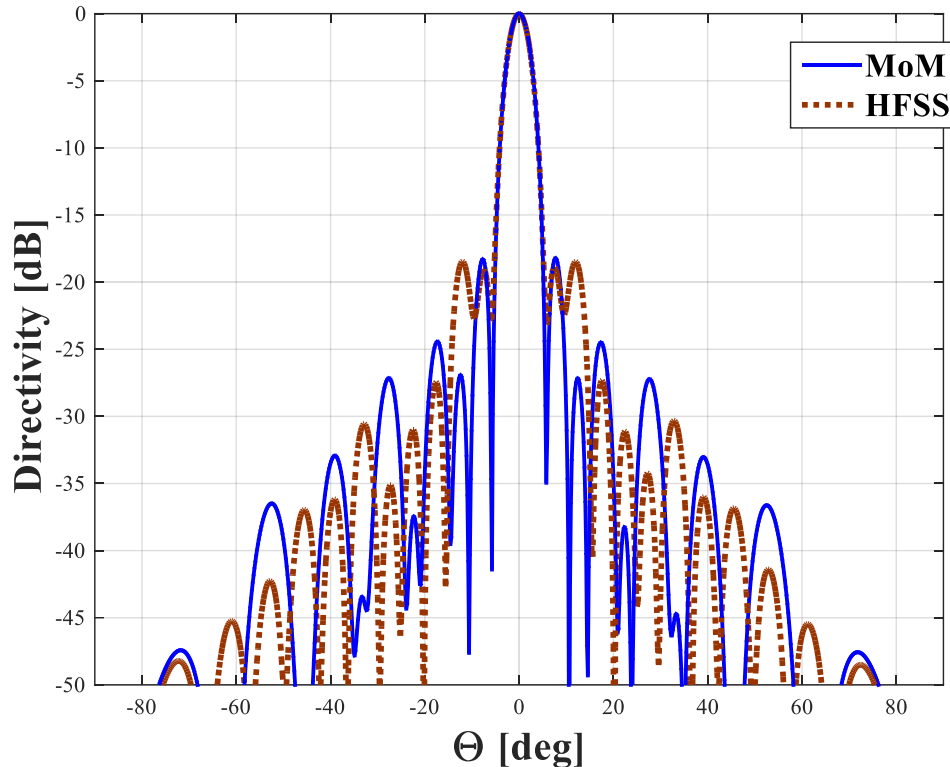
The final example contains five unit cells, centered around the xz plane (normal to the direction of periodicity). All ports are fired simultaneously, and the radiation patterns are calculated, as before, in the $\phi = 0^\circ$ plane. Here the structure had been simulated in HFSS using periodic boundary conditions, since the solver's memory consumption already renders the simulation infeasible on a middle-range computer. One may be concerned by the possible discrepancies between the behaviour of a finite structure, as implemented in the MATLAB code, and the infinite periodic structure of HFSS. However, in this case, the periodic device approximates the finite structure well (or rather the converse), which is a well-known result, though in this case justified only *a posteriori*. Even in this case the code took less time than HFSS to analyse the structure, again with a more modest memory requirement, though not significantly; the computational resources used are shown in the following table.

Table 3.12 Solution data for the five-waveguide, two-layer corporate-fed slot array

Configuration	Intel i7-4790, 3.6 GHz, 8 GB RAM	
Solver	MoM	HFSS
# unknowns	$N_z(2) \times N_\phi(4) \times N_{posts}(2315) + N_{basis\ functions}(175) = 18\,695$	1 372 293
Runtime	39.5 min	298 min
RAM (peak)	6.5 GB	7.01 GB

Figure 3.28 The normalized radiation pattern of a 5-cell corporate-fed slot array at 15.1 GHz, $\phi = 0^\circ$ plane

The total runtime of the code is smaller by a factor of roughly 7, while the RAM used is



comparable to the HFSS analysis. Again, the ad-hoc method is significantly faster and therefore more convenient for any optimization task which might employ it as the main solver.

3.3 Conclusion and future work

A numerical method is only as successful as its ability in predicting measurable quantities of interest. Despite its potential conceptual simplicity, utilitarian advantages or mathematical elegance, it may fall short of its goal – providing accurate results within the specified range of scenarios where it is supposed to hold true. Based on the extensive series of tests, a portion of which were presented in this chapter, we now round up the main characteristics of the method’s overall performance, from which we conclusively deduce its pros and cons.

The preceding discussion can be condensed to the following set of statements:

- I. The method presented in this work offers a conceptually simpler framework suitable for less error-prone construction of solutions to scattering problems of the SIW type -problems pertaining to planar parallel-plate waveguides containing
 - a) single or multi-layered dielectric slabs,
 - b) metal and dielectric cylindrical posts of arbitrary radius,
 - c) narrow coupling and radiating slots.

As such, it enables one to handle a large variety of problems encountered in the design of SIW devices. The conceptual simplicity and mathematical consistency, as well as its advantageous field representation allow one to quickly develop numerical routines applicable to both design and analysis. In addition, that very

same field representation lends itself to application of techniques of asymptotic approximation, potentially speeding up the analysis by an order of magnitude (see e.g. [22]).

- II. Judging by the conducted numerical tests, the method is applicable to both
 - a) closed (resonant) devices of arbitrary shape (of course, provided the waveguide in question is planar), and
 - b) radiating devices whose radiating elements are rectangular slots (although the method could be generalized to arbitrarily shaped ones).
- III. From the perspective of computational resource utilization HFSS, our in-house code outperforms HFSS' FEM solver in all simulated scenarios, with a reduction factor in computation time ranging from 3 to 24, and a reduction factor in the dynamic memory used ranging from 1.1 all the way to 29, depending on the number of DUT (*device under test*) elements and basis functions used. The low-end figures occur when both the number of elements and number of basis functions is large, giving rise to large linear systems which must be solved iteratively. However, in most cases it is sufficient to consider no more than two longitudinal modes, seven azimuthal modes (i.e. modes with the azimuthal wavenumber in the $[-3, 3]$ interval), and five slot basis functions; in a variety of problems, even less is required for excellent accuracy.
- IV. Due to its generality, the proposed approach is applicable to a wide range of dielectric profiles (i.e. configurations of layer thicknesses and permittivities); the sole stipulation being that the multi-layered framework not be used for radiating devices loaded with dielectric slabs whose respective layers have similar permittivities ("similar" meaning $|\varepsilon_i - \varepsilon_j| / \varepsilon_{i,j} < 5\%$ for any two layers i, j). Moreover, the number of unknowns increases significantly less with the increase in permittivity and/or thickness of a dielectric layer compared to HFSS. This is due to use of closed-form eigenfunctions in the stratification coordinate, as opposed to HFSS' tetrahedral-based meshing.

On the other hand, the method possesses some limitations that could be the subject of future work:

- I. As of yet, the analysis of lossy-dielectric-loaded devices and/or lossy metal components is not supported. The inclusion of the said losses would be an important feature, especially at frequencies above 20 GHz.
- II. The method's applicability to very large/complex devices requires further analysis. Though it has been demonstrated that it performs well for devices containing several hundred elements (up to roughly 700), it is necessary to investigate its stability and convergence when the number of elements is on the order of several thousand. It is quite possible that alternative solving routines for relevant linear systems will have to be adopted.
- III. Arbitrary-shaped slots should be supported, as a significant portion of practical devices rely on non-canonically shaped ones, such as dog-bone and crossed slots. For this purpose, one could use a general basis such as Rao-Wilton-Glisson functions. The penalty one would pay in that case, of course, would be the increase in computation time due to both triangulation and computation of a larger number of admittance terms with respect to the entire-domain basis approach.
- IV. The developed MATLAB code, based on the proposed method, should be optimized for faster execution and smaller memory footprint, to enable handling larger structures on medium-range configurations. At present, the code is a straightforward implementation of the proposed algorithm, with no memory management or code optimization techniques applied. Hence, it needs to be

rewritten in a faster, preferably compiled language such as C++ or Fortran. A possible acceleration could be accomplished by loop unrolling [23] due to the presence of a large number of for- and while-loops. A significant speed-up could be accomplished by parallelization using GPU computing (e.g. by porting the code to CUDA C++), a technique gaining momentum in the numerical electromagnetics community due to the widespread availability of powerful graphics processors. As for the memory footprint issue, primarily due to the storage of large matrices generated by mode-matching/MoM subroutines, one could simply store the said matrices to formatted files, clear them from the dynamic memory (RAM) and load them back when necessary. Of course, reading from the hard disk is several orders of magnitude slower than from RAM, but the potential advantage is the possibility of analysing larger structures on RAM-constrained desktops. Additionally, due to the presence of sparse matrices, standard sparse-matrix storage format can be used.

4 REFERENCES

- [1] D. Deslandes and K. Wu, “Integrated microstrip and rectangular waveguide in planar form,” *Microw. Wirel. Compon. Lett. IEEE*, vol. 11, no. 2, pp. 68–70, 2001.
- [2] F. Shigeki, “Waveguide line,” *Jpn. Pat.*, pp. 06–053, 1994.
- [3] J. Hirokawa and M. Ando, “Single-layer feed waveguide consisting of posts for plane TEM wave excitation in parallel plates,” *Antennas Propag. IEEE Trans. On*, vol. 46, no. 5, pp. 625–630, 1998.
- [4] S. T. Choi, K. S. Yang, K. Tokuda, and Y. H. Kim, “A V-band planar narrow bandpass filter using a new type integrated waveguide transition,” *Microw. Wirel. Compon. Lett. IEEE*, vol. 14, no. 12, pp. 545–547, 2004.
- [5] Z. C. Hao, W. Hong, J. X. Chen, H. X. Zhou, and K. Wu, “Single-layer substrate integrated waveguide directional couplers,” *IEE Proc.-Microw. Antennas Propag.*, vol. 153, no. 5, pp. 426–431, 2006.
- [6] W. D’Orazio and K. Wu, “Substrate-integrated-waveguide circulators suitable for millimeter-wave integration,” *Microw. Theory Tech. IEEE Trans. On*, vol. 54, no. 10, pp. 3675–3680, 2006.
- [7] Y. Cassivi and K. Wu, “Low cost microwave oscillator using substrate integrated waveguide cavity,” *Microw. Wirel. Compon. Lett. IEEE*, vol. 13, no. 2, pp. 48–50, 2003.
- [8] K. K. Samanta, D. Stephens, and I. D. Robertson, “Design and performance of a 60-GHz multi-chip module receiver employing substrate integrated waveguides,” *IET Microw. Antennas Propag.*, vol. 1, no. 5, pp. 961–967, 2007.
- [9] D. Deslandes and K. Wu, “Accurate modeling, wave mechanisms, and design considerations of a substrate integrated waveguide,” *Microw. Theory Tech. IEEE Trans. On*, vol. 54, no. 6, pp. 2516–2526, 2006.
- [10] F. Xu, Y. Zhang, W. Hong, K. Wu, and T. J. Cui, “Finite-difference frequency-domain algorithm for modeling guided-wave properties of substrate integrated waveguide,” *Microw. Theory Tech. IEEE Trans. On*, vol. 51, no. 11, pp. 2221–2227, 2003.
- [11] Y. Cassivi, L. Perregrini, P. Arcioni, M. Bressan, K. Wu, and G. Conciauro, “Dispersion characteristics of substrate integrated rectangular waveguide,” *Microw. Wirel. Compon. Lett. IEEE*, vol. 12, no. 9, pp. 333–335, 2002.
- [12] J. Hirokawa and M. Ando, “Complex propagation constant of post-wall waveguide and beam-switching slot array antennas for modern communications,” *COMPLEX Propag. CONSTANT POST-WALL WAVEGUIDE BEAM-Switch. SLOT ARRAY ANTENNAS Mod. Commun.*, 2007.

- [13] X. H. Wu and A. A. Kishk, "Hybrid of Method of Moments and Cylindrical Eigenfunction Expansion to Study Substrate Integrated Waveguide Circuits," *IEEE Trans. Microw. Theory Tech.*, vol. 56, no. 10, pp. 2270–2276, Oct. 2008.
- [14] T. J. Coenen, "Analysis and design of post-wall waveguides for application in SIW," 2010.
- [15] E. Arnieri and G. Amendola, "Analysis of Substrate Integrated Waveguide Structures Based on the Parallel-Plate Waveguide Green's Function," *IEEE Trans. Microw. Theory Tech.*, vol. 56, no. 7, pp. 1615–1623, Jul. 2008.
- [16] E. Arnieri, G. Amendola, and L. Boccia, "Efficient analysis of slotted SIW," in *Antennas and Propagation (EuCAP), 2010 Proceedings of the Fourth European Conference on*, 2010, pp. 1–4.
- [17] M. A. Leontovich, "On the approximate boundary conditions for electromagnetic fields on the surface of well conducting bodies," *Investig. Propag. Radio Waves*, pp. 2–20, 1948.
- [18] M. Albani, A. Mazzinghi, and A. Freni, "Rigorous MoM Analysis of Finite Conductivity Effects in RLSA Antennas," *IEEE Trans. Antennas Propag.*, vol. 59, no. 11, pp. 4023–4032, Nov. 2011.
- [19] M. Casaletti, G. Valerio, J. Seljan, R. Sauleau, and M. Albani, "Efficient analysis of lossy substrate integrated waveguide structures," in *Radio Science Meeting (Joint with AP-S Symposium), 2014 USNC-URSI*, 2014, pp. 108–108.
- [20] G. Amendola, E. Arnieri, and L. Boccia, "Analysis of lossy SIW structures based on the parallel plates waveguide Green's function," *Prog. Electromagn. Res. C*, vol. 33, pp. 157–169, 2012.
- [21] S. Maci, L. Borselli, and L. Rossi, "Diffraction at the edge of a truncated grounded dielectric slab," *Antennas Propag. IEEE Trans. On*, vol. 44, no. 6, pp. 863–873, 1996.
- [22] G. Valerio, M. Casaletti, J. Seljan, R. Sauleau, and M. Albani, "Efficient computation of the coupling between a vertical line source and a slot," *Antennas Propag. IEEE Trans. On*, vol. 61, no. 12, pp. 6084–6093, 2013.
- [23] M. Abrash, *Graphics Programming Black Book*. Coriolis Group Books, 1997.
- [24] J. Volakis, *Antenna Engineering Handbook, Fourth Edition*, 4 edition. New York: McGraw-Hill Professional, 2007.
- [25] J. Bartolić, *Mikrovalna elektronika*. Graphis, 2011.
- [26] C. A. Balanis, *Advanced engineering electromagnetics*, vol. 20. Wiley New York, 1989.
- [27] B. Potelon, J.-C. Bohorquez, J.-F. Favennec, C. Quendo, E. Rius, and C. Person, "Design of Ku-band filter based on substrate-integrated circular cavities (SICCs)," in *Microwave Symposium Digest, 2006. IEEE MTT-S International*, 2006, pp. 1237–1240.
- [28] W. Hong, B. Liu, Y. Wang, Q. Lai, H. Tang, X. X. Yin, Y. D. Dong, Y. Zhang, and K. Wu, "Half mode substrate integrated waveguide: A new guided wave structure for microwave and millimeter wave application," in *Infrared Millimeter*

Waves and 14th International Conference on Terahertz Electronics, 2006. IRMMW-THz 2006. Joint 31st International Conference on, 2006, pp. 219–219.

- [29] K. Wu and others, “On the losses in substrate integrated waveguides,” in *2007 European Microwave Conference*, 2007, pp. 384–387.
- [30] Y. She, R. Fujino, J. Hirokawa, M. Ando, D. Hanatani, and M. Fujimoto, “LTCC oversized rectangular waveguide slot array antenna with air-layer in the radiating part in the millimeter-wave band,” *IEEE Trans. Antennas Propag.*, vol. 61, no. 4, pp. 1777–1783, 2013.
- [31] J. D. Jackson, *Classical Electrodynamics*, 3rd ed. John Wiley & Sons, 1999.
- [32] M. Ettorre, R. Sauleau, L. Le Coq, and F. Bodereau, “Single-folded leaky-wave antennas for automotive radars at 77 GHz,” *Antennas Wirel. Propag. Lett. IEEE*, vol. 9, pp. 859–862, 2010.
- [33] Y. J. Cheng, W. Hong, K. Wu, Z. Q. Kuai, C. Yu, J. X. Chen, J. Y. Zhou, and H. J. Tang, “Substrate integrated waveguide (SIW) Rotman lens and its Ka-band multibeam array antenna applications,” *Antennas Propag. IEEE Trans. On*, vol. 56, no. 8, pp. 2504–2513, 2008.
- [34] K. Tekkouk, “Développement d’antennes multifaisceaux et multicouches fort gain de la bande Ku à la bande V,” Université de Rennes 1, 2014.
- [35] Y.-S. Bang, N. Kim, J.-M. Kim, C. Cheon, Y. Kwon, and Y.-K. Kim, “Micromachined planar probe using half-SIW and half-shielded stripline structure for permittivity measurement,” in *Nanotechnology (IEEE-NANO), 2010 10th IEEE Conference on*, 2010, pp. 1121–1124.
- [36] S. W. Wong, K. Wang, Z.-N. Chen, and Q.-X. Chu, “Design of Millimeter-Wave Bandpass Filter Using Electric Coupling of Substrate Integrated Waveguide (SIW),” *IEEE Microw. Wirel. Compon. Lett.*, vol. 24, no. 1, pp. 26–28, Jan. 2014.
- [37] M. Bozzi and R. Moro, “SIW components and antennas based on eco-friendly materials and technologies: State-of-the-art and future applications,” in *Wireless Sensors and Sensor Networks (WiSNet), 2014 IEEE Topical Conference on*, 2014, pp. 58–60.
- [38] T. Djerafi, O. Kramer, N. Ghassemi, A. B. Guntupalli, B. Youzkatli-El-Khatib, and K. Wu, “Innovative multilayered millimetre-wave antennas for multi-dimensional scanning and very small footprint applications,” in *2012 6th European Conference on Antennas and Propagation (EUCAP)*, 2012, pp. 2583–2587.
- [39] B. Y. El Khatib, T. Djerafi, and K. Wu, “Three-dimensional architecture of substrate integrated waveguide feeder for fermi tapered slot antenna array applications,” *Antennas Propag. IEEE Trans. On*, vol. 60, no. 10, pp. 4610–4618, 2012.
- [40] A. Z. Elsherbeni and A. A. Kishk, “Modeling of cylindrical objects by circular dielectric and conducting cylinders,” *Antennas Propag. IEEE Trans. On*, vol. 40, no. 1, pp. 96–99, 1992.
- [41] L. Tsang, H. Chen, C.-C. Huang, and V. Jandhyala, “Modeling of multiple scattering among vias in planar waveguides using Foldy–Lax equations,” *Microw. Opt. Technol. Lett.*, vol. 31, no. 3, pp. 201–208, 2001.

- [42] H. Chen, Q. Li, L. Tsang, C.-C. Huang, and V. Jandhyala, "Analysis of a large number of vias and differential signaling in multilayered structures," *Microw. Theory Tech. IEEE Trans. On*, vol. 51, no. 3, pp. 818–829, 2003.
- [43] Boping Wu and Leung Tsang, "Fast Computation of Layered Medium Green's Functions of Multilayers and Lossy Media Using Fast All-Modes Method and Numerical Modified Steepest Descent Path Method," *IEEE Trans. Microw. Theory Tech.*, vol. 56, no. 6, pp. 1446–1454, Jun. 2008.
- [44] E. Diaz Caballero, H. Esteban, A. Belenguer, and V. Boria, "Efficient Analysis of Substrate Integrated Waveguide Devices Using Hybrid Mode Matching Between Cylindrical and Guided Modes," *IEEE Trans. Microw. Theory Tech.*, vol. 60, no. 2, pp. 232–243, Feb. 2012.
- [45] M. Casaletti, R. Sauleau, M. Ettorre, and S. Maci, "Efficient Analysis of Metallic and Dielectric Posts in Parallel-Plate Waveguide Structures," *IEEE Trans. Microw. Theory Tech.*, vol. 60, no. 10, pp. 2979–2989, Oct. 2012.
- [46] M. Casaletti, G. Valerio, J. Seljan, M. Ettorre, and R. Sauleau, "A full-wave hybrid method for the analysis of multilayered SIW-based antennas," *Antennas Propag. IEEE Trans. On*, vol. 61, no. 11, pp. 5575–5588, 2013.
- [47] K. Tekkouk, M. Ettorre, R. Sauleau, and M. Casaletti, "Folded Rotman lens multibeam antenna in SIW technology at 24 GHz," in *Antennas and Propagation (EUCAP), 2012 6th European Conference on*, 2012, pp. 2308–2310.
- [48] M. Ettorre and R. Sauleau, "Multi-beam leaky wave pillbox antenna for millimetre-wave applications," in *Antennas and Propagation (EuCAP), 2010 Proceedings of the Fourth European Conference on*, 2010, pp. 1–3.
- [49] A. Mazzinghi, A. Freni, and M. Albani, "Influence of the Finite Slot Thickness on RLSA Antenna Design," *IEEE Trans. Antennas Propag.*, vol. 58, no. 1, pp. 215–218, Jan. 2010.
- [50] W. C. Gibson, *The method of moments in electromagnetics*. CRC press, 2014.
- [51] G. J. Stern and R. S. Elliott, "Resonant length of longitudinal slots and validity of circuit representation: Theory and experiment," *Antennas Propag. IEEE Trans. On*, vol. 33, no. 11, pp. 1264–1271, 1985.
- [52] C.-T. Tai, *Dyadic Green functions in electromagnetic theory*. Institute of Electrical & Electronics Engineers (IEEE), 1994.
- [53] R. F. Harrington, *Time-Harmonic Electromagnetic Fields*, 2nd edition. New York: Wiley-IEEE Press, 2001.
- [54] Z. Sipus, *Analysis of planar and circular cylindrical multilayer structures with application to soft and hard surfaces*. Chalmers University of Technology, 1997.
- [55] K. A. Michalski and J. R. Mosig, "Multilayered media Green's functions in integral equation formulations," *Antennas Propag. IEEE Trans. On*, vol. 45, no. 3, pp. 508–519, 1997.
- [56] J. A. Stratton, *Electromagnetic theory*, vol. 33. John Wiley & Sons, 2007.
- [57] A. Sommerfeld, *Partial differential equations in physics*, vol. 1. Academic press, 1949.

- [58] L. Eyges, *The Classical Electromagnetic Field*, Reprint edition. New York: Dover Publications, 2010.
- [59] W. C. Chew, *Waves and fields in inhomogeneous media*, vol. 522. IEEE press New York, 1995.
- [60] H. Feshbach and P. M. Morse, *Methods of Theoretical Physics, Part I*. McGraw-Hill Book Co., Inc., London, 1953.
- [61] T. Itoh and others, *Numerical techniques for microwave and millimeter-wave passive structures*. Wiley New York, 1989.
- [62] H. Levine and J. Schwinger, “On the theory of diffraction by an aperture in an infinite plane screen. I,” *Phys. Rev.*, vol. 74, no. 8, p. 958, 1948.
- [63] N. Marcuvitz and J. Schwinger, “On the Representation of the Electric and Magnetic Fields Produced by Currents and Discontinuities in Wave Guides. I,” *J. Appl. Phys.*, vol. 22, no. 6, p. 806, 1951.
- [64] L. B. Felsen and N. Marcuvitz, *Radiation and scattering of waves*, vol. 31. John Wiley & Sons, 1994.
- [65] L. E. Ballentine, *Quantum mechanics*, vol. 280. Prentice Hall Englewood Cliffs, 1990.
- [66] A. D. Yaghjian, “Electric dyadic Green’s functions in the source region,” *Proc. IEEE*, vol. 68, no. 2, pp. 248–263, 1980.
- [67] C.-A. Guérin, B. Gralak, and A. Tip, “Singularity of the dyadic Green’s function for heterogeneous dielectrics,” *Phys. Rev. E*, vol. 75, no. 5, May 2007.
- [68] O. D. Kellogg, *Foundations of Potential Theory*. New York: Dover, 1953.
- [69] J. G. Fikioris, “Electromagnetic Field inside a Current-Carrying Region,” *J. Math. Phys.*, vol. 6, no. 11, p. 1617, 1965.
- [70] J. Van Bladel, *Singular Electromagnetic Fields and Sources IEEE Press Series on Electromagnetic Wave Theory*. Wiley New York, 1996.
- [71] C.-T. Tai, “On the eigenfunction expansion of dyadic Green’s functions,” *Proc. IEEE*, vol. 61, no. 4, pp. 480–481, 1973.
- [72] L. Tsang, J. A. Kong, and K.-H. Ding, *Scattering of Electromagnetic Waves, Theories and Applications*, vol. 27. John Wiley & Sons, 2004.
- [73] N. Marcuvitz, “Field representations in spherically stratified regions,” *Commun. Pure Appl. Math.*, vol. 4, no. 2–3, pp. 263–315, 1951.
- [74] L. B. Felsen, “Alternative field representations in regions bounded by spheres, cones, and planes,” *Antennas Propag. IRE Trans. On*, vol. 5, no. 1, pp. 109–121, 1957.
- [75] J. Schwinger, *The theory of obstacles in resonant cavities and wave guides*. Radiation Laboratory, Massachusetts Institute of Technology, 1943.
- [76] B. Friedman, *Principles and techniques of applied mathematics*. New York, 1961.
- [77] G. W. Hanson and A. B. Yakovlev, *Operator theory for electromagnetics: an introduction*. Springer Science & Business Media, 2001.

- [78] S. Weinberg, *The quantum theory of fields*, vol. 2. Cambridge university press, 1996.
- [79] R. E. Collin, "On the incompleteness of E and H modes in wave guides," *Can. J. Phys.*, vol. 51, no. 11, pp. 1135–1140, 1973.
- [80] N. Marcuvitz, *Waveguide Handbook, Radiation Laboratory Series, Vol. 10*. McGraw-Hill, New York, 1951.
- [81] E. C. Titchmarsh, *Eigenfunction Expansions Associated with Second-order Differential Equations*, First edition. edition. Oxford at the Clarendon Press, 1958.
- [82] R. E. Collin, *Field Theory of Guided Waves*, 2 edition. New York: Wiley-IEEE Press, 1990.
- [83] M. Abramowitz, I. A. Stegun, and others, *Handbook of mathematical functions*, vol. 1. Dover New York, 1972.
- [84] M. Reed and B. Simon, *Methods of modern mathematical physics. vol. 1. Functional analysis*, vol. 2. Academic press New York, 1972.
- [85] O. S. Ifeoma, T. A. Rahman, R. Ngah, and I. S. Zakwoi, "Effect of Dielectric Waveguide in the Design of RLSA Antenna: a Review," *Adv. Mater. Res.*, vol. 701, pp. 136–140, 2013.
- [86] G. Martinelli and M. Salerno, "Fondamenti di Elettrotecnica, vol. I e II," *Siderea Seconda Ed.*, 1996.
- [87] B. Wu and L. Tsang, "Signal integrity analysis of package and printed circuit board with multiple vias in substrate of layered dielectrics," *Adv. Packag. IEEE Trans. On*, vol. 33, no. 2, pp. 510–516, 2010.
- [88] C.-T. Tai and P. Rozenfeld, "Different representations of dyadic Green's functions for a rectangular cavity," *IEEE Trans. Microw. Theory Tech.*, vol. 24, pp. 597–601, 1976.
- [89] B. Tomasic and A. Hessel, "Linear phased array of coaxially-fed monopole elements in a parallel plate waveguide," DTIC Document, 1991.
- [90] R. F. Harrington and D. T. Auckland, "Electromagnetic transmission through narrow slots in thick conducting screens," *Antennas Propag. IEEE Trans. On*, vol. 28, no. 5, pp. 616–622, 1980.
- [91] Z. Sipus, M. Lanne, and L. Josefsson, "Moment method analysis of circular cylindrical array of waveguide elements covered with a multilayer radome," *IEE Proc. - Microw. Antennas Propag.*, vol. 153, no. 1, p. 29, 2006.
- [92] P. Y. Ufimtsev, "Method of edge waves in the physical theory of diffraction," DTIC Document, 1971.
- [93] R. G. Kouyoumjian and P. H. Pathak, "A uniform geometrical theory of diffraction for an edge in a perfectly conducting surface," *Proc. IEEE*, vol. 62, no. 11, pp. 1448–1461, 1974.
- [94] R. S. Elliott, *Antenna Theory & Design*, Revised Edition edition. Hoboken, N.J: Wiley-IEEE Press, 2003.

- [95] S. M. Rao, D. Wilton, and A. W. Glisson, "Electromagnetic scattering by surfaces of arbitrary shape," *Antennas Propag. IEEE Trans. On*, vol. 30, no. 3, pp. 409–418, 1982.
- [96] A. Frenkel, "On entire-domain basis functions with square-root edge singularity [EM scattering]," *Antennas Propag. IEEE Trans. On*, vol. 37, no. 9, pp. 1211–1214, 1989.
- [97] T. S. Bird, "Analysis of mutual coupling in finite arrays of different-sized rectangular waveguides," *Antennas Propag. IEEE Trans. On*, vol. 38, no. 2, pp. 166–172, 1990.
- [98] R. F. Harrington, "Matrix methods for field problems," *Proc. IEEE*, vol. 55, no. 2, pp. 136–149, 1967.
- [99] V. H. Rumsey, "Reaction concept in electromagnetic theory," *Phys. Rev.*, vol. 94, no. 6, p. 1483, 1954.
- [100] M. Cohen, "Application of the reaction concept to scattering problems," *Antennas Propag. IRE Trans. On*, vol. 3, no. 4, pp. 193–199, 1955.
- [101] J. S. Schwinger, W. Y. Tsai, L. L. De Raad, and K. A. Milton, *Classical electrodynamics*. Perseus, 1998.
- [102] M. Albani, A. Mazzinghi, and A. Freni, "Asymptotic approximation of mutual admittance involved in MoM analysis of RLSA antennas," *Antennas Propag. IEEE Trans. On*, vol. 57, no. 4, pp. 1057–1063, 2009.
- [103] A. Quarteroni, R. Sacco, and F. Saleri, *Numerical mathematics*, vol. 37. Springer Science & Business Media, 2010.
- [104] M. Albani, G. La Cono, R. Gardelli, and A. Freni, "An efficient full-wave method of moments analysis for RLSA antennas," *Antennas Propag. IEEE Trans. On*, vol. 54, no. 8, pp. 2326–2336, 2006.
- [105] W. A. Johnson, A. Q. Howard, and D. G. Dudley, "On the irrotational component of the electric Green's dyadic," *Radio Sci.*, vol. 14, no. 6, pp. 961–967, 1979.
- [106] R. W. P. King, *Fundamental electromagnetic theory*. Dover Publications, 1963.
- [107] E. Gandini, M. Ettorre, M. Casaletti, K. Tekkouk, L. Le Coq, and R. Sauleau, "SIW Slotted Waveguide Array With Pillbox Transition for Mechanical Beam Scanning," *IEEE Antennas Wirel. Propag. Lett.*, vol. 11, pp. 1572–1575, 2012.
- [108] H. Manual, "v11. 0," *Ansoft Corp*, 2012.
- [109] D. Deslandes and K. Wu, "Single-substrate integration technique of planar circuits and waveguide filters," *Microw. Theory Tech. IEEE Trans. On*, vol. 51, no. 2, pp. 593–596, 2003.
- [110] J. D. Joannopoulos, S. G. Johnson, J. N. Winn, and R. D. Meade, *Photonic crystals: molding the flow of light*. Princeton university press, 2011.
- [111] N. Nasimuddin, "Microstrip antennas," *Rij. InTech*, 2011.
- [112] G. B. Arfken and H. J. Weber, *Mathematical Methods For Physicists International Student Edition*. Academic press, 2005.
- [113] J. Hunter and B. Nachtergaele, "Lecture notes on applied analysis," Jul-2005.

- [114] I. M. Gelfand and G. E. Shilov, “Generalized Functions vol 1–3 (New York: Academic) Gelfand IM and Vilenkin N Ya 1964,” *Gen. Funct.*, vol. 4, 1964.
- [115] V. Daniele, “New expressions of dyadic Green’s functions in uniform waveguides with perfectly conducting walls,” *Antennas Propag. IEEE Trans. On*, vol. 30, no. 3, pp. 497–499, 1982.

5 APPENDICES

APPENDIX A – DERIVATION OF DUAL TE S-POTENTIALS AND THE REGULARIZATION OF THE GREEN'S DYADIC

As noted in subsection 2.3.2 A., dealing with the evaluation of slot admittance, the appearance of a double derivative of the TE S-potential in z/z' leads to a conundrum, due to the necessity of its explicit evaluation, if one intends to end up with a useful, closed-form expression. This short appendix provides the reader with a condensed exposition of the origin of this particular problem, along with its complete resolution within the framework of scalar Green's functions formalism presented in [64]. In addition, the correct derivation of the S-potentials is presented, which consistently leads to physically sound fields, as opposed to some recent works where the same formalism was utilized. Moreover, we show how to regularize the Green's dyadic in a relatively simple way, i.e. we demonstrate how the second delta-term in (5.1) is cancelled by the corresponding clandestine term contained implicitly in the TE part of the Green's dyadic.

We begin by reiterating the general Green's dyadic expression phrased in terms of scalar S-potentials

$$\begin{aligned} \underline{\mathbf{G}}^{\text{HM}}(\mathbf{r}, \mathbf{r}') = & -\frac{1}{k(\mathbf{r}')^2} \left(\hat{\mathbf{z}} \otimes \hat{\mathbf{z}} + \frac{\nabla_t \otimes \nabla_t}{\nabla_t^2} \right) \delta(\mathbf{r} - \mathbf{r}') \\ & + (\nabla \times \hat{\mathbf{z}}) \otimes (\nabla' \times \hat{\mathbf{z}}) \mathcal{S}'(\mathbf{r}, \mathbf{r}') \\ & + \frac{1}{\omega^2 \varepsilon(z') \mu(z)} (\nabla \times \nabla \times \hat{\mathbf{z}}) \otimes (\nabla' \times \nabla' \times \hat{\mathbf{z}}) \mathcal{S}''(\mathbf{r}, \mathbf{r}'), \end{aligned} \quad (5.1)$$

from which one notes that the last term will contain the "offending" double-derivative term. Indeed, we can easily identify the exact term upon using the identity $\nabla \times \nabla \times \hat{\mathbf{z}} = \nabla(\nabla \cdot \hat{\mathbf{z}}) - \nabla^2 \hat{\mathbf{z}} = \partial_z \nabla_t - \nabla_t^2 \hat{\mathbf{z}}$. It is clear that the double-derivative term will have the form $\alpha'' (\partial_z \nabla_t) (\partial_z \nabla_t) \mathcal{S}''(\mathbf{r}, \mathbf{r}')$, $\alpha'' \equiv 1/\omega^2 \varepsilon(z') \mu(z)$. Now, we recall that the slot admittance is defined as

$$\mathbf{Y}_{i,j} = -j\omega \varepsilon(z') \iint \mathbf{b}_j(\mathbf{r}) \cdot \underline{\mathbf{G}}^{\text{HM}}(\mathbf{r}, \mathbf{r}') \cdot \mathbf{b}_i(\mathbf{r}') \, d\mathbf{r} \, d\mathbf{r}' \quad (5.2)$$

which, according to previous considerations, contains the term

$$\partial_{zz'}^2 \mathbf{Y}_{i,j} = -j\omega \varepsilon(z') \iint \mathbf{b}_j(\mathbf{r}) \cdot \left[\alpha'' (\partial_z \nabla_t) (\partial_z \nabla_t) \mathcal{S}''(\mathbf{r}, \mathbf{r}') \right] \cdot \mathbf{b}_i(\mathbf{r}') \, d\mathbf{r} \, d\mathbf{r}' . \quad (5.3)$$

It can be simplified upon a two-fold application of the Green's theorem, allowing us to move the ∇_t and ∇_t' operators onto basis functions $\mathbf{b}_{j/i}$, respectively

$$\partial_{zz'}^2 \mathbf{Y}_{i,j} = -j\omega \varepsilon(z') \iint \nabla_t \cdot \mathbf{b}_j(\mathbf{r}) \left[\alpha'' \partial_z \partial_z \mathcal{S}''(\mathbf{r}, \mathbf{r}') \right] \nabla_t' \cdot \mathbf{b}_i(\mathbf{r}') \, d\mathbf{r} \, d\mathbf{r}' . \quad (5.4)$$

Since the basis functions pertaining to thin slots are directed along the largest dimension (which we denote as $\hat{\mathbf{u}}_i$ and $\hat{\mathbf{u}}_j$, respectively), the transverse derivative operators become simple u-derivatives

$$\partial_{zz'}^2 \mathbf{Y}_{i,j} = -j\omega \varepsilon(z') \iint \partial_{u_j} \mathbf{b}_j(\mathbf{r}) \left[\alpha'' \partial_z \partial_z \mathcal{S}''(\mathbf{r}, \mathbf{r}') \right] \partial_{u_i} \mathbf{b}_i(\mathbf{r}') \, d\mathbf{r} \, d\mathbf{r}' . \quad (5.5)$$

Though simplified, this admittance term contains a double-derivative of the S-potential, which has to be handled carefully. Specifically, the direct differentiation yields a formal, but

incorrect solution inconsistent with the basic symmetry properties of transmission-line Green's functions (2.78). Therefore, we proceed by exhibiting the Green's function/S-potential in the original spectral form [64, p. 447] (8a)

$$\begin{aligned} \partial_z \partial_{z'} \mathcal{S}''(\mathbf{r}, \mathbf{r}') &= \partial_z \partial_{z'} \frac{-1}{\nabla_t^2} \frac{1}{2\pi} \sum_n e^{-jn(\phi-\phi')} \int_0^\infty J_n(k_t \rho) J_n(k_t \rho') g_z''(z, z'; \sqrt{k^2 - k_t^2}) k_t dk_t \\ &= \frac{-1}{\nabla_t^2} \frac{1}{2\pi} \sum_n e^{-jn(\phi-\phi')} \int_0^\infty J_n(k_t \rho) J_n(k_t \rho') d_z d_{z'} g_z''(z, z'; \sqrt{k^2 - k_t^2}) k_t dk_t, \end{aligned} \quad (5.6)$$

where in passing from the first to the second line we have exchanged the integral and differential operators, since the S-potential and all its higher-order derivatives are interpreted as distributions.

Now, it would be convenient if we could reexpress the derivative in z' in terms of the z one, since we do not know how to evaluate it directly. Fortunately, we may resort to the transmission-line (denoted as TL from here on) Green's functions symmetry properties for aid. Indeed, recalling that the TE TL Green's function g_z'' is actually a scaled "impedance" Green's function $Z''(z, z') = j\omega\mu(z') g_z''(z, z')$, and that the impedance GF enjoys the symmetry property $Z''(z, z') = Z''(z', z)$, we can apply the derivative in z' as

$$d_z Z''(z, z') = d_z Z''(z', z). \quad (5.7)$$

However, note that the RHS of (5.7) is nothing more than the LHS of the impedance GF transmission-line equation (2.77), and implies

$$\begin{aligned} d_z Z''(z', z) &= -j\kappa''(z') Z''(z) T^{I''}(z', z) \\ &= j\kappa''(z') Z''(z') T^{V''}(z, z'), \end{aligned} \quad (5.8)$$

where use has been made of the symmetry property $T^{I''}(z', z) = -T^{V''}(z, z')$. Now, upon applying the z -derivative, and using the T^V TL equation

$$-d_z T^{V''}(z, z') = j\kappa''(z) Z''(z) Y''(z, z') - \delta(z - z'), \quad (5.9)$$

we arrive to the expression

$$d_z d_z g_z''(z, z') = \frac{\mu(z)}{\mu(z')} \kappa''(z')^2 \tilde{g}_z''(z, z') + \delta(z - z'), \quad (5.10)$$

where $\tilde{g}_z''(z, z') = (j\kappa''(z') Y''(z'))^{-1} Y''(z, z')$, and $Y''(z') = \kappa''(z') / \omega\mu(z')$. Moreover, the TE admittance Green's function $Y''(z, z')$ can be easily shown to satisfy

$$\left(d_z^2 + \kappa''(z)^2\right) Y''(z, z') = -j\kappa''(z') Y''(z') \delta(z - z'). \quad (5.11)$$

At this point we can further simplify the Fourier integral (5.6) by inserting (5.10) into it, yielding

$$\begin{aligned}
 \partial_z \partial_{z'} \mathcal{S}^n(\mathbf{r}, \mathbf{r}') &= \frac{-1}{\nabla_t^2} \frac{1}{2\pi} \sum_n e^{-jn(\phi-\phi')} \int_0^\infty J_n(k_t \rho) J_n(k_t \rho') d_z d_{z'} g_z''(z, z'; \sqrt{k^2 - k_t^2}) k_t dk_t, \\
 &= \frac{-1}{\nabla_t^2} \frac{1}{2\pi} \sum_n e^{-jn(\phi-\phi')} \int_0^\infty J_n(k_t \rho) J_n(k_t \rho') \left(\frac{\mu(z)}{\mu(z')} \kappa''(z')^2 \check{g}_z''(z, z') + \delta(z - z') \right) k_t dk_t, \\
 &= \mathbf{I}_{zz'}^{(1)} + \mathbf{I}_{zz'}^{(2)}.
 \end{aligned} \tag{5.12}$$

First let us focus on the second, delta-function containing integrand, which we can rewrite as

$$\mathbf{I}_{zz'}^{(2)} = \frac{-1}{\nabla_t^2} \frac{1}{2\pi} \delta(z - z') \sum_n e^{-jn(\phi-\phi')} \int_0^\infty J_n(k_t \rho) J_n(k_t \rho') k_t dk_t. \tag{5.13}$$

However, the integrand is recognized as the completeness relation for Bessel functions [112, p. 696]

$$\int_0^\infty J_n(k_t \rho) J_n(k_t \rho') k_t dk_t = \frac{\delta(\rho - \rho')}{\rho}, \tag{5.14}$$

leading to

$$\mathbf{I}_{zz'}^{(2)} = \frac{-1}{\nabla_t^2} \frac{\delta(\rho - \rho')}{\rho} \delta(z - z') \frac{1}{2\pi} \sum_n e^{-jn(\phi-\phi')}, \tag{5.15}$$

which, in turn, contains the azimuthal harmonic completeness relation

$$\frac{1}{2\pi} \sum_n e^{-jn(\phi-\phi')} = \delta(\phi - \phi'). \tag{5.16}$$

Hence, the second term is actually

$$\mathbf{I}_{zz'}^{(2)} = \frac{-1}{\nabla_t^2} \frac{\delta(\rho - \rho')}{\rho} \delta(z - z') \delta(\phi - \phi') = \frac{-1}{\nabla_t^2} \delta(\mathbf{r} - \mathbf{r}'). \tag{5.17}$$

However strange this term might appear at the moment, one should recall that a singular term of the exact same form appears in the Green's dyadic (5.1) of opposite sign, implying that (5.17) cancels it exactly, leaving only the principal volume correction as the remaining singularity! Indeed, the second singular term appearing in (5.1) is

$$\mathbf{T}_\delta = -\frac{1}{k(\mathbf{r}')^2} \frac{\nabla_t \otimes \nabla_t}{\nabla_t^2} \delta(\mathbf{r} - \mathbf{r}') = -\frac{1}{\omega^2 \varepsilon(z') \mu(z')} \frac{\nabla_t \otimes \nabla_t}{\nabla_t^2} \delta(\mathbf{r} - \mathbf{r}'), \tag{5.18}$$

whereas the corresponding term of the TE dyadic term is, containing (5.17), is

$$\mathbf{T}_\delta'' = -\frac{1}{\omega^2 \varepsilon(z') \mu(z)} \frac{\nabla_t \otimes \nabla_t'}{\nabla_t^2} \delta(\mathbf{r} - \mathbf{r}') = \frac{1}{\omega^2 \varepsilon(z') \mu(z)} \frac{\nabla_t \otimes \nabla_t}{\nabla_t^2} \delta(\mathbf{r} - \mathbf{r}'), \tag{5.19}$$

where use has been made of the relation $\nabla_t = \nabla_t'$. However, one notes that these terms have permeabilities differing in space-coordinate dependence; namely, \mathbf{T}_δ contains $\mu(z')$,

whereas T_δ'' contains $\mu(z)$! One may rightfully ask how it is possible that the two terms annihilate each other. The answer lies in a property of the delta function in z . Firstly, it should be recalled that $\delta(\mathbf{r}-\mathbf{r}')$ can be factored as

$$\delta(\mathbf{r}-\mathbf{r}') = \frac{\delta(\rho-\rho')}{\rho} \delta(z-z') \delta(\phi-\phi'). \quad (5.20)$$

Secondly, the functions one can use to represent the z -delta $\delta(z-z')$ are not in the domain of the $\frac{\nabla_t \otimes \nabla_t}{\nabla_t^2}$ operator. Hence, it follows that their commutator is zero, i.e.

$$\left[\frac{\nabla_t \otimes \nabla_t}{\nabla_t^2}, \delta(z-z') \right] = \frac{\nabla_t \otimes \nabla_t}{\nabla_t^2} \delta(z-z') - \delta(z-z') \frac{\nabla_t \otimes \nabla_t}{\nabla_t^2} = 0. \quad (5.21)$$

Therefore, we can freely exchange the order of the transverse operator and the z -delta. The final step, leading to the cancellation of the aforementioned singular terms, rests on a simple application of the delta function definition

$$\int_{-\infty}^{\infty} \frac{a(z')}{a(z)} \delta(z-z') dz = \int_{-\infty}^{\infty} \delta(z-z') dz = 1. \quad (5.22)$$

Applying this property to \mathbf{T}_δ'' as

$$\begin{aligned} 1 &= \int_a^b \delta(z-z') dz = \int_a^b \frac{\mu(z')}{\mu(z)} \delta(z-z') dz \\ &\Rightarrow \delta(z-z') = \frac{\mu(z')}{\mu(z)} \delta(z-z') \end{aligned} \quad (5.23)$$

finally leads to

$$\mathbf{T}_\delta + \mathbf{T}_\delta'' = -\frac{1}{\omega^2 \varepsilon(z') \mu(z')} \frac{\nabla_t \otimes \nabla_t}{\nabla_t^2} \delta(\mathbf{r}-\mathbf{r}') + \frac{1}{\omega^2 \varepsilon(z') \mu(z')} \frac{\nabla_t \otimes \nabla_t}{\nabla_t^2} \delta(\mathbf{r}-\mathbf{r}') = \underline{0}. \quad (5.24)$$

Therefore, the Schwinger-Marcuvitz-Felsen formalism, in addition to being simpler and operationally more convenient, is self-consistent.

At this point, a comparison of singular terms obtained between various methods of Green's dyadic derivation is in order.

Firstly, we note that a similar approach based on Felsen's methodology was used by Albani et al. in [104] and [18]. In the 2006 paper, correct S-potentials were derived, although the cancellation of the \mathbf{T}_δ operator was not shown explicitly. In passing from that one to the 2011 paper, dealing with propagation in lossy-conducting-plates PPWs, the authors have picked up a dubious logarithmic term as part of the S-potential [18, p. 4025] (12)

$$\mathcal{S}_t(\boldsymbol{\rho}, \boldsymbol{\rho}'; k_t) = \frac{1}{k_t^2} \left[\frac{1}{4j} H_0^{(2)}(k_t |\boldsymbol{\rho}-\boldsymbol{\rho}'|) + \frac{1}{2\pi} \ln(\alpha |\boldsymbol{\rho}-\boldsymbol{\rho}'|) \right], \quad (5.25)$$

where subscript t denotes the transverse part of the S-potential, and α is an arbitrary constant. This form is wrong from multiple perspectives. Firstly, from a physical perspective, since the admittance between two magnetic currents is expressed as an integral whose kernel contains an S-potential (see [18, p. 4026] (14)), it becomes clear that the admittance grows unboundedly, since the logarithmic term is unbounded at infinity. This can be seen more clearly if we represent the Neumann function in the $H_0^{(2)}$ in series form [83, p. 358]

$$Y_0(z) = \frac{2}{\pi} \left\{ \left[\ln\left(\frac{1}{2}z\right) + \gamma \right] J_0(z) + \sum_{k=1}^{\infty} (-1)^{k+1} [\gamma + \psi_0(k+1)] \frac{\left(\frac{1}{4}z^2\right)^k}{k!} \right\}, \quad (5.26)$$

where $z \equiv k_t |\mathbf{\rho} - \mathbf{\rho}'|$, ψ_0 is the digamma function [83, p. 360], and γ is the Euler-Mascheroni constant. Then from (5.25) it follows that the logarithmic term may be bundled with the logarithmic term of Y_0 as $\frac{2}{\pi} \ln\left(\frac{1}{2}z\right) J_0(z) - \frac{2}{\pi} \ln\left(\frac{\alpha}{k_t}z\right)$. If α is arbitrary, then any choice of α except $\alpha = k_t / 2$ will lead to a constant term rendering any subsequent sum or integral containing (5.25) divergent. If, however, $\alpha = k_t / 2$ is chosen, then the extra logarithmic term will asymptotically regularize (5.25) for $k_t \rightarrow 0$; unfortunately, as either $k_t \rightarrow \infty$ or $|\mathbf{\rho} - \mathbf{\rho}'| \rightarrow \infty$ (provided the other remains finite), it will diverge since $J_0(z) \rightarrow 0$ for $z \gg 1$, rendering the extra logarithmic term dominant.

However, if the magnetic currents' partial contributions add out-of phase on average, the admittance may be finite as $|\mathbf{\rho} - \mathbf{\rho}'| \rightarrow \infty$. Unfortunately, in general it is not possible, so only trivial (zero-amplitude) currents will produce a finite admittance when $|\mathbf{\rho} - \mathbf{\rho}'| \rightarrow \infty$. Therefore, we are lead to the conclusion that (5.25) is not a valid form of the transverse portion of the S-potential, if the Green's dyadic is defined as in (5.1)!

A possible reason why this was not noted was that the constant α may be chosen to one's preference (at least according to the authors), and the slots used in numerical examples were at too modest a distance from each other for this behavior to have been noted.

An attempt can be made at mitigating the situation, by adhering to guidelines of Felsen and Marcuvitz [64, p. 448] – instead of dealing with the S-potential \mathcal{S} explicitly, one should consider the function $\nabla'_t \mathcal{S}$, obtained by “borrowing” a ∇'_t operator from the $\nabla' \times \hat{\mathbf{z}}$ and $\nabla' \times \nabla' \times \hat{\mathbf{z}}$ in (5.1). It is defined as

$$\nabla'_t \mathcal{S}(\mathbf{r}, \mathbf{r}') = \frac{j}{\pi} \int_{-\infty}^{\infty} \nabla'_t \mathcal{S}_t(\mathbf{\rho}, \mathbf{\rho}'; k_t) g_z(z, z'; \sqrt{k^2 - k_t^2}) k_t dk_t, \quad (5.27)$$

and allows one to apply the $-1/\nabla_t^2$ operator under the integral sign, while still maintaining the convergence of the integral. This then implies a redefinition of the Green's dyad, consequently making the subsequent analysis significantly more tedious since one has to deal with vectors instead of scalars at this stage, which is a high price to pay. In that case, however, we still end up with derivatives of the logarithmic term which are, in fact, spurious (i.e. lead to fields not satisfying Maxwell equations). Even worse, they do not get annihilated

by any other terms of the Green's dyadic. Therefore, sooner or later one must discard them explicitly, but this procedure lacks mathematical rigor. In sum, (5.25) is an invalid form, and should be avoided.

To explicitly see how the error can come about, consider again the Green's dyadic, repeated here for convenience

$$\begin{aligned} \underline{\mathbf{G}}^{\text{HM}}(\mathbf{r}, \mathbf{r}') &= -\frac{1}{k(\mathbf{r}')^2} \left(\hat{\mathbf{z}}\hat{\mathbf{z}} + \frac{\nabla_t \otimes \nabla_t}{\nabla_t^2} \right) \delta(\mathbf{r} - \mathbf{r}') \\ &\quad + (\nabla \times \hat{\mathbf{z}}) \otimes (\nabla \times \hat{\mathbf{z}}) \mathcal{S}'(\mathbf{r}, \mathbf{r}') \\ &\quad + \frac{1}{\omega^2 \varepsilon(z') \mu(z)} (\nabla \times \nabla \times \hat{\mathbf{z}}) \otimes (\nabla \times \nabla \times \hat{\mathbf{z}}) \mathcal{S}''(\mathbf{r}, \mathbf{r}') . \end{aligned}$$

The possibility of using this representation relies on the ability to consistently define the S-potentials, which are, by definition, related to scalar Green's functions as

$$\mathcal{S}(\mathbf{r}, \mathbf{r}') = -\frac{1}{\nabla_t^2} \mathbf{G}(\mathbf{r}, \mathbf{r}') . \quad (5.28)$$

Now, as was shown in subsection 2.2.1.6, p. 48, one can tackle the explicit evaluation of (5.28) by expressing the Green's function as a Fourier integral

$$\mathcal{S}(\mathbf{r}, \mathbf{r}') = \frac{-1}{\nabla_t^2} \frac{1}{2\pi} \sum_n e^{-jn(\phi-\phi')} \int_0^\infty J_n(k_t \rho) J_n(k_t \rho') g_z(z, z'; \sqrt{k^2 - k_t^2}) k_t dk_t . \quad (5.29)$$

The question now is how to represent the action of the $-1/\nabla_t^2$ operator. Do we move it inside the sum, and if we do, how does it act on the summands? Firstly, we can recast (5.29) into a more compact form using the standard trick of extending the range of integration from $[0, \infty)$ to $(-\infty, \infty)$ by the identity $J_n(z) = (H_n^{(2)}(z) + H_n^{(1)}(z))/2$, and the circuital relation $H_n^{(1)}(ze^{j\pi}) = -e^{jn\pi} H_n^{(2)}(z)$, yielding

$$\mathcal{S}(\mathbf{r}, \mathbf{r}') = \frac{-1}{\nabla_t^2} \frac{1}{4\pi} \sum_n e^{-jn(\phi-\phi')} \int_{\infty e^{-j\pi}}^\infty J_n(k_t \rho_<) H_n^{(2)}(k_t \rho_>) g_z(z, z'; \sqrt{k^2 - k_t^2}) k_t dk_t , \quad (5.30)$$

where the lower integration limit $\infty e^{-j\pi}$ indicates that the integration contour goes slightly below the negative real axis where the logarithmic branch cut due to the Hankel function was stipulated, i.e. the branch cut is avoided. In addition, $\rho_> = \max(\rho, \rho')$ and $\rho_< = \min(\rho, \rho')$. Furthermore, we may exchange the summation and the integration operator

$$\mathcal{S}(\mathbf{r}, \mathbf{r}') = \frac{-1}{\nabla_t^2} \frac{1}{4\pi} \int_{\infty e^{-j\pi}}^\infty \sum_n e^{-jn(\phi-\phi')} J_n(k_t \rho_<) H_n^{(2)}(k_t \rho_>) g_z(z, z'; \sqrt{k^2 - k_t^2}) k_t dk_t . \quad (5.31)$$

Since the z Green's function does not depend on the index of the sum, one can then apply the Gegenbauer addition theorem for cylindrical harmonics, giving

$$\mathcal{S}(\mathbf{r}, \mathbf{r}') = \frac{-1}{\nabla_t^2} \frac{j}{\pi} \int_{\infty e^{-j\pi}}^\infty \frac{1}{4j} H_0^{(2)}(k_t |\boldsymbol{\rho} - \boldsymbol{\rho}'|) g_z(z, z'; \sqrt{k^2 - k_t^2}) k_t dk_t . \quad (5.32)$$

At this stage, we have several options at our disposition of how to proceed. One is to exchange the $-1/\nabla_t^2$ and the integral operator. Then two essentially equivalent procedures lead to a convergence issue. Firstly, since the integral defines a Fourier integral of a distribution, one can identify the $-1/\nabla_t^2$ operator as [113, Ch. 11], [64, Sec. 5.2b]

$$\frac{-1}{\nabla_t^2} = \frac{1}{k_t^2} , \quad (5.33)$$

turning the integral into

$$\mathcal{S}(\mathbf{r}, \mathbf{r}') = \frac{j}{\pi} \int_{-\infty}^{\infty} \frac{1}{k_t^2} \frac{1}{4j} H_0^{(2)}(k_t |\boldsymbol{\rho} - \boldsymbol{\rho}'|) g_z(z, z'; \sqrt{k^2 - k_t^2}) k_t dk_t . \quad (5.34)$$

One immediately notes that this integral is not well-defined due to the $k_t \rightarrow 0$ non-integrable singularity of order $O(\ln(k_t)/k_t)$. An option one has at making sense of it is to perform regularization (see e.g. [114] vol. I). However, this is quite difficult since it opens the question of whether it can be done uniquely. Namely, a Cauchy principle value redefinition does not exist, since the integrand is both too singular due to the logarithmic term of the Hankel function and not odd in k_t so that the negative and positive contribution around the singular point cancel. Another option may be to throw out terms in the series representation of the Hankel function up to order $O(z)$ (recall that $z = k_t |\boldsymbol{\rho} - \boldsymbol{\rho}'|$). In that case we might end up with a finite generalized function representing the potential, though it is highly questionable whether that function will lead to fields satisfying Maxwell equations. Perhaps in some weak sense, yes, but the question then is whether it may be suitable for implementation in a numerical code, and whether it gives good predictions. This is a point to be investigated.

From the discussion above, it follows that the $-1/\nabla_t^2$ operator *should not* be moved inside the integral, unless its introduction into the integrand results in a well-defined integral (possibly in an improper sense). Leaving it outside makes possible the evaluation of the Green's function in closed form, which will be represented in the k_t basis, upon applying the residue theorem

$$\mathcal{S}(\mathbf{r}, \mathbf{r}') = \frac{-1}{\nabla_t^2} \sum_i \frac{1}{4j} H_0^{(2)}(k_{ti} |\boldsymbol{\rho} - \boldsymbol{\rho}'|) w(z') \varphi_i(z) \varphi_i(z') , \quad (5.35)$$

where $w(z')$ is the weight of the Sturm-Liouville problem in the z -coordinate. If now we recall the proposition put forth in subsection 2.2.1.6, p. 49, the ∇_t^2 operator becomes $-k_{ti}^2$ in this basis, and therefore, within the framework of the Borel functional calculus (Theorem VIII. 5, [84])

$$\mathcal{S}(\mathbf{r}, \mathbf{r}') = \sum_i \frac{1}{4j} \frac{H_0^{(2)}(k_{ti} |\boldsymbol{\rho} - \boldsymbol{\rho}'|)}{k_{ti}^2} w(z') \varphi_i(z) \varphi_i(z') . \quad (5.36)$$

This, in fact, is the correct form of the S-potential. Similar results were obtained for bounded cross-section geometries in [115], and both bounded and unbounded in [104], containing a single-layer dielectric medium. Of course, we are dealing with piecewise-constant, stratified planar media, which contain the single-layer medium scenario as a special case.

As for the incorrect form of the S-potential, it could have come from the purely formal calculation

$$\begin{aligned}
 \frac{1}{k_t^2} \frac{-1}{\nabla_t^2} (\nabla_t^2 + k_t^2) g_t(\boldsymbol{\rho}, \boldsymbol{\rho}') &= \frac{1}{k_t^2} \frac{-1}{\nabla_t^2} (-\delta(\boldsymbol{\rho} - \boldsymbol{\rho}')) \\
 \Rightarrow \frac{-1}{k_t^2} \left(\mathbf{1} + \frac{k_t^2}{\nabla_t^2} \right) g_t(\boldsymbol{\rho}, \boldsymbol{\rho}') &= \frac{1}{k_t^2} \frac{-1}{\nabla_t^2} \delta(\boldsymbol{\rho} - \boldsymbol{\rho}') \quad (5.37) \\
 \frac{-1}{\nabla_t^2} g_t(\boldsymbol{\rho}, \boldsymbol{\rho}') &= \frac{1}{k_t^2} \left[g_t(\boldsymbol{\rho}, \boldsymbol{\rho}') - \frac{1}{\nabla_t^2} \delta(\boldsymbol{\rho} - \boldsymbol{\rho}') \right],
 \end{aligned}$$

where one then proclaims

$$-\frac{1}{\nabla_t^2} \delta(\boldsymbol{\rho} - \boldsymbol{\rho}') = \frac{-1}{2\pi} \ln(\alpha |\boldsymbol{\rho} - \boldsymbol{\rho}'|), \quad (5.38)$$

or

$$\begin{aligned}
 -\delta(\boldsymbol{\rho} - \boldsymbol{\rho}') &= \nabla_t^2 \left(\frac{-1}{2\pi} \ln(\alpha |\boldsymbol{\rho} - \boldsymbol{\rho}'|) \right) \\
 \Rightarrow g_t(\boldsymbol{\rho}, \boldsymbol{\rho}') &= \frac{-1}{2\pi} \ln(\alpha |\boldsymbol{\rho} - \boldsymbol{\rho}'|). \quad (5.39)
 \end{aligned}$$

Herein lies the key error – the logarithmic Green’s function is truly the solution to the Poisson equation (5.39), but for a *different* ∇_t^2 operator! Indeed, an operator is not defined only by its form, but by its domain as well. The domain of the transverse Laplacian operator ∇_t^2 we have started with is the vector space of functions satisfying the Sommerfeld radiation conditions. However, such a Laplacian cannot be inverted to yield (5.38). Therefore, the moral of the story is – there are ∇_t^2 operators, and then there are *other* ∇_t^2 operators.

Hence, the solution (5.39) is purely formal, since the ∇_t^2 operator’s domain is on functions satisfying the Sommerfeld radiation condition, which stipulates the finiteness of fields and is a necessary condition for the uniqueness of solution. On the other hand, (5.39) is outside the said domain, rendering the potential divergent. Therefore, as stated already, a differentiation of the potential must be effected which then produces convergent fields; however, the problem is then the interpretation of the derivatives of the logarithmic terms, and their consistent removal.

Now, returning to the original problem, the evaluation of the first integrand rests on the possibility of deriving the “odd” $\tilde{g}_z''(z, z')$ function in closed form. In what follows we show how it can be done in a straight-forward way. Firstly, we note from (5.11) that the impedance TE Green’s function $Y''(z, z')$ represents the current at point z excited by a negative TE voltage source connected in series at point z' of the considered transmission line. Hence, the boundary conditions are such that

$$\begin{aligned}
 d_z Y''(z, z') &= 0 \Big|_{z=z_1, z_2} \\
 [Y''(z, z')]_{d_n-\varepsilon}^{d_n+\varepsilon} &= 0, \\
 \left[-\frac{1}{j\kappa''(z)Y''(z)} d_z Y''(z, z') \right]_{d_n-\varepsilon}^{d_n+\varepsilon} &= 0,
 \end{aligned} \tag{5.40}$$

where $z_{1,2}$ are the z -coordinates of bounding PEC plates, $[x]_a^b$ denotes the difference between the bracketed quantity at point b and point a , i.e. $x(b) - x(a)$, d_n is the z -coordinate of the interface between two adjacent dielectric layers, and ε is an arbitrarily small positive real number. The same boundary conditions apply to the dual TE Green's function $\check{g}_z''(z, z')$. For concreteness, we will assume that the PPW has two layers, which is the case we investigate in numerical experiments. Of course, the method of the derivation of the dual Green's function can be easily extended to the case of an arbitrary number of layers. Now, as done for all the other scalar Green's functions, we shall derive this by the characteristic Green's function approach, which as a first step requires one to find the characteristic eigenfunction. First, we look for a function $\check{y}(z)$ which satisfies the same boundary conditions as the ones found in (5.40), and satisfies the homogeneous Sturm-Liouville equation

$$\left(w(z) d_z \frac{1}{w(z)} d_z + \kappa''^2 \right) \check{y}(z) = 0, \tag{5.41}$$

where $w(z) = (\kappa''(z)Y''(z))^{-1}$. From the first boundary condition in (5.40), we guess its general form as

$$\check{y}(z) = \begin{cases} A \cos(\kappa_1 z) & , \quad 0 \leq z \leq t_1 \\ B \cos(\kappa_2 (h - z)) & , \quad t_1 \leq z \leq h \end{cases} \tag{5.42}$$

$t_{1,2}$ being the layer thicknesses (indexed from the bottom up) and $h = t_1 + t_2$. From here one relates the unknown coefficients A and B by enforcing the continuity of \check{y} at the layer interface $z = t_1$ as

$$B = A \frac{\cos(\kappa_1 t_1)}{\cos(\kappa_2 t_2)}. \tag{5.43}$$

Using this in (5.42) and applying the continuity of $w(z)d_z \check{y}(z)$, interpreted as the dual TE voltage, one obtains the dual TE eigenfunction dispersion relation which is, in fact, the one for TE modes (2.148)

$$Y_1'' \text{ctg}(\kappa_{i,1}'' t_1) + Y_2'' \text{ctg}(\kappa_{i,2}'' t_2) = 0, \tag{5.44}$$

i denoting the mode index. Hence, the dual TE functions have the same spectrum as the standard TE ones! As it is more convenient to deal with normalized eigenfunctions, we perform the weighted scalar product to obtain the modal normalization constant

$$\begin{aligned}
 \langle \check{y}_i, \check{y}_i \rangle &= A^2 \left[\int_0^{t_1} \cos^2(\kappa_{i,1}'' z) w(z) dz + \int_{t_1}^h \left(\frac{\cos(\kappa_{i,1}'' t_1)}{\cos(\kappa_{i,2}'' t_2)} \right)^2 \cos^2(\kappa_{i,2}'' (h-z)) w(z) dz \right] = 1 \\
 \Rightarrow \check{c}_i'' &= A = \frac{1}{\sqrt{I_1 + I_2}}, \\
 I_1 &= w_1 \left(\frac{t_1}{2} + \frac{\sin(\kappa_{i,1}'' t_1) \cos(\kappa_{i,1}'' t_1)}{2\kappa_{i,1}''} \right), \\
 I_2 &= w_2 \left(\frac{\cos(\kappa_{i,1}'' t_1)}{\cos(\kappa_{i,2}'' t_2)} \right)^2 \left(\frac{t_2}{2} + \frac{\sin(\kappa_{i,2}'' t_2) \cos(\kappa_{i,2}'' t_2)}{2\kappa_{i,2}''} \right).
 \end{aligned} \tag{5.45}$$

Then, as shown in subsection 2.2.1.7, the characteristic Green's function can be written down as

$$\check{g}_{zi}''(z, z'; \lambda_z) = \sum_i w(z') \frac{\check{y}_i(z) \check{y}_i(z')}{\lambda_z - \lambda_{zi}'}, \tag{5.46}$$

where $w(z') = (\kappa_i''(z') Y_i''(z'))^{-1}$ and $\lambda_{zi}' = \kappa_i''^2$, i.e. the i -th solution of the dispersion relation (5.44). Hence, inserting this form into the construction integral (2.90) we obtain the dual TE scalar Green's function, and by applying the inverse transverse Laplacian operator, the pertinent S-potential is finally obtained.

$$\check{S}''(\mathbf{r}, \mathbf{r}') = \sum_i w(z') \frac{1}{4j} \frac{H_0^{(2)}(k_i'' |\mathbf{p} - \mathbf{p}'|)}{k_i''^2} \check{y}_i(z) \check{y}_i(z'). \tag{5.47}$$

It is interesting to consider the limit of this potential when $\varepsilon_2 \rightarrow \varepsilon_1$ ($t_1 \rightarrow h, t_2 \rightarrow 0$). Actually, it is enough to consider the limit of the product of the weight and the square of the normalization constant

$$\lim_{\varepsilon_2 \rightarrow \varepsilon_1} w_i(z') \check{c}_i''^2 = \frac{\varepsilon_m}{h}, \tag{5.48}$$

where ε_m is the Neumann number, which is equal to 1 for $m = 0$ and 2 otherwise. Since the TE dispersion equation becomes equal to the TM one, it follows that the dual TE S-potential will have the same spectrum as the TM S-potential. In fact, according to (5.48), it becomes equal to the TM S-potential! This agrees with results obtained by Albani et al. [104]. However, one should be careful with its numerical implementation for multilayered scenarios, since its limiting behavior is unstable. Namely, when one has dielectric layers having permittivities close to each other, and when the thickness of one of the layers becomes small compared to the total height of the PPW under consideration (roughly less than a tenth of the total height), (5.47) does not start behaving as the single-layer TM S-potential. This is due to the behavior of the TE dispersion equation (5.44), which does not "mimick" the single-layer TM dispersion equation for layer thicknesses and permittivities tending to the single-layer case.

APPENDIX B – DIELECTRIC-POST SCATTERING IN AN SIW DEVICE

As was indicated in section 2.2.1.8, when dielectric posts are present in an SIW device, TE and TM modes cannot exist independently. To be specific, even though one can devise excitations injecting solely TM modes into a PPW, the boundary conditions on dielectric posts require the existence of *both* TM and TE modes. Hence, one cannot apply boundary conditions for each mode separately, as is the case when only PEC posts are present, leading to more involved construction of and solution to linear systems in post-scattering amplitudes. This section deals with demonstrating how the post-scattering amplitudes may be obtained in the most straightforward way.

We begin by reiterating the problem – consider a PPW filled by either a single- or a multi-layer dielectric medium, with a number of dielectric and PEC posts embedded inside. The specific post arrangement is not important, unless the PPW is excited by a waveguide port; then there must exist an array of PEC posts confining the field to a limited volume of the PPW sufficiently strongly. Otherwise the approximation of the equivalence principle used to model the waveguide port fails to hold. If a coaxial port is present, no such restrictions are necessary. Finally, with all the requirements specified, what is the electromagnetic field inside the PPW?

As was shown in section 2.2.1.8, the starting point to the answer is to write down the boundary conditions on each and every post; if the post under consideration is PEC, the boundary condition to be satisfied is

$$\hat{\mathbf{n}}_q \times \left(\mathbf{E}_{imp} + \sum_{p \neq q} \mathbf{E}_p + \mathbf{E}_q \right) = 0 \Big|_{\partial R_q}, \quad (5.49)$$

where $\hat{\mathbf{n}}_q$ is the normal to the surface of post q , \mathbf{E}_{imp} is the electric field in the PPW due to an impressed source, with all obstacles (i.e. posts, slots etc.) removed, \mathbf{E}_p is the electric field which post p scatters toward post q , and \mathbf{E}_q is the electric field scattered by post q (∂R_q being its bounding surface). If, on the other hand, the post is dielectric, one enforces

$$\begin{aligned} \hat{\mathbf{n}}_q \times \left(\mathbf{E}_{imp} + \sum_{p \neq q} \mathbf{E}_p + \mathbf{E}_q^s \right) &= \hat{\mathbf{n}}_q \times \mathbf{E}_q^{int} \Big|_{\partial R_q} \\ \hat{\mathbf{n}}_q \times \left(\mathbf{H}_{imp} + \sum_{p \neq q} \mathbf{H}_p + \mathbf{H}_q^s \right) &= \hat{\mathbf{n}}_q \times \mathbf{H}_q^{int} \Big|_{\partial R_q}. \end{aligned} \quad (5.50)$$

Keeping in line with the formalism used to analyze post-scattering, we expand the magnetic fields in the second boundary condition of (5.50) as

$$\begin{aligned} &\hat{\mathbf{n}}_q \times \left(\sum_{\underline{s}} \chi_{\underline{s}q}^e \mathbf{M}_{\underline{s}q}^e + \chi_{\underline{s}q}^h \mathbf{N}_{\underline{s}q}^h + \sum_{p \neq q} A_{pq}^e \mathbf{M}_{pq}^e + A_{pq}^h \mathbf{N}_{pq}^h + \sum_q A_q^e \mathbf{M}_q^e + A_q^h \mathbf{N}_q^h \right) \\ &= \hat{\mathbf{n}}_q \times \left(\sum_q B_q^e \hat{\mathbf{M}}_q^e + B_q^h \hat{\mathbf{N}}_q^h \right) \Big|_{|\boldsymbol{\rho} - \boldsymbol{\rho}_q| = a_q}, \end{aligned} \quad (5.51)$$

where \underline{s} denotes the index multiplet (i, m, r, q) containing all the indexes pertaining to the field launched by an impressed source – i denoting the source, m the order of the longitudinal mode, r the order of the azimuthal mode, whereas q denotes the post. Likewise, \underline{p} and \underline{q} denote the index multiplets of the fields scattered by arbitrary posts p and q , and superscripts e and h denote the TM and TE functions, respectively. χ are amplitudes of modes excited by impressed sources, whereas the functions denoted by over-hats signify vector modes of the field expansion *inside the dielectric post*.

We proceed as before, by noting first that the field is expressed in the coordinate system centered on post q , and that each of the expansions in (5.51) is, among other bases, over the angular (azimuthal) spectrum, i.e. in the $\{e^{-jr\phi_q}\}$ base. Since the terms in the expansions belonging to different r are orthogonal, the only way for (5.51) to hold is if it holds for every r *independently!* In other words, we multiply (5.51) by $e^{jv\phi_q}$ ($v \in \mathbb{Z}$) and integrate it over ϕ_q from 0 to 2π , which annihilates all terms $r \neq v$. Hence, we have simplified the enforcement of (5.51) by having performed the scalar product in ϕ_q , allowing us to focus only on terms $r = v$. In order to obtain a further simplification, we might try to perform the scalar product in z , which will, hopefully, enable us to consider only terms of fixed order m . Though this was possible for problems of scattering in PPWs loaded with PEC posts, unfortunately, this is not the case here since taking the scalar product of (5.51) with a longitudinal eigenfunction (TE or TM) of order l will not annihilate all terms $m \neq l$; as a consequence, we are forced to consider several different modes at once. To see this, we first digress slightly to reconsider the general form of \mathbf{M} and \mathbf{N} functions, given by

$$\begin{aligned}\mathbf{M}_{m,n,q}^e(\boldsymbol{\rho}, \boldsymbol{\rho}_q, z) &= \nabla \times \hat{\mathbf{z}} Z_n(k_m^e |\boldsymbol{\rho} - \boldsymbol{\rho}_q|) e^{-jn\phi_q} i_m^e(z), \\ \mathbf{N}_{m,n,q}^h(\boldsymbol{\rho}, \boldsymbol{\rho}_q, z) &= c_N \nabla \times \nabla \times \hat{\mathbf{z}} Z_n(k_m^h |\boldsymbol{\rho} - \boldsymbol{\rho}_q|) e^{-jn\phi_q} v_m^h(z),\end{aligned}$$

Z_n being either Bessel functions J_n or Hankel functions of the second kind $H_n^{(2)}$, c_N being a suitable \mathbf{N} function constant (depending on the stratification), and i_m^e and v_m^h being the longitudinal TM and TE eigenfunctions, respectively, as defined in section 2.2.1.6. The \mathbf{N} function can be cast into a somewhat more illuminating form upon using the identity $\nabla \times \nabla \times \hat{\mathbf{z}} = \nabla(\nabla \cdot \hat{\mathbf{z}}) - \nabla^2 \hat{\mathbf{z}} = \partial_z \nabla_t - \nabla_t^2 \hat{\mathbf{z}}$

$$\begin{aligned}\mathbf{N}_{m,n,q}^h(\boldsymbol{\rho}, \boldsymbol{\rho}_q, z) &= c_N (\partial_z \nabla_t - \nabla_t^2 \hat{\mathbf{z}}) Z_n(k_m^h |\boldsymbol{\rho} - \boldsymbol{\rho}_q|) e^{-jn\phi_q} v_m^h(z) \\ &= c_N \nabla_t Z_n(k_m^h |\boldsymbol{\rho} - \boldsymbol{\rho}_q|) e^{-jn\phi_q} \partial_z v_m^h(z) + c_N \hat{\mathbf{z}} (k_m^h)^2 Z_n(k_m^h |\boldsymbol{\rho} - \boldsymbol{\rho}_q|) e^{-jn\phi_q} v_m^h(z) \\ &= \partial_z \mathbf{N}_{m,n,q}^h(\boldsymbol{\rho}, \boldsymbol{\rho}_q, z) + \Delta_t \mathbf{N}_{m,n,q}^h(\boldsymbol{\rho}, \boldsymbol{\rho}_q, z).\end{aligned}$$

(5.52)

Moreover, to facilitate manipulation of (5.51), we simplify it by considering the action of the post-surface normal $\hat{\mathbf{n}}_q$ cross-product on the terms in the expansion. Firstly, we note that in the case of \mathbf{M} functions, the cross-product acts as $\hat{\mathbf{n}}_q \times \nabla \times \hat{\mathbf{z}} = -(\hat{\mathbf{n}}_q \cdot \nabla) \hat{\mathbf{z}} = -\partial_{n_q} \hat{\mathbf{z}}$, where ∂_{n_q} denotes the derivative in the direction normal to the post surface. As for the \mathbf{N} functions, it can be shown, by fairly straightforward algebra, that any term in the expansions

of (5.51) containing the aforementioned functions can be simplified using $\hat{\mathbf{n}}_q \times \nabla \times \nabla \times \hat{\mathbf{z}} = \hat{\mathbf{n}}_q \times (\partial_z \nabla_t - \nabla_t^2 \hat{\mathbf{z}}) = \partial_z \partial_{\phi_q} \hat{\mathbf{z}} + \nabla_t^2 \hat{\phi}_q$. Now, using these relations in (5.51), we obtain two equations to be solved for; one for the z-component of (5.51)

$$\begin{aligned} & -\partial_{n_q} \left(\sum_{\underline{s}} \chi_{\underline{s}q}^e \Phi_{\underline{s}q}^e + \sum_{\underline{p} \neq q} A_{\underline{p}q}^e \Phi_{\underline{p}q}^e + \sum_q A_q^e \Phi_q^e \right) + \partial_z \partial_{\phi_q} \left(\sum_{\underline{s}} \chi_{\underline{s}q}^h \Phi_{\underline{s}q}^h + \sum_{\underline{p} \neq q} A_{\underline{p}q}^h \Phi_{\underline{p}q}^h + \sum_q A_q^h \Phi_q^h \right) \\ & = -\partial_{n_q} \sum_q B_q^e \hat{\Phi}_q^e + \partial_z \partial_{\phi_q} \sum_q B_q^h \hat{\Phi}_q^h \Big|_{|\rho - \rho_q| = a_q} \end{aligned} \quad (5.53)$$

whereas for the ϕ_q - component, surprisingly relating only TE components, we obtain

$$\sum_{\underline{s}} \chi_{\underline{s}q}^h \Phi_{\underline{s}q}^h + \sum_{\underline{p} \neq q} A_{\underline{p}q}^h \Phi_{\underline{p}q}^h + \sum_q A_q^h \Phi_q^h = \sum_q B_q^h \hat{\Phi}_q^h; \quad (5.54)$$

the Φ functions are scalar potentials pertinent to each of the types of fields, whose explicit forms will be given shortly. At this point, one should recall that these functions contain longitudinal eigenfunctions i_m^e and v_m^h . If the dielectric filling the waveguide is not stratified, then we can directly proceed to finding the A^h amplitudes by solving (5.54) in the exact same manner as one does when only PEC posts are present – by performing the scalar product between (5.54) and v_l^h , one obtains for each longitudinal mode a linear system of the form

$$\underline{\mathbf{T}}_m^h (\underline{\mathbf{A}}_m^h, \underline{\mathbf{B}}_m^h) = \underline{\Omega}_m^h, \quad (5.55)$$

whose solution yields the scattering amplitudes vector $(\underline{\mathbf{A}}_m^h, \underline{\mathbf{B}}_m^h)$. This is possible since both the field outside and inside the dielectric cylinders can be expanded using identical longitudinal eigenfunctions v_l^h , which are orthonormal $\langle v_m^h(z), v_l^h(z) \rangle = \delta_{ml}$. If, on the other, the guide's dielectric filling is stratified, this is not true, and one must consider a more general linear system since the scalar products between longitudinal eigenfunctions outside and inside the cylinders will in general not be zero.

First, let us see how the **single-layer** filling scenario could be handled. To recapitulate, the scalar product with a generic-order azimuthal eigenfunction has already been performed. This implies that for a given post q we can consider an equation which, of all its terms in the expansion of the field scattered off it, will contain only the terms having a fixed-order azimuthal dependence, i.e. $r = v$. The scalar potentials and coefficients in (5.54) are, explicitly,

$$\begin{aligned} \chi_{q,m,r}^h &= -j\omega\varepsilon \frac{1}{k^2} \frac{1}{4j} \frac{1}{k_m^{h2}} \int \left(D_2' H_r^{(2)}(k_m^h R_q') e^{jr\phi_q} v_m^h(z') \right) \cdot \mathbf{M}(\mathbf{r}') d\mathbf{r}', \\ \Phi_{s,m,r}^h &= J_r(k_m^h R_q) e^{-jr\phi_q} v_m^h(z), \end{aligned}$$

$$\begin{aligned}\Phi_{p \neq q, m, n}^h &= (-1)^{n-r} J_r(k_m^h R_q) H_{n-r}^{(2)}(k_m^h R_{pq}) e^{-jr\phi_q} e^{-j(n-r)\phi_{qp}} v_m^h(z), \\ \Phi_{q, m, n}^h &= H_r^{(2)}(k_m^h R_q) e^{-jr\phi_q} v_m^h(z), \\ \hat{\Phi}_{q, m, n}^h &= J_r(k_{q, m}^h R_q) e^{-jr\phi_q} v_m^h(z),\end{aligned}$$

where $R_q' = |\boldsymbol{\rho}' - \boldsymbol{\rho}_q|$, $R_q = |\boldsymbol{\rho} - \boldsymbol{\rho}_q|$, and $R_{pq} = |\boldsymbol{\rho}_p - \boldsymbol{\rho}_q|$. In addition, we reiterate the general form of longitudinal eigenfunctions and the associated orthonormality relation

$$\begin{aligned}v_m^h(z) &= \sqrt{\frac{2}{h}} \sin(\kappa_m^h z), \\ \langle v_m^h, v_l^h \rangle &= \delta_{ml}.\end{aligned}\tag{5.56}$$

First, we write down the boundary conditions for all the posts (PEC and dielectric), obtaining for each post equations of the form (5.53) and (5.54). Then, by taking the scalar product of (5.54) of each post with v_l^h , a set of equations for each considered mode l is obtained

$$\sum_{p \neq q} A_{l, v, p}^h \Phi_{l, v, p, q}^h + A_{l, v, q}^h \Phi_{l, v, q}^h - B_{l, v, q}^h \hat{\Phi}_{l, v, q}^h = - \sum_i \chi_{i, l, v}^h \Phi_{i, l, v, q}^h \Big|_{|\boldsymbol{\rho} - \boldsymbol{\rho}_q| = a_q}.\tag{5.57}$$

The obtained system of linear equations may be rewritten as

$$\sum_{p \neq q} A_{l, v, p}^h S_{l, n, v, p, q}^h + A_{l, v, q}^h R_{l, v, q}^h - B_{l, v, q}^h T_{l, v, q}^h = \sum_i \Omega_{i, l, v, q}^h,\tag{5.58}$$

where

$$\begin{aligned}S_{l, n, v, p, q}^h &= \frac{1}{K} (-1)^{n-v} H_{n-v}^{(2)}(k_l^h R_{pq}) e^{-j(n-v)\phi_{pq}}, \\ R_{l, v, q}^h &= \frac{1}{K} \frac{H_v^{(2)}(k_l^h a_q)}{J_v(k_l^h a_q)}, \\ T_{l, v, q}^h &= \frac{1}{K} \frac{J_v(k_{q, l}^h a_q)}{J_v(k_l^h a_q)}, \\ \Omega_{i, l, v, q}^h &= -\chi_{q, l, v}^h = -j\omega\varepsilon \frac{1}{K^2} \frac{1}{4j} \frac{1}{k_l^{h2}} \int \left(D_2' H_v^{(2)}(k_v^h R_q') e^{jv\phi_q} v_l^h(z') \right) \cdot \mathbf{M}(\mathbf{r}') d\mathbf{r}'.\end{aligned}\tag{5.59}$$

Casting this equation in matrix form, and solving for A^h , B^h amplitudes, we completely determine the total TE field. On the other hand, we still have to solve (5.53) for A^e , B^e , which we reiterate here for convenience

$$\begin{aligned}-\partial_{n_q} \left(\sum_{\underline{s}} \chi_{\underline{s}q}^e \Phi_{\underline{s}q}^e + \sum_{p \neq q} A_{p\underline{q}}^e \Phi_{p\underline{q}}^e + \sum_{\underline{q}} A_{\underline{q}}^e \Phi_{\underline{q}}^e \right) + \partial_z \partial_{\phi_q} \left(\sum_{\underline{s}} \chi_{\underline{s}q}^h \Phi_{\underline{s}q}^h + \sum_{p \neq q} A_{p\underline{q}}^h \Phi_{p\underline{q}}^h + \sum_{\underline{q}} A_{\underline{q}}^h \Phi_{\underline{q}}^h \right) \\ = -\partial_{n_q} \sum_{\underline{q}} B_{\underline{q}}^e \hat{\Phi}_{\underline{q}}^e + \partial_z \partial_{\phi_q} \sum_{\underline{q}} B_{\underline{q}}^h \hat{\Phi}_{\underline{q}}^h \Big|_{|\boldsymbol{\rho} - \boldsymbol{\rho}_q| = a_q}.\end{aligned}$$

To solve the system of equations we proceed as before; firstly by taking the scalar product with a generic azimuthal eigenfunction of order ν , yielding

$$\begin{aligned}
 & \sum_{i,m} \chi_{i,m,r=\nu}^e \Phi_{i,m,r=\nu,q}^e + \sum_{p \neq q, m, n} A_{m,n,p}^e \Phi_{m,n,r=\nu,p,q}^e + \sum_m A_{m,r=\nu,q}^e \Phi_{m,r=\nu,q}^e \\
 & + \sum_{i,m} \chi_{i,m,r=\nu}^h \Phi_{i,m,r=\nu,q}^h + \sum_{p \neq q, m, n} A_{m,n,p}^h \Phi_{m,n,r=\nu,p,q}^h + \sum_m A_{m,r=\nu,q}^h \Phi_{m,r=\nu,q}^h \quad (5.60) \\
 & = \sum_m B_{m,r=\nu,q}^e \hat{\Phi}_{m,r=\nu,q}^e + \sum_m B_{m,r=\nu,q}^h \hat{\Phi}_{m,r=\nu,q}^h \Big|_{|\rho-\rho_q|=a_q},
 \end{aligned}$$

where, with a slight abuse of notation, it is understood that $\Phi^e \equiv -\partial_{n_q} \Phi^e$, $\Phi^h \equiv \partial_z \partial_{\phi_q} \Phi^h$, and the ϕ_q dependence of the potential functions has been integrated out.

One notes that this leads to a system of equations in $N_{posts} \times N_z \times N_\phi$ unknowns (assuming the TE scattering amplitudes have been found from (5.58)), N_z being the number of longitudinal, while N_ϕ the number of azimuthal modes considered. In order to arrive to a simplified linear system, we take the scalar product of the equations of the form (5.60) for each post with a generic longitudinal TM eigenfunction $i_l^e(z)$. It should be clear that the orthonormality of the longitudinal TM eigenfunction set will lead to the annihilation of all TM terms of order $r \neq l$. Fortunately, for the single-layer case this same scalar product with TE terms will result in their annihilation as well, since

$$\langle \partial_z v_m^h(z), i_l^h(z) \rangle = \kappa_m^h c_m^h c_l^e \int_0^h \cos(\kappa_m^h z) \cos(\kappa_l^e z) = \kappa_m^h \delta_{ml}, \quad (5.61)$$

Now, if we are to arrive to a fully determined linear system, we can perform the scalar product of each of the equations with longitudinal TM eigenfunctions up to the maximal order considered, i.e.

$$\begin{aligned}
 & \sum_{i,m} \chi_{i,m,r=\nu}^e \Phi_{i,m,r=\nu,q}^e + \sum_{p \neq q, m, n} A_{m,n,p}^e \Phi_{m,n,r=\nu,p,q}^e + \sum_m A_{m,r=\nu,q}^e \Phi_{m,r=\nu,q}^e \\
 & + \sum_{i,m} \chi_{i,m,r=\nu}^h \Phi_{i,m,r=\nu,q}^h + \sum_{p \neq q, m, n} A_{m,n,p}^h \Phi_{m,n,r=\nu,p,q}^h + \sum_m A_{m,r=\nu,q}^h \Phi_{m,r=\nu,q}^h \\
 & = \sum_m B_{m,r=\nu,q}^e \hat{\Phi}_{m,r=\nu,q}^e + \sum_m B_{m,r=\nu,q}^h \hat{\Phi}_{m,r=\nu,q}^h \left| i_l^h(z) \right\rangle,
 \end{aligned}$$

resulting in

$$\begin{aligned}
 & \sum_i \chi_{i,m=l,r=\nu}^e \tilde{\Phi}_{i,m=l,r=\nu,q}^e + \sum_{p \neq q, n} A_{m=l,n,p}^e \tilde{\Phi}_{m=l,n,r=\nu,p,q}^e + A_{m=l,r=\nu,q}^e \tilde{\Phi}_{m=l,r=\nu,q}^e \\
 & + \sum_i \chi_{i,m=l,r=\nu}^h \tilde{\Phi}_{i,m=l,r=\nu,q}^h + \sum_{p \neq q, n} A_{m=l,n,p}^h \tilde{\Phi}_{m=l,n,r=\nu,p,q}^h + A_{m=l,r=\nu,q}^h \tilde{\Phi}_{m,l,r=\nu,q}^h \\
 & = B_{m=l,r=\nu,q}^e \tilde{\hat{\Phi}}_{m=l,r=\nu,q}^e + B_{m=l,r=\nu,q}^h \tilde{\hat{\Phi}}_{m=l,r=\nu,q}^h, \quad (5.62)
 \end{aligned}$$

where the tilde denotes the result of the scalar product with a longitudinal eigenfunction, i.e. $\tilde{\Phi} = \langle \Phi_m, i_l(z) \rangle$. If the TE scattering amplitudes are known, we can bundle the TE terms with the excitation terms to give

$$\begin{aligned}
 & \sum_{p \neq q, n} A_{m=l, n, p}^e \tilde{\Phi}_{m=l, n, r=v, p, q}^e + A_{m=l, r=v, q}^e \tilde{\Phi}_{m=l, r=v, q}^e - B_{m=l, r=v, q}^e \tilde{\Phi}_{m=l, r=v, q}^e \\
 &= - \sum_i \mathcal{X}_{i, m=l, r=v}^e \tilde{\Phi}_{i, m=l, r=v, q}^e - \sum_i \mathcal{X}_{i, m=l, r=v}^h \tilde{\Phi}_{i, m=l, r=v, q}^h - \sum_{p \neq q, n} A_{m=l, n, p}^h \tilde{\Phi}_{m, n, r=v, p, q}^h \\
 & \quad - A_{m=l, r=v, q}^h \tilde{\Phi}_{m, r=v, q}^h - B_{m=l, r=v, q}^h \tilde{\Phi}_{m=l, r=v, q}^h
 \end{aligned} \tag{5.63}$$

from which we can readily arrive to the final linear system to be solved in a few steps. Firstly, we recognize that all the potential functions Φ are expressed in the coordinate system centered on a given post q , i.e. $\Phi = \Phi(|\mathbf{p} - \mathbf{p}_q|, \phi_q) = \Phi(R_q, \phi_q)$, and that $\partial_{n_q} = R_q^{-1} \partial_{R_q}$. Hence, the explicit form of the potential functions involved is

$$\begin{aligned}
 \tilde{\Phi}_{i, l, v, q}^e &= -\frac{k_l^e}{R_q} J_v'(k_l^e a_q), & \tilde{\Phi}_{i, l, v, q}^h &= -jv\kappa_l^h J_v(k_l^h a_q), \\
 \tilde{\Phi}_{l, n, v, p, q}^e &= (-1)^{n-r+1} k_l^e \frac{H_{n-v}^{(2)}(k_l^e R_{pq})}{a_q} e^{-j(n-v)\varphi_{pq}} J_v'(k_l^e a_q), & \tilde{\Phi}_{l, n, v, p, q}^h &= -jv\kappa_l^h (-1)^{n-r} H_{n-v}^{(2)}(k_l^h R_{pq}) e^{-j(n-v)\varphi_{pq}} J_v(k_l^h a_q), \\
 \tilde{\Phi}_{l, v, q}^e &= -\frac{k_l^e}{a_q} H_v^{(2)'}(k_l^e a_q), & \tilde{\Phi}_{l, v, q}^h &= -jv\kappa_l^h H_v^{(2)'}(k_l^h a_q).
 \end{aligned} \tag{5.64}$$

It should be noted that for angular order $v=0$ the TE terms vanish due to the presence of the $-jv$ factor (resulting from differentiation with respect to ϕ_q), therefore the TM and TE modes are formally decoupled, but since the higher-order TE modes are involved - which do couple with higher-order TE modes - this fact does not alleviate the complexity of solution.

Finally, the system (5.63) can be recast into a more convenient form upon dividing each of the pertinent equations by $J_v'(k_l^e a_q)/a_q$, yielding

$$\begin{aligned}
 & \sum_{p \neq q, n} A_{l, n, p}^e \mathbf{S}_{l, n, v, p, q}^e + A_{l, v, q}^e \mathbf{R}_{l, v, q}^e - B_{l, v, q}^e \mathbf{T}_{l, v, q}^e \\
 &= \sum_i \Omega_{i, l, v, q}^e \zeta_{i, l, v, q}^e - \sum_i \Omega_{i, l, v, q}^h \zeta_{i, l, v, q}^h - \sum_{p \neq q, n} A_{l, n, p}^h \mathbf{S}_{l, n, v, p, q}^h \\
 & \quad - A_{l, v, q}^h \mathbf{R}_{l, v, q}^h - B_{l, v, q}^h \mathbf{T}_{l, v, q}^h,
 \end{aligned} \tag{5.65}$$

where

$$\begin{aligned}
 \mathbf{S}_{l,n,v,p,q}^e &= (-1)^{n-r} k_l^e H_{n-v}^{(2)}(k_l^e R_{pq}) \\
 \mathbf{S}_{l,n,v,p,q}^h &= j\nu(-1)^{n-r} (c_l^e c_l^h) (\kappa_l^h a_q) H_{n-v}^{(2)}(k_l^e R_{pq}) \frac{J_\nu(k_l^h a_q)}{J_\nu'(k_l^e a_q)} \\
 \mathbf{R}_{l,v,q}^e &= k_l^e \frac{H_\nu^{(2)'}(k_l^e a_q)}{J_\nu'(k_l^e a_q)} \\
 \mathbf{R}_{l,v,q}^h &= j\nu(c_l^e c_l^h) (\kappa_l^h a_q) \frac{H_\nu^{(2)}(k_l^h a_q)}{J_\nu'(k_l^e a_q)} \\
 \mathbf{T}_{l,v,q}^e &= k_{q,l}^e \frac{J_\nu'(k_{q,l}^e a_q)}{J_\nu'(k_l^e a_q)} \\
 \mathbf{T}_{l,v,q}^h &= j\nu(c_l^e c_l^h) (\kappa_l^h a_q) \frac{J_\nu(k_{q,l}^h a_q)}{J_\nu'(k_l^e a_q)} \\
 \Omega_{i,l,v,q}^e &= -j\omega\varepsilon \frac{1}{4j} \frac{1}{k_l^e} \int (D_1' H_\nu^{(2)}(k_l^e R_q') e^{j\nu\phi_q'} i_l^e(z')) \cdot \mathbf{M}_i(\mathbf{r}') d\mathbf{r}' \\
 \Omega_{i,l,v,q}^h &= -j\omega\varepsilon \frac{1}{4jK^2} \frac{1}{k_l^{h2}} \int (D_2' H_\nu^{(2)}(k_v^h R_q') e^{j\nu\phi_q'} v_l^h(z')) \cdot \mathbf{M}_i(\mathbf{r}') d\mathbf{r}' \\
 \zeta_{i,l,v,q}^e &= k_l^e \\
 \zeta_{i,l,v,q}^h &= j\nu(c_l^e c_l^h) (\kappa_l^h a_q) \frac{J_\nu(k_l^h a_q)}{J_\nu'(k_l^e a_q)} .
 \end{aligned}
 \tag{5.66}$$

Then it is a simple matter of writing this system down in matrix form and solving for the TM scattering amplitudes, which completes the mode-matching analysis.

A few comments on the features of such systems inherent in the analysis of practical devices is in order. Firstly, most such devices are designed to allow the propagation of solely the lowest order TM mode ($m=0$ or 1 , depending on the mode numbering convention), with the next-to-lowest modes severely suppressed. As such, the amplitudes of both the TM and TE higher-order modes scattered off of posts are negligible compared to the lowest-order mode at even modest distances from the source/scatterer. Consider, for example, the structure analyzed in 3.2.4, composed of stacked guides, each 1.54 mm high and loaded with a Rogers Duroid 4003 dielectric slab of permittivity $\varepsilon = 3.55$, operating at 14.25 GHz. A simple back-of-the-envelope calculation shows that the amplitude of the next-to-lowest modes (TM or TE) is on the order of 10^{-6} compared to the lowest-order mode, already at a distance of half a wavelength away (roughly 0.56 cm)! Therefore, in most scenarios one is safe to neglect higher order modes without notably sacrificing accuracy. For example, we could have substantially simplified the analysis expounded in this appendix had we simply set all

modal scattering amplitudes A_m, B_m to zero for $m > 0$, which would lead us, essentially, to an analysis similar to the one presented in subsection 2.2.1.8.

If the PPWs are loaded with layered dielectrics, and dielectric posts are present (e.g. air holes, phase-shifting or reflection-cancelling posts etc.) the scattering can be treated in the exact same way as for the single-layer case, though in that case there is an ambiguity in defining the scalar product in z analogous to (5.61) which leads to a discrete set of equations (along with the standard scalar product in ϕ). Namely, one encounters the scalar product between the z -derivatives of the TE modal functions and the TM ones, i.e. $\langle \partial_z v_m^h, i_l^e \rangle$, which can be defined in several ways. Firstly, one can use the definition of the TE scalar product

$$\langle \partial_z v_m^h, i_l^e \rangle = \int_{z_1}^{z_2} \partial_z v_m^h(z) i_l^e(z) \frac{dz}{\mu(z)}, \quad (5.67)$$

which we argue to be less “natural” than the alternative, which is the TM scalar product

$$\langle \partial_z v_m^h, i_l^e \rangle = \int_{z_1}^{z_2} \partial_z v_m^h(z) i_l^e(z) \frac{dz}{\varepsilon(z)}. \quad (5.68)$$

By “less natural” we mean “less convenient” in the following sense. The majority of the field energy will be carried by TM modes, i.e. they will have significantly larger amplitudes than TE modes. Taking the scalar product as defined in (5.68) of (5.60) will have the effect of annihilating the TM terms $m \neq l$, while the TE terms will persist, but will be of small amplitude. In practice, one can then completely neglect the TE terms, leaving only TM modes of order $m = l$. This leads to a simpler linear system than the one that would have resulted had we adopted (5.67) as the scalar product definition, i.e. the T-matrices will be less populated.

The preceding discussion makes the following observations clear:

- I. When an SIW device contains only PEC posts, if the source launches only a single type of modes into the PPW, i.e. either TM or TE, the scattered field will contain only those modes.
- II. If, on the other hand, the PPW contains dielectric posts, and if the source launches only a single type of modes, the scattered field will contain the other type of modes. In most cases of interest, the dielectric posts will weakly scatter the other type, which will decay severely even at relatively small distances from the scatterer.
- III. From II. It follows that one can simplify the post-scattering problem by neglecting the weakly scattered type of modes without significantly affecting the accuracy of the solution.
- IV. When more than one mode propagates in an SIW device containing dielectric posts, there will be significant mode-coupling, leading to larger-sized matrices that have to be inverted and, consequently, a significantly larger computation time with respect to the low mode-coupling scenario, which can be estimated as follows. Consider the T-matrices inherent in the low-mode coupling scenarios. There will be one for each longitudinal mode, of size $\dim(\mathbf{T}) = N_\phi \times N_{posts}$. Let us assume that the inversion scheme is a standard Gauss-Seidel method, which is of complexity $O(n^3)$, n being the number of rows or columns of the matrix to be inverted. Hence, the time necessary to compute the inverse of $2N_z$ such matrices will be roughly $\tau(\mathbf{T}^{-1}) = 2N_z \times (N_\phi \times N_{posts})^3$. Consider now the more exact

mode-coupling scenario where, generally, the coupling between all modes must be taken into account. Then the T-matrix is of size $\dim(\underline{\mathbf{T}}) = 2N_z \times N_\phi \times N_{posts}$, and the time necessary to invert it is $\tau(\underline{\mathbf{T}}^{-1}) \propto (2N_z \times N_\phi \times N_{posts})^3$; the ratio of the times is then roughly $\tau(\underline{\mathbf{T}}^{-1}) / \tau(\underline{\mathbf{T}}^{-1}) \approx 4N_z^2$. To give a sense of how much this might be in practice, one usually considers no more than $N_z = 3$, giving the computational time larger by a factor of 36 if either mode-coupling is strong and we must use the exact approach to mode-matching (as expounded in this appendix) or the mode-coupling is low but we are being rigorous by using the more exact approach (i.e. we do not neglect higher-order modes).

APPENDIX C – BIBLIOGRAPHY RELATED TO THE THESIS

Journal papers

M. Casaletti, G. Valerio, **J. Seljan**, M. Ettorre, and R. Sauleau, "A full-wave hybrid method for the analysis of multilayered SIW-based antennas," *Antennas Propag. IEEE Trans. On*, vol. 61, no. 11, pp. 5575–5588, 2013.

G. Valerio, M. Casaletti, **J. Seljan**, R. Sauleau, and M. Albani, "Efficient computation of the coupling between a vertical line source and a slot," *Antennas Propag. IEEE Trans. On*, vol. 61, no. 12, pp. 6084–6093, 2013.

Conference papers, talks

J. Seljan, G. Valerio, M. Casaletti, K. Tekkouk, M. Ettorre, and R. Sauleau (2014, April). Hybrid MoM/mode-matching method for SIW devices housing layered dielectric substrates. In *Antennas and Propagation (EuCAP), 2014 8th European Conference on* (pp. 3605-3608). IEEE.

J. Seljan, M. Casaletti, G. Valerio, M. Ettorre, R. Sauleau, and S. Maci, "Novel mode-matching technique for the efficient analysis of complex multi-layer SIW and SISW-based structures," in *Proc. Nat. Radio Sci. meeting, Chicago, Illinois, USA, 8 – 14 Jul. 2012*.

E. Gandini, K. Tekkouk, **J. Seljan**, M. Casaletti, G. Valerio, M. Ettorre, R. Sauleau, "Substrate integrated waveguide structures: analysis and design of multiple beam antennas," in *Proc. 7th Working Group and 9th Management Committee, Istanbul, Turkey, 8 - 9 Oct. 2012*.

M. Casaletti, G. Valerio, **J. Seljan**, M. Ettorre, and R. Sauleau, "A full-wave hybrid method for the fast analysis of SIW-based antennas," *VII Eur. Conf. Antennas Propag. (EuCAP), Gothenburg, Sweden, 8-12 Apr. 2013*.

M. Casaletti, G. Valerio, **J. Seljan**, M. Ettorre, and R. Sauleau, "Méthode de raccordement modal pour l'analyse rapide d'antennes SIW," *XVIII Journées Nationales Microondes, Paris, France, 15-17 May 2013*.

M. Casaletti, G. Valerio, **J. Seljan**, M. Ettorre, and R. Sauleau, "Efficient analysis of SIW-based antenna geometries through a rigorous MoM mode-matching approach," accepted for presentation at *Antennas Propag. Symp. (APS), Lake Buena Vista, Florida, USA, 7 – 12 Jul. 2013*.

M. Albani, M. Casaletti, M. Ettorre, G. Valerio, **J. Seljan**, and R. Sauleau, "A new synthesis technique for near-field focusing systems," accepted for presentation at *Nat. Radio Sci. meeting, Lake Buena Vista, Florida, USA, 7 – 12 Jul. 2013*.

G. Valerio, M. Casaletti, **J. Seljan**, M. Ettorre, and R. Sauleau, "Optimized analysis of slotted substrate integrated waveguides by a method-of-moments mode-matching hybrid approach," accepted for presentation at *Int. Conf. Electromagn. Advanced Appl. (ICEAA), Turin, Italy, 9-13 Sep. 2013*.

J. Seljan, M. Casaletti, G. Valerio, "Efficient Analysis of Metallic and Dielectric Posts in Parallel-Plate Waveguide Structures", given at the Dept. of Radiocommunications, FER, Zagreb, 2012.

BIOGRAPHY

Josip Seljan was born in 1986 in Karlovac, Croatia where he graduated from high school in 2005. In the same year he enrolled to the electrical engineering programme at the Faculty of Electrical Engineering and Computing, Zagreb, graduating in 2011 with a master's thesis on Green's functions for gap waveguides based on asymptotic boundary conditions, under prof. Zvonimir Šipuš. In 2011 he started his Ph.D. on integral-equation based analysis of SIW devices at the Institut d'Electronique et de Télécommunications de Rennes, under the supervision of doctor Mauro Ettorre and professor Ronan Sauleau.

His research interests include integral equation methods and functional analysis in electromagnetics, as well as the general theory of electrodynamics (with emphasis on the construction and interpretation of work/energy functionals in arbitrary media).

ANNEXE 2

VU :

VU :

Le Directeur de Thèse

(Nom et Prénom)

Le Responsable de l'École Doctorale

VU pour autorisation de soutenance

Rennes, le

Le Président de l'Université de Rennes 1

David ALIS

VU après soutenance pour autorisation de publication :

Le Président de Jury,

(Nom et Prénom)

